MAGNETIC PROPERTIES OF SINGLE AND MULTILAYER STRUCTURED AMORPHOUS AND NANOCRYSTALLINE FeTaC MAGNETIC THIN FILMS

A thesis submitted

by

Akhilesh Kumar Singh

to

Indian Institute of Technology Guwahati

in

Partial fulfillment of the requirement for the award of the degree of Doctor of Philosophy in Physics

Department of Physics
Indian Institute of Technology Guwahati
Guwahati 781 039, Assam, India

April 2014

MAGNETIC PROPERTIES OF SINGLE AND MULTILAYER STRUCTURED AMORPHOUS AND NANOCRYSTALLINE FeTaC MAGNETIC THIN FILMS

A thesis submitted

by

Akhilesh Kumar Singh

to

Indian Institute of Technology Guwahati

in

Partial fulfillment of the requirement for the award of the degree of Doctor of Philosophy in Physics

Department of Physics
Indian Institute of Technology Guwahati
Guwahati 781 039, Assam, India

April 2014

Statement

The work contained in the thesis entitled “Magnetic properties of single and multilayer structured amorphous and nanocrystalline FeTaC magnetic thin films” has been carried out by me under the supervision of Dr. A. Perumal at the Department of Physics, Indian Institute of Technology Guwahati. This work has not been submitted elsewhere for the award of any degree.

April 2014

(Akhilesh Kumar Singh)
Roll No: 09612112
Department of Physics
Indian Institute of Technology Guwahati
Guwahati – 781039
India.

Certificate

It is certified that the work contained in the thesis entitled “Magnetic properties of single and multilayer structured amorphous and nanocrystalline FeTaC magnetic thin films” submitted by Akhilesh Kumar Singh, a Ph. D. student of the Department of Physics, Indian Institute of Technology Guwahati for the award of degree of Doctor of Philosophy has been carried out under the supervision of Dr. A. Perumal. This work has not been submitted elsewhere for the award of any degree.

April 2014

(Dr. A. Perumal)
Associate Professor,
Department of Physics
Indian Institute of Technology Guwahati
Guwahati – 781039
India.

Dedicated to my

beloved parents

Acknowledgements

It is my privilege to express deep sense of gratitude to my thesis supervisor Dr. A. Perumal for his resourceful guidance, constructive criticisms and careful supervision in guiding me throughout my research work. His continuous encouragement and intellectual discussion has been a driving force for me to excel in my work. I am grateful to my doctoral committee members (Prof. S. Ravi, Dr. Dilip Pal and Dr. S. Kanagaraj) for reviewing my research work regularly and providing valuable guidelines/suggestions for the improvement of my research work. I am thankful to Prof. S. Basu, HOD Department of Physics, and Prof. S. Ravi, the former HOD, Department of Physics for their immense supports.

I am very much thankful to Dr. Subhankar Bedanta, NISER Bhubaneswar, India for magnetic domain observation using Kerr microscope. I am also thankful to Prof. K. G. Suresh, Indian Institute of Technology Bombay for thermomagnetization measurements using SQUID magnetometers.

I express my sincere thanks to Dr. Sidananda Sarma, a scientific officer in the department of physics, for guiding me to handle the various high precision instruments in the department of physics.

Mr. Chandan Borgohain, Dr. Kula Kamal Senapati and Mr. Madhurjya Borah, scientific officers of CIF, have patiently and enthusiastically extended their expertise in handling various instruments that I have used for my research work.

I am fortunate to have my senior Dr. Debabrata Mishra and other lab seniors Dr. B. Samantaray, Dr. S. Mohanty. Dr. Sangeetha and Dr. Rahul Das, who helped me in various ways throughout my research work.

Shyni, Tribedi, Padam, Santosh, Mukesh, Batakrushna, Indrajeet, Brahmananda, Bhargab, Bhagaban, Anabil, Barnali, Arnab, Nisha, Bipul, Ranganadha, Junmoni, Mahesh, Ramesh and all the research scholars of physics department will always be remembered for the wonderful time we shared together. I thank Bhargab, Anabil, Bhagban and all my friends for the memorable life in IIT Guwahati campus.

I am deeply obligated to my beloved parents, brothers, sisters and all my family members for their moral support and constant encouragements for my progress. Finally my sincere thanks are due to all those have been helped me in whatever manner and bring me to this position, some of whom I may have inadvertently forgotten to mention in this acknowledgement.

Akhilesh Kumar Singh

PREFACE

The tendency to miniaturize the dimensions of electronic devices during last two decades has created a demand for new materials and new methods for their production. Thin films of various magnetic alloys play a key role in miniaturization of integrated circuits in various magnetoelectronic devices. Hence, searches for suitable magnetic thin films with enhanced soft magnetic properties have been carried out widely not only for practical applications in modern magnetic devices such as soft underlayer in perpendicular magnetic recording media, magnetic flux amplifier, high-density magnetic recording read heads and magnetoresistive random access memories, but also for gaining fundamental knowledge on low-dimensional systems. In general, the magnetic thin films were prepared in amorphous form. However, they exhibit a strong thickness dependence of magnetic properties, which depend strongly on the constituent elements. In addition, thickness dependent properties do not show unique behaviour and hence the estimation of magnetic properties is rather difficult. Nevertheless, most of the Fe based magnetic alloys display degraded magnetic properties at higher thicknesses mainly due to the change in the magnetic domain structure resulting from the development of perpendicular magnetic anisotropy. On the other hand, the controlled post deposition annealing of these amorphous precursors develops the characteristic two-phase microstructure in which nano-sized crystals of soft ferromagnetic crystalline phase are embedded in a ferromagnetic amorphous matrix. In addition, this two-phase microstructure exhibits excellent soft magnetic properties, high thermal stability and low media noise. Alternatively, to control the development of perpendicular magnetic anisotropy and the domain structure for improving the soft magnetic properties at a larger film thickness, the multilayer structured thin films have been proposed. The study of magnetic multilayer thin films has resulted variety of fascinating phenomena and has been the subject of extensive investigations from both theoretical and experimental points of view. While such artificial structures are suggested for various applications in modern magnetoelectronic devices from the application point of view, they also expected from fundamental point of view to provide an understanding of surface magnetism and transport phenomena, such as interlayer magnetic coupling, the magnetostatic interaction induced by the interface roughness (topological coupling), the effects of thickness and number of spacer layers

on the structural and magnetic properties, and disorder magnetic states, etc. Therefore, the controlled growth and tailorable properties of such nanostructured multilayer films have become a very active field in the research for the realization of futuristic magnetic devices. Furthermore, the investigation of temperature dependent magnetic properties of multilayer structured soft magnetic thin films has not been reported in detail.

Hence, the present thesis aims (i) to understand the effect of film thickness and (ii) the multilayer structures with different spacer layer thicknesses on the temperature dependent magnetic properties of FeTaC magnetic thin films and (iii) to investigate the effect of post deposition annealing at different temperatures (T_A) on the formation of two-phase microstructure and the resulting magnetic properties and the correlation between them. The present thesis comprises of seven chapters.

Chapter 1 presents a brief introduction to the content of the thesis along with a review of literature relevant to the thesis work. The motivation and aim of thesis works are also included in this chapter. **Chapter 2** summarizes the fundamental aspects of magnetism and various models utilized in the analysis of the data for the presently investigated films. In **Chapter 3**, the experimental techniques used for the preparation of single and multilayer structured films and characterization of these films are outlined.

In **Chapter 4**, the effect of amorphous FeTaC (t) film thickness on the temperature dependent magnetic properties is reported over a wide range of temperatures (5 K - 500 K). Magnetic hysteresis (M-H) loops obtained at room temperature illustrate narrow loops with high remanence magnetization and low coercivity (H_C) for the films with thickness less than 50 nm. In particular, 50 nm thick film displays in-plane uniaxial anisotropy. With increasing film thickness more than 50 nm, the nature of the M-H loops changes to transcritical loop due to the development of perpendicular anisotropy, which forms magnetic strip domain patterns. As a result, H_C increases largely (> 20 Oe). The temperature dependent M-H loops reveal a prominent shift towards a negative field axis at lower film thickness. The variations of H_C, saturation magnetization (M_S) and perpendicular anisotropy constant show a dependence on the film thickness. Temperature dependent zero-field-cooled (ZFC) and field-cooled (FC) magnetization data (M-T) exhibit bifurcations between them for FeTaC ($t \geq 100$ nm) films. High temperature M-T data reveal a film thickness dependence of effective reduction in magnetization and marginal increase in Curie

temperature with decreasing film thickness. The magnetic phase transition from ferromagnetic state to paramagnetic state exhibits thickness dependent critical exponents transforming from 3D Heisenberg model for 20 nm thick film to 3D Ising model for the films having thickness larger than 50 nm.

Chapter 5 discusses effects of multilayer structures and the thickness of the spacer layers on the structural and magnetic properties of FeTaC films with Ta spacer layer, i.e., [[FeTaC (y nm)/Ta (x nm)]$_n$ /FeTaC (y nm)] in two sections. While the first section describes the effect of number of multilayers (n = 0 – 4) on the magnetic properties by fixing the space layer thickness at 1 nm, the second section focuses on the spacer layer thickness (x = 0 – 6) and temperature driven magnetic properties in multilayer structured FeTaC thin films with n = 3. The total thickness of FeTaC film was retained at 200 nm and the thickness of each layer in multilayer films was controlled using the relation y = 200 / (n + 1) with n varying between 0 and 4. Similarly, the thickness of the spacer layer was varied systematically between 0 and 6 nm. XRD and TEM analysis confirmed the presence of amorphous structure in all the multilayer films. *Effect of number of multilayers* (n): Room temperature *M-H* loops are found to be strongly dependent on multilayer films, i.e., the transcritical loop observed in 200 nm thick single layer film fades out progressively with increasing n values and for the films with n > 2, *M-H* loops transform from transcritical to narrow flat loops with high remanence magnetization. As a result, H_C decreases largely by two orders of magnitude in multilayer films. In addition, the *M-H* loops observed at low temperatures display multistep magnetization reversal behaviour due to the individual switching of FeTaC layer in multilayer film and number of steps in the magnetization reversal significantly depends on number of multilayers. The variations of H_C and M_S with temperature also show a strong dependence on the multilayer structures. The bifurcation observed in the ZFC and FC data for 200 nm thick single layer film shifts to lower temperature in multilayer films with increasing n up to 3 and disappears eventually for n = 4 indicating that the existence of magnetic disorder in large thickness single layer film can be fine-tuned methodically using multilayer structure. However, high temperature *M-T* curves of all the multilayer films obtained under saturated conditions were appeared to be similar without any significant changes in T_C. *Effect of spacer layer thickness* (x): The shape of the room temperature *M-H* loops for multilayer films with different x (1- 6 nm) remains same, but H_C decreases significantly with increasing x up to 4 and increases slightly for x = 6. Temperature dependent *M-H* loops

reveal a change in the loop shape from flat loop to the transcritical one for the film with x = 1 due to the direct exchange coupling between FeTaC layers through the pinhole present in the thin (1 nm) Ta spacer layers. Such behaviours were not observed for the films with spacer layer thickness larger than 1 nm due to the formation of well separated FeTaC layers by the Ta spacer layers and the disappearance of direct exchange coupling between FeTaC layers. In addition, *M-H* loops measured at different temperatures exhibit spacer layer thickness dependent multistep magnetization reversal behaviour at low temperature (below 70 K) mainly due to enhanced interface roughness with decreasing temperature. Furthermore, the bifurcation point observed between ZFC and FC data for x = 0 film shifted to lower temperature and disappeared for the films with $x \geq 2.5$ nm. The observed results confirm the spacer layer thickness and temperature driven magnetic properties in multilayer FeTaC films. Nevertheless, the magnetic phase transition from ferromagnetic state to paramagnetic state does not depend on the spacer layer thickness and hence T_C remains constant for all the films with different spacer layer thicknesses. The observed results confirm the enhancement in the soft magnetic properties with number of multilayers and spacer layer thickness in multilayer FeTaC films.

Chapter 6 describes the effects of post deposition annealing on the microstructure and magnetic properties of the single and multilayer films. All the films were post annealed (T_A) ex-situ systematically at 200 ºC, 300 ºC and 400 ºC for 30 minutes duration in a separate home-made high vacuum annealing set up. The structural analysis performed using XRD and TEM reveals that (i) all the films annealed at or below 200 ºC exhibit amorphous nature. (ii) With increasing T_A above 200 ºC, the precipitation (at 300 ºC) and subsequent growth (at 400 ºC) of α-Fe nanocrystals in the residual amorphous matrix were observed. The obtained results are divided into two parts: *Effect of number of multilayers*: *M-H* loop of 200 ^{o}C annealed single layer film and multilayer films illustrates a flat loop with a large reduction in H_C at room temperature. This could be attributed to annihilation of perpendicular anisotropy in the as-deposited films and as a result, a transformation from strip domain pattern to in-plane magnetization was observed. Temperature dependent *M-H* loops show multilayer structure dependent multistep magnetization reversal behaviour only below 70 K. With increasing $T_A \geq 300$ ºC, the multistep magnetization reversal behaviour was observed for multilayer films even at room temperature. The variation of

room temperature H_C with increasing n strongly depends on T_A. In addition, the nature of the loops, number of the steps and position of the steps in the magnetization reversal process of the *M-H* loops observed at different temperatures depends intensely on number of multilayers and T_A due to the change in interlayer coupling between FeTaC layers and the microstructure of the FeTaC films. On the other hand, the values of T_C obtained from high temperature *M-T* curves decrease significantly with increasing number of multilayers for the films annealed at 200 ºC and 300 ºC, but remain almost constant for the films annealed at 400 ºC. Similarly, for a given multilayer structure, the values of T_C (i) decrease significantly for the films annealed at 200 ºC as compared to the as-deposited films due to the release of stress accumulated during the films' deposition and (ii) increase largely for the 400 ºC annealed films due to the formation of α-Fe nanocrystals. *Effect of spacer layer thickness*: The magnetic properties of the multilayer films of different spacer layer thicknesses (x) also strongly depend on T_A. As compared to the as-deposited films (x = 1, n = 3), the annealed films do not show a large variation in the nature of *M-H* loops measured at different temperatures. Nevertheless, spacer layer thickness dependent multistep magnetization reversal behaviour was observed for the films annealed at different T_A. Interestingly, temperature dependent H_C displays an unusual behaviour in the annealed multilayer films (at 300 ºC), i.e., H_C decreases initially and then increases with decreasing temperature resulting a broad minimum in the $H_C(T)$ versus T curve. The position of the broad minimum in the curve shifts to lower temperature with increasing the spacer layer thickness. On the other hand, the multilayer films annealed at 400 ºC depict a continuous increase in H_C with decreasing temperature and the rate of decrease of $H_C(T)$ displays a strong dependence on the spacer layer thickness. Similarly, the temperature dependent saturation magnetization and the field required for saturating the magnetization along the film plane depend on the microstructure of the multilayer films. On the other hand, the values of T_C obtained from the high temperature *M-T* curves vary significantly with the thickness of the spacer layers and T_A.

Chapter 7 provides a summary of the results obtained in the thesis and explores possible directions of future work in this topic. References and list of publications which have originated out of this thesis work and the publications from other collaborative research works are listed at the end of the thesis.

CONTENTS

Chapter 1

Prologue

1.1. Introduction:

A key trend in recent science and technology is the exploitation of phenomena occurring at length scales between 1 and 500 nm, which has led to the emergence of new fields such as nanoelectronics, nanobiology and nanochemistry. During the last few decades, the tendency to miniaturize the dimensions of electronic devices has created a demand for new materials and new methods for their production. Thin films of various magnetic alloys play a major role in miniaturization of integrated circuits in magnetoelectronic devices including consumer electronics. Hence, searches for suitable magnetic thin films with enhanced soft magnetic properties (high saturation magnetization (M_S), low coercivity (H_C), large relative permeability, controllable magnetic anisotropy and good thermal stability) have been carried out widely not only for practical applications in modern magnetic devices such as soft underlayer in perpendicular magnetic recording (PMR) media, magnetic flux amplifier, high-density magnetic recording read heads and magnetoresistive random access memories, but also for gaining fundamental knowledge on low-dimensional systems [NAOE1998, HART1999, KHIZ20041, PIRA2007, SAKI2008].

In order to obtain soft magnetic thin films, it is very much essential to understand the correlation between the structural and magnetic properties so that a well-defined magnetic domain structure can be achieved in the magnetic thin films. Therefore, extensive studies have been carried out since past two decades on various amorphous single layer thin films such as FeCuNbSiB [NAOE1998, FUJI2006], FeAlSi [TATE1998], CoNbZr [HIRA2000], FeTa(C)N [WEIV2000, JIAN2005], FeTaC [TANA2002], Fe-Zr-N [CRAU2002], CoTaZr [LEED2006] and CoFeB [GUER2007] and multilayer structured thin films of Fe/Ta and Fe:N/Ta:N [NAOE1996], Fe/Zr [CAST19971], FeCoTa:N/Ti [NAKA1997], FeCuNbSiB/Al [NAOE1998], Fe/Cu [OLIV1999], FeAlSi/C [NAKA2001], CoCrTa/Ru/CoTaZr and CoCrPt/Ru/CoFe [WUAY2002, JUNG2006], Fe(Ta,Ti,Nb)C/Ta [TANA20032], NiFe/IrMn/ NiFe/CoTaZr [TANA20031], CoTaZr/Ru/CoTaZr [ACHA2004] and Fe/Al [BRAJ2010]. Although the magnetic alloys with amorphous structure exhibit large M_S, low H_C due to random magnetic anisotropy and high electrical resistivity [KIMY2000, KIMJ2003, LIW2005], the thermal stability of these alloys is considerably low. As a result, the amorphous alloys and the multilayer structured films with amorphous magnetic alloys are found not suitable for high temperature applications. Another class of materials exhibiting outstanding soft magnetic properties is nanocrystalline materials [YOSH19881, HERZ1992, PETZ2002], which are generally obtained by a controlled annealing of the amorphous

precursors at different temperatures under high vacuum. The responsibility for the excellent soft magnetic properties in the nanocrystalline materials is their characteristic two-phase microstructure in which nano-sized (< 20 nm) crystals of a soft ferromagnetic phase are embedded in a ferromagnetic amorphous matrix [SELL2006]. Such microstructure not only yields an averaging out of magnetocrystalline anisotropy, but enhances the saturation magnetization and the permeability [HERZ1995, OHNU2003] as shown in figure 1.01. In addition, the strong ferromagnetic inter-granular exchange interaction and long range ferromagnetic ordering in the nanocrystalline materials result in very high Curie temperature (T_C) as compared to the amorphous materials [HERN1995, GORR1996]. Furthermore, magnetostriction (see figure 1.02) and noise properties of the nanocrystalline materials are very low [KIKU2000]. Therefore, these nanocrystalline materials find wide applications in high performance magnetic components such as noise absorbers, magnetic switch cores, current sensors and for high frequency and high temperature applications.

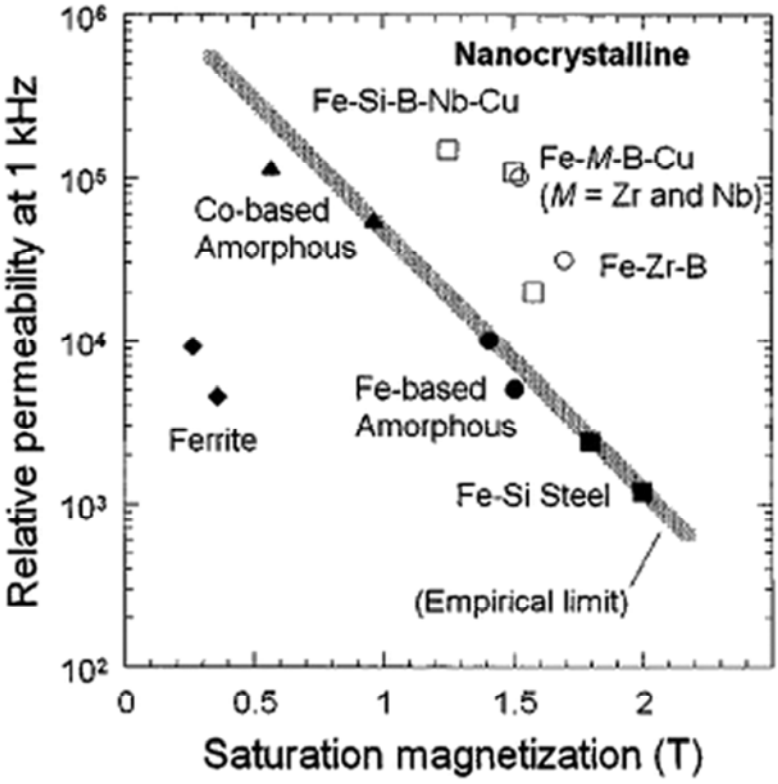

Figure 1.01: Relative permeability and saturation magnetization of various soft magnetic materials. The open circles and open squares denote FINEMET [YOSH19882, YOSH2001] and NANOPERM [SUZU1993, BITO1997] materials, respectively.

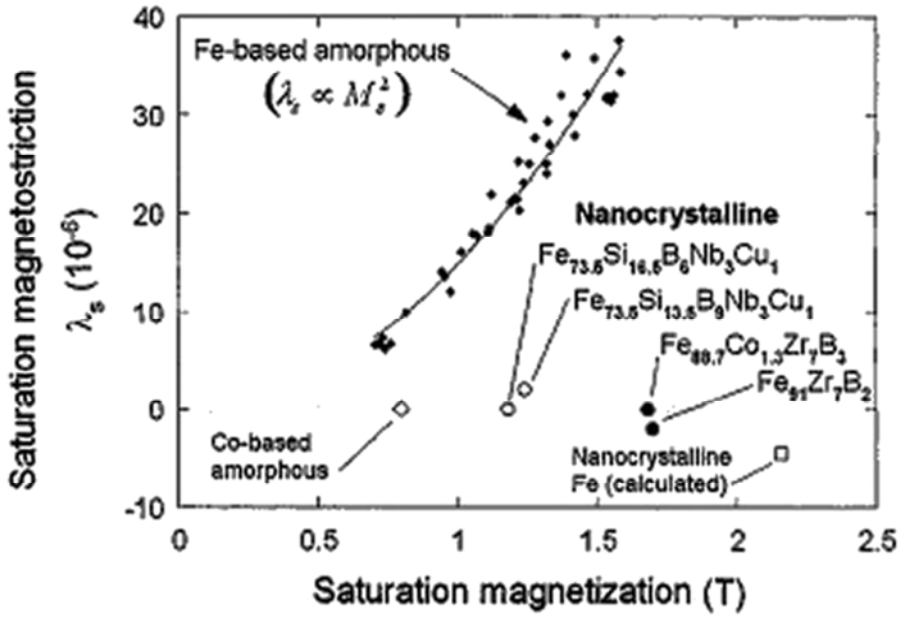

Figure 1.02: Relation between saturation magnetostriction and saturation magnetization for amorphous [ITOS1980] and nanocrystalline [YOSH19882, YOSH19891, SUZU1994] soft magnetic materials.

1.2. Motivation behind the work with historical perspective from the literature:

With the recent interests in the development of various magnetoelectronic devices such as high density magnetic recording read heads, magnetoresistive random access memories, and soft underlayer in the PMR media, it is very much important to study the magnetic properties of those alloys that are commonly used in such applications. Particularly, in double-layered PMR medium, the recording layer with a perpendicular anisotropy is fabricated on top of a soft magnetic thin film with suitable intermediate layers. This double-layered medium and a single-pole type head is considered as one of the ideal solutions for high density PMR [TAKA2000, KHIZ20042]. However, the design and property optimization of a magnetic thin film for soft underlayer application is one of the key issues [CAIN1996]. Since the past decade, extensive studies have been carried out on various magnetic thin films both in single layer form [CoNbFe, Co(Ta,Nb)Zr, FeAlSi, FeTaN, FeCoNi and FeTaC] and multilayer form [Fe:N/Ta:N, FeCoTa:N/Ti, FeCuNbSiB/Al, FeAlSi/C, CoCrTa/Ru/CoTaZr, CoCrPt/Ru/ CoFe, Fe(Ta,Ti,Nb)C/Ta, NiFe/IrMn/NiFe/CoTaZr and CoTaZr/Ru/CoTaZr] to arrive at suitable soft underlayer. As an underlayer of a double-layered PMR medium [ZHAN2003, PIRA2007, PERU2010], FeTaC based alloy films have been reported to show good soft magnetic properties [LAIC2003, TANA20032, JIAN2005, PERU2009] for soft underlayer

applications in $L1_0$ ordered FePt based PMR media prepared on heat resistant substrates [CHEN20071, PERU2008].

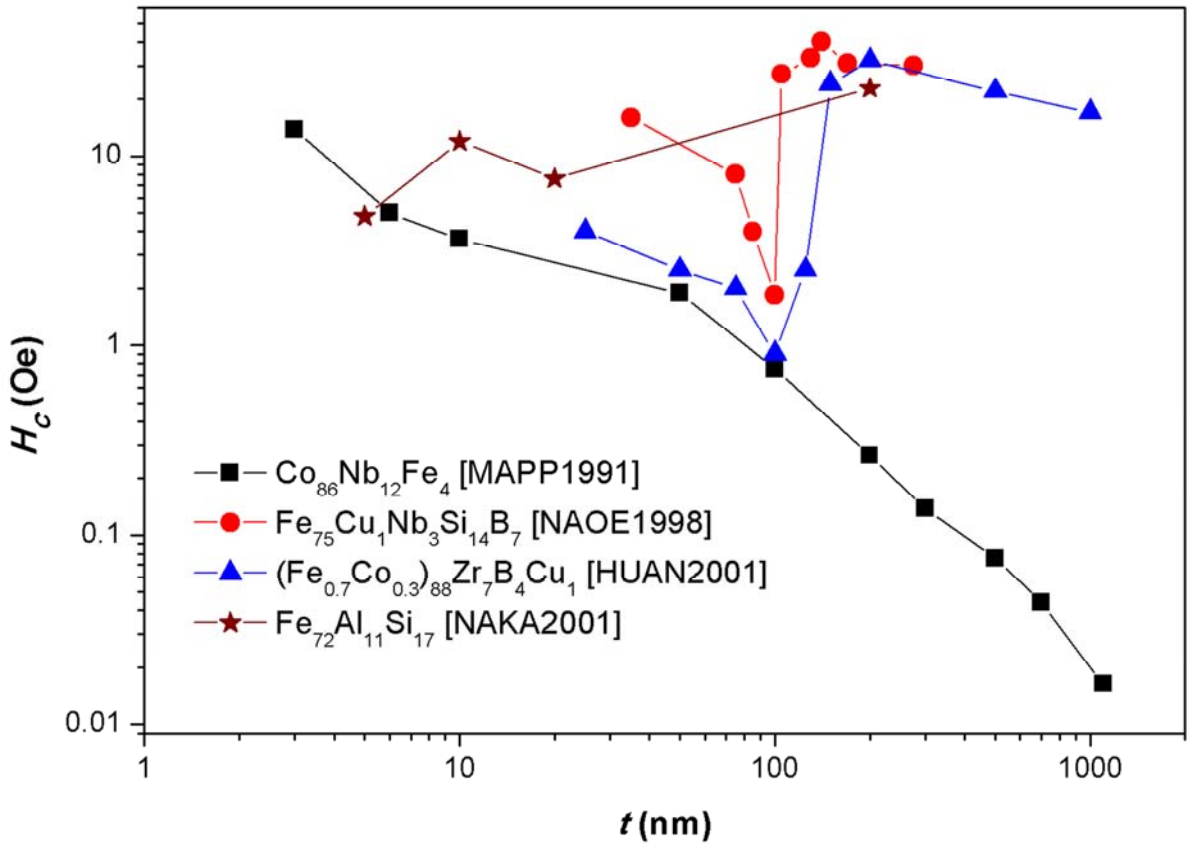

Figure 1.03: Thickness dependent coercivity in magnetic thin films.

However, it has been revealed from a careful review of the literature that the soft magnetic properties of the magnetic films display a strong dependence on the film thickness and the growth conditions of the films. Interestingly, the thickness dependent magnetic properties of the films do not show unique behaviour (see figure 1.03) and depend strongly on the constituent elements [MAPP1991, NAOE1998, HUAN2001, NAKA2001]. The variations of H_C of various types of the magnetic thin films extracted from the literature are summarized as a function of film thickness (t) in figure 1.03. It is clearly evident from figure 1.03 that the thickness dependent H_C of the magnetic films exhibit a random behaviour depending on the constituent elements in the alloys. For example, Mapps et al [MAPP1991] reported that H_C of CoNbFe films decreases almost continuously over a wide range of film thicknesses (5 nm – 1000 nm). But, Huang et al [HUAN2001] showed that the room temperature H_C of single layer FeCoZrBCu (HITPERM) films decreases slightly with increasing thickness from 25 nm to 100 nm, but shows a rapid increase for the thickness larger than 100 nm. In contrast, Naoe et al [NAOE1998] reported that H_C of FeCuNbSiB

alloy decreases largely with increasing thickness from 25 to 100 nm followed by a rapid increase in H_C values for the thickness between 100 and 150 nm. However, H_C decreases slightly on further increasing the film thickness above 200 nm. In addition, they reported that the variation of H_C with thickness depends strongly on the growth condition of the magnetic films. On the other hand, Nakamura et al [NAKA2001] reported an oscillatory nature in H_C in FeSiAl alloy films at lower thicknesses (< 30 nm) and a high value of H_C at larger thickness. These results suggest that the estimation of soft magnetic properties of the thin films is rather difficult without performing thickness dependent studies on magnetic thin films. Nevertheless, most of the Fe based magnetic alloys display degraded magnetic properties at higher thicknesses mainly due to the change in the magnetic domain structure with increasing film thickness [LIUZ2006] resulting from the development of perpendicular magnetic anisotropy [NAOE1998, CRAU2002, SING2012]. As a result, they show severe noise properties [NAKA2001, TANA2002]. These results further illustrate that the equilibrium magnetic domain structure in thick magnetic films is governed by the competition of various energy terms (exchange, dipolar and anisotropy energies) and conversely the orientation of magnetization is determined by the effective anisotropy constant. Interestingly, these types of soft magnetic thin films also display spin-reorientation transition from in-plane single domain like state to out-of-plane multidomain state or vice-versa with increasing film thickness or change in the substrate temperature during sample preparation [SHAR2006, LIXW2007, COIS2008]. Nevertheless, most of the published results narrate thickness dependent studies at room temperature from the application point of view without any detailed or systematic investigations on the thickness and/or temperature dependent magnetic properties aimed at understanding the magnetic nature of the films at different thicknesses.

In order to control the development of effective anisotropy at larger film thickness and to improve soft magnetic properties of magnetic thin films, the multilayer structured thin films having ferromagnetic layers separated by non-magnetic (metallic and non-metallic nature) layers were reported [NAKA1997, NAOE1998, HUAN2001, NAKA2001, TANA2002, TANA20032]. It is well known that the study of magnetism and magnetic interactions between the ferromagnetic layers in multilayer structured thin films has resulted in the discovery of variety of fascinating phenomena and generated enormous interest among scientists from both theoretical and experimental points of view [HART1999, SPAL2011, VOLK2011]. While such artificial structures in nanoscale length are suggested for various

applications in modern magnetoelectronic devices as summarized earlier [TSAN1994, OSHI2002, KHIZ20041, PIRA2007, IKED2008, BERG2011] from the application point of view, they are also expected to provide an understanding of surface magnetism and transport phenomena, such as interlayer magnetic coupling [KORE2012, KRAV2012], dipolar interaction between ferromagnetic layers [HILL1993, MAJC2007], magnetostatic interaction induced by the interface roughness (topological coupling) [SHIZ1994, ZHAN19961], effects of thickness and number of spacer layers on structural and magnetic properties [HERN2008], disorder magnetic states, surface anisotropy, magneto-optical effect and different types of magnetoresistance, etc. Another key advantage of artificial magnetic nanostructures is their ability to surpass the performance of naturally occurring magnetic compounds. Therefore, the controlled growth and tailorable properties of such nanostructured multilayer films have become a very active field of research for the realization of futuristic magnetic devices.

Nakamura et al [NAKA2001] showed that the noise signal observed in thick FeSiAl film decreases strongly with decreasing thickness of FeSiAl film. This behaviour was attributed to the change in the microstructure and magnetic domain structure with decreasing film thickness resulting a decrease in H_C (see Table 1.01). Similarly, Tanahashi et al [TANA20032] reported that a laminated type Fe based soft magnetic thin film displays lower H_C as compared to the single layer thick film. This observation was explained on the basis of magnetostatic interaction between the ferromagnetic layers, which reduces the stray field by forming local magnetic loops. Alternatively, Huang et al [HUAN2001] reported that the improvement of soft magnetic properties in HITPERM based multilayer thin films is very much dependent on the thicknesses of both the ferromagnetic and spacer layers. Interestingly, such multilayer films exhibited a spacer layer thickness dependent multistep magnetization reversal process at lower temperatures. Naoe et al [NAOE1998] reported that the introduction of Al non-magnetic layer sandwiched between FeCuNbSiB multilayer thin films causes a large reduction (nearly two orders) in H_C for Al thickness of 2 nm and show oscillatory nature with increasing Al thickness up to 10 nm. Feng et al [FENG1994, FENG1995] studied the effect of various types of interlayer such as Al, Cr, Cu and Ag on the magnetic properties of CoCrTa films and showed that the variations of H_C strongly depend on the thickness of the spacer layers, i.e., H_C decreases with increasing the thickness of the spacer layers. Herndon et al [HERN2008] have also reported a similar trend of H_C variation with Al_2O_3 spacer thickness in self-assembled single-domain iron nanoparticles embedded in an alumina thin film matrix separated by Al_2O_3 spacer layers. The variation of magnetic properties has been

attributed to three types of magnetic interactions such as exchange interaction, strong dipolar interaction and weak dipolar interaction depending on the spacer layer thickness. The above results evidently reveal the advantage of the multilayer structured films in controlling the soft magnetic properties and its applicability in devices. In addition, various parameters such as layer structure, microstructure, magnetic domain structure in multilayer thin films, thickness of spacer and ferromagnetic layers, number of spacer layers, interface roughness and magnetization of ferromagnetic layers and temperature play a major role on controlling the soft magnetic properties of multilayer films. However, the origin of improvement in soft magnetic properties of the multilayer thin films, their stability against spacer layer thickness, and the effect of temperature on the magnetic interaction between the ferromagnetic layers have not been well addressed so far. Furthermore, the study of effects of microstructure and temperature driven interlayer interactions in the multilayer films in correlation with the resulting magnetic properties has not been reported in detail.

Table 1.01: Magnetic parameters (saturation induction (B_S), remanence (B_r) and H_C) of various magnetic thin films with different multilayer structures. Numerals given within the parenthesis indicate thickness in nanometer.

Sl.	Layer structure	B_S (Tesla)	B_r (Tesla)	H_C (Oe)	Reference
1.	FeAlSi (200)	-	-	23	[NAKA2001]
2.	FeAlSi (20)	-	-	7.5	[NAKA2001]
3.	$[FeAlSi (5)/C (4)]_{n=20}$	-	-	0.5	[NAKA2001]
4.	FeNbC (200)	1.5	0.8	0.47	[TANA20032]
5.	$[FeNbC (100)/Ta (2.5)]_2$	1.5	< 0.1	0.04	[TANA20032]
6.	$[FeNbC (67)/Ta (2.5)]_3$	1.5	< 0.1	0.07	[TANA20032]
7.	$[FeNbC (50)/Ta (2.5)]_4$	1.5	< 0.1	0.12	[TANA20032]
8.	FeTaC (200)	1.7	0.7	0.42	[TANA20032]
9.	$[FeTaC (100)/Ta (2.5)]_2$	1.7	< 0.1	0.07	[TANA20032]
10.	$[FeTaC (67)/Ta (2.5)]_3$	1.7	< 0.1	0.15	[TANA20032]
11.	$[FeTaC (50)/Ta (2.5)]_4$	1.7	0.1	0.24	[TANA20032]
12.	FeTiC (200)	1.3	0.6	0.65	[TANA20032]
13.	$[FeTiC (100)/Ta (2.5)]_2$	1.3	< 0.1	0.12	[TANA20032]
14.	$FeTiC (67)/Ta (2.5)]_3$	1.3	< 0.1	0.08	[TANA20032]
15.	$FeTiC (50)/Ta (2.5)]_4$	1.3	0.1	0.20	[TANA20032]

16.	FeCoZrBCu (200)	1.75	0.7	33	[TANA20032]
17.	[FeCoZrBCu (75)/SiO2 (2)]$_2$	-	-	0.25	[HUAN2001]
18.	FeCuNbSiB (140)	-	-	40.0	[NAOE1998]
19.	FeCuNbSiB (70)/Al(2)/ FeCuNbSiB (70)	-	-	1.0	[NAOE1998]

In this context, it may be noted that the study of magnetic properties of those alloys which are typically used in various magnetoelectronic devices is very much essential. This is mainly due to the fact that magnetic properties such as H_C, magnetic anisotropy, and magnetic interaction between the ferromagnetic layers in the multilayer films are strongly affected by the growth conditions, which are altered at a surface or an interface. When averaged over the entire volume of the film, these properties can therefore be expected to depend strongly on the surface to volume ratio (film thickness). Among various soft magnetic thin films, FeTaC alloy films depict excellent soft magnetic properties and low media noise [TANA2002, PERU2009]. It was reported that the soft magnetic properties depend strongly on the alloy composition and the composition of $Fe_{80}Ta_8C_{12}$ shows superior soft magnetic properties [HASE1995, TANA2002, PERU2009]. However, a systematic investigation of magnetic properties of FeTaC films as a function of thickness, different multilayer structures and post deposition annealing temperatures to improve the magnetic properties is still missing.

1.3. Objective of the thesis work:

a) To prepare amorphous $Fe_{80}Ta_8C_{12}$ single layer films of different thicknesses (t = 20, 50, 100 and 200 nm) directly on oxidised Si substrate at ambient temperature using magnetron sputtering technique.

b) To prepare multilayer structured [[FeTaC (y nm)/Ta (x nm)]$_n$/FeTaC (y nm)] films directly on oxidised Si substrate at ambient temperature using magnetron sputtering technique. Thickness of the individual ferromagnetic FeTaC layers (y) in multilayer films will be controlled using the relation $y = 200/(n+1)$, where 200 nm is total thickness of FeTaC in multilayer films, n is number of repitation varying between 0 and 4, and x is the thickness of non-magnetic Ta spacer layer varying between 0 and 6 nm.

c) To study the effect of film thickness on the room temperature and temperature dependent magnetic properties of FeTaC (*t*) films over a wide range of temperatures.

d) To understand effects of number of multilayers and thickness of the spacer layers on the room temperature and temperature dependent magnetic properties in the temperature range of 5 K to 500 K.

e) To investigate effect of post deposition annealing temperatures on the formation of nanocrystalline microstructure and the resulting magnetic properties of single and multilayer thin films and the correlation between them.

f) To understand the role of perpendicular anisotropy and temperature dependent interlayer magnetic coupling in shaping the magnetic properties of multilayer thin films with amorphous and nanocrystalline ferromagnetic FeTaC layers.

Chapter 2

Fundamental Aspects and Theoretical Modeling

2.1. Introduction:

Magnetism, the phenomenon by which materials avow an attractive or repulsive force, has been known for thousands of years. The history of magnetism is coeval with the history of science. However, the underlying principles and mechanisms that explain the magnetic properties of the materials are still complex and elusive. It is well known that most of the modern technological devices such as electrical power generators, transformer, electric motors, sensors, computers, and components of sound and video reproduction system rely on magnetism and magnetic materials. Recently, the tendency to miniaturize the dimensions of electronic devices has created a demand for new materials and new methods for their production. Therefore, the understanding of development of magnetic properties in new materials and optimization of the magnetic properties for different applications are very much essential. This chapter provides a brief description of origin of magnetism in solids, the phenomenon of ferromagnetism and the various phenomena affecting the ferromagnetic properties of materials.

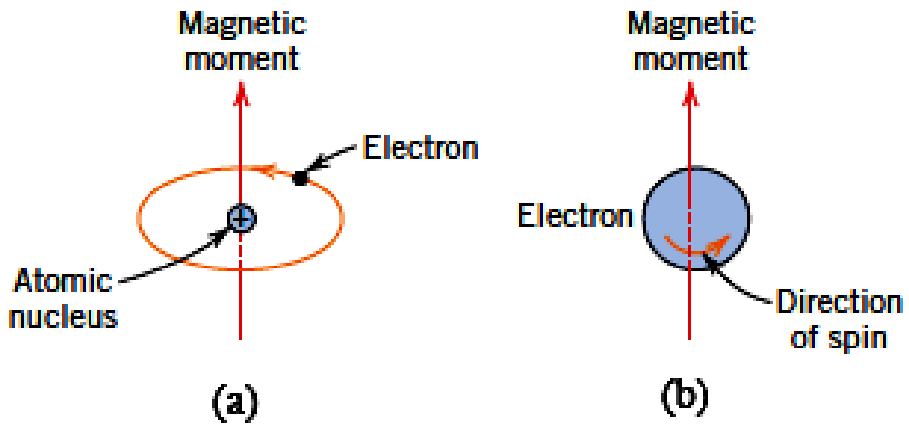

Figure 2.01: Demonstration of the magnetic moment associated with (a) an orbiting electron and (b) a spinning electron.

2.2. Origin of magnetism:

The macroscopic magnetic properties of materials are a consequence of magnetic moments associated with individual electrons [KITT2004, OHAN2000]. Each electron in an atom has magnetic moments originating from two different sources: (a) One is orbital motion of electron around the nucleus, generating a small magnetic field and having magnetic moment along the axis of rotation (see figure 2.01(a)) and (b) Other magnetic moment originates from the electron spin, which is directed along the spin axis as shown in figure 2.01(b). This

reveals that the each electron in an atom may be thought of as being a small magnet having permanent orbital and spin magnetic moments. Furthermore, in an atom, electrons are occupied according to the Pauli's Exclusion Principle and Hund's rule. The net magnetic moment for an atom is the sum of the magnetic moments of the each of constituting electrons, including both orbital and spin contributions and taking into the account of moment cancellation. For an atom having completely filled electron shells or subshells, when all electrons are considered, there is a total cancellation of both the moments. Thus, materials composed of atoms having completely filled electron shells are not capable of being permanently magnetized.

Based on number of unpaired electrons in atom, their orientation in the orbitals and the spin-orbit interaction between the electron orbital angular momentum and spin angular momentum and their response in the external applied field, materials are classified into diamagnetic, paramagnetic, ferromagnetic, antiferromagnetic and ferrimagnetic [KRON2003]. Diamagnetism is a manifestation of Lenz law, i.e., if one applies a field to a system of moving charges, then their motions change in such a way that they create a magnetization that opposes the original applied field [OHAN2000]. Such effect is present in all the materials, but is often obscured by other types of magnetism. For some solid materials, each atom possesses a permanent dipole moment by virtue of incomplete cancellation of electron spin and/or orbital magnetic moments. The orientations of these atomic magnetic moments are random in the absence of an external magnetic field and result no net macroscopic magnetization. However, these atomic dipoles are free to rotate and paramagnetism occurs when they preferentially align, by rotation, with an external field [KITT2004]. Both diamagnetic and paramagnetic materials are generally considered to be non-magnetic because they exhibit magnetization only under the application of an external field. On the other hand, certain materials possess a permanent magnetic moment resulting from strong interaction between the magnetic moments even in the absence of an external field. This dominates over the thermal energy and reveals an alignment of magnetization in a particular direction. Such behaviours are displayed by the transition metals and some of the rare earth metals. In an antiferromagnetic material, moments of equal magnitude are aligned in an antiparallel arrangement with zero net moment in the absence of external field at temperatures below the ordering temperature called Néel temperature [KITT2004]. Some ceramics exhibit a permanent magnetization, termed ferrimagnetism. When two antiferromagnetically coupled sublattices in a material have unequal moments because of the

different species on the different sites, the net moment is not zero. Such materials are called ferrimagnets.

As the primary motivation of the thesis work is to study the ferromagnetic properties of magnetic thin films, we focus only on the phenomenon of ferromagnetism and the various phenomena affecting the ferromagnetic properties of materials in the rest of this chapter.

2.3. Ferromagnetism:

The atomic moments in ferromagnetic materials exhibit very strong interactions, which are produced by electronic exchange forces and result in either a parallel or an antiparallel alignment of atomic moments. As a result, a large net magnetization even after removing the external applied magnetic field exists in ferromagnetic materials. Therefore, there are two distinct characteristics: (1) their spontaneous magnetization and (2) existence of magnetic ordering temperature. Spontaneous magnetization is the net magnetization that exists inside a uniformly magnetized microscopic volume even in the absence of external magnetic field. The magnitude of this magnetization at absolute temperature depends on the spin magnetic moments of electrons. Although electronic exchange forces in ferromagnets are very large, thermal energy eventually overcomes the exchange energy and produces a randomizing effect leading to paramagnetism, i.e., with increasing temperature, a transition from ferromagnetic state to paramagnetic state occurs at a temperature called Curie temperature (T_C).

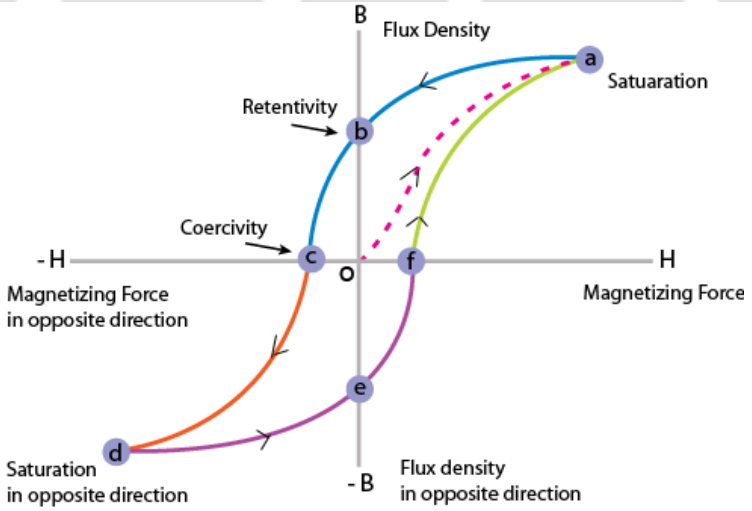

Figure 2.02: Magnetic hysteresis loop of a ferromagnetic material.

All ferromagnetic materials exhibit magnetic hysteresis behaviour, i.e., the formation of loop under the application of magnetic field (*M-H* loop) as displayed in figure 2.02. A

great deal of information about the magnetic properties of a ferromagnetic material can be acquired by studying its hysteresis loop. The loop is generated by measuring the magnetic flux of a ferromagnetic material while the magnetizing field is changed continuously. Ferromagnetic materials that have never been exposed to magnetic field or have been thoroughly demagnetized follow the dashed line (starting from the origin '**o**') as applied field is increased and reach the point '**a**' where almost all of the magnetic domains are aligned to field direction and an additional increase in the magnetizing field produces a very little or no increase in magnetic flux. The magnetization obtained at this point is called saturation magnetization (M_S). When the field is reduced to zero, the curve moves from point '**a**' to '**b**'. At this point, some magnetic flux remains in the material even at zero magnetic field. This is called as retentivity and indicates the remanence or level of residual magnetism in the material. As the magnetic field is reversed, the curve moves to point '**c**', where the magnetization reaches to zero. This point is called as coercivity (H_C) or coercive force. On further increasing the field in the negative direction, materials become magnetically saturated but in the opposite direction (point '**d**'). Reducing the field to zero brings the curve to point '**e**'. At this point, the level of residual magnetism is almost equal to that achieved in the other direction (point '**b**'). Increasing the field back in the positive direction returns the magnetization to zero. Subsequently, the curve takes a different path from point '**f**' back to the saturation point (point '**a**') where it completes the loop. From the *M-H* loop, the following magnetic parameters can be determined: (i) *Retentivity*: a material's ability to retain a certain amount of magnetization when the magnetizing field is removed after achieving saturation, (ii) *Residual magnetism or Residual flux*: The magnetic flux density that remains in a material when the magnetic field is zero. Note that residual magnetism and retentivity are the same when the material has been magnetized to the saturation point. However, the level of residual magnetism may be lower than the retentivity value if the magnetic field did not reach the saturation level, (iii) *Coercivity*: The magnitude of reverse magnetic field is required to make the magnetization to zero; (iv) *Permeability*: A property of a material that describes the ease with which a magnetic flux is established in the component. These hysteresis parameters are not solely intrinsic properties but are dependent on various parameters such as grain size, domain state, internal stresses and temperature. Since the hysteresis parameters are dependent on grain size, they are useful for magnetic grain sizing of natural samples. The elements Fe, Ni, and Co and their alloys are typical examples of ferromagnetic materials.

Ferromagnetic materials are mainly divided into two groups as shown in figure 2.03: (a) hard ferromagnetic materials which exhibit very high H_C (> 1000 Oe). These materials are

mainly used as permanent magnets and media for data storage and (b) soft magnetic materials with low H_C (< 100 Oe) are used for transformer core, read head and magnetic sensor applications.

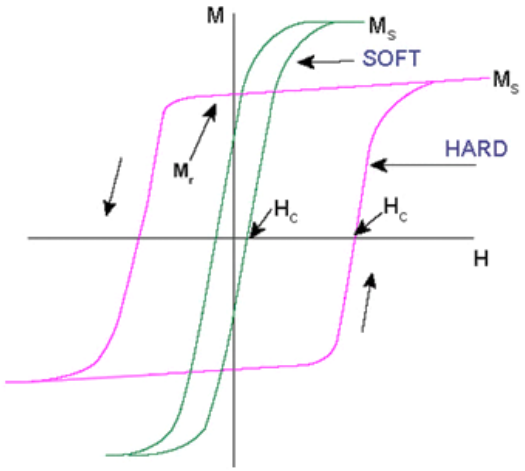

Figure 2.03: Typical magnetic hysteresis loops of soft and hard ferromagnetic materials.

2.4. Exchange Interaction:

Weiss (1907) reported that in addition to any externally applied field *H*, there is an internal molecular field or exchange field in a ferromagnet proportional to its magnetization.

$$\overrightarrow{B_E} = \lambda \vec{M} \qquad (2.01)$$

where, λ is a constant independent of temperature. According to eqn.(2.01), each spin sees the average magnetization of all the other spins. This molecular field is not really a magnetic field and therefore does not enter into the Maxwell equations. For example, there is no current density $\vec{j}$ related to $\overrightarrow{B_E}$ by $\vec{\nabla} \times \vec{H} = 4\pi\vec{j}/c$. The magnitude of the molecular field may be as high as 1000 Tesla. Now the question is what is the origin of such huge internal molecular field? For instance, the magnetic field at distance *r* due to a magnetic dipole of dipole moment *m* is [KITT2004],

$$\overrightarrow{B_{dip}} = \left(\frac{\mu_0 M}{4\pi r^3}\right)[2cos\theta\overrightarrow{e_r} + sin\theta\overrightarrow{e_\theta}] \qquad (2.02)$$

The order of magnitude of B_{dip} (= $\mu_0 H_{dip}$) is $\mu_0 M/4\pi r^3$ and taking $m = 1\mu_B$ and r = 0.1 nm provides $B_{dip} \approx 1$ Tesla or 10 kG only. This reveals that the huge molecular field is not due to the magnetic dipole interaction. This lingered as a mystery until Heisenberg introduced the

concept of exchange interaction in 1928 [HEIS1928]. The origin of the Heisenberg exchange interaction is electrostatic, but the explanation involves quantum mechanics. The charge distribution of a system of two spins depends on whether the spins are parallel or antiparallel. Pauli's exclusion principle dismisses that no two identical electrons occupy the same quantum state simultaneously. However, it does not exclude two electrons of opposite spin. Therefore, the electrostatic energy of a system depends on the relative orientation of the spins: the difference in energy defines the exchange energy. The energy of interaction between the atoms *i* and *j* bearing electron spins S_i and S_j is defined from the Heisenberg model as [OHAN2000],

$$E_{exch} = -2\sum_{i<j} J_{ij} S_i . S_j \qquad (2.03)$$

where, J_{ij} is the exchange integral and is related to the overlap of the charge distribution of the atoms *i* and *j*. Assuming that the exchange interaction is the same for each nearest-neighbour pair, eqn.(2.03) turns out to be

$$E_{exch} = -2J\sum_{i<j}^{nn} S_i . S_j \qquad (2.04)$$

For parallel orientation of the magnetization (ferromagnet), *J* should be positive and for antiparallel alignment of spins, *J* should be negative. The variation of *J* with respect to inter-atomic distance is shown in figure 2.04. This curve is also known as the Bethe-Slater curve.

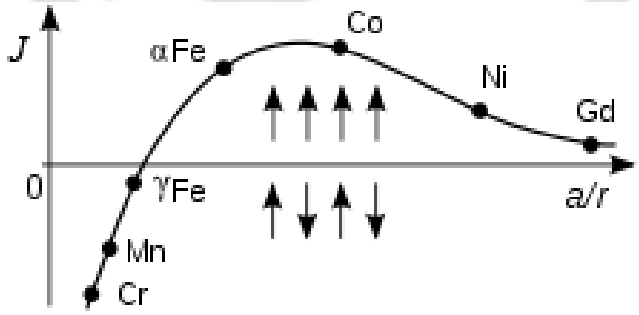

Figure 2.04: Bethe-slater curve: Elements above (below) the horizontal axis are ferromagnetic (antiferromagnetic).

It is clear from the figure 2.04 that the value of *J* and hence the short-range exchange interaction depends strongly on the inter-atomic distance. The eqn.(2.04) can further be

simplified by considering the energy of a particular atom *i* interacting with its *j* nearest neighbour:

$$E_{exch}^{i} = -2JS_i \sum_j S_j \tag{2.05}$$

while for the entire material,

$$E_{exch} = -\frac{1}{2}\sum_j E_{exch}^{i} \tag{2.06}$$

Thus, the discrete, pairwise interaction can be replaced by assuming that the magnetic moment $\mu_m^i = g\mu_B S_i$ at site *i* interacts with a molecular field H_{eff} given by the net effect of the *z* nearest neighbour spins:

$$E_{exch}^{i} = -\mu_0 \mu_m^i H_{eff} = -g\mu_0\mu_B S_i H_{eff} \tag{2.07}$$

where, g is the landé g-factor, μ_B is Bohr magneton (= 9.27×10^{-24} J.T^{-1}) and μ_0 is the permeability of the free space (= $4\pi\times10^{-7}$ H/m or 1.256×10^{-6} H/m). Comparing eqn.(2.07) with eqn.(2.05) provides the effective field as,

$$H_{eff} = \frac{2J}{g\mu_0\mu_B}\sum_j S_j \cong \frac{2zJ}{g\mu_0\mu_B}\langle S_j\rangle \tag{2.08}$$

Here, the sum over *z* neighbouring spins has been replaced by *z* times the average spin value $\langle S_j\rangle$. Using $M = N_v g\mu_B\langle S_j\rangle$, eqn.(2.08) gives,

$$H_{eff} \cong \frac{2zJ}{N_v g^2 {\mu_B}^2 \mu_0} M \tag{2.09}$$

From eqn.(2.09), it can be seen that the H_{eff} is the Weiss molecular field defined as $H_{mol} = \lambda M$, provided

$$\lambda = \frac{2zJ}{N_v g^2 {\mu_B}^2 \mu_0} \tag{2.10}$$

Using the value of molecular field coefficient λ as 10^3, *J* is calculated to be 2×10^{-21} J or 0.01 eV/atom. Exchange interactions are weaker than the Coulomb interactions that distinguish

levels of different principal and orbital quantum numbers, but stronger than spin-orbit interaction. Following the treatment of Weiss molecular field that $T_C = \lambda C$, with $C = N_v {\mu_m}^2 \mu_0 / 3k_B$, the expression for T_C can be obtained from eqn.(2.10) as

$$T_C = \frac{2zJ{\mu_m}^2}{g^2{\mu_B}^2 3k_B} = \frac{2zJs(s+1)}{3k_B} \tag{2.11}$$

where, $\mu_m = \sqrt{g\mu_B s(s+1)}$. Another important relation between exchange energy and the magnetization is defined as,

$$\frac{E_{exch}^{ij}}{V} = \frac{s^2 a^2 J N_v'}{2}\left(\frac{\nabla M}{M}\right)^2 = A\left(\frac{\nabla M}{M}\right)^2 \tag{2.12}$$

where, *a* is the distance between the spins, *A* is called the exchange stiffness constant having 1-2×10^{-11} J/m for most ferromagnets, and N_v' is number of nearest neighbour atoms per unit volume. Therefore, it is clear from the above equations that the exchange energy or the Heisenberg exchange interaction depends strongly on temperature due to the dependence of interatomic distance on temperature. In particular, the disorder ferromagnetic system is the subject of low T_C due to the low value of *J*.

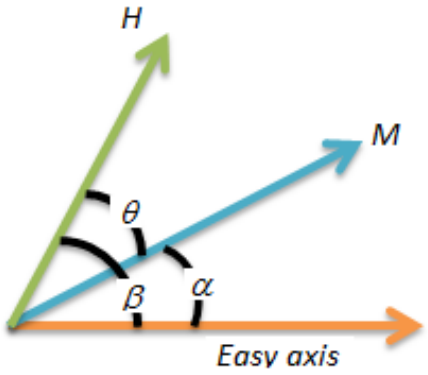

Figure 2.05: Schematic diagram of magnetization, applied field, and easy axis for a given material.

2.5. Anisotropy:

When a physical property of any materials depends on the direction, that property is said to exhibit anisotropy. In magnetism, the preference of magnetization to lie in a particular direction of sample is called magnetic anisotropy. As anisotropy plays an important role in

tuning the nature of *M–H* loop, it is much essential to understand the various possible sources of the magnetic anisotropy and its influence on the control of the magnetic properties. Figure 2.05 displays a typical situation where for zero applied field, the magnetization would point along the easy axis shown (α = 0). When a field is applied, the magnetization is pulled towards the field direction and approaches closer to the field direction with increasing the applied field. For any intermediate values of α, the magnetization is being attracted in opposite directions, i.e., up by the field and down by the anisotropy.

Let us assume that all the magnetization is pointing in the same direction in a magnetic material and the material exhibits an easy axis of magnetization. In such scenario, we can describe the energy per unit volume of the magnetization of this material by

$$E = K\,sin^2\alpha \tag{2.13}$$

where, *K* is called anisotropy constant with an unit of energy per unit volume (J/m^3). Hence, the energy term, *E*, is also energy per unit volume. In general, the magnitude of uniaxial anisotropy is described in terms of the anisotropy field, which is defined as the field needed to saturate the magnetization of a uniaxial crystal in the hard axis direction, as given in eqn.(2.14)

$$H_k = \frac{2K}{\mu_0 M} \tag{2.14}$$

In general, the energy of the magnetization is given by,

$$E = K\,sin^2\alpha - \mu_0 MH\,cos(\beta - \alpha) \tag{2.15}$$

where, the first term is anisotropy energy. The second term is due to the magnetic field and the difference in the angle (β - α) is the angle between ***H*** and ***M***. In order to get equilibrium, we required first derivative to be zero. Therefore, taking derivative of eqn.(2.15) with respect to the angle results,

$$\frac{dE}{d\alpha} = 2K \sin\alpha \cos\alpha - \mu_0 MH\,sin(\beta - \alpha) = 0 \tag{2.16}$$

Taking the value of β as 90^o for the equilibrium angle for the magnetization relative to the easy axis and considering the eqn.(2.14) gives➔

$$\sin\alpha = \frac{H}{H_k} \tag{2.17}$$

The above eqn. indicates that when field is zero, the magnetization points along the easy axis and when the field is equal to H_k, the magnetization points along the direction of field. For any intermediate value of the applied field, the magnetization points at a value of angle given by eqn.(2.17) rotating smoothly between the easy axis and the applied field.

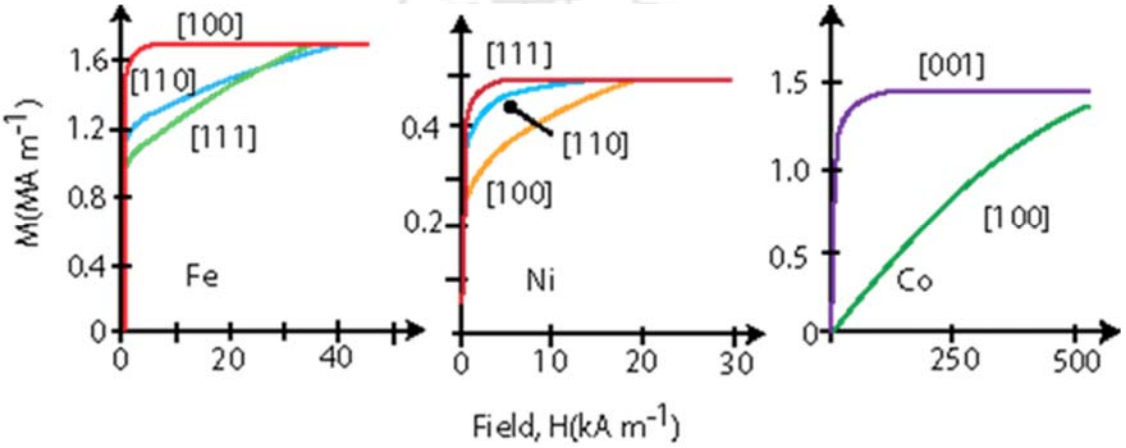

Figure 2.06: Magnetization of single crystals of Iron, Nickel and Cobalt.

2.5.1. Magnetocrystalline anisotropy:

Figure 2.06 depicts initial magnetization curves of single crystals of different 3*d* ferromagnetic elements. It is seen that the materials approach to saturation in different ways when magnetized in different directions. For example, iron display a ⟨100⟩ as easy directions and ⟨111⟩ as hard directions, while nickel exhibits ⟨111⟩ as easy axis and ⟨100⟩ as hard directions. This behaviour can be understood by analyzing the development of anisotropy energy in different symmetries as given below:

For Hexagonal:

$$E_a = K_1 \sin^2\theta + K_2 \sin^4\theta + K_3 \sin^6\theta + K_3' \sin^6\theta \sin 6\phi \tag{2.18}$$

For Tetragonal:

$$E_a = K_1 \sin^2\theta + K_2 \sin^4\theta + K_2' \sin^4\theta \cos 4\phi + K_3 \sin^6\theta + K_3' \sin^6\theta \sin 6\phi \tag{2.19}$$

For Cubic:

$$E_a = K_{1c}(\alpha_1^2\alpha_2^2 + \alpha_2^2\alpha_3^2 + \alpha_3^2\alpha_1^2) + K_{2c}(\alpha_1^2\alpha_2^2\alpha_3^2) \qquad (2.20)$$

where, α_i are the direction cosines of the magnetization. K_{1c} term is equivalent to $K_{1c}(\sin^2\theta\, cos^2\phi \sin^2\phi + \cos^2\theta \sin^2\theta)$. When, $\theta = 0$, $\phi = 0$, this term reduces to eqn.(2.13) [COEY2010].

Figure 2.07: Schematic drawing of broadside and head-to-tail configurations for a pair of ferromagnetically coupled magnetic moments.

Origin of magnetocrystalline anisotropy: There are two distinct sources of magnetocrystalline anisotropy: (i) single-ion contributions and (ii) two-ion contributions. The first one is essentially due to the electrostatic interaction of the orbitals containing the magnetic electrons with the potential created at the atomic site by the rest of the crystal. This crystal field interaction stabilizes a particular orbital and by spin-orbit interaction, the magnetic moment is aligned in a particular crystallographic direction. For example, a uniaxial crystal having 2×10^{28} ions/m^3 described by a spin Hamiltonian DS^2 with D/k_B = 1 K and S = 2 will have anisotropy constant $K_1 = nDS^2 = 1.1\times10^6$ J/m^3. On the other hand, the later contribution replicates the anisotropy of the dipole-dipole interaction. Considering the broadside and head-to-tail configurations of two dipoles each with moment m, as shown in figure 2.07, the energy of the head-to-tail configuration is lower by $3\mu_0 m^2/(4\pi r^3)$ and hence the magnets tend to align head-to-tail. In non-cubic lattices, the dipole interaction is an appreciable source of ferromagnetic anisotropy.

2.5.2. Shape anisotropy:

Shape anisotropy arising due to the asymmetric shape of the material is important for thin films where one dimension is very short as compared to other dimensions. The demagnetization field inside the material or the stray field outside the magnetic material depends on the magnetization and shape of the material [JILE1997, OHAN2000, BLUN2001]. The magnetostatic energy of a ferromagnetic ellipsoid as shown in figure 2.08 with magnetization M_S is given as

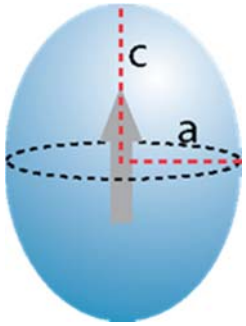

Figure 2.08: Magnetization of a prolate ellipsoid of revolution with c > a and no magnetocrystalline anisotropy. c-axis is the easy direction of magnetization.

$$E_m = \frac{1}{2}\mu_0 V N M_S^2 \tag{2.21}$$

The anisotropy energy is related to the difference in energy ΔE when the ellipsoid is magnetized along its hard and easy directions. N is the demagnetization factor tensor for the easy direction. N'=(1/2)(1-N) is the demagnetization factor tensor for the hard directions. Hence,

$$\Delta E_m = \frac{1}{2}\mu_0 V M_S^2 \left[\frac{1}{2}(1-N) - N\right]$$

$$\Delta E_m = \frac{1}{4}\mu_0 V M_S^2 [1-3N]$$

$$K_{sh} = \frac{1}{4}\mu_0 M_S^2 [1-3N] \tag{2.22}$$

In addition, the demagnetization factor tensor that relates the demagnetization field with a specimen magnetization as a function of position is given by [NEAL1994]

$$N(r) = -\frac{1}{4\pi}\iiint d^3r' \nabla' \left(\nabla' \left(\frac{1}{r-r'}\right)\right) \tag{2.23}$$

This tensor is given by an integral over the object volume and can be evaluated either inside or exterior to the body. The value of tensor N significantly depends on the specimen shape, which are difficult to obtain in closed-form. It may be calculated exactly for an ellipsoidal shape only. In many symmetrical materials such as any ellipsoids of revolution, the demagnetization factor tensor only has three principal components, i.e.,

$$\begin{pmatrix} H_1 \\ H_2 \\ H_3 \end{pmatrix} = -\begin{pmatrix} N_1 & 0 & 0 \\ 0 & N_2 & 0 \\ 0 & 0 & N_3 \end{pmatrix}\begin{pmatrix} M_1 \\ M_2 \\ M_3 \end{pmatrix} \quad (2.24)$$

where, $N_1 + N_2 + N_3 = 1$ (in SI) and $N_1 + N_2 + N_3 = 4\pi$ (Gaussian). The demagnetization factors for the selected shapes are summarized in Table 2.01. A detailed calculation of demagnetization factor for various objects can be found in [NEAL1994].

Table 2.01: Demagnetization factors (in Gaussian units) of selected shapes:

Shape	N_1	N_2	N_3
Sphere	$4\pi/3$	$4\pi/3$	$4\pi/3$
Long Cylinder along z-axis	2π	2π	0
Infinite plate normal to *z*-axis	0	0	4π
Strip film normal to *z*-axis (with t – thickness, W – Width, L – Length; $t \le W \le L$)	0	$8t/W$	4π

The shape anisotropy is zero for a sphere, as $N = 1/3$. Shape anisotropy is fully effective in samples which are so small that they do not break up into domains [COEY2010].

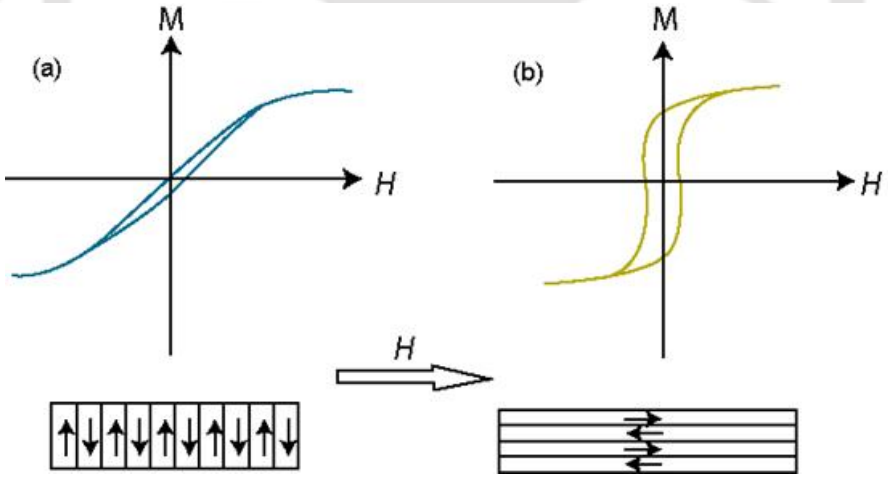

Figure 2.09: Magnetization of a thin film with induced anisotropy created by annealing in a magnetic field. The sheared (open) loop in a (b) is observed when the measuring field H is applied perpendicular (parallel) to the annealing field direction.

2.5.3. Induced anisotropy:

In some materials, the magnetic anisotropy can be induced by many ways: (i) fabricate a film in the presence of a magnetic field, (ii) heat treat the materials in the presence of external

applied magnetic field and (iii) apply uniaxial stress. In the first two cases, after such treatment, the material may exhibit an easy axis of magnetization that points in the direction of the magnetic field. This induced anisotropy is certainly independent of any crystalline anisotropy or any other form of anisotropy that might be present. Figure 2.09 shows the typical example of inducing the anisotropy in ferromagnetic materials by field annealing.

In the last case, the uniaxial anisotropy is induced by applying uniaxial stress (σ) in a ferromagnetic solid [KRON2003]. The magnitude of the stress-induced anisotropy is

$$K_{u\sigma} = \frac{3}{2}\sigma\lambda_S \tag{2.25}$$

where, λ_S is the saturation magnetostriction. Both the single-ion and two-ion anisotropy contribute to the stress induced anisotropy. The highest values of uniaxial anisotropy are found in hexagonal and other uniaxial crystals. Smallest values are found in cubic alloys and amorphous ferromagnets.

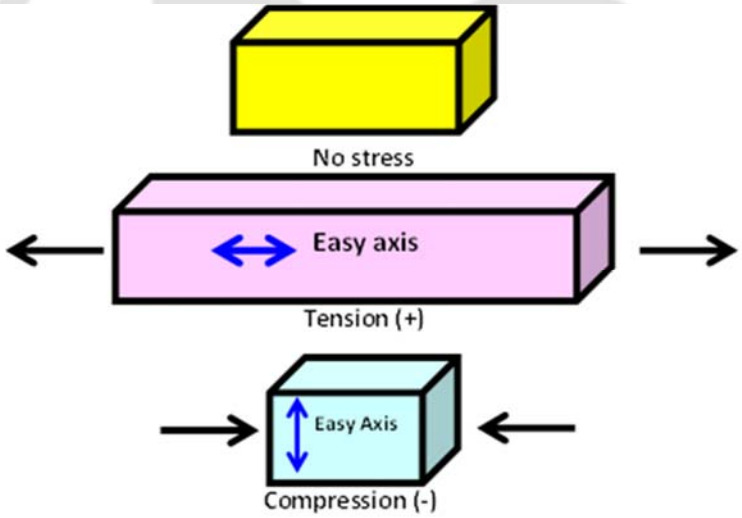

Figure 2.10: Schematic drawing of bars to demonstrate inducing an easy-axis in a material with the positive magnetostriction.

2.5.4. Magnetostrictive anisotropy:

Another important form of anisotropy in magnetic materials is due to magnetostriction, a change of volume of an isotropic crystal due to magnetic order. Magnetostriction relates the stress in a magnetic material to an anisotropy created by that stress. Figure 2.10 shows schematic views of bars with different applied stress conditions. If λ is positive, then application of a tensile stress to the bar creates an easy axis in the direction of the applied

stress. If a compressive stress is applied, then the direction of the easy axis created will be perpendicular to the stress direction. On the other hand, if the magnetostriction constant for the material is negative, then the above phenomena would be reversed: a tensile stress will create an easy axis perpendicular to the stress direction and a compressive stress will create an easy axis in the direction of the applied stress.

2.5.5. Magnetic surface anisotropy:

The direction of orientation of magnetic moments in the ultrathin film strongly affects the magnetic properties and hence attracts enormous interest since past decades. It has been reported that in ultrathin films, magnetic moment orients along perpendicular direction of the film plane up to certain critical thickness. The preferred uniaxial direction of magnetization is due to the magnetic surface anisotropy, which has the following origins: a) the lack of the neighbours or reduced symmetry at the interface gives rise to magnetocrystalline surface anisotropy [NEEL1954], b) strain at the interface due to the lattice mismatch between the substrate and the film and c) the interface roughness. The direction of magnetization in the ultrathin films is determined by the competition between shape (or dipolar anisotropy) and the magnetic surface anisotropy, i.e., when the thickness of the films is below the critical thickness, the surface anisotropy dominates over the shape anisotropy. On the other hand, the shape anisotropy dominates over the surface anisotropy above critical thickness resulting in-plane orientation of the magnetization [PESC1987, GARR2005, YILD20091, YILD20092, HIND2011]. Critical thickness and the easy direction of uniaxial surface anisotropy depend strongly on the deposition conditions, nature of substrate, temperature, materials and microstructure of the film [BRUN1989]. For example, the magnetization of Ni [111] ultrathin films deposited in Au/Ni/Au [111] multilayers always lies within the plane of films [BRUN1989]. On the other hand, the easy axis of magnetic surface anisotropy of *bcc* Fe [100] grown on Ag [100] is normal to the film plane [HEIN1987, KOON1987]. The critical thickness below which the spontaneous magnetization becomes perpendicular is 2.4 monolayers. Similarly, the magnetic surface anisotropy of Fe [110] grown epitaxially on GaAs and W[110] strongly differs from the previous result and the easy axis of magnetization lies along film plane. In addition, Fe [110]/Ag [111] shows perpendicular magnetization for thickness less than 2 ML. Furthermore, hexagonal closed packed (HCP) Co deposited at room temperature on atomically flat polycrystalline Au[111] and covered by Au exhibits perpendicular magnetization for thickness less than 12 Å (6 ML) [CHAP1988].

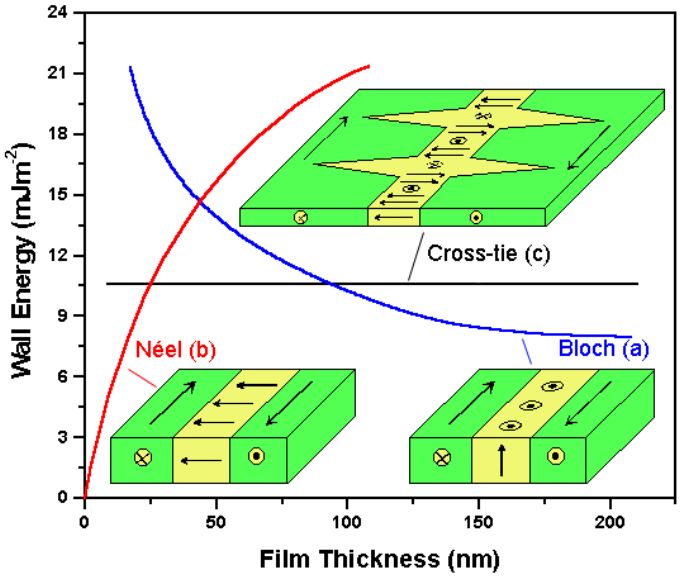

Figure 2.11: Comparison of domain wall energies for a (a) Bloch, (b) Néel and (c) Cross-tie wall for a permalloy film as function of film thickness [PRUT1964] and illustrative diagrams of the respective domain wall spin configuration.

2.6. Magnetic domains and domain walls:

Magnetic domains are the regions inside a ferromagnetic material that are magnetized in different directions so that the net magnetization is nearly zero. The surfaces or the walls separating one domain from another are called as domain walls. The main cause of formation of magnetic domains and domain walls is to reduce the magnetostatic energy of a finite and uniformly magnetized sample. The size of the domain and domain wall, and orientation of magnetization within the domain and domain walls are determined by the minimization of the total energy of the system. This energy includes exchange anisotropy, magnetocrystalline anisotropy, magnetostatic energy, magnetoelastic energy and domain wall energy [OHAN2000]. The width of a domain wall is dependent upon the exchange energy which prefers the magnetization to rotate slowly from one orientation to the other leading to wide walls, whereas the anisotropy and demagnetizing energies prefer the magnetization to switch immediately to the opposite direction and therefore results narrow walls. The thickness of the domain wall is determined by the equilibrium between these energies. There are three types of domain walls exist in thin films as shown in figure 2.11: Bloch wall, Néel wall, and Cross tie wall. In Bloch wall, magnetization rotates about an axis perpendicular to the wall as shown in figure 2.11(a). Hence, for thin films, the rotation of magnetization would be perpendicular to the film plane resulting a high stray field on the surface. A Néel wall is

defined by the magnetization rotating in the plane of the film which reduces the magnetostatic energy of the wall (see figure 2.11(b)), since the magnetization is not pointing in an unfavorable directions (out of plane) as with a Bloch wall. A cross-tie wall is defined by a mixture of spins pointing out and in the plane, and is identifiable by spike walls which form to ensure flux closure (see figure 2.11(c)) [CRAI1965]. It is found that in thin films Néel walls have lower magnetostatic energy than Bloch walls and are therefore more energetically favorable. The variations of different types of wall energies in permalloy film are shown as a function of thickness in figure 2.11. The cross-tie walls appear in between the transition region from Bloch wall to Néel wall. The widths of the domain walls also vary as a function of film thickness where Bloch walls become narrower and Néel walls become wider with decreasing film thickness [MIDD1963]. The typical length and energy scales related to different types of domain walls are defined as [OHAN2000],

Wall Type	Length scale	Energy Density
Bloch wall	$\delta_{Bw} = \pi\sqrt{\frac{A}{K}}$	$\sigma_{Bw} = 4\sqrt{AK}$
Néel wall	$\delta_{Nw} = \pi\sqrt{\frac{2A}{\mu_0 M_S^2}}$	$\sigma_{Nw} = 2\pi\sqrt{AK}$

where K is anisotropy constant, A is exchange stiffness constant having 1-2×10^{-11} J/m for most ferromagnets and M_S is saturation magnetization. There are several types of domains observed both in bulk materials and in thin films: (a) star like domain patterns observed in $Fe_{40}Ni_{40}P_{14}B_6$ (metglass), (b) the laminar domain structure observed in the $Fe_{40}Ni_{40}B_{20}$ alloys and (c) the strip domain structure observed in thin films above certain critical thickness [KRON2003]. The development of anisotropy perpendicular to the film plane arising due to the stress accumulated during the deposition of the film aligns the magnetization perpendicular to the film plane with strip domain patterns [MURA1966, PRAD1997, CRAU2002]. The equation for the critical thickness above which the strip domain appears was derived from the micromagnetic equation with appropriate approximations and the boundary conditions [HUBE2009] and given by,

$$t_{critical} = \frac{2\pi}{1 - \frac{\mu_0 M_S H_{Sat}}{2K}}\sqrt{\frac{A}{K}} = \frac{2\pi}{1 - S}\sqrt{\frac{A}{K}} \qquad (2.26)$$

where, $t_{critical}$ is the critical thickness, S is the dimensionless quantity, and H_{Sat} is the critical field beyond which the strip domains are unstable. These strip domains are periodical oscillations of the magnetization within a laminar conventional domain structure [CRAU2002, KRON2003, AMOS2008, HUBE2009]. The advantage of such strip domain structure along with the closer domains is the absence of stray field outside the specimen. The approximation for formation of the closer domains is given by [KRON2003],

$$Q = \frac{2K}{\mu_0 M_S^2} \ll 1 \tag{2.27}$$

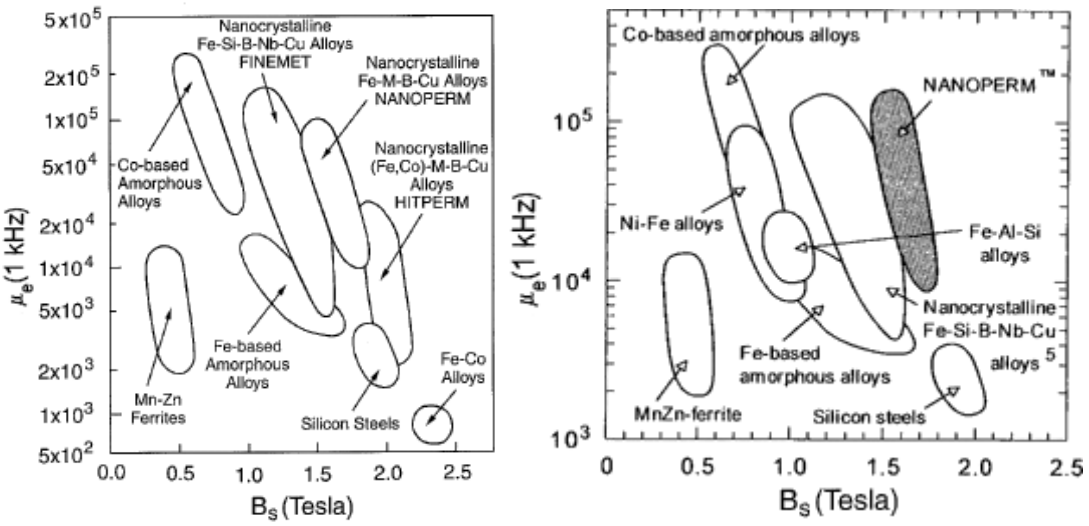

(a) *(b)*

Figure 2.12: Relation between permeability (at 1 kHz) and saturation induction for soft magnetic materials (a) [MAKI1995] and (b) [YOSH19892].

It is clear from eqn.(2.27) that the formation of closer domains depends strongly on the anisotropy present in the material and the values of M_S. Soft magnetic materials in general exhibit a low anisotropy and relatively high M_S. As a result, above approximation of formation of closer domains are more suitable for soft magnetic materials. For small Q (< 0.1), the critical thickness for the formation of stripe domains is approximately $t_{critical} = 2\pi\sqrt{A/K}$ in zero applied field. When Q approaches one, the critical thickness vanishes, i.e., stripe domains are therefore expected even for ultrathin films and reported experimentally in ultrathin cobalt films by Allenspach et al [ALLE1990]. In this case, the surface anisotropy

adds to the perpendicular anisotropy for ultra-thin films so that the effective value of Q becomes larger than unity.

2.7. Magnetic properties of amorphous and nanocrystalline materials:

Reducing the structural correlation length of solids to nanoscale results in dramatic changes in their physical properties, which are usually not predictable on the basis of their macroscopic properties. In particular, the enhancement of soft magnetic properties in Fe based nanostructures is one of the examples of such size effects. After the development of $Fe_{74.5}Si_{13.5}B_9Nb_3Cu_1$ by Yoshizawa et al [YOSH19882], the magnetic softening effect in nanostructures has opened the possibility of promising exploration for material developments in soft magnetic materials for magnetic cores for the purpose of magnetic flux multiplication. It has been reported that amorphous materials exhibit low H_C [KOBL1978, INOU1997] and high permeability. While the permeability of Co based amorphous materials is high as compared to Fe based amorphous alloys, M_S of Co based alloys is considerably lower than the Fe based amorphous alloys. In addition, the magnetostriction of Fe based amorphous alloys is quite high [ITOS1980, INOU1997] as compared to Co based alloys [OHAN1987, MCHE1999]. However, FeCo based amorphous alloys exhibit low value of permeability but relativity high M_S as compared to any other Fe based or Co based alloys. Figure 2.12 summarizes the relation between the permeability and saturation induction for various soft magnetic materials. Another advantage of amorphous materials is high electrical resistivity due to absence of long rang atomic ordering and makes them suitable for high frequency device applications. However, they exhibit low T_C due to absence of long range ferromagnetic ordering and weak ferromagnetic exchange interaction. Therefore, they are not suitable for high temperature applications.

Another class of material exhibiting superior soft magnetic properties is nanocrystalline materials having grain size in the range of 10-15 nm [YOSH19881, YOSH19882, HERZ1992, PETZ2002]. These nanocrystalline materials are prepared by a controlled annealing of the amorphous precursors and they exhibit two phase microstructure, in which the fine nano-crystals are embedded in the residual amorphous matrix. When the average size of the crystals is lower than the ferromagnetic exchange correlation length, it exhibits not only excellent soft magnetic properties (high B_S and low H_C), but the magnetocrystalline anisotropy is averaged out [HERZ1990, HERZ1995]. Furthermore, the magnetostriction of nanocrystalline materials turns out be quite low as compared to amorphous materials (see figure 2.13) [YANG2011]. In addition, the noise properties of the

nanocrystalline materials are observed to be low [KIKU2000, KIKU2001] ensuing the applicability of the nanocrystalline materials for high frequency applications. Strong ferromagnetic inter-granular exchange interaction and long range ferromagnetic ordering in nanocrystalline materials shift T_C to a high value [HERN1995, GORR1996]. Hence, nanocrystalline materials are clearly the most advanced family of soft magnetic materials with better thermal stability and suitability for high temperature applications.

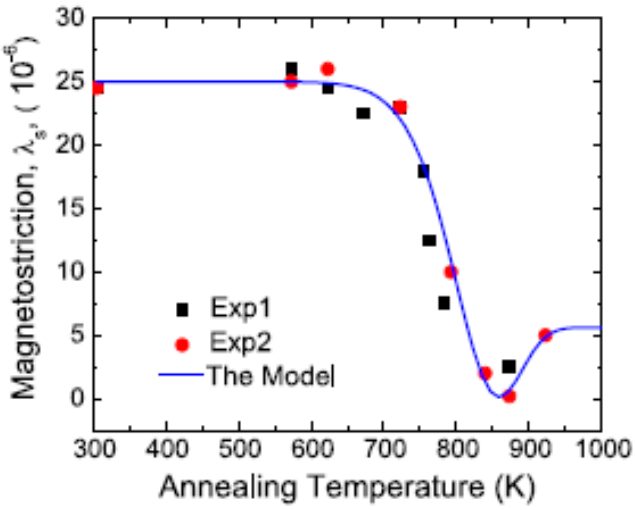

Figure 2.13: The relation between effective magnetostriction and annealing temperature for nanocrystalline magnetic alloys [YANG2011].

2.7.1. Random anisotropy model:

In conventional polycrystalline materials, magnetization follows individual easy magnetic directions of the structural units and the magnetization process is determined by the local magnetocrystalline anisotropy constant *K* of the grains. However, this rule is applicable only when the grain diameter is larger than the ferromagnetic exchange correlation length. Otherwise, magnetocrystalline anisotropy of the grains is suppressed due to the smoothing part of ferromagnetic exchange interaction. The situation resembles much in the case of amorphous alloys where the atomic scale local anisotropy is randomly average out and hence no anisotropy net-effect on the magnetization process [ALBE1978, HERZ1990]. Consequently, in the nanocrystalline materials, the critical scale below which this averaging mechanism takes place is given by [SELL2006],

$$L_0 = \varphi_0 \sqrt{\frac{A}{|K|}} \qquad (2.28)$$

where, φ_0 is a dimensionless parameter in the order of one and L_0 is the basic correlation length. For Fe-based alloys, this basic exchange correlation length is typically 30-50 nm [SELL2006]. On the other hand, the relation between H_C and anisotropy is given as,

$$H_C \approx \frac{\Delta K}{\mu_0 M_S} \frac{L_{ex}}{L_k} \tag{2.29}$$

where, L_{ex} is ferromagnetic exchange correlation length and L_k is wavelength of the anisotropy fluctuation [HERZ1990]. The lower bound for L_k is given by L_{ex} which is the scale below which the magnetic moments are aligned parallel due to exchange interaction. In this case, eqn.(2.29) simplifies to,

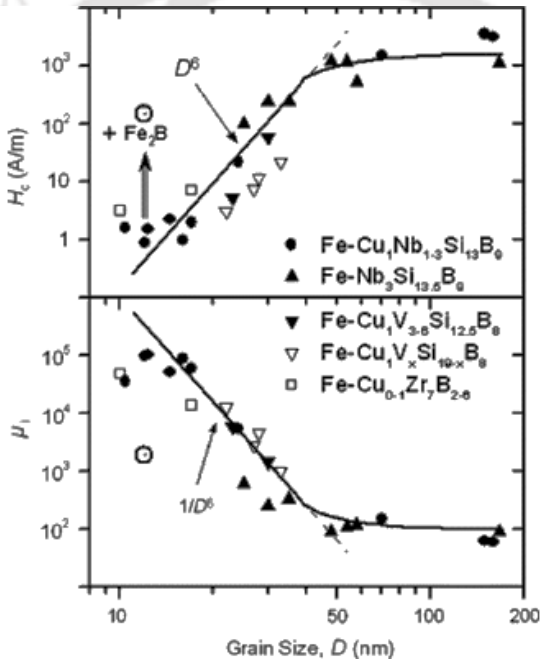

Figure 2.14: Variations of coercivity and permeability with grain size for different nanocrystalline alloys [HERZ2005].

$$H_C \approx \frac{\Delta K}{\mu_0 M_S} \tag{2.30}$$

It is clear from above equation that H_C is directly proportional to the anisotropy and inversely proportional to saturation magnetization. The average anisotropy constant of N coupled grains is given by

$$\langle K \rangle = \frac{K}{\sqrt{N}} \tag{2.31}$$

Using above relations, G. Herzer [HERZ1989] find out a relation between anisotropy and grain size as [SELL2006],

$$\langle K \rangle = K \left(\frac{D}{L_0} \right)^6 \tag{2.32}$$

This reveals that anisotropy depends on 6th power of grain size with an approximation $D < L_0$. Observed experimental results as shown in figure 2.14 also support the dependence of coercivity on 6th power of grain size in the grain size range of 10 to 40 nm and vary on a different order with the further increase in grain size above 40 nm.

2.7.2. Extended RAM:

The RAM model discussed above is valid for single phase system. However, in real materials, a large number of structural phases with additional anisotropies has been observed. Such long-range anisotropies eventually determine the soft magnetic properties of optimized nanocrystalline alloys and the contribution from random anisotropies tends to be negligible. Hence, the original model has to be extended accordingly [HERZ1995, SUZU19981, SUZU19982, HERZ2005]. As a result, the average anisotropy constant <*K*> of a coupled three dimensional multiphase system with anisotropies randomly oriented on a scale smaller than a magnetic correlation length L_{ex} can be described by

$$\langle K \rangle = \sqrt{K_u^2 + \sum_v x_v \, \beta_v^2 K_{1,v}^2 \left(\frac{D_v}{L_{ex}} \right)^3} \tag{2.33}$$

where, K_u denotes uniaxial anisotropy which is uniform on a scale much larger than L_{ex}. The random contributions are represented by the local anisotropy constant $K_{1,v}$, the grain size D_v and the volume fraction x_v of the individual structural phases labeled by the index v. The parameter β_v mainly involves conventions used for defining the anisotropy constants for different symmetries [SELL2006]. In case of thin film, in which the smallest sample dimension is comparable or less than the exchange length, eqn.(2.33) can be rewritten as,

$$\langle K \rangle = \sqrt{K_u^2 + \sum_v x_v \, \beta_v^2 K_{1,v}^2 \left(\frac{D_v}{L_{ex}} \right)^n} \tag{2.34}$$

where, the value of n is taken as 2. Taking $L_{ex} = \varphi_0\sqrt{A/\langle K\rangle}$, the value of <$K$> can be defined as,

$$\langle K\rangle = \frac{1}{2}\left(\Delta K + \sqrt{\Delta K^2 + 4K_u^2}\right) \tag{2.35}$$

with

$$\Delta K = \sum_v x_v\,\beta_v\;K_{1,v}\left(\frac{D_v}{L_{0,v}}\right)^2$$

where, $L_{0,v} = \varphi_{0,v}\sqrt{A/\left|K_{1,v}\right|}$. It may be noted that the eqn.(2.35) provide D^2 dependence for ΔK and hence for H_C.

2.8. Two-layers model in amorphous single layer magnetic thin films:

The fabrication of magnetic thin films directly on the substrates causes possible inter diffusion between the film and the substrate due to dynamics of film deposition and an instantaneous increase of substrate temperature during film deposition [ZENG2005, LIXW2007]. Therefore, there will be a mixed interface between the alloy film and the substrate. Such interface is more obvious in fabricating amorphous magnetic thin films, as the films are normally deposited at a significantly high deposition rate (> 3 nm/min) to achieve amorphous structure. The formation of such mixed interface of about 2 nm thick is shown evidently by Li et al LIXW2007] in CoZrNb amorphous films deposited directly on Si substrate. It may be noted that the thickness of such mixed interface strongly depends on the deposition rate of the film, nature of the elements in the film and the substrate. This reveals that the actual film has a magnetic layer composed of two magnetic components, i.e., the system can be viewed as two-layers model [HAND2005]. Based on this model, it is assumed that the initial growth of the films directly on the substrate (bottom layer) results somewhat hard magnetic properties with higher coercivity H_{C1} and moment M_1 due to either the local stress induced on the film by the substrate or the interface diffusion caused by the dynamics of the film deposition [LIXW2007]. On the other hand, the remaining film (upper layer) grown continuously on top of the bottom layer has soft magnetic properties with lower coercivity H_{C2} (< H_{C1}) and moment M_2. This two-layers structure is expected to show a considerable shift in the *M-H* loop for the low thickness films (t < 50 nm) as the magnetization reversal of the soft upper layer is believed to be controlled by the hard bottom layer. In addition, the loop shift and temperature dependent magnetization of the films are

expected to be strongly dependent on the measurement temperature, as the temperature dependent magnetic properties of both hard bottom layer and soft upper layer are rather different. Therefore, the investigation of variation of temperature dependent magnetic properties in such two-layers structured films would be quite interesting.

2.9. Interlayer coupling in multilayer thin films:

The study of magnetic properties of materials composed of alternating magnetic and non-magnetic layers has recently attracted much attention, as the interplay between electron transport properties and magnetic behaviour results in variety of fascinating phenomena [VELU1988, DAHL1988]. These artificial structures are promising as potential memory elements, magnetic sensors and magnetic tunneling junctions, etc. One of the technological hurdles is to understand and control the interlayer magnetic coupling between the electrodes. It has been shown that two separate effects such as magnetostatic coupling due to uncompensated poles near the edges and the magnetostatic coupling between the stray fields of domain walls, and Néel coupling due to interface roughness tend to produce extraneous magnetic fields in the plane of the free layer. In addition, the interlayer coupling originates from two different types of interactions such as short-range exchange interaction and long-range exchange interaction.

2.9.1. Exchange coupling:

2.9.1.1. Direct exchange coupling:

Two magnetic layers separated by a thin non-magnetic insulating or metallic spacer layer are directly coupled through pinholes present in the thin spacer layer, i.e., since the pinhole appears mainly due to the formation of non-continuous spacer layer, number of pinholes, which control the strength of the coupling depends on the thickness of the spacer layer, growth conditions, atomic size of the elements present in the spacer and magnetic layers [SAIT2002, STIL2005, PONG2008]. Multilayer films having the direct exchange coupling through the pinholes exhibit strong temperature dependent magnetic properties due to the temperature dependent magnetic properties of diffused magnetic atoms into the non-magnetic layers [OLIV1999].

2.9.1.2. Indirect exchange coupling:

The increase in the spacer layer thickness between the magnetic layers results the interlayer coupling between the ferromagnetic layers through conduction electrons of the non-magnetic

metallic spacer layer. This is called as indirect exchange interaction or Ruderman-Kittel-Kasuya-Yosida (RKKY) interaction. Theory of indirect exchange interaction was first predicted by Ruderman and Kittel [RUDE1954] and later extended by Tadao Kasuya [KASU1956] and Kei Yosida [YOSI1957]. RKKY interaction was implemented in the multilayer structured thin films to understand the magnetization orientation and the giant magnetoresistance of multilayer structured ultra-thin films. It was observed that RKKY coupling aligns the magnetization of adjacent ferromagnetic layers to be either ferromagnetic (parallel alignment) or antiferromagnetic (antiparallel alignment). Hence, the magnetoresistance of the multilayer films exhibits a strong dependence on the spacer layer thickness and shows an oscillating nature with spacer layer thickness. The amplitude of oscillation decreases with increasing spacer layer thickness [BAIB1988, PARK1990, BRUN1991, BRUN1992]. In addition, the coupling also depends on the roughness at the interfaces.

2.9.2. Magnetostatic coupling:

2.9.2.1. Topological coupling:

The topological coupling also known as Néel's orange peel coupling or the dipolar coupling is the magnetostatic interaction induced by the magnetic poles at the interface. These magnetic poles are generated by the interface roughness. Néel carried out the first calculation of topological coupling for semi-infinite magnetic layers with a correlated sinusoidal interface roughness [NEEL1962]. Later, the model was extended by other researchers for the roughness of arbitrary phase and finite magnetic film thickness [ZHAN19961, ZHAN19962, KOOL1999]. The coupling strength depends on the thickness of magnetic layers and spacer layers, magnetization of magnetic layers, roughness amplitude at the interface and wavelength of the roughness profile. Néel coupling between two ferromagnetic layers is defined as [SCHR2000],

$$H_N = \frac{\pi^2}{\sqrt{2}}\left(\frac{h^2}{\lambda t_F}\right) M_S exp\left(-\frac{2\pi\sqrt{2}t_s}{\lambda}\right) \qquad (2.36)$$

where, t_F and t_s are the thickness of the magnetic layer and spacer layers respectively, h and λ are amplitude and wavelength of the roughness, respectively as shown in the figure 2.15(a). The coupling field strongly depends not only on the spacer layer thickness, but also depends on the ferromagnetic layer thickness (see figure 2.15(b)).

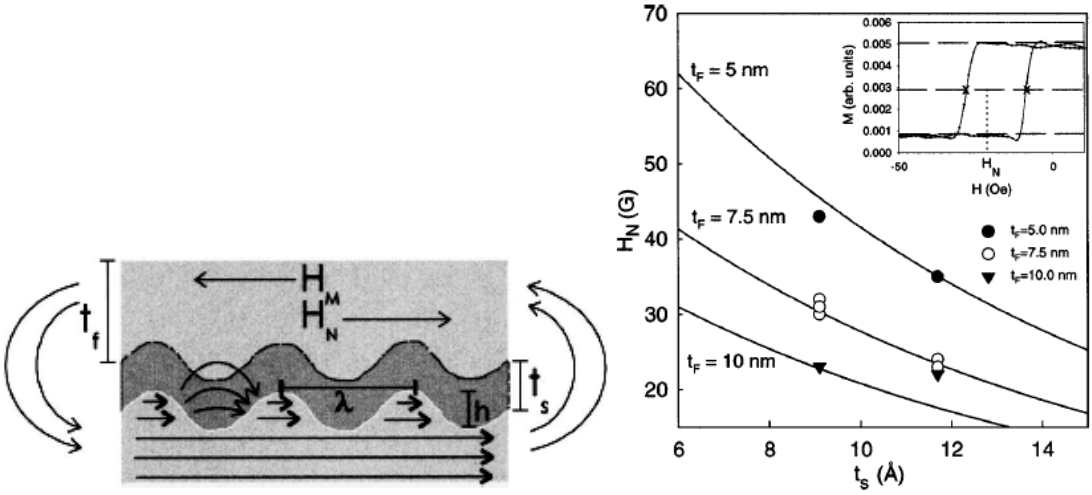

(a) *(b)*

Figure 2.15: (a) Schematic drawing of two dominant interlayer coupling mechanisms, and (b) variations of Néel coupling with spacer layer thickness for different multilayer films [SCHR2000].

2.9.2.2. Stray field coupling:

Another magnetostatic coupling arises due to the magnetic poles at the edges of the film is stray field coupling. The stray field generated from the edges of the one magnetic layer magnetostatically couples the other layers as shown in the figure 2.15(a). Since the coupling is magnetostatic in nature, it depends strongly on the films' dimension and provides a significant interlayer coupling for thicker films [ANGU2000]. The variation of stray field coupling on the films' dimension can be described as [ANGU2000],

$$H_M = A\frac{W^{\alpha}}{L} \qquad (2.37)$$

where, W and L are the width and length of the sample in micron, respectively, A and α (= 0.22) are constants. The value of α varies with the sample dimension, i.e., when the separation between the free layers and the relevant pinned layer is much larger than its width, α approaches to one, whereas in the opposite limit, the value of α should be nearly zero [ANGU2000].

2.9.2.3. Domain wall stray field coupling:

Stray fields emanating from domain walls of a given ferromagnetic layer magnetostatically lock in with the stray fields from walls in adjacent layers as shown in figure 2.16. [CHOP2000, CHOP2005]. The rotation of magnetization within a Néel wall is denoted by the double arrows. The stray field emanating out of the Néel walls, denoted by curved arrows, causes a magnetization fluctuation in the adjacent layers above and below it, giving rise to quasi-Néel walls. This stray field emanating from each domain wall is able to close its flux by magnetostatic locking-in with the stray fields from domain wall in adjacent layers. This

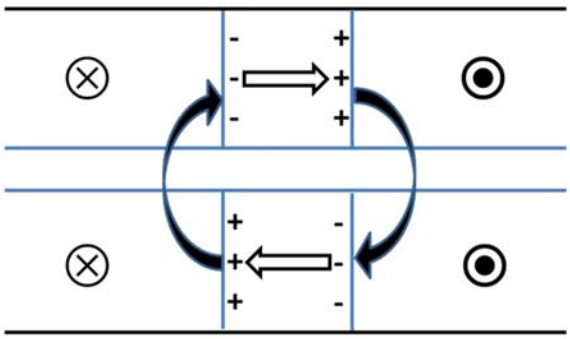

Figure 2.16: Schematic of Néel wall pair separating parallel domains. Superimposed Néel walls are energetically favorable entities due to a more complete flux closure associated with them [CHOP2000].

leads to an overall reduction in the wall energy and hence the coercivity. Magnetic thin films reveal strong thickness dependent magnetic properties. Particularly, ultrathin films having in-plane magnetic anisotropy exhibits in-plane magnetization with large sized domains and Néel wall [OHAN2000]. Similarly, the multilayer thin films with thin ferromagnetic layers also show in-plane magnetization with large sized domains and Néel wall, which results a minimum or zero stray field coupling. On the other hand, the development of multidomain patterns above the critical thickness depends on the net magnetization of the ferromagnetic layers, anisotropy of the films, substrate nature, microstructure of the film and the growth conditions of the thin films [FELD1971, OEPE1990, ALLE1994]. Therefore, at larger thicknesses, the multidomain pattern with Bloch wall is energetically more favorable. This reveals that the domain wall stray field provides a significant coupling among the ferromagnetic layers ensuing a strong variation in the magnetic properties of the multilayer structured films measured at different temperatures.

Chapter 3

Experimental Methods

In the course of the present investigations, several experimental techniques were used for the preparation and characterization of single and multilayer thin films. This chapter provides a brief description of those experimental techniques.

3.1. Techniques used for sample preparation:

3.1.1. Sputtering technique:

The ejection of atoms from the cathode surface by impinging of energetic positive ions of noble gases such as helium, argon, neon and krypton, at a reduced gas pressure under high direct current (DC) voltage gives rise to the sputtering [OHRI1992, WAGE1994, SESH2002]. In 1852, Sir W. R. Grove discovered surface coatings generated in the valve under a glow discharge. This phenomenon was called as spluttering by Sir W. Thomson and soon it was adopted as sputtering. This process involves a momentum transfer between the impinging positive ions and the cathode surface atoms as shown in figure 3.01 and as a result of which a physical removal of atoms takes place.

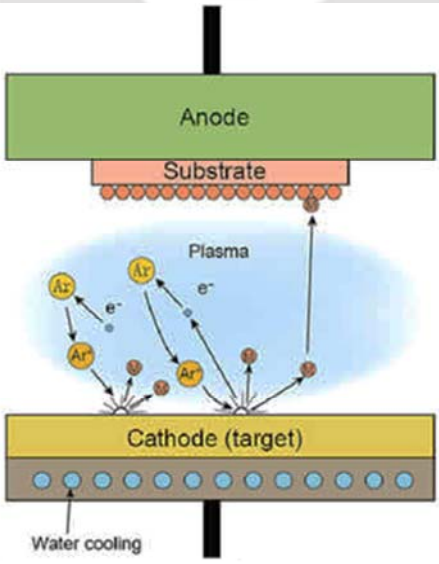

Figure 3.01: Schematic diagram of the sputtering process.

The sputtering yield is defined as ratio between the mean number of emitted atoms to number of incident ions on the target surface.

- The sputtering yield increases with the a) energy, b) mass of the bombarding atoms and c) decrease of angle of incidence to the target.
- A minimum energy is required to start the sputtering process.
- Sputter atoms have higher energy than those of the thermally evaporated atoms.

- The sputter atoms are ejected along the crystallographic directions of the cathode metal lattices.
- Sputtering yield decreases with larger increase of the ion-energy because of the deeper penetration of ions inside the lattice.
- Sputtering is also accompanied by the emission of secondary electrons from the cathode surface.
- The sputtering yield is insensitive to the cathode temperature.
- If the sputtering process does not involve any of the chemical reaction between bombarding gas ions and the cathode, it is known as physical sputtering.
- If some reactions are involved then it is named as reactive sputtering.

The physical deposition process consists of three steps

1. Emission of the particles from a source,
2. Their transport to the substrate, and
3. Condensation on the substrate.

There are four different types of sputtering process (DC, Radio-frequency (RF), Magnetron and Reactive sputtering) used for thin film deposition. We have used DC magnetron sputtering for depositing the films of present investigation.

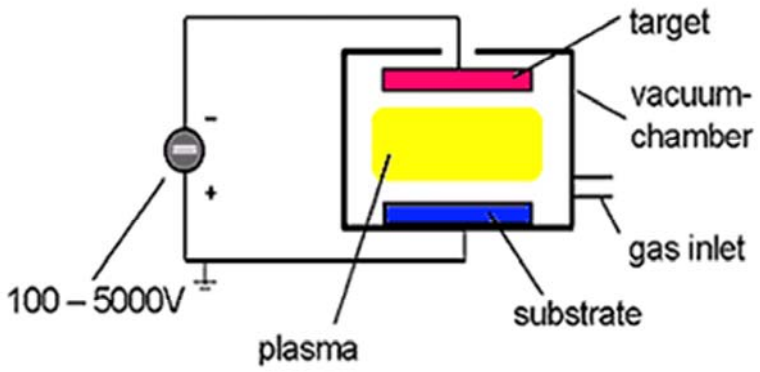

Figure 3.02: Schematic arrangement of DC sputtering technique.

3.1.1.1. DC sputtering technique:

Figure 3.02 depicts a typical arrangement used for DC sputtering. In this case, target and substrate oppose each other in the vacuum chamber having a distance of few centimeters to few tens of centimeters. The target is connected to a negative output of a DC power supply, acting as the cathode whereas substrate and chamber walls act as anode. After the creation of

argon atmosphere with a pressure of about 1 - 100 mTorr, the gas discharge is ignited by applying a DC voltage. The created Ar^+ ions are now accelerated toward the target and eject atoms from the target. These atoms subsequently are deposited on the substrate. At low pressures, the mean free path between collisions is large, the ionization efficiency is low and self-sustained discharges cannot be maintained below few mTorr. As the pressure increases at a fixed voltage, the electron mean free path is decreased, more ions are generated and large current flow. If the pressure is too high, the sputtered atoms undergo increased collisional scattering resulting a low deposition process. The deposition rate is proportional to (a) power consumed, (b) square of current density and (c) 1/(electrode spacing). DC sputtering works with all types of target materials which are conductive in nature.

However, DC sputtering suffers from two major drawbacks as compared to conventional evaporation: (i) low deposition rates and (ii) high thermal load of the substrate due to bombardment of secondary electrons. In order to increase the deposition rate and to control the thermal load, magnetron sputtering as described below in figure 3.03 is utilized for the fabrication of the films.

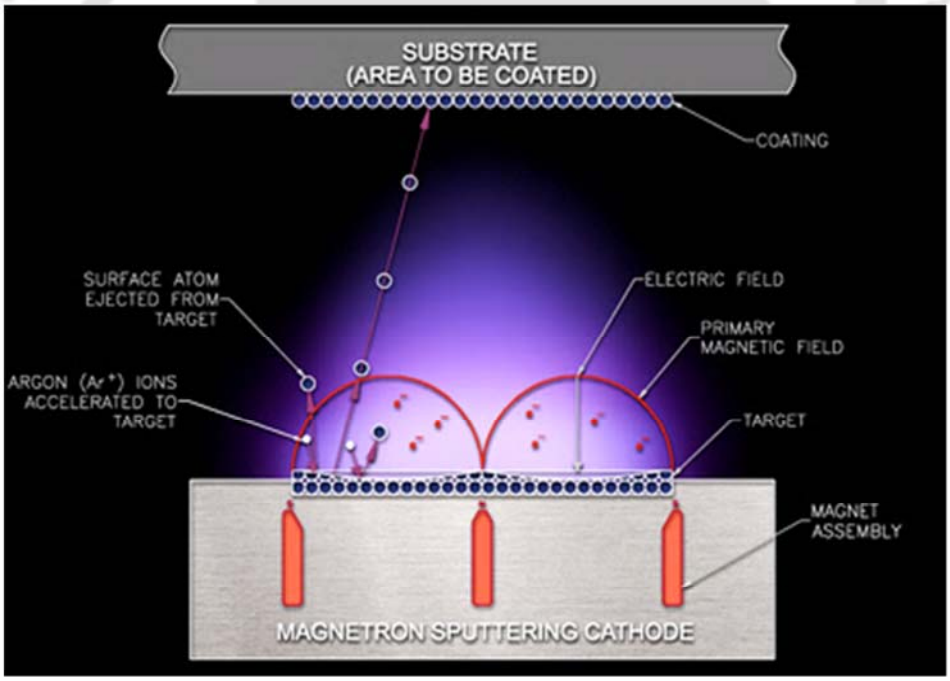

Figure 3.03: Schematic presentation of magnetron sputtering gun assembly.

3.1.1.2. Magnetron sputtering technique:

In magnetron sputtering, electrons ideally don't even reach the anode but are trapped near the target and thereby enhancing the ionization efficiency. This is accomplished by employing a magnetic field oriented parallel to the target and perpendicular to the electric field.

Practically, this is achieved by placing bar magnets behind the target as shown in figure 3.03. The magnetic field lines emanate first normal to the target and then bend with a component parallel to the target surface and finally return to magnet completing the magnetic circuit. Electrons emitted from cathode are initially accelerated toward the anode, but executing a helical motion when they encounter the region of the parallel magnetic field. Therefore, they are bent in an orbit back to the target. The chief reasons of its success are (1) increased sputtering rates (~ 5 - 10 times) due to high plasma density around target, (2) low discharge voltages of 300 to 1000 V due to the reduced plasma impendence resulting from high plasma density and (3) low thermal load of the substrate due to deflection of secondary electrons by the magnetic field.

Figure 3.04: Photographic view of the magnetron sputtering system used in the present work.

Figure 3.04 depicts the typical set up of magnetron sputtering used in the present thesis work for fabricating single and multilayer structured thin films. The chamber is equipped with four different guns for making multilayer films. The substrate was loaded on the rotating substrate holder. Subsequently, the chamber was pumped to high vacuum (< 10^{-6}

Torr) using diffusion pump and rotary pump combination. The argon gas of fixed pressure was permitted into chamber continuously using mass flow controller (MFC) and the argon gas pressure in the chamber was maintained by adjusting the MFC and high vacuum valve. The optimized sputtering Ar gas pressures for FeTaC and Ta films were fixed at 1 mTorr and 10 mTorr, respectively. After stabilizing the constant argon gas pressure in the chamber, a constant DC power was applied to commence the sputtering process. The deposition of the films was carried out after stabilizing the plasma and completing the pre-sputtering process. The nominal thickness of the films is controlled by sputtering time ranging between 1 nm and 6 nm for Ta spacer layer and from 20 nm to 200 nm for FeTaC film. The deposition rate for FeTaC and Ta films was calibrated by using an ex-situ surface profilometer (Vecco, Dektak-150) as described in the next section.

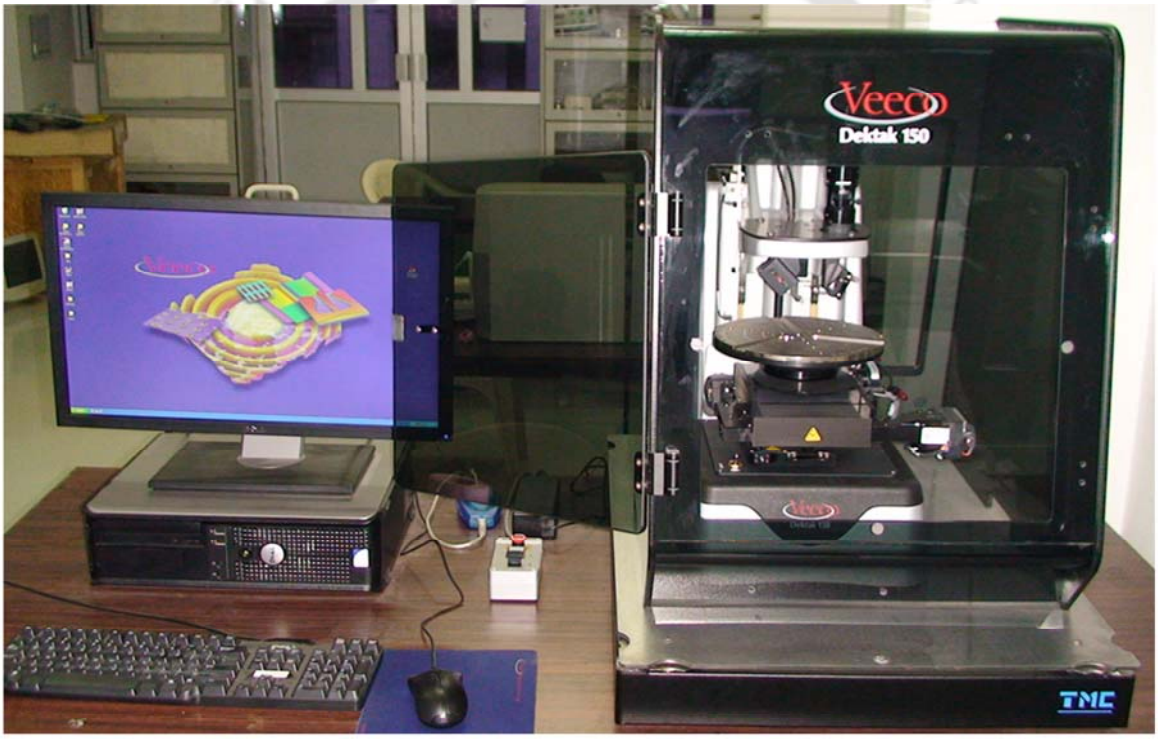

Figure 3.05: Photographic view of Vecco-Dektak 150 surface profilometer.

3.1.2. Deposition rate calibration:

In order to monitor the properties of the films at different thicknesses, it is very much essential to control the thickness of the film deposited under optimized sputtering conditions. Deposition rate of the films studied in the present investigations was calibrated with surface profilometer (Vecco, Dektak-150), as illustrated in figure 3.05. Stylus profilers are versatile measurement tools for studying surface topography. Their primary function is to measure film thickness by scanning step heights and trench depths. The stylus profilers rely on a

small-diameter stylus moving along a surface either by movement of the stylus or movement of the surface of interest. A true stylus profiler moves linearly to obtain the measurement. As the stylus encounters surface features, the stylus moves vertically to measure various surface features, such as deposited film and irregularities. The stylus profiler used in the present work was sponsored by Defence Research & Development Organisation (DRDO), New Delhi under the project scheme of ERIP/ER/0900363/M/01/1185 Dated 16 November 2009. To monitor the thickness of the deposited films, a proper marking using permanent marker was made on top of the cleaned substrate. Subsequently, the deposition was done under controlled sputtering environment (constant Ar gas pressure, DC power and target to substrate distance, etc.) for a given time at ambient temperature. After the completion of the deposition, the film was cleaned through sonication in acetone. As a result, the film deposited on the substrate reveals a clear step. The step size was evaluated using surface profiler as displayed in figure 3.06 and the average deposition rate was eventually calculated by dividing the average thickness measured at various locations on the substrate with deposition time. In order to confirm the reproducibility, more films were made under the same sputtering conditions and analyzed using surface profilometer. Similar procedures were followed for all the films prepared under different sputtering conditions.

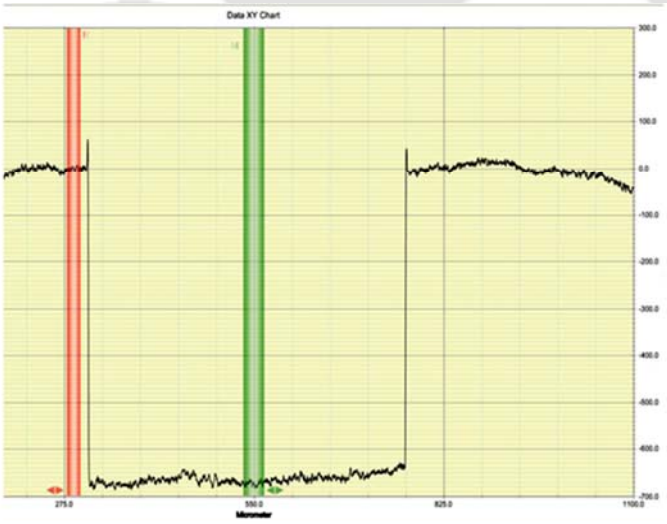

Figure 3.06: A typical scan profile of the surface profilometer.

3.1.3. Post deposition annealing at elevated temperatures:

All the films were deposited at a high deposition rate directly on thermally oxidized Si substrate at ambient temperature for producing amorphous structure. Hence, these films exhibit considerable stress in the as-deposited state and reveal thickness dependent magnetic properties. In order to release the stress accumulated during film deposition and to produce

nanocrystalline microstructure, all the as-deposited films were annealed in a separate custom-made high vacuum chamber at different annealing temperatures (200 ºC, 300 ºC and 400 ºC) for 30 minutes annealing time. The annealing temperature and annealing time were optimized based on the development of nanocrystalline microstructure and magnetic properties of the films. In the annealing process, the substrate with film was kept on a filament heater and attached close to a thermocouple (Chromel-Alumel) to avoid any temperature lag between heater, sample and thermocouple. The chamber was pumped to high vacuum (< 10^{-6} Torr) using diffusion pump and rotary pump combinations. After reaching the desired vacuum, temperature was raised constantly at a rate of 10 ºC/min to the annealing temperature. The sample was annealed at a given annealing temperature within the temperature stability of ±2 ºC accuracy. After the completion of heat treatment at a particular temperature, the heater was switched off and the sample was allowed to cool down naturally to room temperature in presence of vacuum.

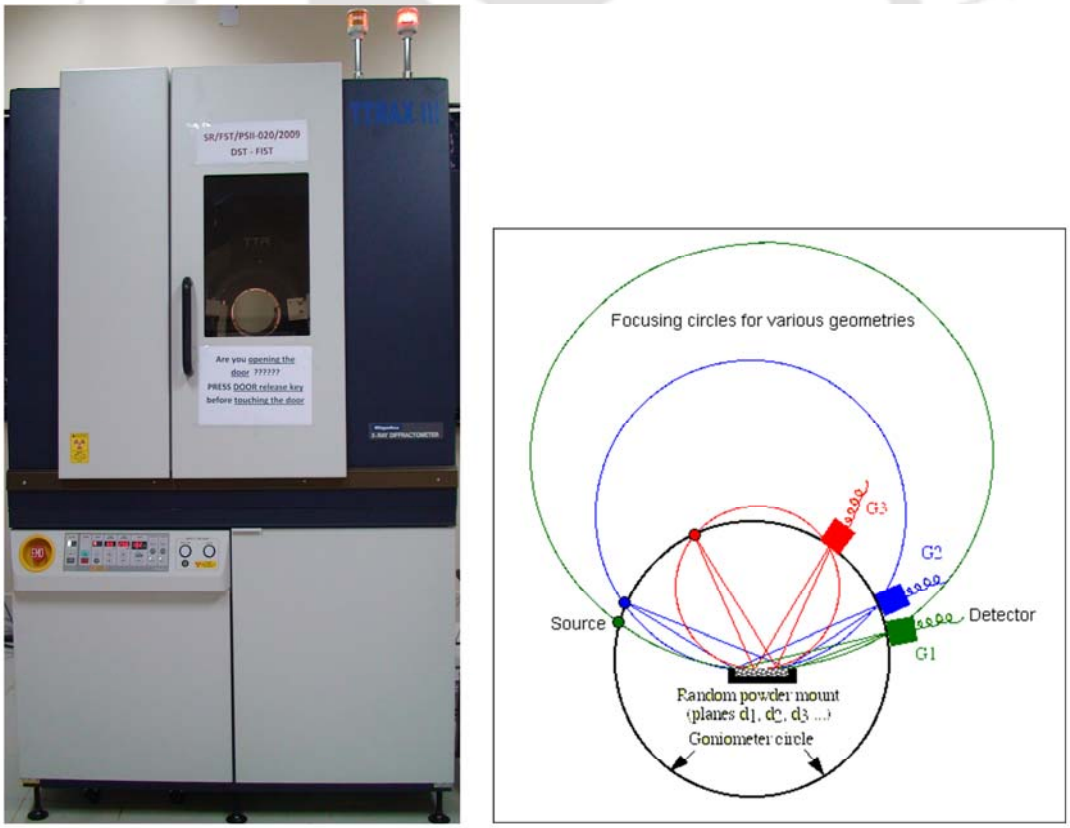

(a) (b)

Figure 3.07: (a) Photographic view of Rigaku TTRAX III 18 kW X-ray diffractometer and (b) Bragg-Brentano diffraction geometry of a powder X-ray diffractometer.

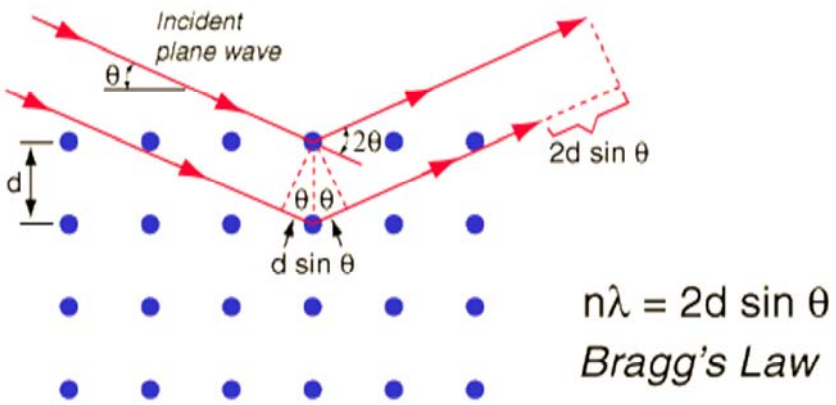

Figure 3.08: Schematic ray diagram of diffraction of X-rays by a crystal.

3.2. Structural property characterization:

3.2.1. X-ray diffraction:

Two different X-ray diffractometers viz. Rigaku RINT 2500 and Rigaku TTRAX III 18 kW (shown in figure 3.07a) were used in the thesis work depending upon their availability. Cu-K_α X-ray radiation with wavelength 1.54056 Å was used in all the cases. The theta-theta (θ–θ) goniometer was used in the reflection (Bragg-Brentano) geometry (see figure 3.07b) [CULL2001]. X-ray diffraction (XRD) technique is useful to identify the existence of various phases, degree of crystalline order and quantitative analysis of secondary phases present in a two-phase system. An ideal crystal has a periodic arrangement of atoms. Diffraction of X-rays occurs through constructive interference of X-rays scattered from atoms of a set of parallel planes in crystal lattice at particular angular positions of the incident wave known as Bragg angles. This condition for obtaining constructive interference is known as Bragg's law and given by the relation

$$2d_{hkl} \sin\theta = n\lambda \qquad (3.01)$$

where, d_{hkl} is inter-planer spacing, θ is glancing angle, λ is wavelength of the X-ray and n is order of diffraction. A sequence of these angles can be used to determine the Miller indices (*hkl*) values and the crystal structure can be identified from the systematic behaviour of these indices. Figure 3.08 shows the diffraction of X-rays from crystal lattice planes illustrating Bragg's law. The structural parameters such as the average size of the crystallites, *d*-spacing, lattice constant and strain present inside the crystallites, *etc* can be determined by a careful analysis of the XRD patterns using various models [CULL2001].

3.2.2. Transmission electron microscope:

Transmission electron microscopy (TEM, TECNAI G^2 F30; JEOL 2100) was used to study the nanocrystalline microstructure of the samples depending on its availability. Figure 3.09 depicts the cut view of TEM (figure 3.09(a)) and schematic ray diagrams for imaging (figure 3.09(b)) and diffraction (figure 3.09(c)) modes. Electrons thermionically emitted from the gun, made of tungsten or LaB_6, are accelerated to 200 keV or higher and first projected onto a thin specimen by means of the condenser lens system. The scattering processes experienced by electrons during their passage through the specimen determine the kind of information obtained. Elastic scattering, involving no energy loss when electrons interact with the potential field of the ion cores, gives rise to diffraction patterns. Inelastic interactions between beam and matrix electrons at heterogeneities such as grain boundaries, dislocations, second-phase particles, defects, density variations, etc., cause complex absorption and scattering effects, leading to a spatial variation in the intensity of the transmitted beam. The transmitted beams are further magnified by a set of intermediate lens and projector lens and finally projected on a fluorescent screen.

Microstructural images are obtained in number of ways. The bright-field image is obtained by intentionally excluding all the diffracted beams and only allowing the central beam passing through the specimen. This is done by placing suitably sized apertures in the back focal plane of the objective lens. Dark-field images are also formed by magnifying a single beam of one of the diffracted beams by means of an aperture that blocks the central beam and the other diffracted beams. In a third method of imaging, the primary transmitted and one or more of the diffracted beams are made to recombine, thus preserving both their amplitudes and phases. This is the technique employed in high-resolution lattice imaging, enabling diffracting planes and arrays of individual atoms to be distinguished. From the high-resolution TEM (HR-TEM) micrograph, average grain size and dislocations can be evaluated. On the other hand, the selected area electron diffraction is done by intentionally excluding the central beam by beam blocker and collecting all the diffracted beams to form the diffraction patterns. The composition analysis of the samples can also be analyzed using X-ray energy dispersive analysis interfaced to TEM. Electrons emitted from the filament (cathode) are accelerated to high energies where they strike the specimen target (anode). In the process, X-rays characteristic of atoms in the irradiated area are emitted. The atoms can be identified by analyzing their energies and the concentration of atoms in the specimen can be determined by counting the number of X-rays emitted.

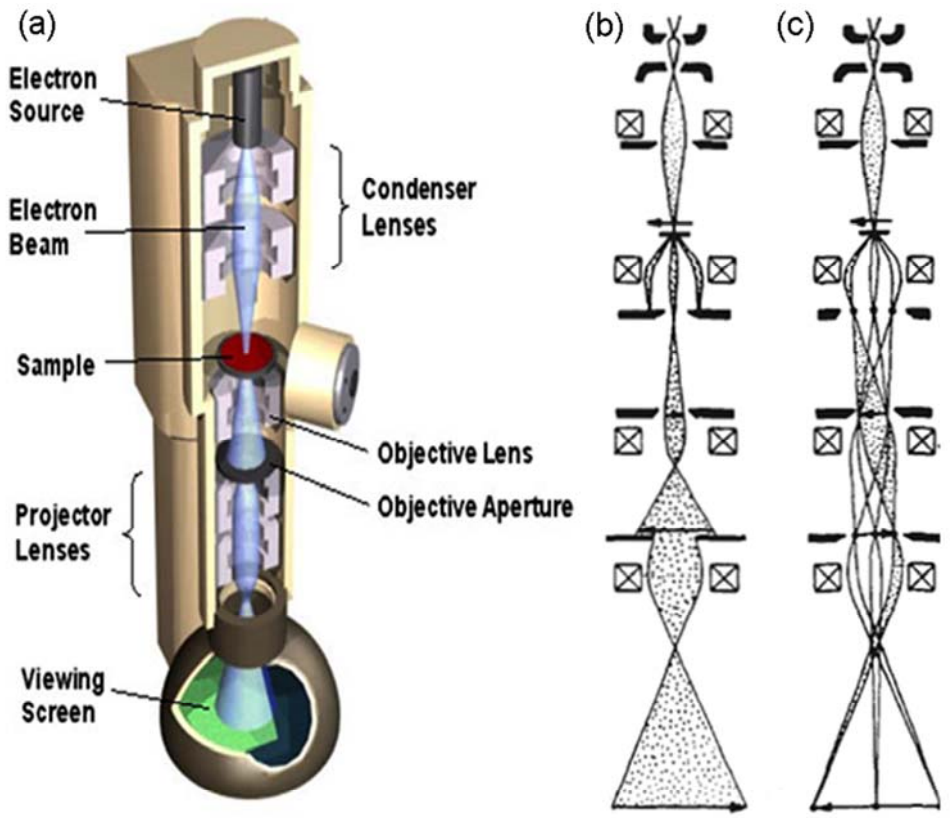

Figure 3.09: (a) Cut view of transmission electron microscope, (b) Schematic ray diagrams of image mode and (c) diffraction mode of TEM.

In the present study, as-deposited films and post deposition annealed films were polished mechanically from substrate side using Gatan Disc grinder to reduce the thickness down to 10 μm and subsequently thinned down using precision ion polishing system (PIPS) to suitable thickness for the TEM observation [REIM1993, BRAN2008].

3.3. Magnetic property characterization:

Magnetic properties of the magnetic materials can be characterized with various experimental techniques such as magnetic property measurement system (MPMS) equipped with superconducting quantum interference device (SQUID) magnetometer and vibrating sample magnetometer (VSM). These techniques are based on the induction methods and have sensitivity of at least 10^{-6} emu. Similarly, the magnetic domain structure of the materials can be imaged using magnetic Kerr microscope. In this section, a brief description of the principle involved in various magnetic measurement and domain imaging techniques employed in the present work is outlined.

Figure 3.10: Photographic view of MPMS XL 7 system.

3.3.1. Magnetic property measurement system:

MPMS system (see figure 3.10) equipped with SQUID magnetometer (MPMS XL 7, USA) was used to characterize magnetic properties in the temperature range of 5 K – 300 K. The fundamental property of superconducting rings is that they can enclose magnetic flux only in multiples of a universal constant called flux quantum, ϕ_0, i.e., an external magnetic field can penetrate a superconductive loop if and only if the magnetic field is an integer multiple of ϕ_0 [ANTO1992]:

$$\phi_0 = \frac{h}{2e} = 2 \times 10^{-15} Wb \qquad (3.02)$$

where, h is the plank constant and e is the charge of electron. Since the flux quantum is the smallest quantity of the magnetic flux, SQUID has an extraordinarily sensitive magnetic detector. SQUIDs actually function as magnetic flux-to-voltage transducers by converting magnetic flux into corresponding voltage. SQUID mainly consists of two Josephson junctions, i.e., two superconducting metals separated by a thin insulating layer, which is

typically a metal oxide [ANTO1992]. As a result, the tunneling super current across the junction has a phase which depends strongly on the magnetic field applied perpendicularly to junction. Furthermore, each junction has a maximum value of the current that can flow without voltage drop across and above which normal electrons need to flow and a finite voltage drop appears. This finite voltage drop causes the supercurrent to cease. In particular, in a superconducting ring interrupted by two Josephson junctions, the application of a magnetic field normal to the ring causes an induced supercurrent to screen the magnetic field. When induced supercurrent exceeds the critical value, it allows the magnetic flux to enter the hollow portion of the ring, in multiples of one quantum unit as discussed earlier. The process repeats for an increasing external applied magnetic field and the flux increases each time by one quantum unit. A pick-up coil, located coaxially to the ring, enables the measurement of the magnetic field by counting the pulses of *emf* induced each time of the magnetic flux changes.

In the present study, the sample was fixed in the suitable sample holder and temperature dependent magnetization measurements were carried out under zero-field-cooled (ZFC) and field-cooled (FC) conditions by applying the field along the film plane and by setting the program. The sample was cooled down to 5 K without applying any field and the magnetization was measured during the warming process under a constant applied, known as ZFC process. Subsequently, the sample was cooled down to 5 K under the same constant field and the magnetization was measured during warming process, called as FC process. The temperature during measurements was controlled using suitable temperature controller (Quantum Design) from 5 K to room temperature.

3.3.2. Vibrating sample magnetometer:

VSM (Lakeshore 7410, USA) was used to characterize room temperature and temperature dependent magnetic properties in the temperature range 20 K – 300 K and 300 K – 1100 K. VSM measures net dipole moment when material is exposed to magnetic field [JANS2004, HORS2006]. The magnetic moment of the material can be obtained either as a function of field called magnetic hysteresis (*M-H*) loop to investigate the evolution of magnetic properties with field or as a function of temperature (*M-T*) to understand the magnetic phase transition of the material. Figures 3.11 and 3.12 display schematic diagram of VSM and a photographic view of VSM used in the present study, respectively.

When a sample is placed in a uniform magnetic field, a dipole moment proportional to the product of the sample susceptibility and the applied field is induced in the sample. If the

sample is made to undergo sinusoidal motion, an electrical signal can be induced in suitably located stationary pickup coils (see figure.3.11). This signal has amplitude proportional to the magnetic moment of the sample, the vibrating amplitude and the vibration frequency. Through the use of lock-in-amplifier and feedback techniques, only that portion of the signal arising from the magnetic moment is picked up and is converted into direct read-out in the unit of magnetization (e.g. emu) on a digital panel meter. VSM consists of the following major parts: a) Vibration exciter and sample holder, b) Water cooled electromagnet and power supply, c) Hall probe, d) pick-up coils, e) Amplifier, f) Control panel system, g) Lock-in amplifier and h) Computer interface.

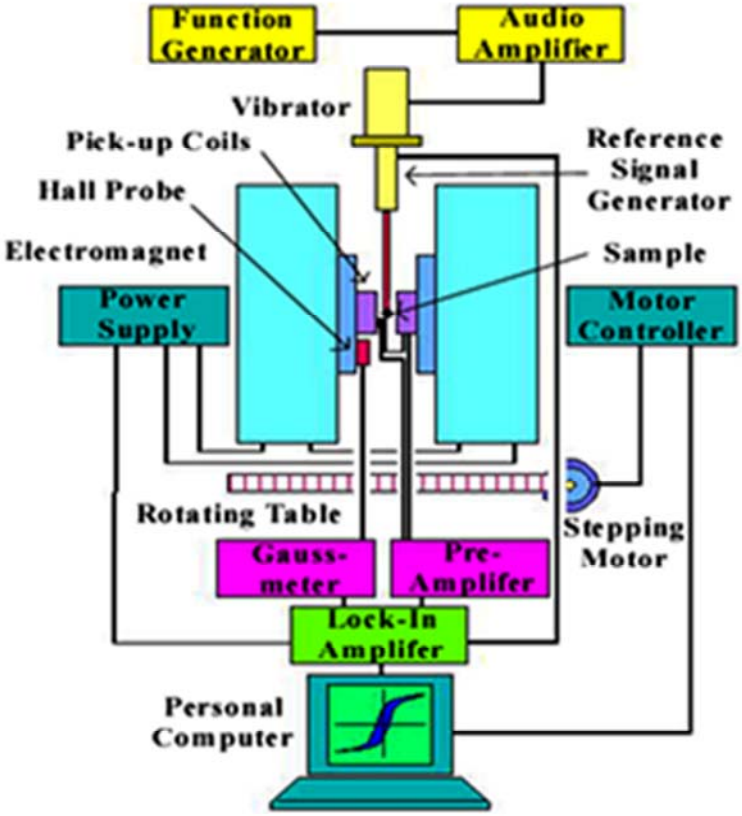

Figure 3.11: Schematic diagram of a vibrating sample magnetometer.

The thin film sample was fixed at the lower end of the sample rod aligning either in-plane or out of plane direction with respect to applied field. Prior to the magnetic measurements, the calibration procedure was carried out using standard Ni sphere sample. The measurement sequence is programmed as per the users choice using the software (IDEASVSM) provided with the instrument such that the program starts either from the maximum field or from the zero applied field. The sequence is made to collect more number of data, which helps to extract the magnetic parameters (saturation magnetization, remenance

magnetization, coercivity, etc.) more accurately. The exciter is vibrated at a frequency of 72 Hz (Lakeshore model 7410) and the signal received from the hall probe and the pick-up coils is converted into the magnetic moment of the sample. The magnetic field is increased automatically in user-defined steps for measuring *M-H* loops. Similarly, for high temperature *M–T* measurements, a high temperature oven attachment capable of providing a controlled heating/cooling of the sample from room temperature to 1223 K was used. For *M–T* measurements, the film was loaded on a high temperature sustainable holder (ceramic holder or quartz rod) after the calibration using standard Ni sample. The oven was purged with nitrogen gas to avoid oxidization of the sample at high temperature. Magnetization was recorded at different temperatures at a constant in-plane applied magnetic field. The heating rate and *M–T* sequences were programmed using the IDEASVSM software.

Figure 3.12: Photographic view of vibrating sample magnetometer (Model: Lakeshore 7410, USA) used in the present investigation.

3.4. Magnetic domain structure analysis:

The magneto-optical Kerr effect (MOKE) represents a change in the intensity or polarization state of the light reflected from a magnetic material. Figure 3.13 depicts a schematic view of

conventional MOKE set up. The light beam from a laser is polarized using a linear polarizer, while a photo elastic modulator (PEM) superimposes periodic quarter-wave retardation ($\pm\lambda/4$) to this beam before it reaches the sample. After the beam is reflected from the sample, the light beam is again made to pass through a linear analyzer and then the signal is collected at the detector. In principle there are three different optical and magnetic geometries of the Kerr effect: (a) Longitudinal MOKE provides a signal proportional to the component of magnetization that is parallel to the film plane and the plane of incidence of the light. (b) In transverse MOKE, the signal is proportional to the component of magnetization that is parallel to the film plane but perpendicular to the plane of incidence of the light. (c) Polar MOKE, in which a signal proportional to the component of magnetization that is perpendicular to the film plane is measured and often performed at normal incidence. There are three important properties to be noted that (i) the Kerr signal is a linear function of the Kerr amplitude K and therefore of the respective magnetization components, (ii) the Kerr signal can be enhanced by increasing the analyzer angle allowing to increase the signal-to-noise ratio and to adjust to the sensitivity of the detector and (iii) the visibility of domains is determined by the Kerr amplitude and not by the Kerr rotation.

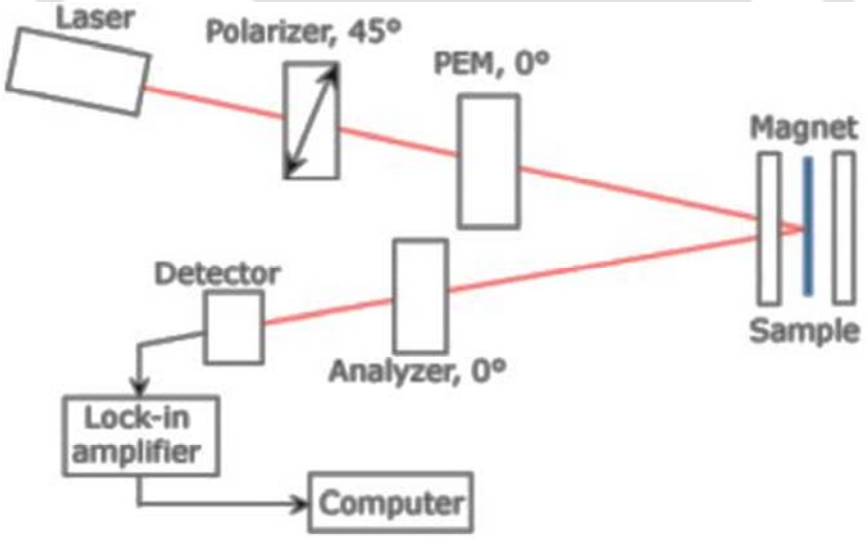

Figure 3.13: Schematic drawing of MOKE set up.

To produce a Lorentz movement that leads to detectable Kerr rotation, an appropriate direction of light incidence and polarization has to be selected for a given magnetization direction. As a simple rule, the Kerr rotation is proportional to the magnetization component parallel to the reflected beam of light. This rule implies that domains that are magnetized parallel to the sample surface require oblique light incidence and that for maximum rotation

the plane of incidence must be parallel to the axis of magnetization with the polarizer set either parallel or orthogonal to the incidence plane (longitudinal Kerr effect, $\vartheta \neq 0$). The Kerr amplitude is then proportional to the sine of the angle of incidence ϑ, and therefore disappears for perpendicular incidence. In this case, maximum rotation is exhibited by domains that are magnetized perpendicularly to the sample surface (polar Kerr effect, $\vartheta = 0$), while in-plane domains do not cause a Kerr amplitude. At oblique incidence, both in-plane and out-of-plane magnetization components generate a superimposed Kerr contrast. The separation of the two components is possible by proper difference images that are obtained at different microscope settings. Also, the transverse Kerr effect leads to in-plane magnetization sensitivity. Here, the in-plane *m* vector is normal to the plane of (oblique) incidence. Light with *E* parallel to this plane generates Kerr amplitude, but its polarization direction is the same as that of the normally reflected beam. The transverse Kerr effect thus causes an amplitude variation, which can be used for measuring purposes. A rotation that is detectable by an analyzer is obtained when the incident light is polarized at 45º to the plane of incidence. Here, the E component perpendicular to the incidence plane is not affected, while the parallel component is modulated in its amplitude on reflection, leading to polarization rotation by superposition [SCHA2007, HUBE2009].

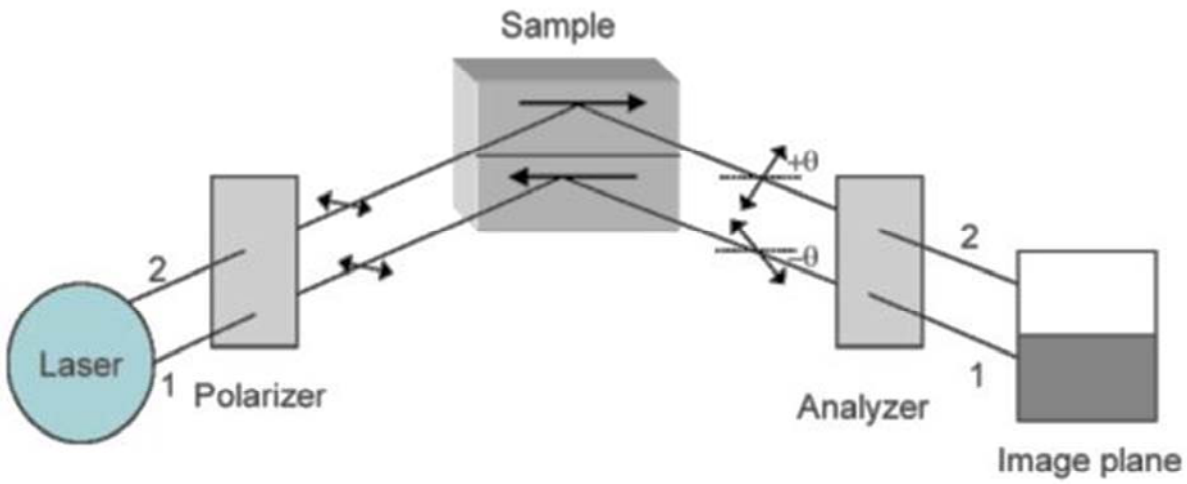

Figure 3.14: Schematic drawing of Kerr microscope.

Kerr microscopy alloys the imaging of magnetic domain and magnetization processes in an optical polarization microscope. This is also based on the MOKE, but only with the difference that the domains are directly imaged. A schematic picture of the setup is shown in figure 3.14. In this set up, the light from a source passes through a polarizer which transmits only plane polarized light. This polarized light is then allowed to fall on the sample. The

resulting light in the image plan strongly depends on the magnetization of the sample. For example, let us consider a simplest case of two domain states which are antiparallel to each other as indicated by arrows in figure 3.14. After reflection from the sample, the plane of polarization of beam 1 is rotated one way by certain angle $-\theta$ and that of beam 2 is rotated by angle $+\theta$, as they encountered oppositely magnetized domains. The light then passes through an analyzer and into a camera to make images. Here, the analyzer is rotated until it is crossed with respect to the reflected beam 1 and the beam is therefore extinguished and the lower domain appears dark. At the same time, the analyzer is not crossed with respect to beam 2 and thus beam 2 is not extinguished resulting the upper domain as light one. This is the mechanism to find a contrast between two different domains.

Figure 3.15: Photographic view of the Kerr microscope (Evico Magnetics Ltd. Germany) used in the present study.

In the present study, magnetic domain images and Kerr loops were obtained using a MOKE microscope (Evico Magnetics Ltd., Germany) as shown in figure 3.15. Imaging was performed using linearly polarized light with Xenon lamp as source. Magnetic domain images were observed in both branches of hysteresis cycle in longitudinal MOKE mode. Hysteresis accompanied by simultaneous imaging has been performed for magnetic fields applied along various in-plane directions (easy and hard axes).

Chapter 4

Thickness dependent properties of FeTaC magnetic thin films

This chapter primarily focuses on the preparation and characterization of FeTaC single layer films deposited directly on thermally oxidized Si substrate at ambient temperature using magnetron sputtering technique and the results of experimental studies carried out on these films with different thicknesses.

4.1. Experimental details:

Amorphous $Fe_{80}Ta_8C_{12}$ (FeTaC) single layer films with different thicknesses t = 20, 50, 100, and 200 nm were deposited on thermally oxidized Si substrates using DC magnetron sputtering technique at ambient temperature. The choice of FeTaC composition was dictated by the fact that this alloy composition exhibits good soft magnetic properties [TANA2002, PERU2009]. The base pressure of the sputtering chamber was better than 10^{-6} Torr. The sputtering Ar gas pressure for FeTaC films was fixed at 1 mTorr and the nominal thickness of FeTaC films was varied by varying the sputtering time during sample preparation. The deposition rate was calibrated by using ex-situ surface profilometer (Vecco, Dektak-150) as discussed in section 3.1.2. Amorphous nature of the film was confirmed by X-ray diffraction (XRD) using a high power (18 kW) and high-resolution Rigaku X-ray diffractometer (TTRAX III) with Cu-K_α radiation (λ = 1.54056 Å) and transmission electron microscopy

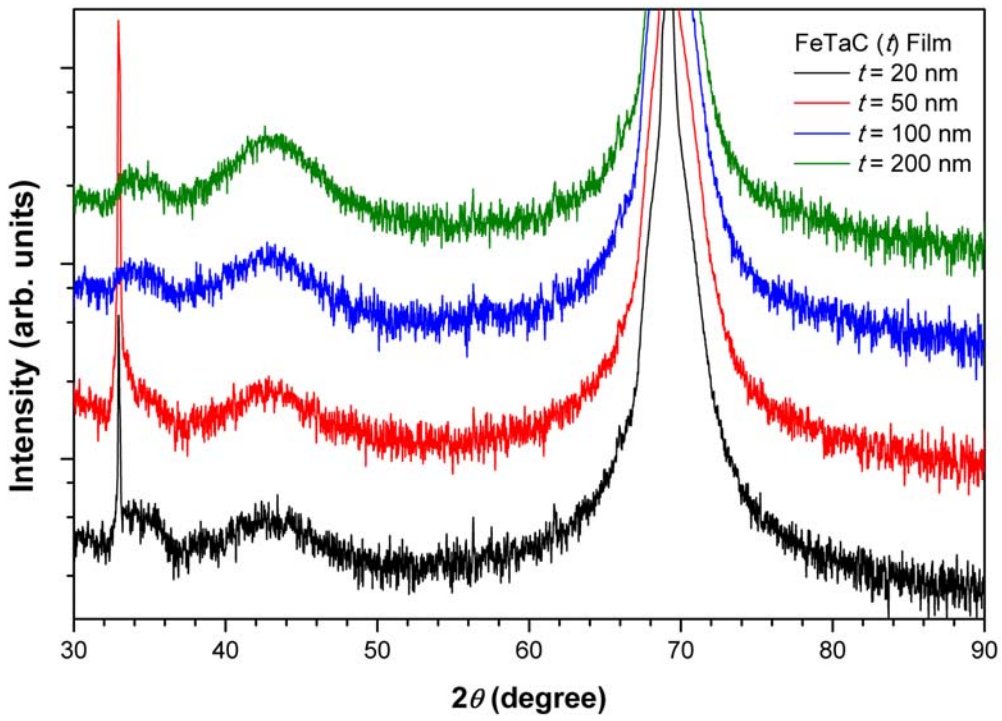

Figure 4.01: Room temperature XRD patterns of FeTaC (t) films with different thicknesses.

(TEM, JEOL 2100 and TECNAI G^2 F30) techniques. Temperature dependent magnetic properties of the films (magnetic hysteresis loops (*M-H*) at different temperatures and thermo-magnetization (*M-T*) data at different constant applied fields) in the temperature range 5 K to 300 K and 20 K to 500 K were investigated by using magnetic property measurement system (MPMS, XL 7, Quantum design) with superconducting quantum interference device (SQUID) magnetometer and vibrating sample magnetometer (VSM, LakeShore Model 7410), respectively. Magnetic domain images and Kerr loops were obtained using magneto-optical Kerr effect (MOKE) microscope (Evico Magnetics Ltd., Germany). Imaging was performed using linearly polarized light with Xenon lamp as source. Magnetic domain imaging was performed in both branches of hysteresis cycle in longitudinal MOKE mode. Hysteresis accompanied by simultaneous imaging has been performed for fields applied both along easy and hard axes (along the film plane), respectively.

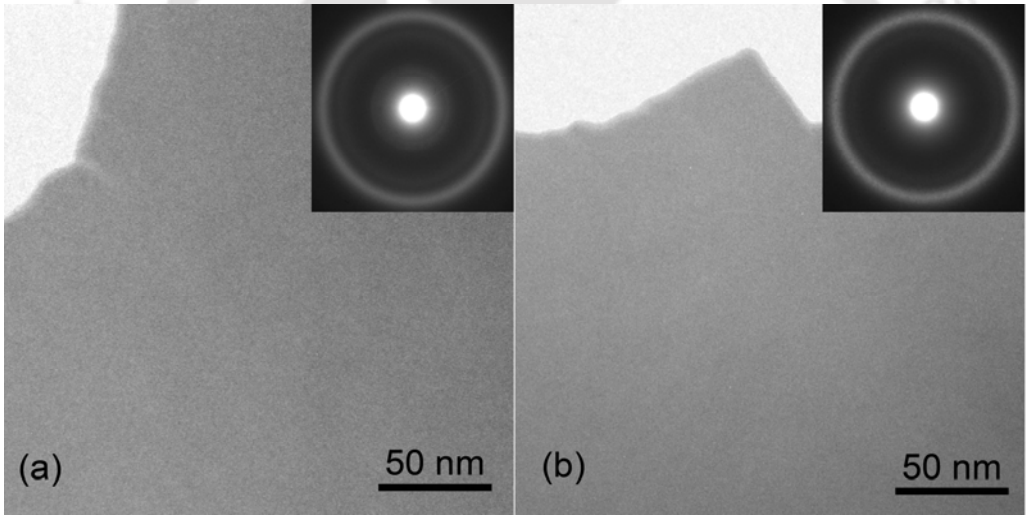

Figure 4.02: Bright-field TEM micrographs and selected area electron diffraction patterns of as-deposited FeTaC (t) films (t = 20 (a) and 200 nm (b)).

4.2. Structural properties:

Figure 4.01 displays the XRD patterns of FeTaC (*t*) films with different thicknesses. All films exhibit broad humps around $2\theta = 43^{o}$ without any sharp peaks characteristic to crystalline phases. This indicates that the films exhibit amorphous structure. It is also to be noted that the crystalline peaks observed at $2\theta = 33.03^{o}$ and $2\theta = 69.19^{o}$ represent Si (200) and Si (400) reflections, respectively, resulting from the thermally oxidized Si substrate [WUYM1998, CHOM2001]. In order to further confirm the local microstructure, all the films were

investigated by TEM technique and the micrographs are depicted in figure 4.02. While the bright-field TEM micrographs reveal the characteristic amorphous microstructure devoid of any local lattice fringes, the selected area electron diffraction patterns display halo diffraction rings corresponding to the amorphous structure. The above results clearly establish that all the as-deposited FeTaC films exhibit amorphous structure.

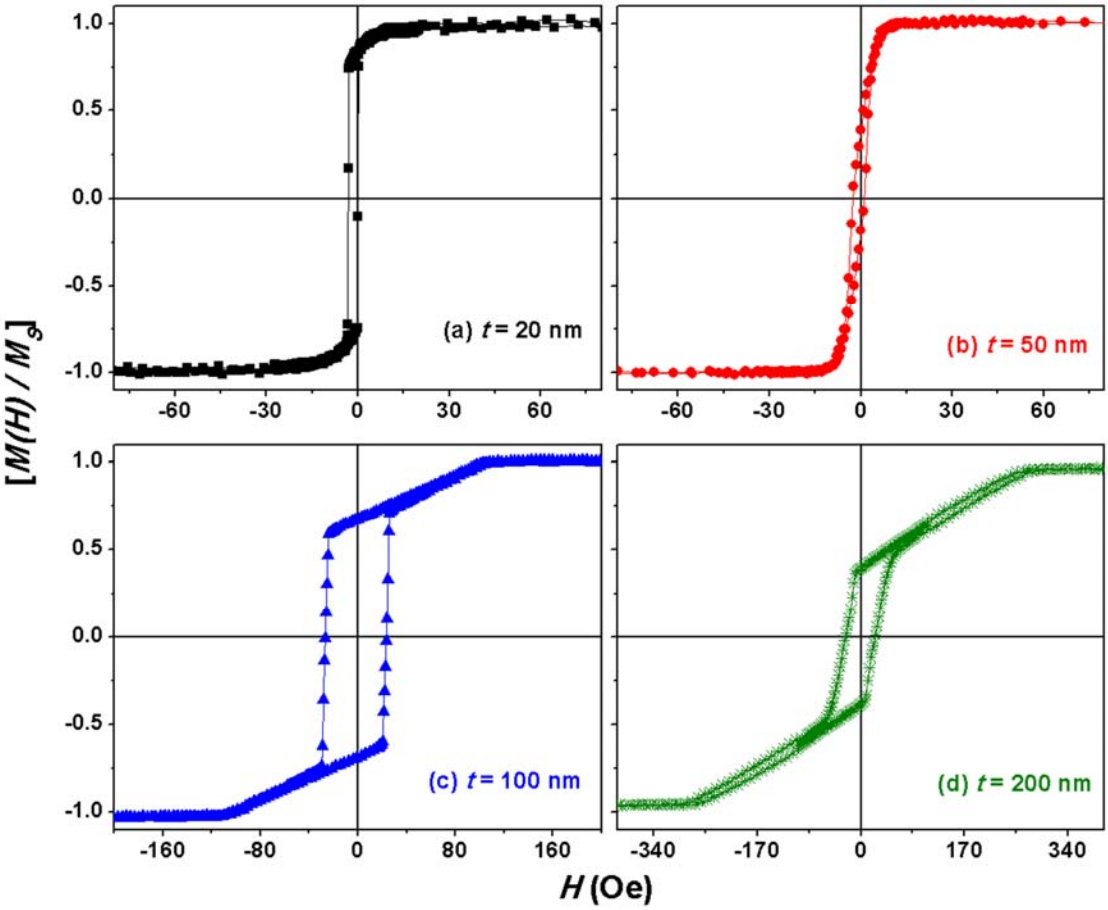

Figure 4.03: Room temperature M–H loops of amorphous FeTaC (t) films.

4.3. Magnetic properties:

4.3.1. Room temperature magnetic properties:

Figure 4.03 displays room temperature normalized in-plane *M-H* loops for FeTaC (*t*) films with different thicknesses. It is observed that FeTaC (20 nm) film exhibits rectangular shaped loop shifted considerably to negative *x*-axis. In addition, the loop has a remanence ratio of around 90% and saturates at low applied magnetic fields. With increasing *t* to 50 nm, the loop shape is changed from rectangular to flat loop characterized by a central range of constant slope combined with a low remanence and a tiny loop around the origin. Interestingly, this

flat loop also saturates at low applied magnetic field. These results suggest that FeTaC (20 nm) film exhibits in-plane anisotropy parallel to the in-plane axis resulting in domains with magnetization parallel to in-plane. The in-plane anisotropy is mainly caused by the formation of aligned ferromagnetic atom pairs due to their strong magnetic exchange coupling during deposition process. The change of the loop shape from rectangular to flat loop may be attributed to the development of magnetic easy axis transverse to the measurement direction which leads to a highly symmetrical structure of transverse domains in the plane. Under the application of external magnetic field, the magnetization vector rotates out of the direction of easy axis, which results in a linear increase of magnetization with field.

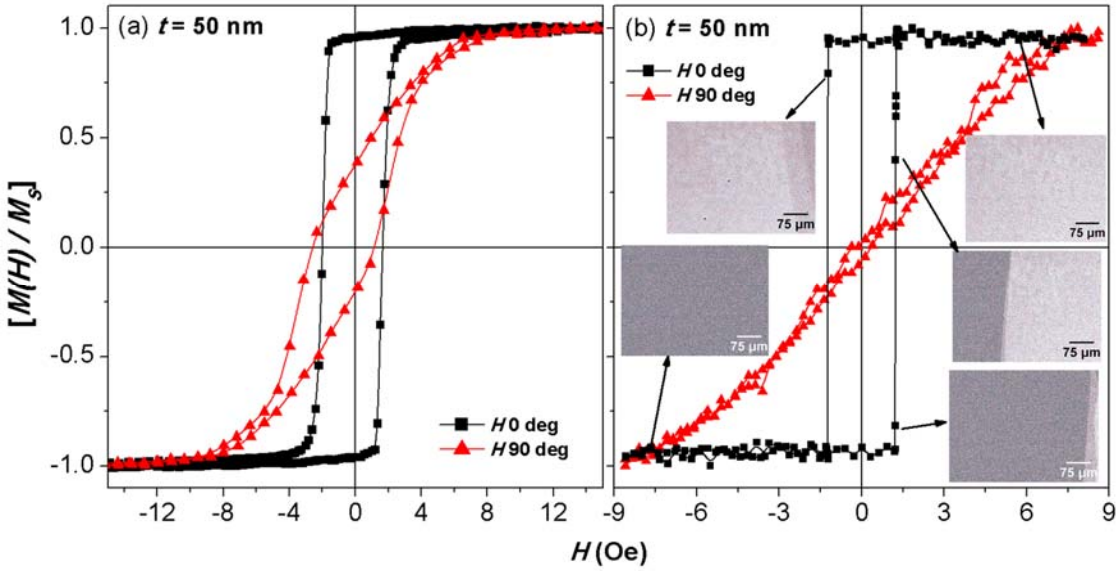

Figure 4.04: Room temperature M–H loops and magnetic domain images of amorphous FeTaC (50 nm) film obtained using (a) VSM and (b) Kerr microscope along two different in-plane directions.

To further investigate the change in the loop shape with increasing the film thickness, *M-H* loops were measured both along length and width directions of the films using VSM and Kerr microscope. While we did not notice any change in the shape of the loops for FeTaC (20 nm) film, FeTaC (50 nm) film exhibited different hysteresis loops as shown in figure 4.04 depending on the measurement direction. As seen in figure 4.04, the loop measured along the length of the film (H = 0 degree) displays a rectangular shaped loop, which changed to flat loop when measured along the width of the film (H = 90 degree). This could be attributed to the magnetic shape anisotropy instigating uniaxial in-plane anisotropy

in the film and hence the change in the shape of the loop from rectangular to flat one might have been caused by the rotation of magnetization vector out of the easy axis direction. This was further confirmed from the Kerr loops and magnetic domain structures obtained using magnetic Kerr microscope as depicted in figure 4.04(b). It is evident from the figure that FeTaC (50 nm) exhibits a clear square loop with low coercivity (H_C) of 1.29 Oe in one direction and a linear variation of magnetization in another direction of the film plane. Also, the domain images show a rapid switching of large sized domains with the applied field. These results confirm the existence of uniaxial in-plane anisotropy in FeTaC (50 nm) film.

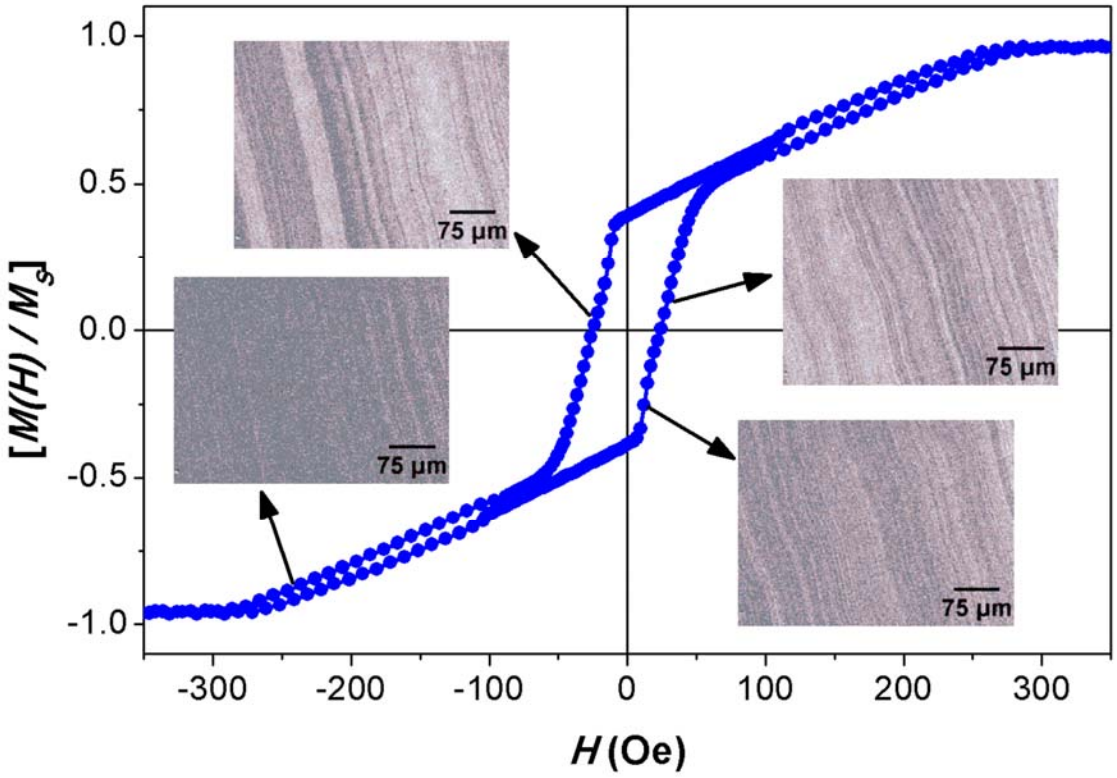

Figure 4.05: Room temperature M–H loop and magnetic domain images of amorphous FeTaC (200 nm) film obtained using VSM and Kerr microscope, respectively.

On the other hand, FeTaC films with thickness above 50 nm exhibit different types of hysteresis loops, which are constituted by two distinct magnetization phases: (i) an in-plane magnetic component accounting for about half of total magnetization, which reverses quickly at fields close to coercive field, and (ii) a linear approach to saturation, whose magnetization rotates progressively under the application of magnetic field in the film plane. The linear region at which the magnetization increases linearly increases with increasing film thickness. The presence of two magnetic phases requires considerably a large applied field (> 100 Oe

for 100 nm and > 250 Oe for 200 nm films) to saturate the films' magnetization as compared to the lower thickness FeTaC ($t \leq 50$) films. This loop shape is often referred as transcritical loop [CHAN2002, CRAU2002, HUBE2009]. The domain structure, obtained using Kerr microscope and shown in figure 4.05 for 200 nm thick FeTaC film, displays a dense stripe domain structure, which is typical for a material having perpendicular anisotropy component

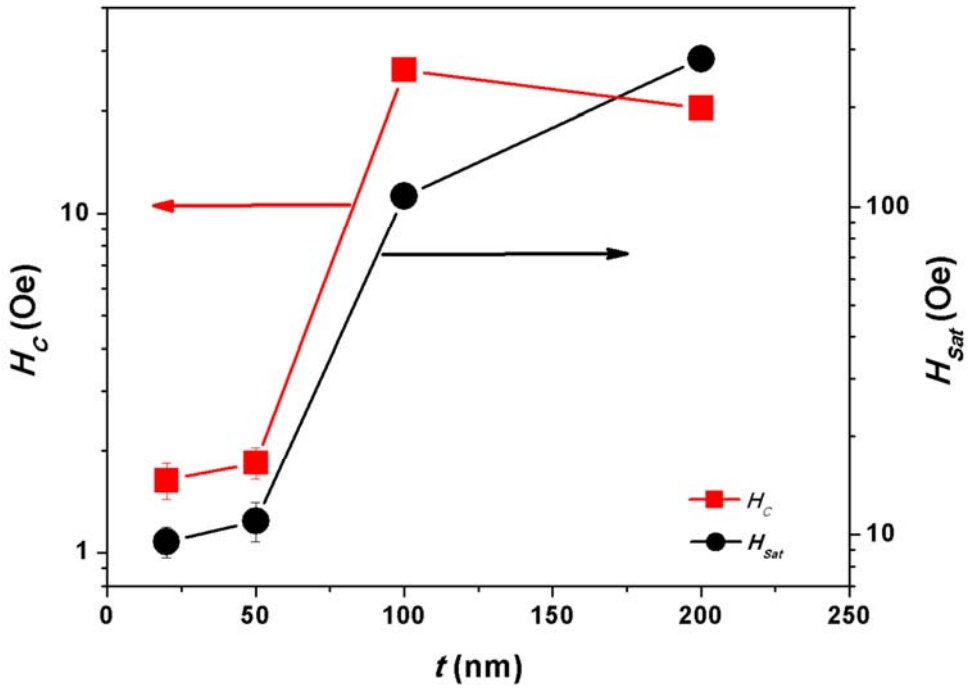

Figure 4.06: The variations of H_C and H_{Sat} with the thickness of amorphous FeTaC (t) films. The line connecting the data points in the figure is guide to the eye only.

[HUBE2009]. Thus, the above results reveal a transition from in-plane orientations of the magnetization to a magnetic stripe domain structure with increasing film thickness above 50 nm. The extracted values of H_C and the field necessary to saturate the magnetization of the films along their plane (H_{Sat}) from the *M–H* loops are summarized in figure 4.06. It is observed that H_C remains almost constant for film thicknesses between 20 and 50 nm followed by a rapid increase to 26 Oe for 100 nm thick film. On further increasing the film thickness to 200 nm, H_C decreases slightly to 20 Oe. The observed variation of H_C with the thickness of the presently investigated films is somewhat similar to the results reported in FeAlSi alloy films [NAKA2001], but contradicts the results reported in CoNbFe [MAPP1991], HITPERM alloy [HUAN2001] and nanocrystalline Fe-Cu-Nb-Si-B alloys [NAOE1998], where the 100 nm thick film had a lowest H_C value, and increasing and/or

decreasing the film thickness away from 100 nm resulted a large change in H_C value. Nevertheless, the observed results suggest that the room temperature magnetic properties of FeTaC ($t \geq 100$) films are degraded drastically. Craus et al [CRAU2002] observed similar behaviour of *M-H* loops and dense strip magnetic domain patterns in FeZrN films. In addition, Youssef et al [YOUS2004] and Liu et al [LIUZ2006] reported similar magnetic properties in FeNi and FeTaN films, respectively. Coisson et al [COIS2008] and Sharma et al [SHAR2006] reported that the transcritical loops are more pronounced in the films deposited at ambient temperature as compared to the films deposited at elevated substrate temperatures. This may be originating from the difficulty of the magnetization reversal by the presence of perpendicular magnetic anisotropy [SAIT1964] induced by the stress [MURA1966, NAKA1997, PRAD2004, SHAR2006, COIS2008, COIS2009] or due to the formation of stripe domain structure depending on the saturation magnetization (M_S) and the perpendicular anisotropy constant ($K_\perp$) [MURA1966, PRAD1997, CRAU2002].

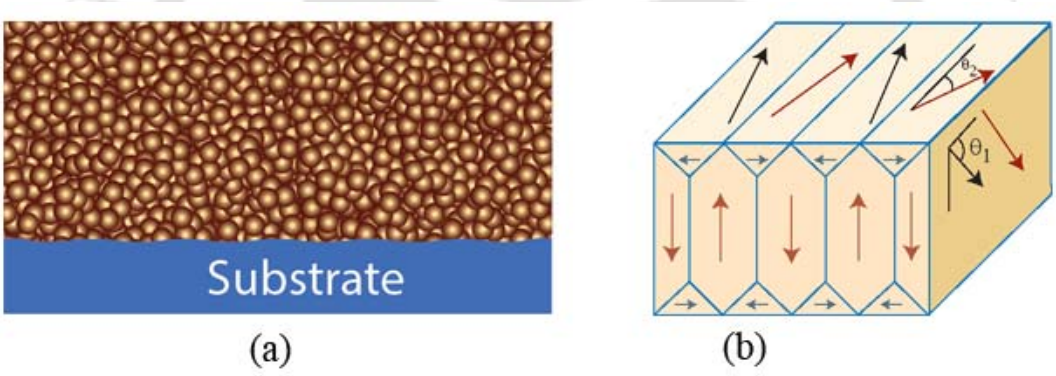

Figure 4.07: Schematic representation of (a) microstructure and (b) magnetic domain structure for amorphous FeTaC ($t \geq 100$) films.

In order to interpret the observed results more qualitatively, we consider that FeTaC films fabricated directly on the oxidized Si substrate has a magnetic layer composed of two layers with different magnetic components, i.e., two-layers model [HAND2005, LIXW2007]. Based on this model, we assume that the initial growth of the films directly on the substrate (bottom layer) results somewhat hard magnetic properties with higher coercivity H_{C1} and moment M_1 due to either the local stress induced on the film by the substrate or the interface diffusion caused by the dynamics of the film deposition and an instantaneous increase of substrate temperature during film deposition [LIXW2007]. On the other hand, the remaining film (upper layer) grown continuously on top of the bottom layer has soft magnetic properties

with lower coercivity H_{C2} (< H_{C1}) and moment M_2. This two-layers structure provides a considerable shift in the *M-H* loop for the low thickness films ($t \leq 50$ nm) as the magnetization reversal of the upper layer is significantly controlled by the bottom layer. The observation of *M-H* loop shift in the presently investigated films is in good agreement with the earlier reported results on similar soft magnetic amorphous films [DIAZ2002, LIXW2007]. Note that the relative shift of the *M-H* loop to the negative *x*-axis decreases by increasing film thickness from 20 to 50 nm. On further increasing the film thickness to 100 and 200 nm, the role of the bottom layer on the magnetization reversal of the upper layer is not realized noticeably due to larger volume fraction between the upper and bottom layers.

On the other hand, the transcritical loops observed in FeTaC ($t \geq 100$) films are correlated to the development of perpendicular anisotropy component resulting from stress quenched in during the film deposition or atomic relaxation. As it is known that the orientation of magnetization in disordered system, as schematically shown in figure 4.07(a), is determined mainly by the magnetoelastic and shape anisotropy terms, and the magnetoelastic term is coupled to the interplay among the stress and magnetization, the formation of stripe domain pattern beyond critical thickness is mainly controlled by the stress. Among the several possible domain structures [HUBE2009], the observed domain structure for FeTaC (200 nm) film can be attributed to weak dense stripe domains in which the neighbouring stripes have aligned along in-plane direction, but their perpendicular components alternate up and down as demonstrated in figure 4.07(b). This can be well interpreted by using the model proposed by Craus et al [CRAU2002] following the model demonstrated by Murayama [MURA1966] and Alvarez-Prado et al [PRAD1997, PRAD2004]. This procedure allows one to ultimately determine the values of $K_{\perp}$ and optimum domain wall width (w). According to the Craus et al's model [CRAU2002], the spins in the bulk domains make an angle θ_1 with the surface and the closure domain spins on the surface make an angle θ_2 with the long axis of the stripes (see figure 4.07(b)). The values of θ_1 can be calculated either from Mössbauer data or from the remanence magnetization data measured using the VSM under the condition that the magnetization in the closure domains remains perpendicular to the direction of the applied magnetic field such that $\theta_2 = \pi/2$. The values of θ_1, playing a crucial role on the magnetic properties of the thicker films, can vary between 0 and 90° depending on the values of fractional change in the remanence (M_r) magnetization with respect to saturation magnetization (M_S) [CRAU2003]. Moreover, there exists a critical thickness, as given in eqn.(4.01) [PRAD1997, COIS2009, HUBE2009],

above which the existence of stripe domains is strongly depend on the values of M_S and $K_\perp$ [MURA1966, PRAD1997].

$$t_{critical} = \left(\frac{2\pi}{1 - \frac{\mu_0 M_S H_{Sat}}{2K}}\right)\sqrt{\frac{A}{K_\perp}} = \left(\frac{2\pi}{1-S}\right)\sqrt{\frac{A}{K_\perp}} \qquad (4.01)$$

where, $t_{critical}$ is critical thickness above which the stripe domain appears, A is exchange stiffness constant taken as 1×10^{-11} J/m, S is the dimensionless quantity, and μ_0 is absolute permeability. It may be noted that the values of H_{Sat} and M_S can be obtained directly from the *M-H* loops. Since we observed the existence of stripe domain structure in the presently investigated FeTaC films, the values of $K_\perp$ were determined by substituting the values of H_{Sat}, M_S, A and the total thickness of FeTaC film (t) in eqn.(4.01). Similarly, the domain wall width (w) is calculated by assuming a Landau domain structure [STIL2005], which is compatible when the sample thickness is larger than $\sqrt{A/K_\perp}$, as in the present case, using

$$w = 2\sqrt{2t\sqrt{\frac{A}{K_\perp}}} \qquad (4.02)$$

The determined values of θ_1, $K_\perp$ and w are found to be 24°, 2.62×10^4 J/m^3 and 128 nm, and 50°, 2.19×10^4 J/m^3 and 185 nm for 100 and 200 nm thick films, respectively. The obtained values of $K_\perp$ and w are in close agreement with those values ($K_\perp$ = 2.18×10^4 J/m^3 and w = 179 nm) reported for the FeSiB (230 nm) alloy thin film [COIS2008]. While the determined values of $K_\perp$ are almost similar for both 100 nm and 200 nm thick FeTaC films at room temperature, the values of H_{Sat} depend strongly on film thickness. This can be attributed to the large variation in bulk domain angle (θ_1) with increasing film thickness.

4.3.2. Low temperature magnetic properties:

To understand the thickness dependent magnetic nature of FeTaC films in more details, we measured *M-H* loops at different temperatures in the temperature range 20 K to 300 K using VSM and the *M-T* data under zero-field-cooled (ZFC) and field-cooled (FC) conditions in the temperature range 5 K to 300 K using MPMS. Figure 4.08 illustrates the expanded view of temperature dependent *M-H* loops measured along the film plane for FeTaC (t) films. While the nature of the loops does not change with the temperature for a particular film, the values

of H_C and H_{Sat} increase with decreasing temperature. Interestingly, the shifting of the *M-H* loops with respect to temperature is more significant for FeTaC (20 nm) film. This could be understood based on the two-layers model [HAND2005] as discussed earlier in this chapter. The observation of *M-H* loop shift in the presently investigated films is in good agreement with the earlier reports on similar soft magnetic amorphous films [DIAZ2002, LIXW2007]. These results suggest that the temperature dependent magnetic properties of the hard layer at the interface between the substrate and film play a significant role on the resulting magnetic properties of the thinner films. However, the role of the bottom layer is not realized noticeably for the films at larger thicknesses.

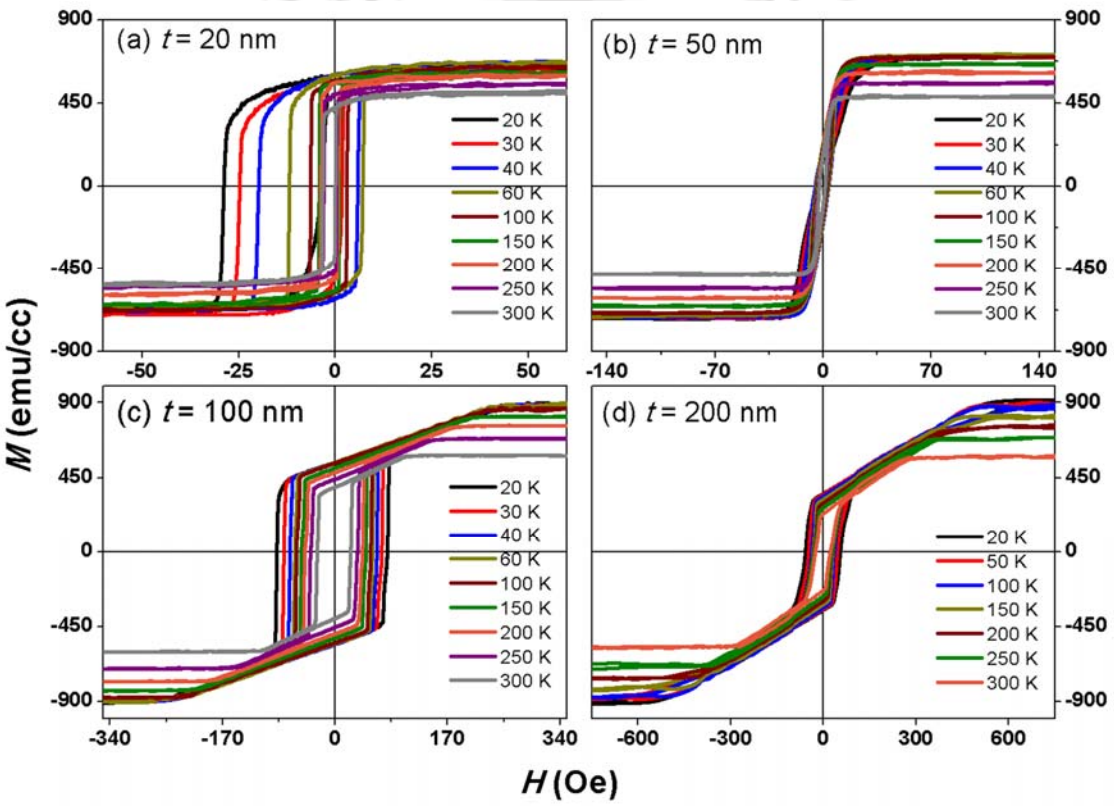

Figure 4.08: M–H loops measured at different temperatures (20 K – 300 K) for amorphous FeTaC (t) films.

Figure 4.09 displays the extracted values of H_C and M_S from the *M-H* loops at different temperatures. As expected for typical ferromagnetic materials, the values of H_C and M_S increase with decreasing temperature from 300 K to 20 K. However, the relative variation of the magnetic parameters with temperature depends strongly on the thickness of the films. For example, $H_C(T)$ of 20 nm thick film displays a slow variation with temperature down to 100 K from 300 K, but exhibits a large increase in H_C below 100 K. This could be correlated

to the enhanced hard magnetic properties of bottom layer at lower temperatures. As the nature of the *M-H* loops of FeTaC films with thickness larger than 100 nm does not change with temperature, the values of $K_{\perp}$ were determined at different temperatures following the eqn.(4.01) and extracting the values of H_{Sat} and M_S from *M-H* loops measured at different temperatures. Figure 4.10 depicts the variations of $K_{\perp}$ and H_{Sat} for the FeTaC ($t \geq 100$) films. It is observed that even though the room temperature values of $K_{\perp}$ are almost similar for 100 and 200 nm thick films, their temperature dependence strongly depends on the thickness of the films. This is mainly due to the strong temperature dependent variation in H_{Sat} values with thickness resulting from the large variation in the angle between the bulk and surface domains as demonstrated in figure 4.07(b).

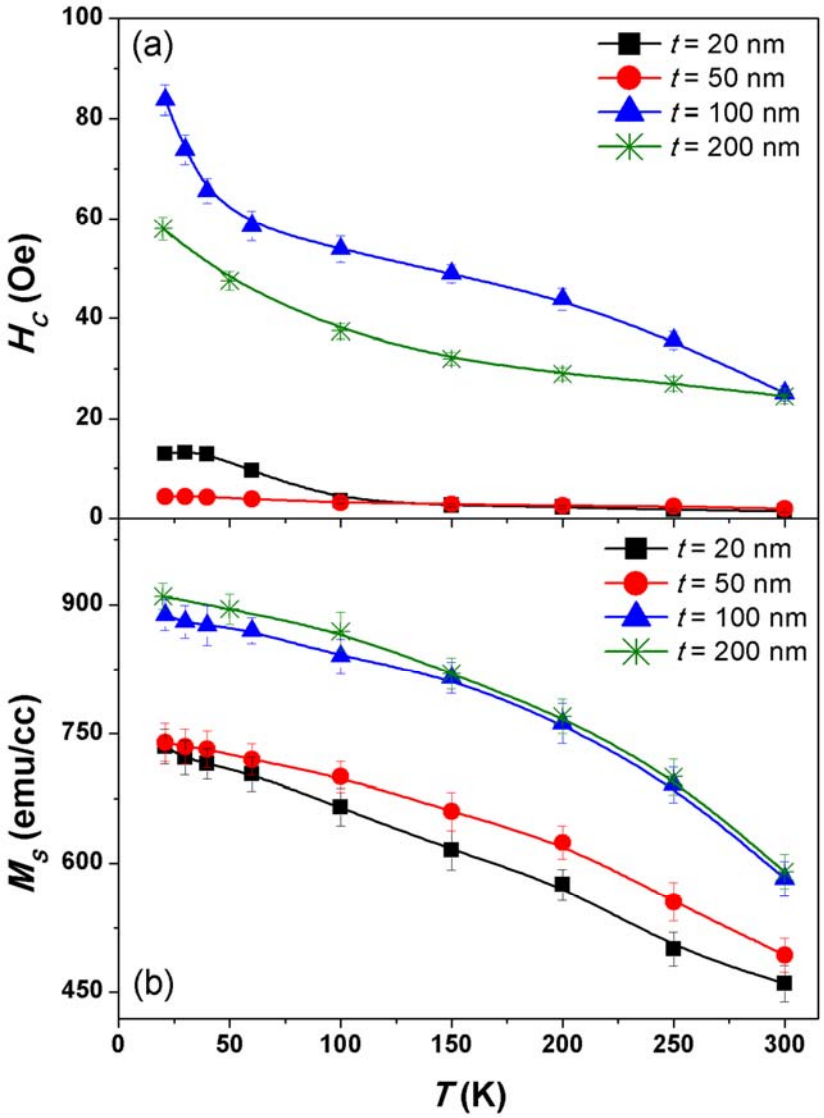

Figure 4.09: Temperature dependent (a) H_C and (b) M_S for amorphous FeTaC (t) films.

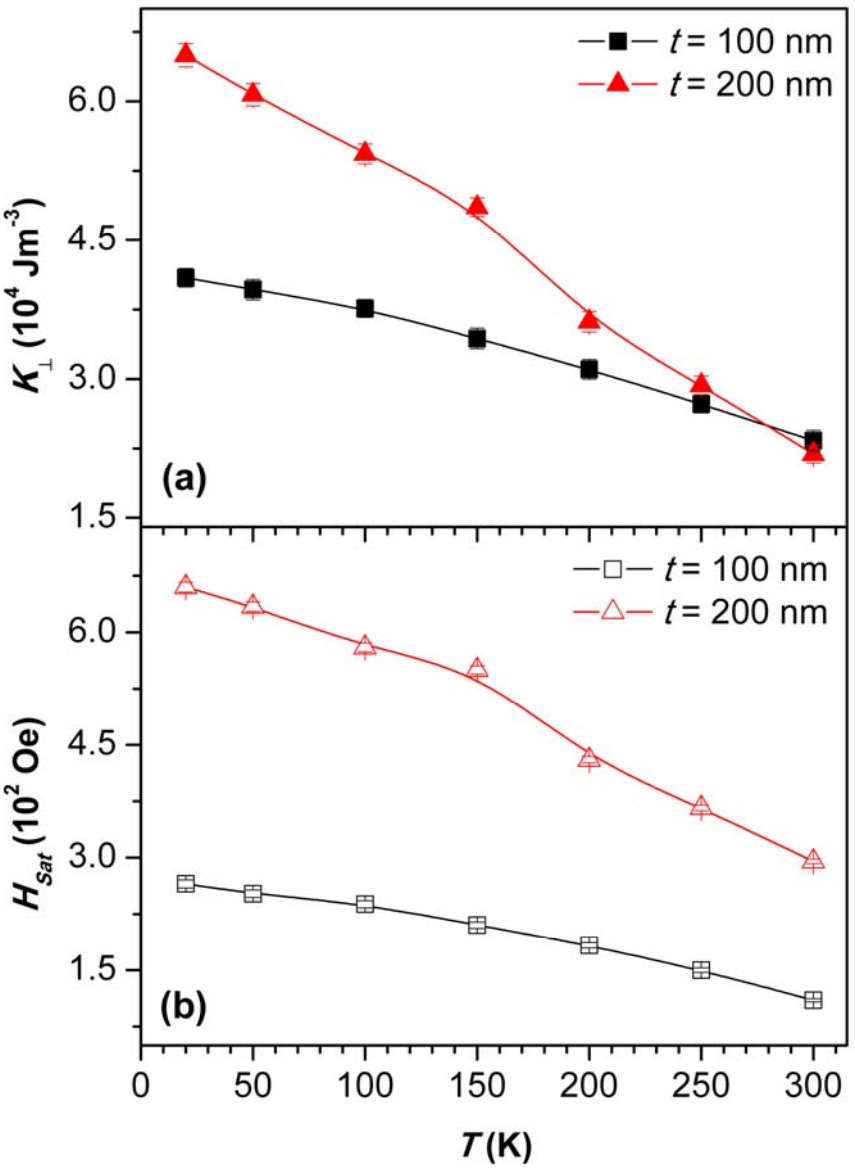

Figure 4.10: Temperature dependent (a) perpendicular anisotropy constant ($K_\perp$) and (b) H_{Sat} for amorphous FeTaC ($t \geq 100$) films.

Figure 4.11 shows normalized *M-T* data measured at 100 Oe applied field under ZFC and FC conditions. In these measurements, the sample was initially cooled down to 5 K under zero-field condition. Magnetization was then recorded as the sample was heated to room temperature under a constant field applied (100 Oe) along the film plane (ZFC process). Subsequently, the sample was again cooled under the same constant applied field of 100 Oe to 5 K and then the magnetization was recorded as the sample was heated under the same in-plane applied field to room temperature (FC process). *M-T* curves depicted in figure 4.11

reveal the following features: (1) For the FeTaC (20 nm) film, the magnetization data measured under ZFC and FC conditions increase gradually with decreasing temperature from 300 K and a very minor bifurcation between the ZFC and FC data was observed below 10 K. (2) A similar behaviour was observed for FeTaC (50 nm) film, but the bifurcation between ZFC and FC data was not observed within the experimental accuracy even down to 5 K. (3) With increasing the film thickness more than 50 nm, both ZFC and FC curves show different

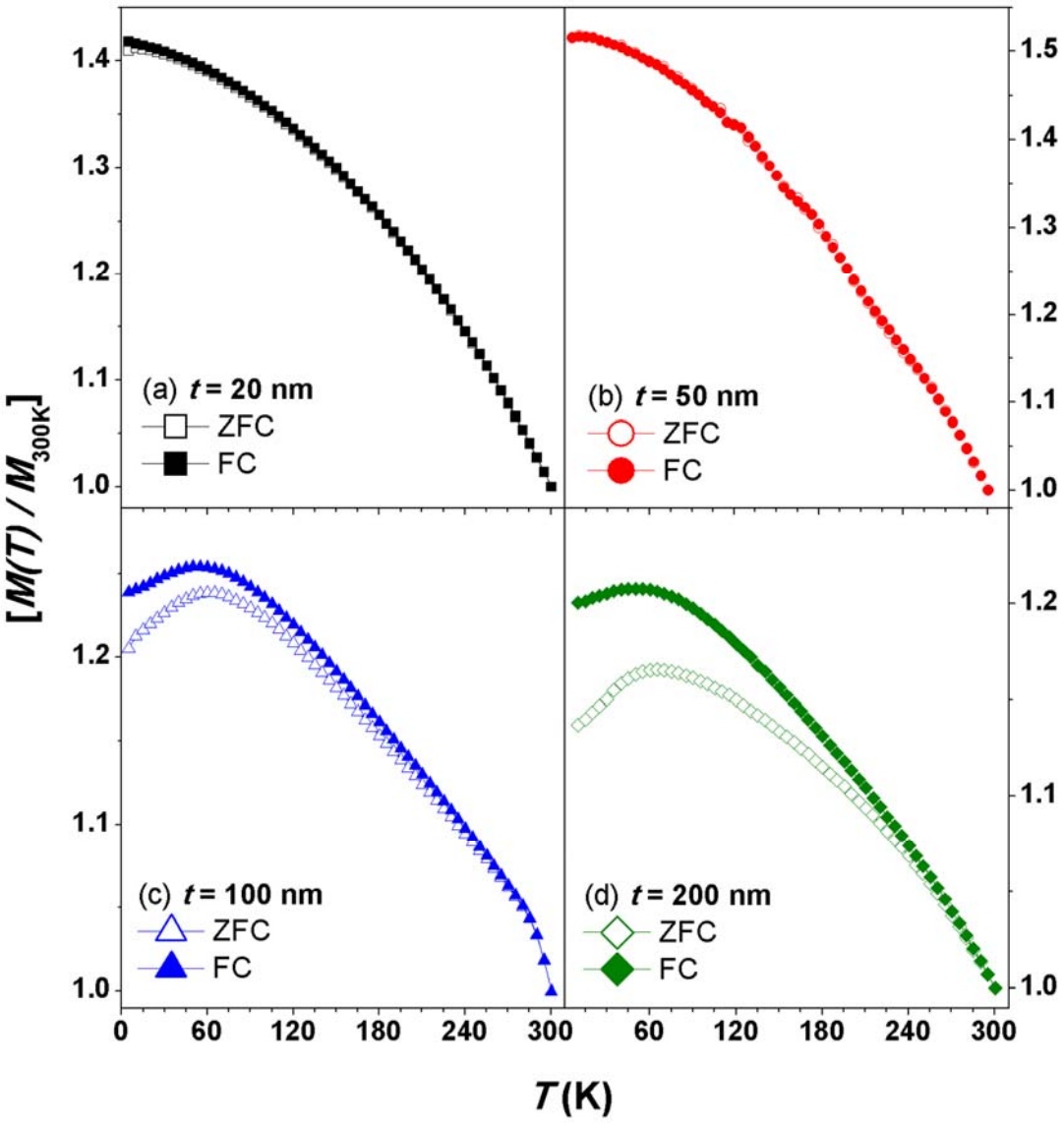

Figure 4.11: Temperature dependent magnetization data measured at an applied field of 100 Oe under ZFC and FC conditions for amorphous FeTaC (t) films. The magnetization data is normalized with respect to room temperature magnetization for each film to show the relative variation of magnetization with temperature.

behaviours, i.e., for FeTaC (100 nm) film, a sharp increase in magnetization down to 290 K followed by a gradual increase in magnetization up to 70 K was observed. On further lowering the temperature, the magnetization decreases leaving a maximum around 60 K. Interestingly, the bifurcation between the ZFC and FC curves was initiated around 250 K and both the curves deviate away from each other down to 5 K. The amount of deviation between the ZFC and FC curves increases with decreasing the temperature, and (4) For FeTaC (200 nm) film, the bifurcation was observed below 270 K and the amount of deviation between the ZFC and FC curves increased largely as compared to FeTaC (100 nm) film. These observations indicate that the existence of in-plane anisotropy with magnetization parallel to the film plane in FeTaC (20 nm) film results good soft magnetic properties. Therefore, the application of 100 Oe external magnetic field is sufficient to saturate the film's magnetization both in ZFC and FC cycles and hence no difference in magnetization data obtained under the ZFC and FC conditions was observed. Also, FeTaC (50 nm) film exhibits a transverse domain structure in the film plane, which could be easily saturated at low applied magnetic field (< 50 Oe) even at low temperature as demonstrated earlier from the temperature dependent *M-H* loops (see figure 4.08). Therefore, as shown in figure 4.11(b), the magnetization data obtained under ZFC and FC conditions did not show any bifurcation between them. On the other hand, when film thickness increased above 50 nm, the perpendicular magnetic anisotropy in the films is enhanced due to the quenched in stress and the large variation in the angle between the bulk and surface domains resulting random (non-collinear) arrangement of spins in the films. This increases the magnetic disorder in the film and needs relatively large applied magnetic field (> 100 Oe) to obtain the saturation (see figure 4.08). Therefore, the ZFC and FC curves obtained under low applied magnetic fields of 100 Oe show significant variations in their magnetization behaviours with decreasing temperature and resulting bifurcation between them. Hence, the presence of bifurcation between the ZFC and FC data can be attributed to the existence of magnetic disorder either due to the non-collinear spin arrangements in Fe rich FeTaC films [HANS1991, CAST19972, HERN2002] or due to the existence of magnetic anisotropy in the system. The observed results suggest that the magnetic disorder is significantly low or almost negligible in the films with thickness up to 50 nm due to the formation of in-plane magnetization structure, but increases with increasing the film thickness more than 50 nm. Thus, the existence of magnetic disorder in larger thickness films also plays a significant role on controlling the magnetic properties.

4.3.3. High temperature magnetic properties:

To study the magnetic properties of the films up to critical temperatures, high temperature *M-T* data were measured at a constant applied field of 500 Oe for all the films using VSM magnetometer. Figure 4.12 illustrates *M-T* data above room temperature, thermal derivative of magnetization (inset 4.12(a)) and inverse susceptibility (inset 4.12(b)) above Curie temperature (T_C) for FeTaC (*t*) films. In order to compare all the magnetization data in a single graph, *M-T* data were normalized with respect to the room temperature magnetization data of that particular sample. It could be clearly seen from the Figure 4.12 that (a) FeTaC (200 nm) film shows an incessant decrease in magnetization up to 410 K. The rate of decrease of magnetization decreases with the further increase in temperature. (2) A similar behaviour was observed for FeTaC (100 nm) film but with a slight shift in the magnetization

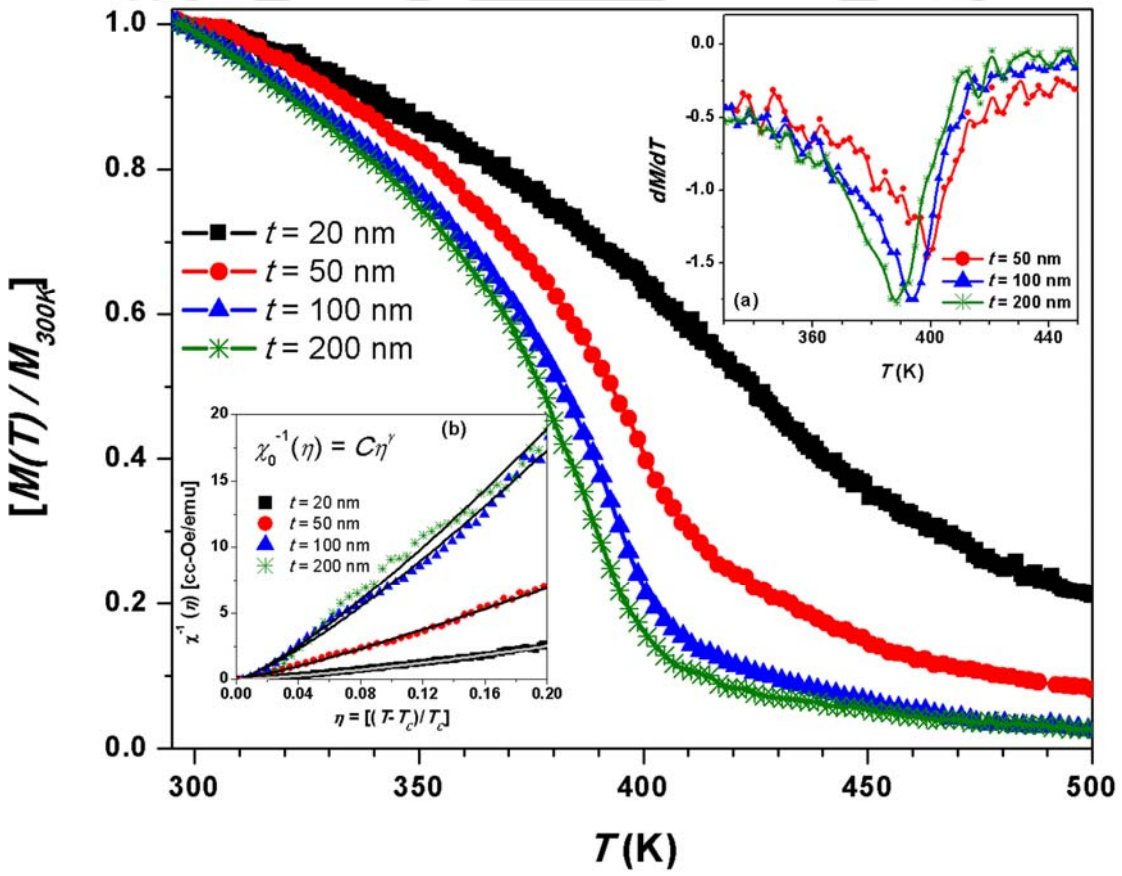

Figure 4.12: M-T data measured at an applied field of 500 Oe for amorphous FeTaC (t) films. Inset: (a) thermal derivative of magnetization as a function of temperature and (b) inverse susceptibility above Curie temperature as a function of reduced temperature range, η. The solid line passing through the data points is the best fit obtained using eqn.(4.03).

curve towards high temperature region around T_C. (3) With decreasing the film thickness to 50 nm, the magnetization curve shifted considerably towards higher temperature along with a non-zero magnetization up to 500 K. (4) On further lowering the thickness to 20 nm, the magnetization decreases very slowly with temperature as compared to other films. (5) The values of T_C were obtained from the thermal derivative of the magnetization data as depicted in inset (a) of Figure 4.12 and listed in Table 4.01. Interestingly, the values of T_C of FeTaC films increase marginally with decreasing film thickness. The above results clearly intimate that the magnetization data obtained at 500 Oe applied field for 200 nm and 100 nm thick FeTaC films exhibit a clear magnetic phase transition from ferromagnetic state to paramagnetic state above 380 K. As a result, the magnetization data above T_C approaches to almost zero values. On the other hand, FeTaC films with 50 and 20 nm thicknesses exhibit a magnetization value (at 500 K) of about 8% and 20%, respectively, with respect to their room temperature magnetization. This suggests that in low thickness films, the magnetic phase transition from the ferromagnetic to paramagnetic state is not completed entirely and depends strongly on the film thickness. This could be explained using the two-layers model as discussed earlier. According to this model, the magnetic contribution from the bottom hard layer on the magnetization reversal of the upper soft layer is more significant only for the low thickness films (< 50 nm). This reveals that with increasing the temperature above 300 K, the magnetization of the upper layer is reversed dominantly resulting a large drop in the magnetization value between 350 K and 450 K. The rate of decrease in magnetization with increasing temperature decreases with decreasing the film thickness from 50 to 20 nm. This could be attributed to the slow reversal behaviour of the bottom layer, which is rather imperceptible to the temperature due to either the interface diffusion [LIXW2007] or the local stresses [GORR2009]. The rough estimation of the bottom layer thickness, by using the relative magnetization value at 500 K and assuming that the magnetization at that temperature is only due to the bottom layer, turns out to be around 2 - 4 nm. This is reasonably in good agreement with the results of cross sectional TEM analysis at the interface between the substrate and film reported on similar amorphous alloy films [LIXW2007].

To understand the effect of film thickness on the magnetic phase transition behaviour, the inverse susceptibility data in the critical region just above T_C were analyzed using simple power law analysis as described below,

$$\chi_0^{-1}(\eta) = C|\eta|^{\gamma} \qquad \eta > 0 \tag{4.03}$$

where η [=$(T-T_C)/T_C$] is reduced temperature range, γ is critical exponent for the magnetic susceptibility and C is critical amplitude. Inset (b) of figure 4.12 demonstrates the inverse susceptibility data as a function of reduced temperature for all the films and the applicability of the fit is represented by solid lines passing through the data points using eqn.(4.03) on the susceptibility data. The resulting parameters from the fit analysis are summarized in Table 4.01 along with the predicted values of critical exponents for the theoretical models of mean field, 3D Heisenberg model and 3D Ising model and other experimental data on similar amorphous systems for comparison. The critical exponent values obtained for the films with thickness between 50 and 200 nm are in good agreement with the value predicted by 3D Ising model and the experimental values reported on similar systems [YAMA1975, KYPR1996]. On the other hand, for the 20 nm thick film, the observed exponent value is close to the 3D Heisenberg model. We have tried to examine the possible explanation for such thickness dependent critical exponents in the presently investigated films. It is well known that the values of critical exponents depend not only on the lattice dimensionality of the spin system and number of components of order parameter, but also depend on the range of microscopic interactions responsible for the phase transition and the transition region considered for the analysis of critical exponents. The effect of dimensionality on the critical behaviour is not expected in the presently investigated samples as the thicknesses of the films are larger in size and do not fall into dimensionality cross over [DUNL2004]. Although the effect of range of microscopic interactions [KARM2006] and the presence of defects [BACK1995] are expected to alter the magnetic phase transition behaviour, their contribution in the presently investigated samples may be discarded as the correlation length is much larger. Therefore, the deviation of critical exponent from the 3D Heisenberg to 3D Ising model could mainly be attributed to the development of perpendicular anisotropy causing a cross over effect [KIMD2002].

Table 4.01: Curie temperature, the values of fit parameters obtained from power law analysis and the comparison of critical exponents with different theoretical models and earlier reports on similar systems.

Sample thickness (nm)	***C* (cc-Oe/emu)**	**γ**	**T_C (K)**
200	141.3	1.248	388
100	130.5	1.254	393

50	47.9	1.291	399
20	22.0	1.347	~ 410
Mean Field theory [PAPO2006]	-	1.000	-
3D Heisenberg	-	1.336	-
3D Ising [PAPO2006]	-	1.240	-
Fe-P-C [YAMA1975]	-	1.300	-
Fe-Cr-B-Si [KYPR1996]	-	1.286	-

4.4. Summary:

The structural and magnetic properties of FeTaC (t) films with different thicknesses prepared directly on thermally oxidized Si substrates at ambient temperature using DC magnetron sputtering technique were systematically carried out in this chapter. The salient features of FeTaC films from the current investigations are as follows:

- Amorphous FeTaC films with different thicknesses (t = 20 – 200) could be prepared directly on thermally oxidized Si substrate at ambient temperature using DC magnetron sputtering technique.
- Amorphous nature of all the as-deposited FeTaC films was confirmed through XRD and TEM studies.
- FeTaC ($t \leq 50$) films exhibit soft magnetic nature due to the in plane orientation of the magnetization.
- Increasing the film thickness above 50 nm degraded the soft magnetic properties due to the transition from in-plane magnetization to stipe domain magnetic structure caused by the growth of the perpendicular anisotropy.
- The shift in the temperature dependent M-H loops of the FeTaC ($t \leq 50$) films is discussed using two-layers model.
- Although the room temperature value of $K_{\perp}$ is almost similar for 100 and 200 nm thick films, their temperature dependence strongly depends on the thickness of the films.

- Low temperature thermo-magnetization data reveal that the magnetic disorder increases with increasing the film thickness above the critical value.
- Curie temperature of FeTaC (*t*) films increases marginally and the magnetic susceptibility critical exponent displays a cross over from 3D Ising model to 3D Heisenberg model values with decreasing the FeTaC thickness.
- The observed results were discussed on the basis of the development of perpendicular anisotropy, magnetic disorder and transition from in-plane magnetization to stripe domain structure with increasing FeTaC film thickness.

Chapter 5

Structural and magnetic properties of multilayer FeTaC / Ta films

The thickness dependent magnetic properties of FeTaC single layer films discussed in chapter 4 revealed that soft magnetic properties depend strongly on the film thickness and degrade in films of larger ($t \geq 100$ nm) thicknesses. This is mainly due to the growth of perpendicular anisotropy, which results in the formation of dense strip domain structure. As a result, the orientation of magnetization is randomized by the effective anisotropy with a negative influence on the soft magnetic properties. It is well known that the soft magnetic thin films with low H_C and high relative permeability are required in applications such as magnetic recording [KHIZ20041, KHIZ20042, PIRA2007], communication devices [SHIR1990] and automotive industry. In these applications, the ferromagnetic thin film is used either as a magnetic flux guide or as magnetic flux amplifier at high frequency applications, provided these films have a simple magnetic domain structure with the magnetization oriented at a particular direction [RIET1997, KAZI2013]. Therefore, the control of domain structure, orientation of magnetization in a particular direction and the understanding of the resulting magnetic properties are very much important in the process of optimizing the performance of such films for device applications. In this chapter, we shall demonstrate that the degradation of in-plane soft magnetic properties observed in FeTaC ($t \geq 100$) single layer films can be systematically controlled by fabricating stacks of thin FeTaC films decoupled by suitable non-magnetic (Ta) spacer layers. This chapter will cover the structural and magnetic properties of multilayer structured [[FeTaC (y nm)/Ta (x nm)]$_n$/FeTaC (y nm)] films in two sections: While the first section describes the effect of number of multilayers ($n = 0 – 4$) on the magnetic properties by fixing the space layer thickness at 1 nm, the second section

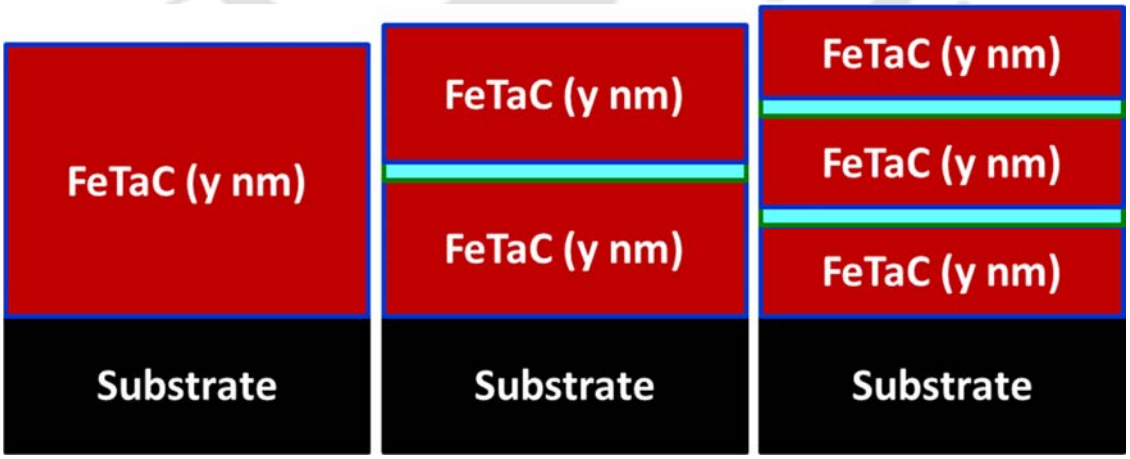

Figure 5.01: Schematics of multilayer [[FeTaC (y nm)/Ta (1 nm)]$_n$/FeTaC (y nm)] films with n = 0, 1 and 2.

focuses on the spacer layer thickness variation and temperature driven magnetic properties in multilayer structured thin films with $n = 3$.

5.1. Experimental details:

Amorphous multilayer [[FeTaC (y nm)/Ta (x nm)]$_n$/FeTaC (y nm)] films were deposited directly on thermally oxidized Si substrates at ambient temperature using DC magnetron sputtering technique as schematically shown in figure 5.01 using targets of FeTaC and Ta loaded in two separate magnetron guns. Here, x is the thickness of the Ta spacer layer varied between 1 nm and 6 nm, and the individual FeTaC layer thickness (y) in multilayers was controlled using the relation $y = 200/(n+1)$, where n is number of Ta spacer layers inserted between FeTaC layers and varied systematically between 0 and 4. The total thickness of FeTaC layer in multilayer films is fixed at 200 nm. The substrate was loaded on the rotating substrate holder and moved to the respective targets of FeTaC and Ta after making each layer sequentially. The base pressure of the chamber was better than 10^{-6} Torr. The optimized sputtering Ar gas pressures for FeTaC and Ta films were fixed at 1 mTorr and 10 mTorr, respectively. The deposition rate of both FeTaC and Ta were calibrated by using ex-situ

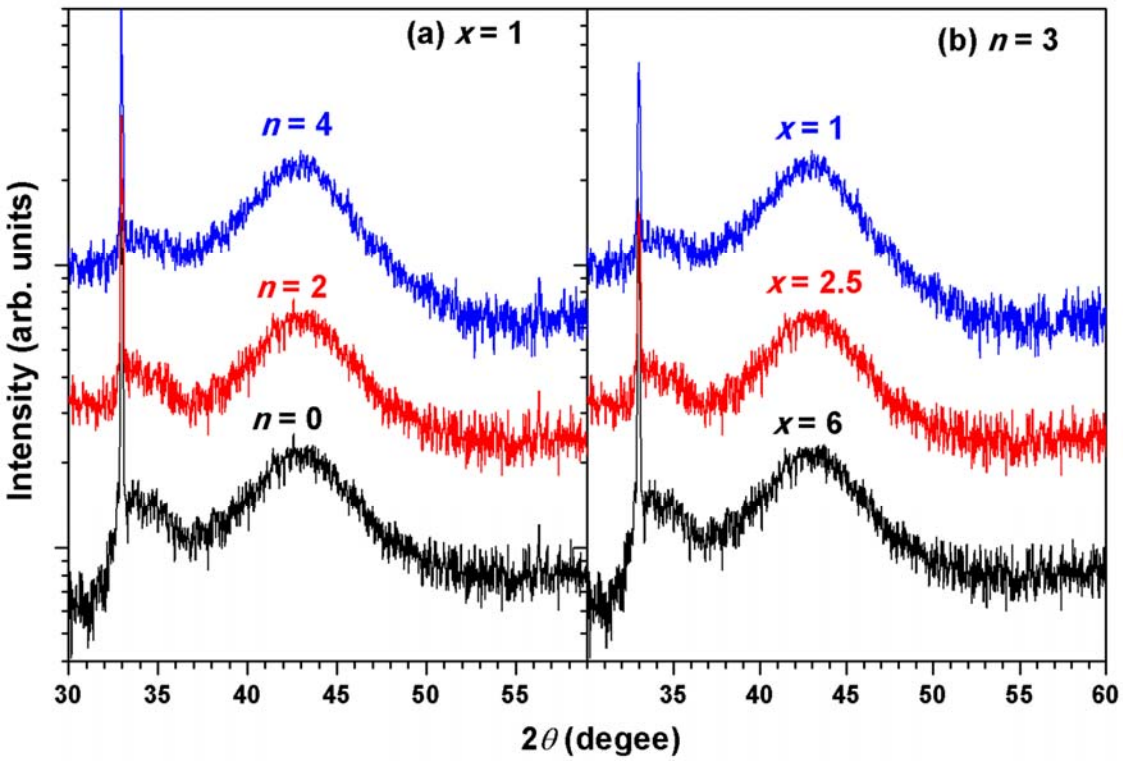

Figure 5.02: Room temperature XRD patterns of as-deposited multilayer [[FeTaC (y nm)/Ta (x nm)]$_n$/FeTaC (y nm)] films with different (a) n and (b) x values.

surface profilometer (Vecco, Dektak-150) as described in section 3.1.2. Amorphous nature of the films was confirmed by X-ray diffraction (XRD) using a high power Rigaku TTRAX III diffractometer with Cu-K_α radiation and transmission electron microscopy (TEM, JEOL 2100 and TECNAI G^2 F30) techniques. Temperature dependent magnetic properties of the films in the temperature range 5 K to 500 K were investigated by using magnetic property measurement system (MPMS XL 7, Quantum Design, USA) with superconducting quantum interference device (SQUID) magnetometer and vibrating sample magnetometer (VSM, LakeShore Model 7410, USA).

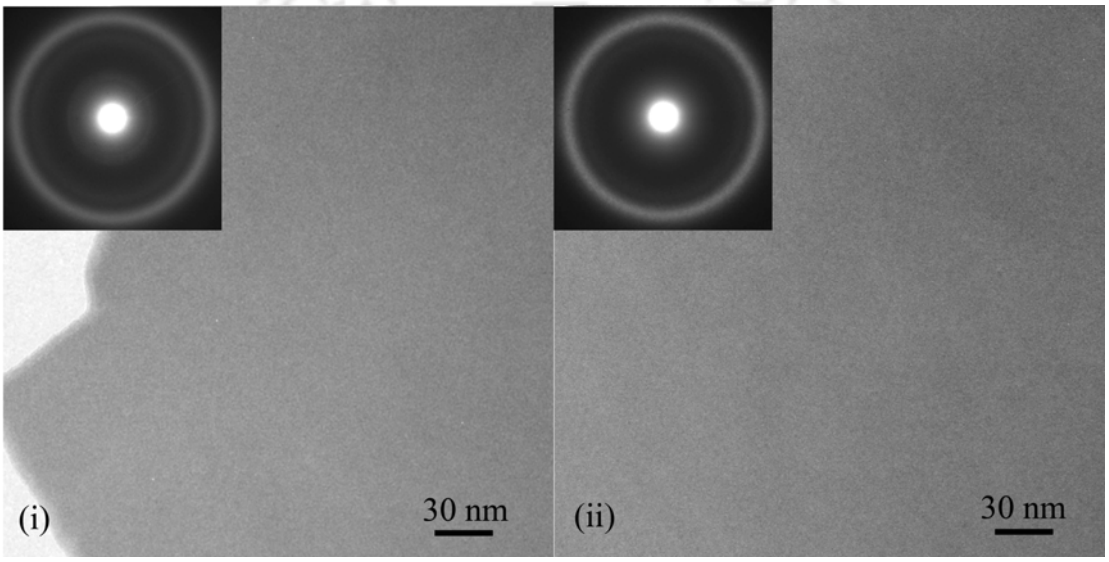

Figure 5.03: Bright-field TEM images and selected area electron diffraction patterns of as-deposited multilayer [FeTaC (50 nm)/Ta (x nm)]$_3$/FeTaC (50 nm)] films with (i) x = 0 and (ii) 2.5.

5.2. Structural properties:

The structural properties of multilayer [[FeTaC (y nm)/Ta (x nm)]$_n$/FeTaC (y nm)] films characterized using XRD and microscopic techniques are depicted in figures 5.02 and figure 5.03, respectively. All the films exhibit broad humps around 2θ = 43º without any sharp peaks typical of crystalline phases. This indicates the existence of amorphous structure in all the as-deposited films. The sharp XRD peak observed at 2θ = 33.03º represents Si(200) Bragg reflection resulting from thermally oxidized Si substrate [CHOM2001]. To further confirm the local microstructure, all the films were investigated by TEM technique and the micrographs are depicted in figure 5.03 for multilayer films with n = 3 and x = 0 and 2.5.

While the bright-field TEM micrographs reveal the characteristic amorphous microstructure devoid of any local lattice fringes, the selected area electron diffraction patterns display halo diffraction rings corresponding to the amorphous structure. The above results clearly establish that all the as-deposited multilayer films exhibit amorphous structure.

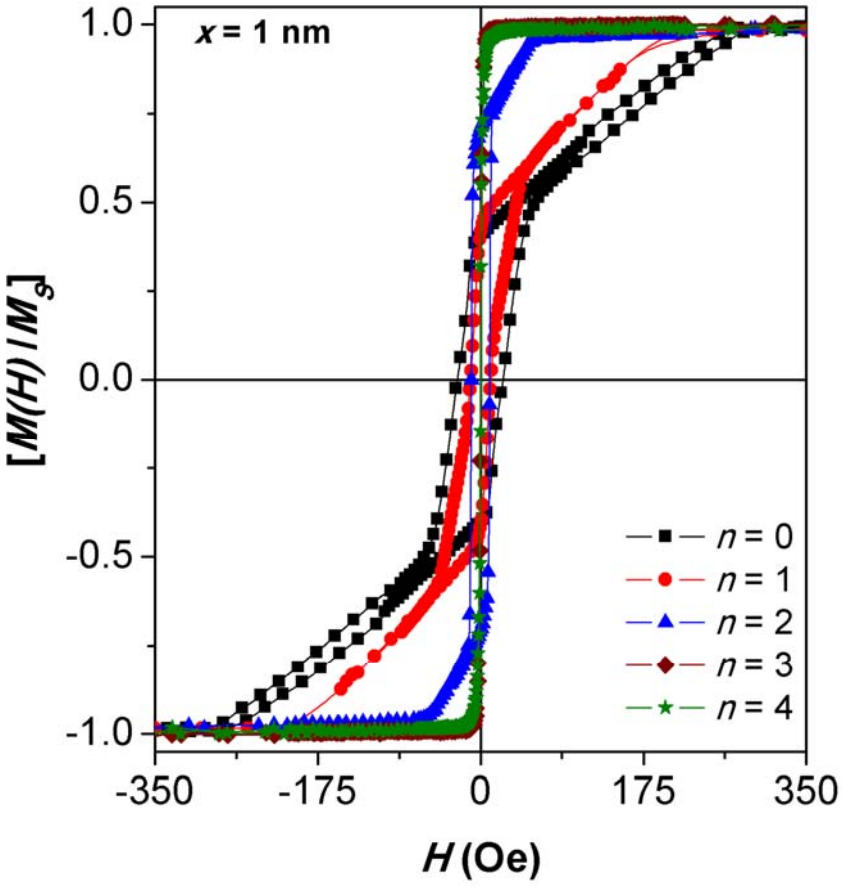

Figure 5.04: Room temperature normalized M-H loops measured along a film plane for as-deposited multilayer [[FeTaC (y nm)/Ta (1 nm)]$_n$/FeTaC (y nm)] films with different n values.

5.3. Magnetic properties:

The magnetic properties of multilayer films were investigated in two different aspects: (i) effects of number of multilayers (n) and temperature on the magnetic properties by fixing the Ta spacer layer thickness (x) and (ii) effects of spacer layer thickness and temperature on the magnetic properties by fixing number of Ta spacer layers (n). The value of n was varied between 0 and 4 by keeping x at 1 nm in the first case, while the later part had the n value as 3 and varied the values of x between 0 and 6 nm.

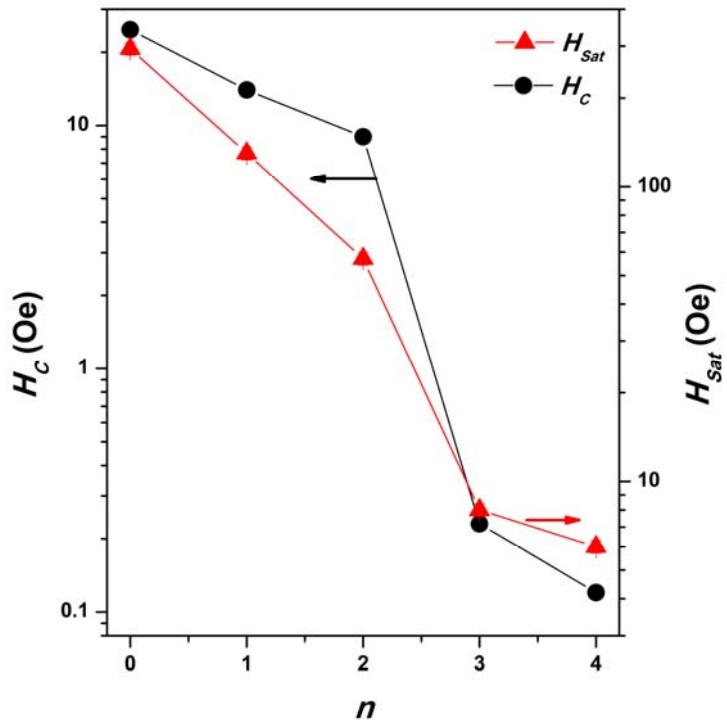

Figure 5.05: The variations of H_C and H_{Sat} with number of multilayers for as-deposited multilayer [[FeTaC (y nm)/Ta (1 nm)]$_n$/FeTaC (y nm)] films.

5.3.1. Effect of multilayer structure on the magnetic properties:

5.3.1.1. Room temperature magnetic properties:

Figure 5.04 displays the room temperature normalized *M-H* loops of multilayer films with different *n* values. As discussed earlier in chapter 4, the single layer film (x = 0, n = 0) exhibits the transcritical loop. The shape of the transcritical loop remains the same with increasing the values of *n* up to 2 due to the existence of strip domain patterns, but the values of coercivity (H_C) and the field required for saturating the *M-H* loops along the film plane (H_{Sat}) decrease significantly and the remanence values increase marginally with increasing *n* values. On further increasing the *n* values (≥ 3), the shape of the *M-H* loops changes from transcritical to flat loop, which saturates at much smaller applied fields. This can be attributed to the change in the domain structure of FeTaC films from strip domain patterns to in-plane orientation of magnetization. In other words, for $n \geq 3$ films, the thickness of individual FeTaC layers in multilayer films is less than 50 nm resulting in-plane orientation of magnetization in each FeTaC layer as described in chapter 4. The extracted values of H_C and H_{Sat} from the *M-H* loops are plotted as a function of *n* in figure 5.05. It is observed that both the values of H_C and H_{Sat} decrease almost linearly at a rate of 7.9 Oe/*n* and 119 Oe/*n* for *n*

values up to 2. On the other hand, H_C and H_{Sat} decrease rapidly to 0.23 Oe and 8 Oe for n = 3 and reaches to 0.12 Oe and 6 Oe for n = 4 films. The linear variations of H_C and H_{Sat} with increasing n up to 2 can be attributed to the change in the size of the strip domain patterns and the orientation of magnetization in the plane, while the large reduction in the H_C and H_{Sat} for $n \geq 3$ is due to the change in the domain structure from strip domain pattern to in-plane orientation of magnetization. Huang et al [HUAN2001] reported a similar H_C variation in FeCoZrBCu/SiO_2 multilayer films, i.e., H_C decreases largely from 25 Oe for a single layer FeCoZrBCu (150 nm) film to 0.25 Oe for the multilayer film of [FeCoZrBCu(150 nm)/ SiO_2(2 nm)]$_2$/ FeCoZrBCu (150 nm)/glass substrate. Similarly, Naoe et al [NAOE1998] reported a large decrease in H_C of FeCuNbSiB (140 nm) single layer film into multilayer [[FeCuNbSiB (y nm)/Al(x nm)]$_n$/ FeCuNbSiB (y nm)] films. These results confirm that the room temperature magnetic properties of multilayer FeTaC films are enhanced, as the intervening Ta layers play a dominant role in reducing the H_C and H_{Sat} values. This could be

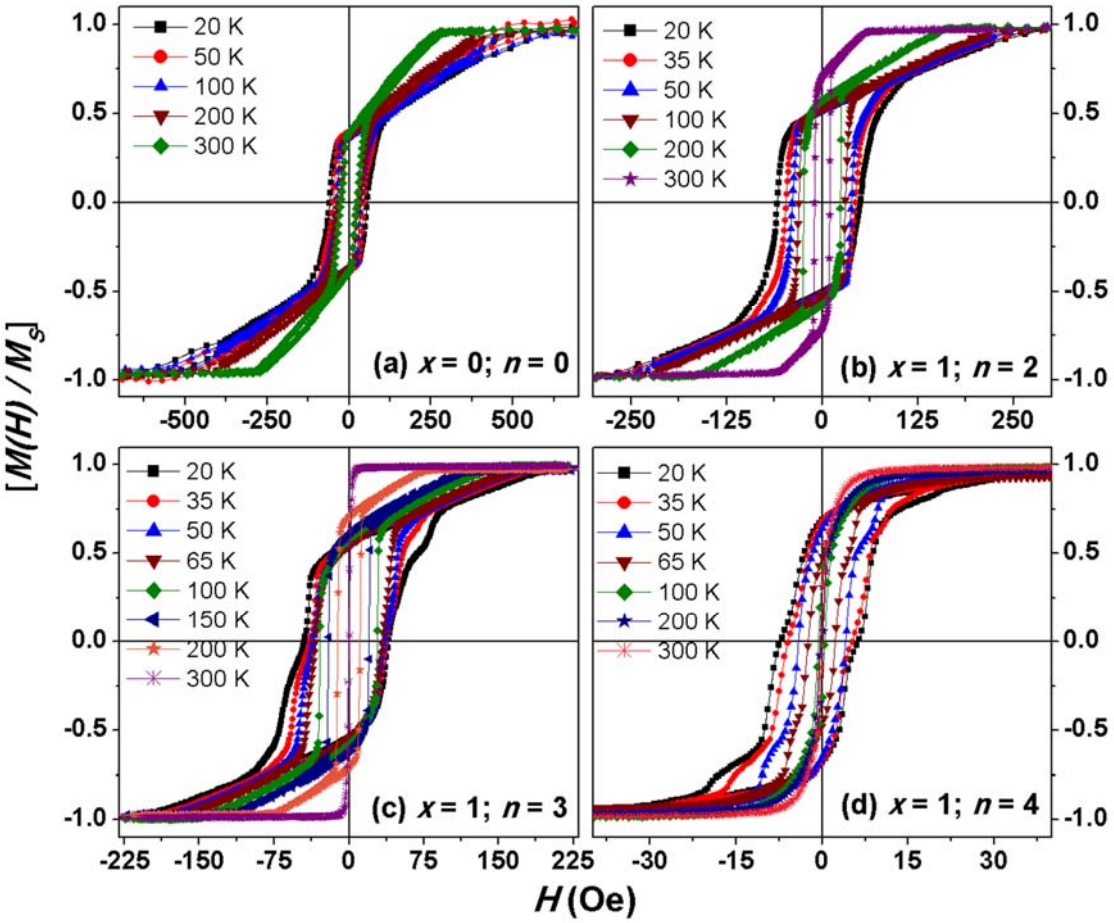

Figure 5.06: Temperature dependent normalized M-H loops for as-deposited multilayer [[FeTaC (y nm)/Ta (1 nm)]$_n$/FeTaC (y nm)] films.

attributed to the fact that the appearance of the perpendicular anisotropy in ferromagnetic FeTaC layers is suppressed by the insertion of Ta spacer layer and hence the soft magnetic properties are improved because of the magnetostatic coupling between the ferromagnetic layers [NAOE1998, TANA20032].

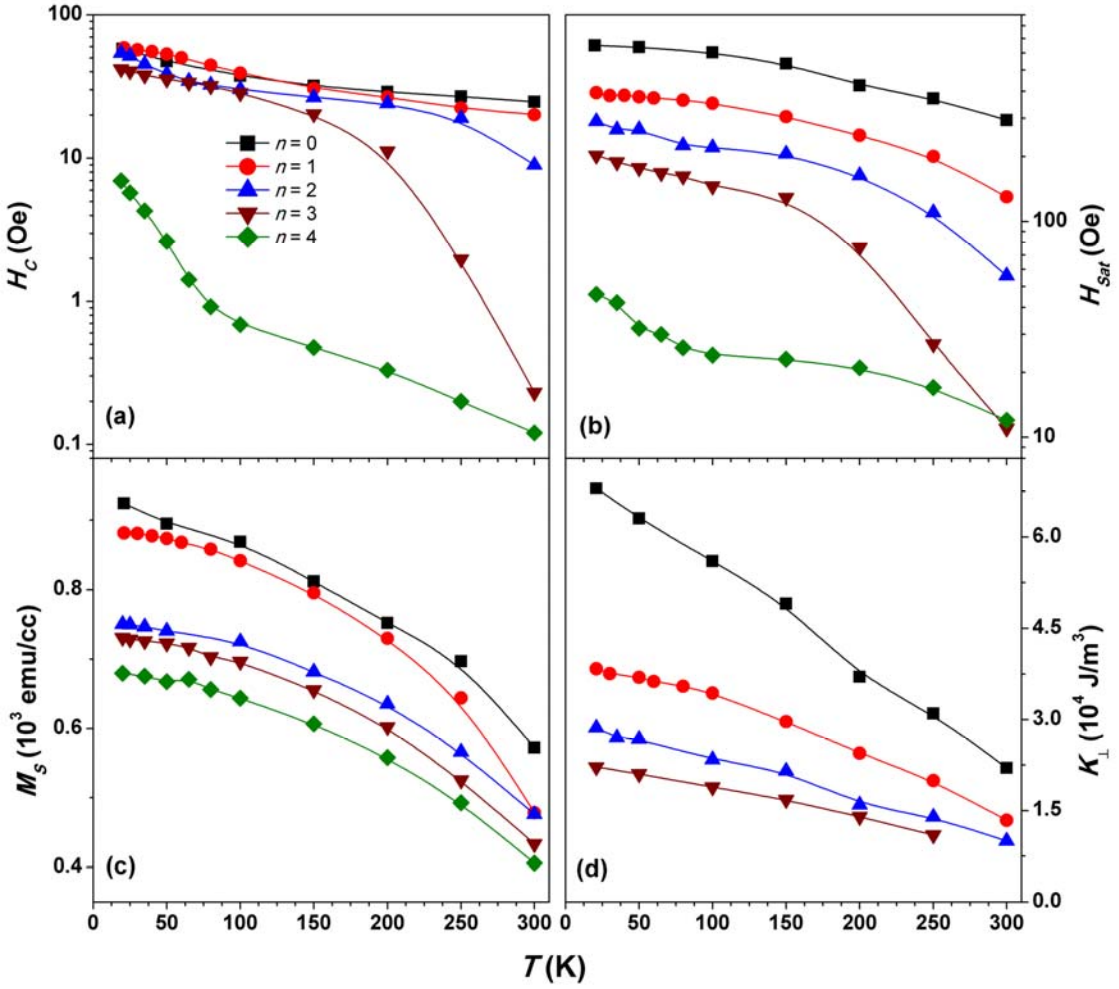

Figure 5.07: The variations of (a) H_C, (b) H_{Sat} (c) M_S and (d) perpendicular anisotropy constant with temperature for as-deposited multilayer [[FeTaC (y nm)/Ta (1 nm)]$_n$/FeTaC (y nm)] films.

5.3.1.2. Low temperature magnetic properties:

Temperature dependent magnetic properties of FeTaC multilayer films were investigated by recording *M-H* loops at different temperatures and temperature dependent magnetization curves (*M-T*) under zero-field cooled (ZFC) and field-cooled (FC) conditions in the temperature range 5 to 300 K using VSM and SQUID magnetometers. Figure 5.06 depicts

temperature dependent normalized *M-H* loops measured in the temperature range 20 K to 300 K for single layer FeTaC (200 nm) film and multilayer films with different *n* values. As like single layer films, the shape of the *M-H* loops is not changed with temperature for multilayer films with $n \leq 2$. However, the values of H_C and H_{Sat} increase with decreasing temperature. This is a typical behaviour observed in many soft magnetic materials. With increasing $n = 3$,

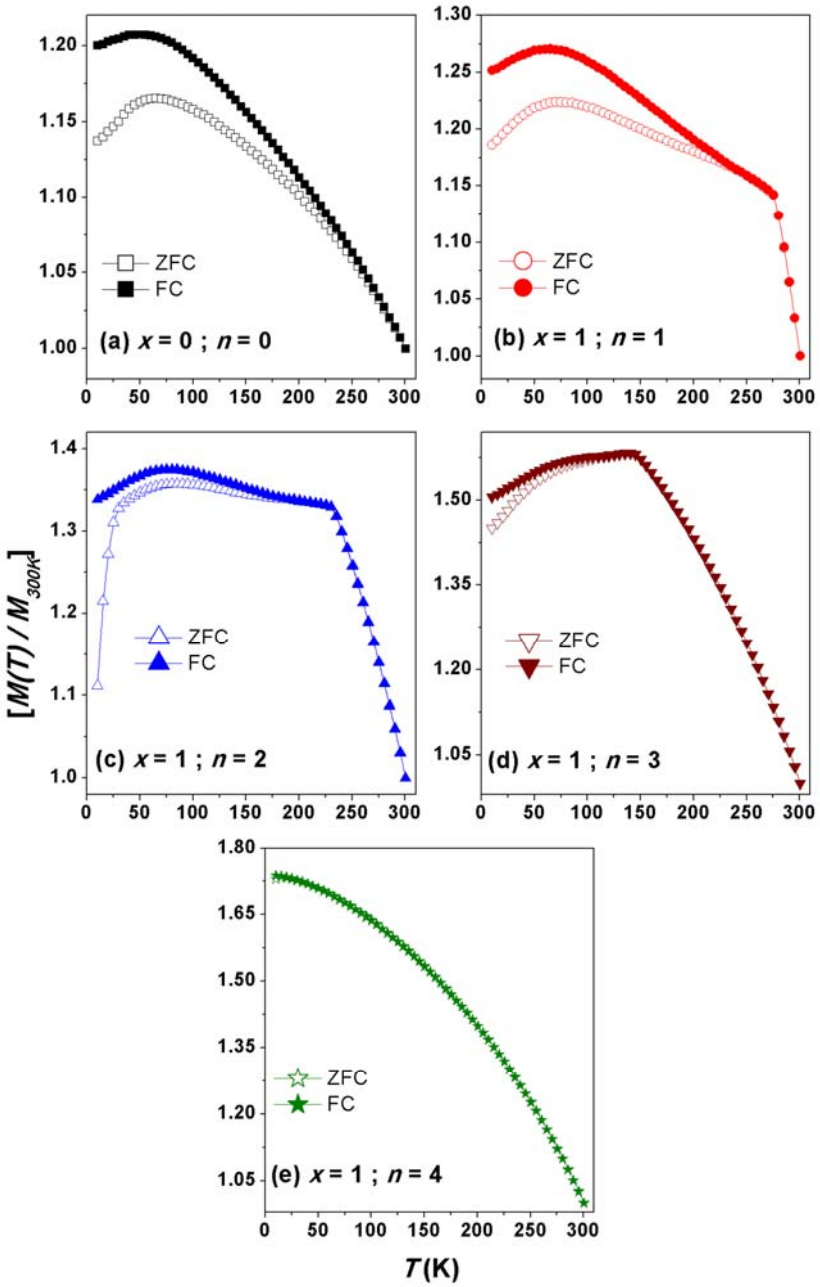

Figure 5.08: Low temperature M-T data for as-deposited multilayer [[FeTaC (y nm)/Ta (1 nm)]$_n$/FeTaC (y nm)] films measured at 100 Oe applied field under ZFC and FC conditions.

the shape of the loops is changed from flat loop to transcritical one with decreasing temperature and hence the values of H_C and H_{Sat} increased largely. A detailed explanation regarding this shape change is discussed in section 5.3.2.2. In addition, for the films with $n \geq 3$, the *M-H* loops exhibit a pronounced multistep magnetization reversal process at temperatures below 70 K. The number of steps in the magnetization reversal behaviour depends on number of multilayers. The observed results could be understood on the basis of competition between the magnetostatic coupling between FeTaC ferromagnetic layers and the interface roughness. With increasing the values of *n*, the average magnetization of the individual ferromagnetic layer decreases and interface roughness increases. As a result, the demagnetization field associated with the roughness increases and results in the domain formation especially at the interfaces [NEEL1962, ZHAN19961, ZHAN19962, KOOL1999]. Hence, a sequential switching of the ferromagnetic layers in multilayer films is observed. With increasing temperature above 70 K, thermal activation diminishes the topological coupling, resulting smooth and narrow hysteresis curves caused by the magnetostatic coupling. As a result, the values of H_C decrease with increasing temperature. To understand the effective variations of the magnetic parameters with number of multilayers, the values of H_C, H_{Sat} and saturation magnetization (M_S) from the temperature dependent *M-H* loops are plotted in figure 5.07 against temperature. For single layer and multilayer films with $n \leq 2$, H_C increases almost linearly in logarithmic scale with decreasing temperature. This is a typical behaviour observed in many soft magnetic materials. In contrast, the multilayer film with $n = 3$ exhibit a large increase in H_C with decreasing temperature from 300 K to 150 K followed by a linear increase at lower temperatures as observed for the other films. On the other hand, for multilayer films with $n = 4$, the variation of H_C against temperature exhibits two distinct slopes: H_C varies at a slow rate of 0.0028 Oe/K in the temperature range between 300 K and 100 K and a faster rate of 0.1187 Oe/K in the temperature range from 80 K to 20 K. The large variation in H_C for temperatures below 80 K is caused by the individual switching of the ferromagnetic layers (see figure 5.06(d)) due to the enhanced interface roughness with increasing the values of *n*. $H_{Sat}(T)$ exhibits almost the similar variations of $H_C(T)$ with temperature for each of multilayer films. The values of M_S decrease not only with increasing temperature for all multilayer films, but also decrease significantly with increasing the values of *n*. The decrease in magnetization with increasing number of interfaces is reported by Saipriya et al [SAIP2012] in SnO_2/Cu-Zn multilayer films and by Abid et al [ABID1999] in Ni/V multilayer films and attributed to the presence of magnetically dead

layer at the interface of non-magnetic/ferromagnetic layers due to the inter diffusion between magnetic and non-magnetic layers. A similar behaviour is also expected for the currently investigated multilayer films. Nevertheless, the observed results suggest that the temperature dependent magnetic properties strongly depend on the multilayer structure. As multilayer films with n up to 3 exhibit strip domain patterns, the calculation of perpendicular anisotropy was extended at low temperatures using the procedure followed for single layer films in chapter 4. Figure 5.07(d) displays the variations of perpendicular anisotropy constant ($K_{\perp}$) with temperature for different multilayer films. The values of $K_{\perp}$ decrease not only with increasing temperature for a given multilayer film, but also decrease with increasing number of multilayers. This could be attributed to the suppression of perpendicular anisotropy in the ferromagnetic FeTaC layer by the insertion of Ta spacer layer and the improvement of soft magnetic properties by the magnetostatic coupling between the ferromagnetic layers [NAOE1998, TANA20032].

Figure 5.08 depicts normalized *M-T* data measured at an applied field of 100 Oe under ZFC and FC conditions in the temperature range of 5 K to 300 K for multilayer thin films with different values of n. In these measurements, the sample was initially cooled to 5 K under zero-field condition. Magnetization was then recorded as the sample was heated to room temperature under a constant field applied along the film plane (ZFC process). Subsequently, the sample was cooled under the same constant applied field to 5 K and then the magnetization was recorded as the sample was heated to room temperature (FC process). *M-T* curves reveal the following features: (i) For single layer film, the magnetization increases gradually with decreasing temperature and a bifurcation between the ZFC and FC data was observed below 270 K, (ii) a sharp increase in magnetization down to 273 K from 300 K followed by a bifurcation at about 225 K was observed for the film with n = 1, (iii) with increasing n up to 3, the temperature zone of sharp increase in magnetization shifts from 273 K for n = 1 to 144 K for n = 3 along with the shift of bifurcation from 225 K to 73 K, and (iv) for multilayer films with n = 4, the bifurcation point almost disappeared and the magnetization data obtained under ZFC and FC conditions are found to be nearly the same within experimental accuracy. These observations indicate that the existence of in-plane anisotropy with magnetization parallel to the film plane in multilayer films with n = 4 results good soft magnetic properties. Therefore, the application of 100 Oe external magnetic field is well enough to saturate the film's magnetization (see figure 5.06(d)) both in ZFC and FC cycles and hence no difference in magnetization data obtained under the ZFC and FC

conditions was observed. However, with decreasing the *n* values, the perpendicular anisotropy in the films is not suppressed due to the large variation in the angle between the bulk and surface domains resulting random (non-collinear) arrangement of spins in FeTaC ferromagnetic layers with decreasing temperature. This increases the magnetic disorder in the film. Moreover, the applied field required to saturate the films' magnetization along the film plane increases (> 200 Oe) with decreasing the *n* values (see figures 5.06 (a) – (c)). Therefore, the ZFC and FC curves obtained under low applied magnetic fields (< 200 Oe) show a variation in their magnetization behaviour with decreasing temperature resulting bifurcation between them. Hence, the presence of bifurcation between the ZFC and FC data can be attributed to the existence of magnetic disorder either due to the non-collinear spin arrangements in Fe rich FeTaC films [HANS1991, CAST19972, HERN2002] or due to the existence of random magnetic anisotropy in the system. These results reveal a dependence of magnetic nature on number of multilayers at different temperatures. They also suggest that the change in the domain structure of the individual ferromagnetic layers with decreasing thickness and magnetostatic coupling between the ferromagnetic layers diminishes the

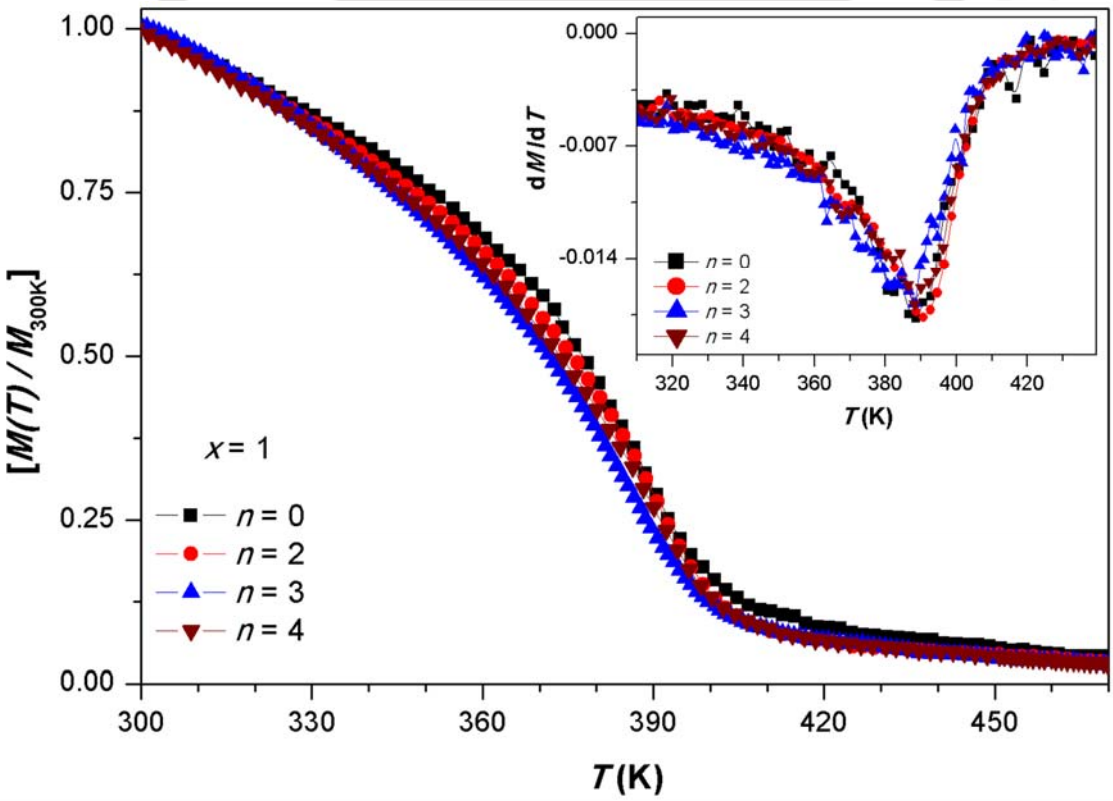

Figure 5.09: High temperature M-T data measured at 500 Oe applied field for as-deposited multilayer [[FeTaC (y nm)/Ta (1 nm)]$_n$/FeTaC (y nm)] films.

magnetic disorder. This improves the magnetic properties of multilayer films. Also, it is demonstrated that the amount of magnetic disorder exists in single layer film of larger thickness at low temperatures can be fine-tuned with the multilayer structure.

5.3.1.3. High temperature magnetic properties:

To understand the magnetic nature of multilayer films up to critical temperature, high temperature *M-T* data were obtained for all the films under the field of 500 Oe applied in the film plane. In order to compare the nature of all the *M-T* curves, the magnetization of each curve is normalized with respect to their room temperature magnetization value and the plots of temperature dependent normalized magnetization data are depicted in figure 5.09. It is seen clearly that all the films show an incessant decrease in magnetization up to 400 K and the rate of decrease of magnetization decreases with a further increase in temperature. Interestingly, the magnetization of all the films varies almost similarly with temperature and exhibits a clear magnetic phase transition from ferromagnetic state to paramagnetic state. Curie temperature (T_C) was obtained from the thermal derivative of magnetization data as displayed in inset of figure 5.09 and found to be about 390 K. T_C values are found to be nearly the same for both single layer and multilayer films within the experimental accuracy.

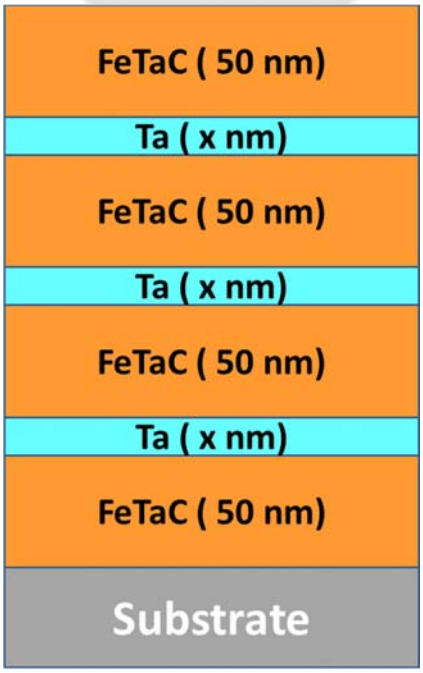

Figure 5.10: Schematic representation of as-deposited multilayer [FeTaC (50 nm)/Ta (x nm)]$_3$/FeTaC (50 nm)] films taken for the study of spacer layers driven magnetic

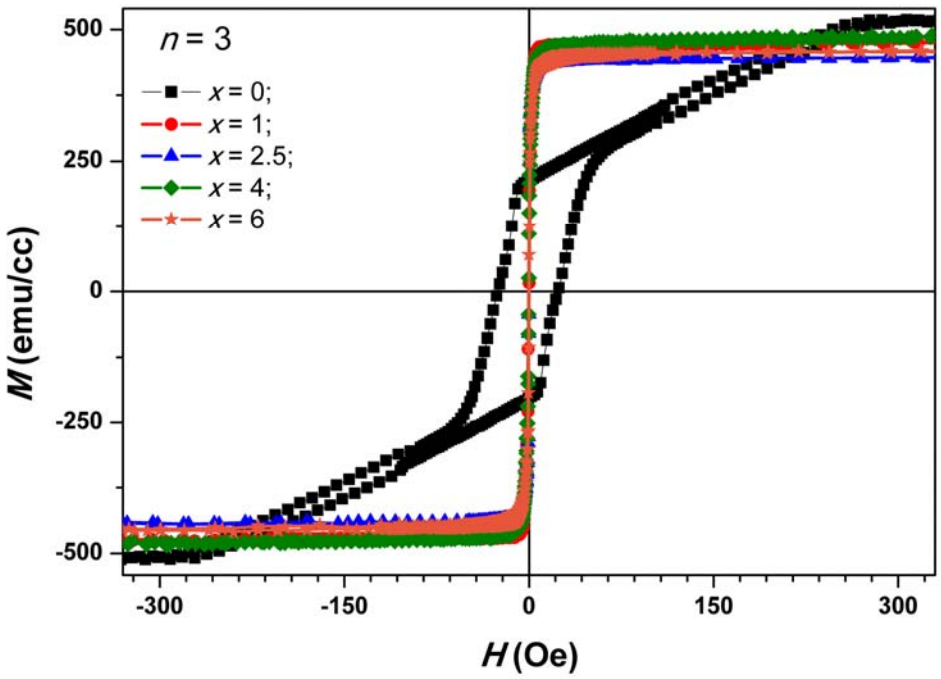

Figure 5.11: Room temperature M-H loops measured along film plane for as-deposited multilayer [[FeTaC (50 nm)/Ta (x nm)]$_3$/FeTaC (50 nm)] films with different spacer layer thicknesses.

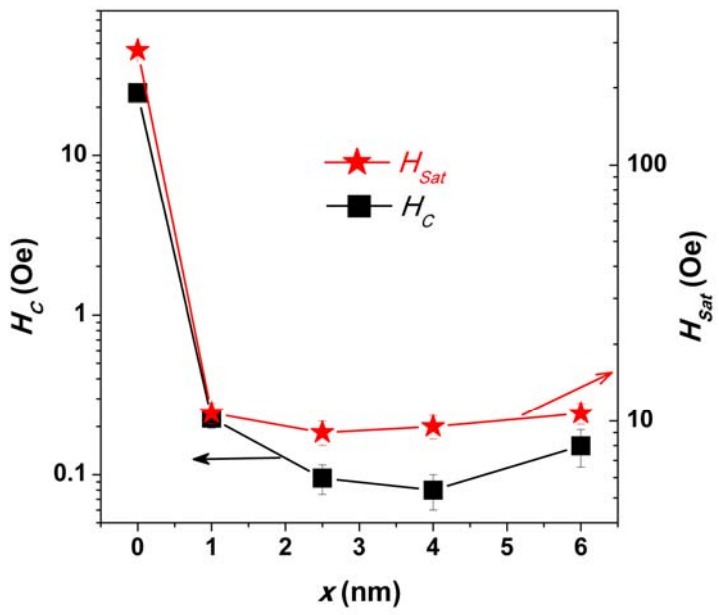

Figure 5.12: The variations of H_C and H_{Sat} for as-deposited multilayer [[FeTaC (50 nm)/Ta (x nm)]$_3$/FeTaC (50 nm)] films with different spacer layer thicknesses.

5.3.2. Spacer layer and temperature driven magnetic properties:

Since multilayer films with $n = 3$ display a strong temperature dependent magnetic properties (see figures 5.06 and 5.07), we have taken this multilayer structure for further investigation by varying the spacer layer thickness. Therefore, this section focuses on the magnetic

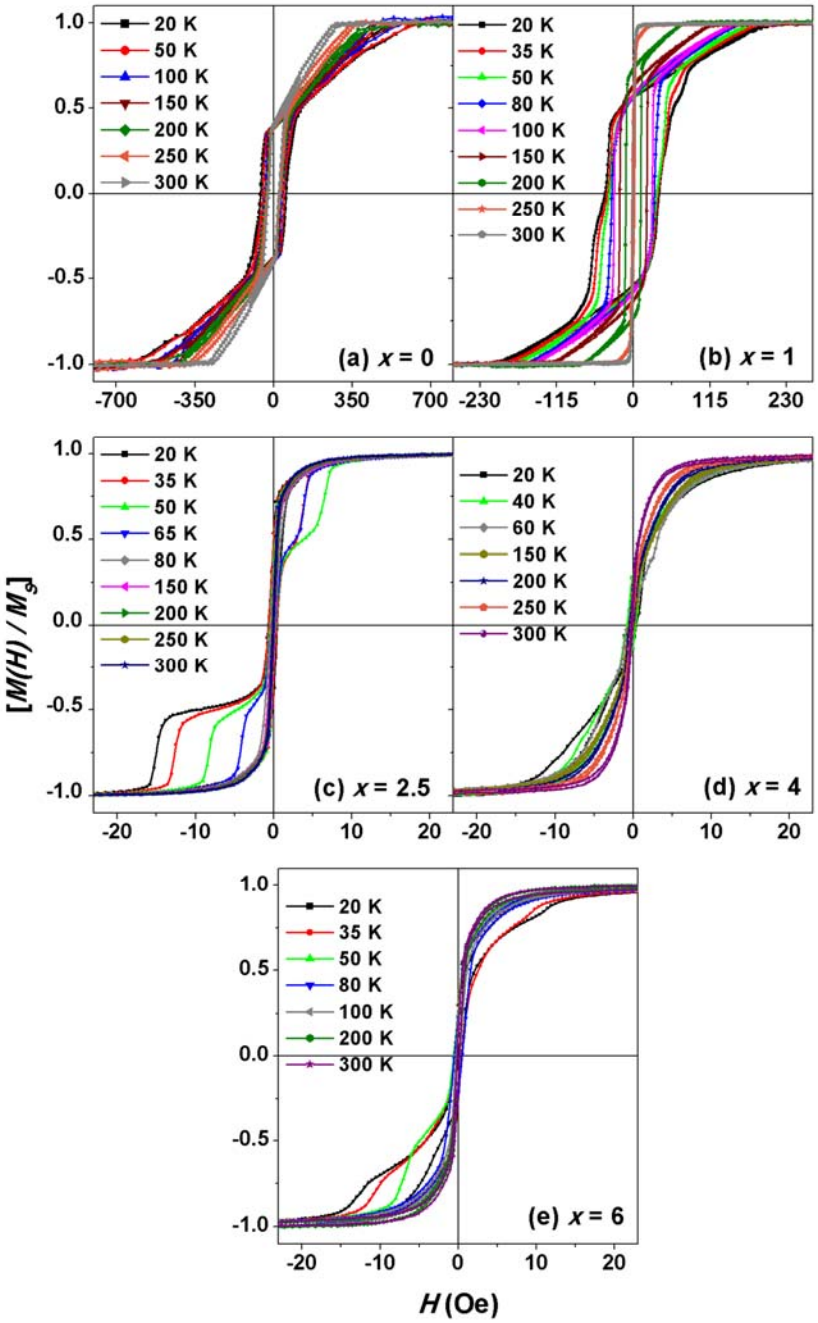

Figure 5.13: M-H loops measured at different temperatures for as-deposited multilayer [FeTaC (50 nm)/Ta (x nm)]$_3$/FeTaC (50 nm)] films with x = 0, 1, 2.5, 4 and 6.

properties of multilayer [[FeTaC (50 nm)/Ta (x nm)]$_3$/FeTaC (50 nm)] films over a wide range of temperatures. The spacer layer thickness (x) was varied systematically between 1 and 6 nm, as schematically shown in figure 5.10.

5.3.2.1. Room temperature magnetic properties:

Figure 5.11 depicts room temperature *M-H* loops measured along film plane for multilayer films with different x values. It is observed that *M-H* loop of a single layer film (x = 0) exhibits transcritical loop as discussed in chapter 4 [CHAN2002, CRAU2002, HUBE2009]. The introduction of thin Ta spacer layers (x = 1, n = 3) changes the shape of *M-H* loop from transcritical to almost a flat loop, which saturates at quite low applied magnetic field (~ 10 Oe). On further increasing x up to 6 nm, the shape of the *M-H* loop did not change significantly. In order to monitor the effect of spacer layer thickness on the magnetic parameters of multilayer films, the values of H_C and H_{Sat} are extracted from figure 5.11 and depicted in figure 5.12 as a function of x. H_C decreases largely from 25 Oe for x = 0 film to 0.23 Oe for x = 1 film followed by a gradual reduction in H_C up to x = 4 (H_C ~ 80 mOe) and increases slightly for x = 6 film. Similarly, H_{Sat} decreases rapidly from 280 Oe for x = 0 film to around 10 Oe for x = 1 film and remains almost constant for films with $x \geq 1$. Huang et al [HUAN2001] reported that the reduction in H_C not only depends on the ferromagnetic layer thickness, but also vary with the spacer layer thickness. On the other hand, the results obtained by Feng et al [FENG1994, FENG1995] for various type of interlayers such as Al, Cr, Cu and Ag in CoCrTa films show that H_C reduces with increasing the spacer layer thickness. Herndon et al [HERN2008] have also reported a similar nature of H_C variation with Al_2O_3 spacer thickness. The above results confirm that the room temperature magnetic properties of single layer FeTaC (200 nm) films are enhanced by the multilayer structure, as intervening Ta spacer layers play a dominant role in controlling the magnetic properties.

5.3.2.2. Low temperature magnetic properties:

To understand the effect of spacer layers' thickness on magnetic nature of multilayer films, temperature dependent magnetic properties were investigated by measuring *M-H* loops at different temperatures in the temperature range 20 K to 300 K using the VSM and *M-T* data in the temperature range 5 K to 300 K and 300 K to 500 K using the SQUID and the VSM magnetometers, respectively. Figure 5.13 illustrates normalized *M-H* loops measured along film plane for multilayer [[FeTaC (50 nm)/Ta (x nm)]$_3$/FeTaC (50 nm)] films with x = 0, 1, 2.5, 4, and 6 nm using VSM in the temperature range from 20 K to 300 K. For x = 0 film, the

shape of the *M-H* loops is not changed with decreasing temperature, but the values of H_C and H_{Sat} are found to increase with decreasing temperature. This is a typical behaviour observed in many soft magnetic materials [HUAN2001, HERN2008, BRAJ2010]. On the other hand, as discussed earlier, the shape of the *M-H* loops of x = 1 film is found to be strongly depending on the temperature: (i) *M-H* loop observed at 300 K depicts almost a flat loop which saturates at very low applied magnetic field (~ 10 Oe). (ii) With decreasing temperature below 300 K, the shape changes from flat loop to those observed for x = 0 film and the values of H_C and H_{Sat} increase largely. (iii) On further decreasing the temperature below 80 K, the *M-H* loops display a step like magnetization reversal process with different H_C values. With increasing the spacer layer thickness more than 1 nm, narrow *M-H* loops were observed in the temperature range 80 K to 300 K. However, the film with x = 2.5 exhibits a clear multistep magnetization reversal behaviour below 80 K. Such multistep reversal process shows an oscillatory behaviour with increasing x, i.e., with increasing the values of x from 1 to 2.5, a clear stepped hysteresis was observed, which disappeared at x = 4 and reappeared again at x = 6 film. The above results suggest that while the multilayer film with x = 1 exhibits a strong temperature dependent magnetic nature, the observation of multistep magnetization reversal process in multilayer films is strongly depend on the Ta spacer layer thickness.

In order to understand the observed results, the variations in microstructure and magnetic domain structure of the films are presented schematically in figure 5.14. It may be noted that the transcritical loop observed in x = 0 film is generally correlated to the development of perpendicular anisotropy component resulting from stress quenched in during the film deposition [MURA1966, PRAD2004, SHAR2006, COIS2008, COIS2009] as discussed in chapter 4. As it is known that the orientation of magnetization in disordered system (see figure 5.14(a)) is determined mainly by the magnetoelastic and shape anisotropy terms, and the magnetoelastic is coupled to the interplay among the stress and magnetization, the formation of stripe domain pattern beyond critical thickness is mainly controlled by the stress. Among the several possible domain structures [HUBE2009], the observed domain structure for x = 0 film can be attributed to weak dense stripe domains in which the neighbouring stripes have aligned along in-plane direction, but their perpendicular components alternate up and down as demonstrated in figure 5.14(b). On the other hand, the introduction of thin spacer layers in multilayer films revealed a drastic change in loop shape from transcritical to flat loop. This is caused mainly by partitioning of a single layer FeTaC (200 nm) film into four equal FeTaC layers with each of 50 nm thickness (see figure 5.10)

having an in-plane magnetic structure as depicted in figure 5.14(d) and demonstrated in figure 4.04. This can be understood that FeTaC films having thicknesses below $t_{critical}$ as defined in eqn.(4.01) do not display any out-of-plane component even in the as-prepared state, where the stresses quenched in during the deposition have not been relieved out completely. This suggests that the stress induced perpendicular anisotropy in thin FeTaC

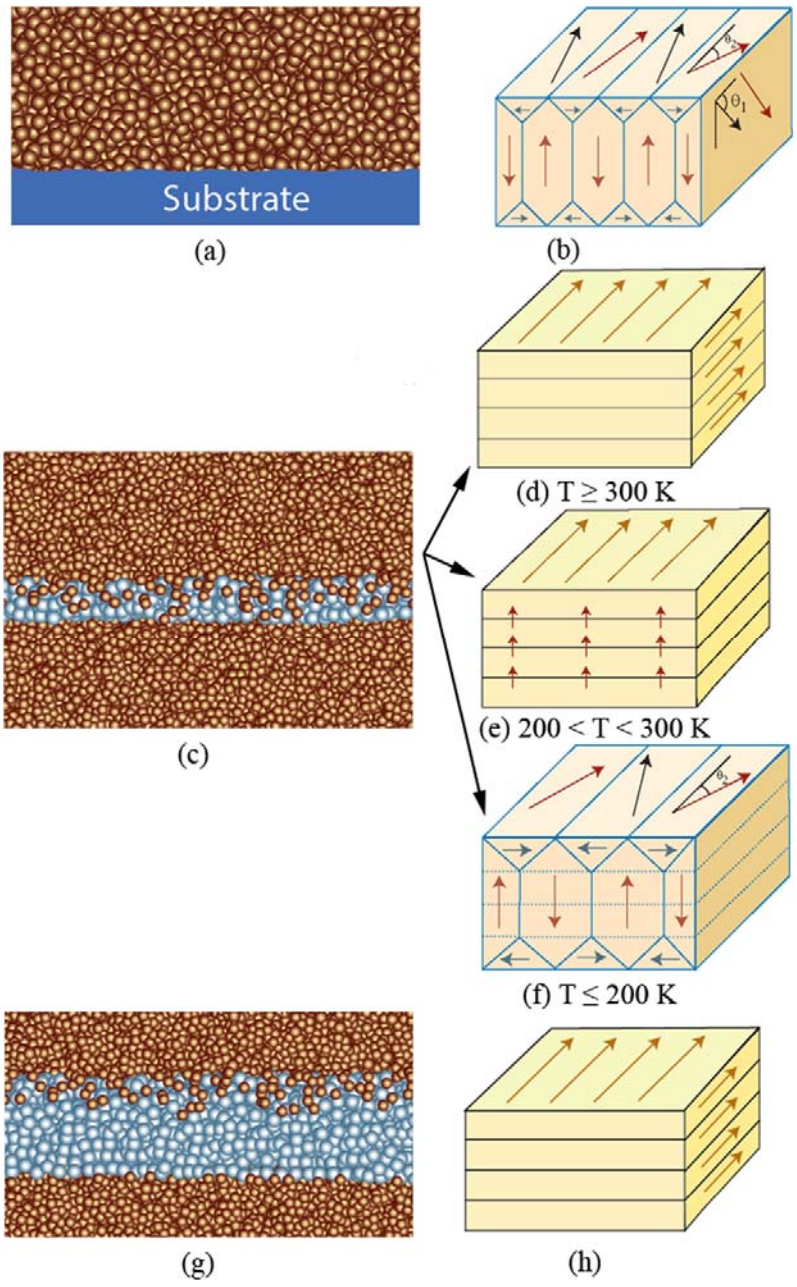

Figure 5.14: Schematic of variations in microstructure ((a) x = 0, (c) x = 1, and (g) x = 2.5) and magnetic domain structure ((b) x = 0, (d,e,f) x = 1, and (h) x ≥ 2.5) of as-deposited multilayer [FeTaC (50 nm)/Ta (x nm)]$_3$/FeTaC (50 nm)] films.

films is not sufficient to overcome shape anisotropy. Consequently, the magnetization lies mainly within the plane of the film [OHAN2000, PORR2002, HUBE2009]. Furthermore, the uniaxial anisotropy may result from forming aligned ferromagnetic atom-pairs due to their strong magnetic exchange coupling during film deposition process [HUAN2001]. Therefore, the flat loop observed in x = 1 film at 300 K is mainly due to the magnetostatic coupling between FeTaC ferromagnetic layers having in-plane anisotropy with magnetization parallel to the film plane. However, with decreasing temperature below 300 K, the loop shape of x = 1 film is again changed to those shapes observed for x = 0 film. This results a large increase in H_C for temperature down to 100 K and varies almost linearly (in logarithmic scale) with a further decrease in the temperature. This could be attributed to a nucleation of strip domain structure across the interface of the films at $T \leq 250$ K due to the presence of possible pinholes in the non-magnetic layer [STIL2005]. Note that 1 nm thick Ta spacer layer is ideally expected to have a maximum of 3 to 4 atomic layers of Ta atoms between two ferromagnetic layers. In order to prepare FeTaC films with amorphous structure, the films were deposited at a significantly high deposition rate (> 4 nm/min). As a result, one would expect a possible inter-diffusion at the interface between FeTaC and Ta layers, which may alter the magnetic properties of multilayer films. Since FeTaC alloy films contain Fe, Ta and C atoms, the diffusion of all these atoms into Ta layer during FeTaC layer deposition on top of the Ta layers cannot be ruled out [BRAN1992]. However, the inter-diffusion of Ta and C atoms into the Ta layers may not affect the magnetic properties of multilayer films due to the non-magnetic nature of these elements. On the other hand, the probability of Fe atoms diffusing into the Ta layers is quite high due to a higher Fe concentration in FeTaC alloy films and its smaller size as compared to Ta atoms [BRAN1992]. This causes a significant change in the magnetic properties of multilayer films. Although the interfacial profile cannot be estimated quantitatively from the current investigation, the observed results support that the pinhole, as depicted in figure 5.14(c), is referred to a possible inter-diffusion of Fe atoms into the Ta layers. A similar scenario has been reported in different systems [CLAR1994, OLIV1999]. Oliveria et al [OLIV1999] proposed that inter diffused Fe atoms form either as isolated manner or as cluster nature. Therefore, the existence of Fe atoms in the Ta layers is expected to show possible temperature dependent properties. It is understood from the *M-H* loop of x = 1 film at 300 K that the inter-diffused Fe atoms may not contribute to the magnetic properties possibly due to its paramagnetic state. In such scenario, the interaction between the two ferromagnetic layers is mainly dominated by the magnetostatic coupling (see

figure 5.14(d)) causing a flat loop with low H_C. However, with decreasing temperature below 250 K, the paramagnetic nature of Fe atoms transforms into ferromagnetic one and facilitates a direct exchange interaction between the ferromagnetic layers through pinholes as pointed out by arrows in figure 5.14(e). This feature permits the nucleation of stripe domains below 250 K (see figure 5.14(f)) and therefore, the *M–H* loop changes from flat loop to transcritical one below 250 K. The development of perpendicular anisotropy was calculated using the procedure described earlier and plotted in figure 5.07(d). A comparison of $K_\perp$ data between x = 0 and 1 films reveals that despite having the stripe domain like structure in x = 1 film, the anisotropy is relatively smaller due to the interlayer exchange interaction between FeTaC layers through pinhole coupling.

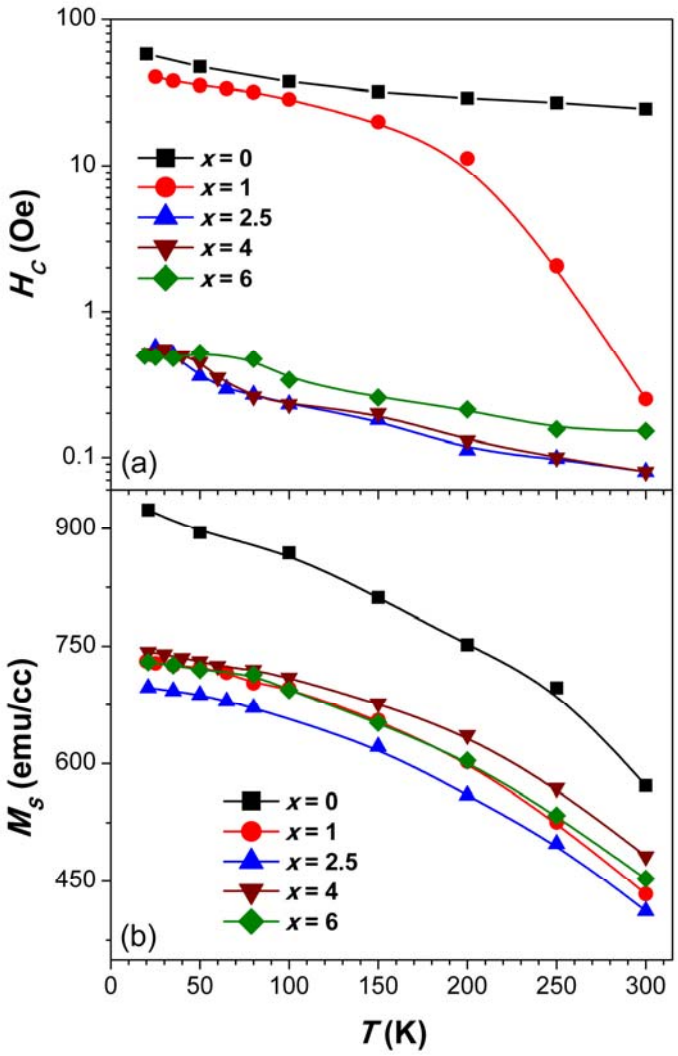

Figure 5.15: The variations of (a) H_C and (b) M_S with temperature for as-deposited multilayer [FeTaC (50 nm)/Ta (x nm)]$_3$/FeTaC (50 nm)] films.

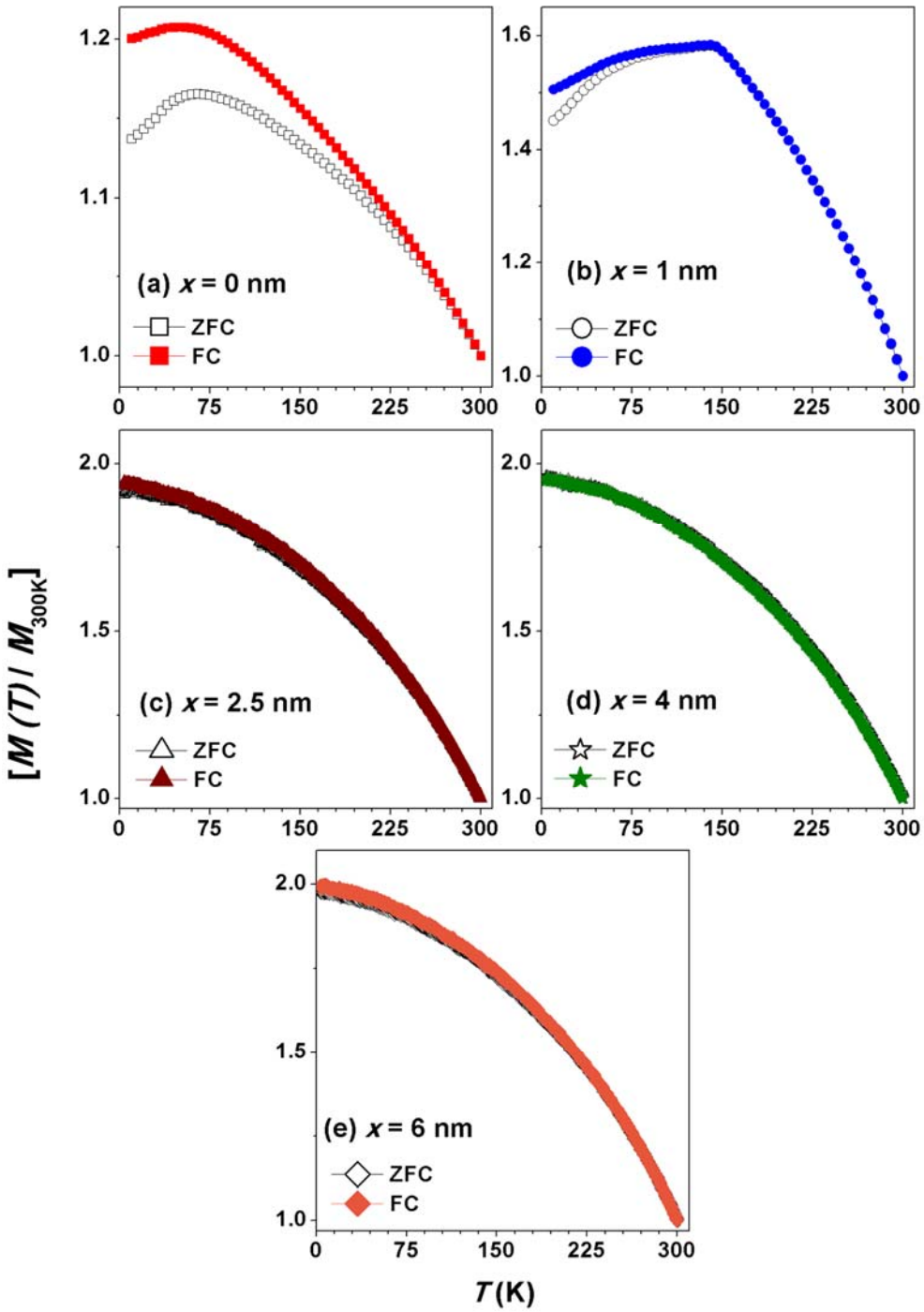

Figure 5.16: Low temperature M-T data measured at an applied field of 100 Oe under ZFC and FC conditions for as-deposited multilayer [FeTaC (50 nm)/Ta (x nm)]$_3$/FeTaC (50 nm)] films.

On further increasing the Ta layer thickness (> 1 nm), number of Ta atomic layers formed between the ferromagnetic layers increases, which conceivably limits the inter-

diffusion of Fe atoms within top few layers. Therefore, the direct exchange coupling between the ferromagnetic layers across the interface is faded out, as the ferromagnetic layers are well separated by the Ta layers (see figure 5.14(g)). Therefore, the interaction between the ferromagnetic layers can be related mainly to the magnetostatic coupling (see figure 5.14(h)) resulting a flat loop. With decreasing the temperature below 70 K, multilayer films with $x \geq 2.5$ exhibit multistep magnetization reversal process which is sensitive to the Ta spacer thickness. This can be attributed to the dependence of magnetostatic coupling between the ferromagnetic layers on the thickness of the spacer layers, which exhibits itself in a blocked phenomenon resulting a sequential switching of the ferromagnetic layers and gives rise to a stepped hysteresis. The formation of multistep magnetization reversal process in multilayer films is also caused by an enhancement in the interface roughness [ZHAN19962], which reduces the interaction between ferromagnetic layers and the demagnetization associated with the interface roughness increases, resulting a sequential switching of FeTaC layer in multilayer films. Similar variation of the steps in the *M-H* loops with spacer layer thickness is reported by Huang et al [HUAN2001] for multilayer HITPERM/SiO_2 films. The steps in the *M-H* loops are sensitive to the SiO_2 spacer layer thickness and for 2 nm of SiO_2 thickness, the step is more prominent. The extracted values of $H_C(T)$ and $M_S(T)$ from the temperature dependent *M-H* loops are plotted in the figure 5.15. For all multilayer films except for $x = 1$ film, the values of H_C increase progressively in logarithmic scale with decreasing temperature. As the multilayer film with $x = 1$ has shown a strong temperature dependent magnetic nature, $H_C(T)$ also exhibited two distinct regions: a large increase in H_C in the temperature range 300 K to 150 K followed by a linear variation, as similar to the one observed for $x = 0$ film in the temperature range 150 K to 20 K. On the other hand, the values of M_S increase with decreasing temperature for all the films with different spacer layer thicknesses. In addition, we observed a considerable decrease in magnetization with the multilayer structure due to the magnetic dead layer as discussed earlier.

Figure 5.16 shows the *M-T* data taken under ZFC and FC conditions for multilayer films with different values of *x*. *M-T* curves depicted in figure reveal that (i) For $x = 0$ film, the magnetization increases gradually with decreasing temperature, but a bifurcation between the ZFC and FC data was observed at temperatures below 270 K. (ii) Upon introducing thin Ta spacer layers ($x = 1$), a sharp increase in magnetization down to 144 K from 300 K followed by a bifurcation at about 73 K was observed. (iii) On further increasing the Ta spacer layer to 2.5 nm, the magnetization increases largely with decreasing temperature and

the bifurcation point is shifted to a lower temperature of around 30 K, and (iv) disappeared eventually for the films with $x \geq 4$, which confirms that the magnetization data obtained under the ZFC and FC conditions are the same and hence no bifurcation was observed within the experimental accuracy down to 5 K. These results reveal a dependence of magnetic nature on the thickness of the spacer layers at different temperatures. This can be correlated to the fact that the perpendicular magnetic anisotropy observed in $x = 0$ film produces random (non-collinear) arrangement of spins [CAST19972, HANS1991, HERN2002, BRAJ2010], which increases the magnetic disorder in the film. Therefore, this film needs a significantly large applied magnetic field (> 500 Oe) to saturate the film's magnetization. The ZFC and FC magnetization data obtained under low applied magnetic fields ($< H_{Sat}$) illustrate a difference in their magnetization behaviour with decreasing temperature and exhibiting a bifurcation between them. Upon introducing thin spacer layers of 1 nm, the film exhibits a similar variation in magnetization with temperature both in ZFC and FC conditions down to 150 K. On further decreasing temperature below 150 K, the bifurcation between ZFC and FC

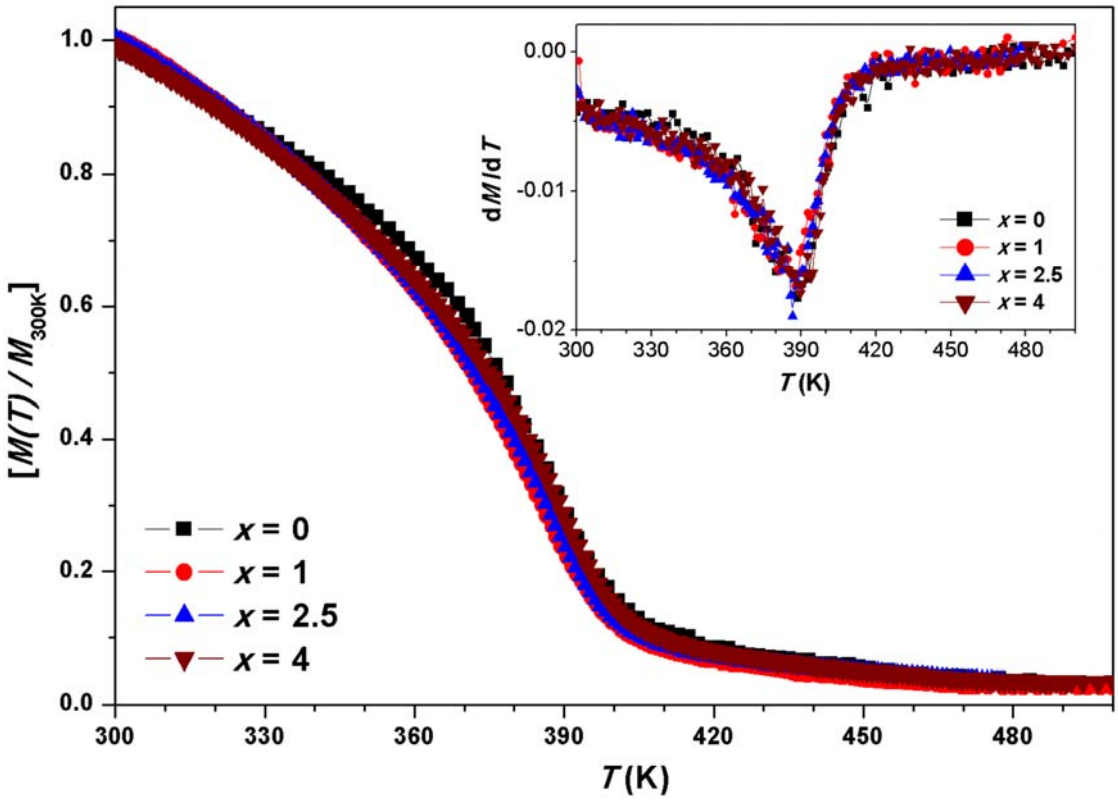

Figure 5.17: High temperature M-T data measured at an applied field of 500 Oe for as-deposited multilayer [FeTaC (50 nm)/Ta (x nm)]$_3$/FeTaC (50 nm)] films. Inset: thermal derivative of magnetization as a function of temperature.

appears mainly due to the nucleation of stripe domain structure resulting from pinhole coupling. Thus, one needs considerably a larger applied magnetic field (> 100 Oe) to destabilize the stripe domain magnetic structure at lower temperatures. On further increasing the thickness of the spacer layers, the interaction between the ferromagnetic layers having in-plane anisotropy is mainly directed by the magnetostatic coupling. Hence, the total system behaves as a collective nature of all the individual magnetic properties of FeTaC layer and a low value of applied field (< 50 Oe) is adequate to saturate the films' magnetization. As a result, the magnetization data obtained under ZFC and FC conditions with the applied field of 100 Oe do not display any difference between them, leading to no bifurcation between ZFC and FC data.

5.3.2.3. High temperature magnetic properties:

Figure 5.17 depicts *M-T* data above room temperature measured at a constant applied field of 500 Oe using the VSM and the thermal derivative of magnetization data for all the films. To compare all data in a single graph, *M-T* data were normalized with respect to room temperature magnetization data of that particular sample. It is seen clearly that all the films show an incessant decrease in magnetization up to 400 K and the rate of decrease of magnetization decreases with a further increase in temperature. Interestingly, the magnetization of all the films varies similarly with temperature and exhibits a clear magnetic phase transition from ferromagnetic state to paramagnetic state. T_C obtained from the thermal derivative of magnetization data (inset of figure 5.17) is determined to be about 390 K, which does not change with the multilayer structure. This can be understood from the fact that the applied magnetic field of 500 Oe is noble enough to obtain saturation in all multilayer films with different spacer layer thicknesses. So, the variation of magnetization with temperature follows a similar nature and exhibits a well-defined second order magnetic phase transition from ferromagnetic state to paramagnetic state around 390 K. The observed results confirm that the magnetic disorder observed in a single layer film with higher thickness is drastically reduced in multilayer films due to the transition from magnetic stripe domain structure to in-plane orientation of the magnetization.

Thus, multilayer films with an appropriate thickness of the spacer layers are very much indispensable in controlling the soft magnetic properties of higher thickness magnetic thin films. The observed results also suggest that the stacks of FeTaC films with in-plane magnetization decoupled by suitable non-magnetic Ta spacer layers are promising for the

application of soft magnetic underlayer in magnetic recording and magnetic flux amplifier in high frequency device applications.

5.4. Summary:

The structural and magnetic properties of multilayer [[FeTaC (y nm)/Ta (x nm)]$_n$/FeTaC (y nm)] films with different multilayers and the spacer layer thicknesses prepared directly on thermally oxidized Si substrates were systematically carried out in this chapter. The salient features of multilayer films from the current investigations are as follows:

- Amorphous multilayer [[FeTaC (y nm)/Ta (x nm)]$_n$/FeTaC (y nm)] films with different multilayers (n = 0 – 4) and spacer layer thicknesses (x = 0 to 6 nm) could be prepared using DC magnetron sputtering technique at ambient temperature.
- Amorphous nature of the as-deposited multilayer films was confirmed through XRD and TEM studies.
- Room temperature coercivity and the field necessary to saturate the magnetization decrease drastically with increasing number of multilayers, while they show weak dependence on the spacer layer thickness for a given multilayer structure.
- The improvement in the magnetic properties of multilayer films is due to the transition from magnetic stripe domain structure causing a transcritical hysteresis loop to the in-plane orientation of the magnetization parallel to the film plane.
- Temperature dependent magnetic study reveals that the shape of the *M-H* loops depend strongly on number of multilayers and spacer layer thickness. The multilayer film with x = 1 showed a strong temperature dependent magnetic nature induced by the direct exchange coupling through the pinholes.
- Multilayer films exhibit pronounced multistep magnetization reversal process at temperatures below 70 K and thermal activation results in smooth and narrow hysteresis loops for temperatures above 70 K. The number of steps in the reversal behaviour depends on number of multilayers and thickness of the spacer layers.
- The magnetic disorder observed at low temperature in a single layer film decreases and the bifurcation observed between ZFC and FC data shifts to lower temperature and disappears eventually for multilayer films with increasing number of multilayers and thickness of the spacer layers.
- The magnetic parameters (coercivity, field necessary to saturate the magnetization and perpendicular anisotropy constant) of multilayer films depend strongly on

temperature and vary at different rates for different multilayers and spacer layer thicknesses.

- The saturation magnetization in multilayer films decreases significantly with increasing number of multilayers due to increase in the magnetic dead layers with increasing number of interfaces.
- High temperature magnetic properties measured under saturated conditions and Curie temperature of multilayer films are not influenced by the multilayer structure.
- The observed results were discussed on the basis of change in the magnetic structure from stripe domain structure to in-plane magnetization, effective reduction of perpendicular anisotropy and magnetic disorder with increasing number of multilayers, thickness of the spacer layers and measurement temperatures.

Chapter 6

Effect of post deposition annealing on the structural and magnetic properties of FeTaC single and multilayer films

As demonstrated in the earlier chapters, the soft magnetic properties of FeTaC films depend strongly on the film thickness in single layer films, and number of multilayers and thickness of the spacer layers in multilayer films. In addition, most of the amorphous films exhibit a strong temperature dependent saturation magnetization (M_S) and low Curie temperature (T_C). Furthermore, the values of M_S decrease with increasing number of multilayers in multilayer films. All the as-deposited multilayer films exhibit a pronounced multistep magnetization reversal process only at temperatures below 80 K due to the interface roughness induced by number of interfaces. Therefore, to improve the soft magnetic properties (high M_S, low coercivity (H_C) and high T_C) in FeTaC films, the as-deposited amorphous precursors were annealed ex-situ systematically at different temperatures (T_A). It is well-known that the process of post deposition annealing not only develops two-phase microstructure in which the fine-nanocrystals are embedded in the amorphous matrix [MCHE1999, SELL2006], but also promotes the interface roughness due to the possible interlayer mixing in multilayer films. As a result, the magnetic properties and the magnetization reversal process in multilayer films are expected to show different properties as compared to amorphous precursors. However, no systematic investigations of effect of post deposition annealing process and the measurement temperature on the nature of the coupling between the ferromagnetic layers and the properties of multilayer films could be found in the literature. Hence, we have annealed all the as-deposited films systematically ex-situ at different temperatures and the resulting magnetic properties are discussed in this chapter.

6.1. Experimental details:

All the as-deposited amorphous FeTaC (200 nm) film and multilayer [[FeTaC (y nm)/Ta (x nm)]$_n$/FeTaC (y nm)] films with n = 1 - 4 and x = 1 - 4 nm deposited at ambient temperature directly on thermally oxidized Si substrates were annealed ex-situ in a separate home-made high vacuum (< 10^{-6} Torr) annealing set-up at different T_A of 200 ºC, 300 ºC and 400 ºC for 30 minutes duration. The annealing temperature and annealing time were optimized based on the development of nanocrystalline microstructure and magnetic properties of films. In the annealing process, the samples were kept on a filament heater and attached closely to a thermocouple (Chromel-Alumel) to avoid any temperature lag between heater, sample and thermocouple. The chamber was pumped to a high vacuum of better than 10^{-6} Torr using diffusion pump and rotary pump combinations. After reaching the desired vacuum, temperature was raised constantly at a rate of 10 ºC/minute to T_A. The samples were annealed at a given T_A within the temperature stability of ±2 ºC accuracy. After the completion of the

heat treatment at a particular T_A, the heater was switched off and the samples were allowed to cool down naturally to room temperature in the presence of vacuum. Crystal structure and microstructure properties of annealed films were confirmed by X-ray diffraction (XRD) using a Rigaku TTRAX III diffractometer with Cu-K_α radiation (λ = 1.54056 Å) and transmission electron microscopy (TEM, JEOL 2100 and TECHNAI G^2 F30) techniques. Temperature dependent magnetic properties in the temperature range 20 K to 1100 K were investigated by using vibrating sample magnetometer (VSM, Lake Shore Model 7410).

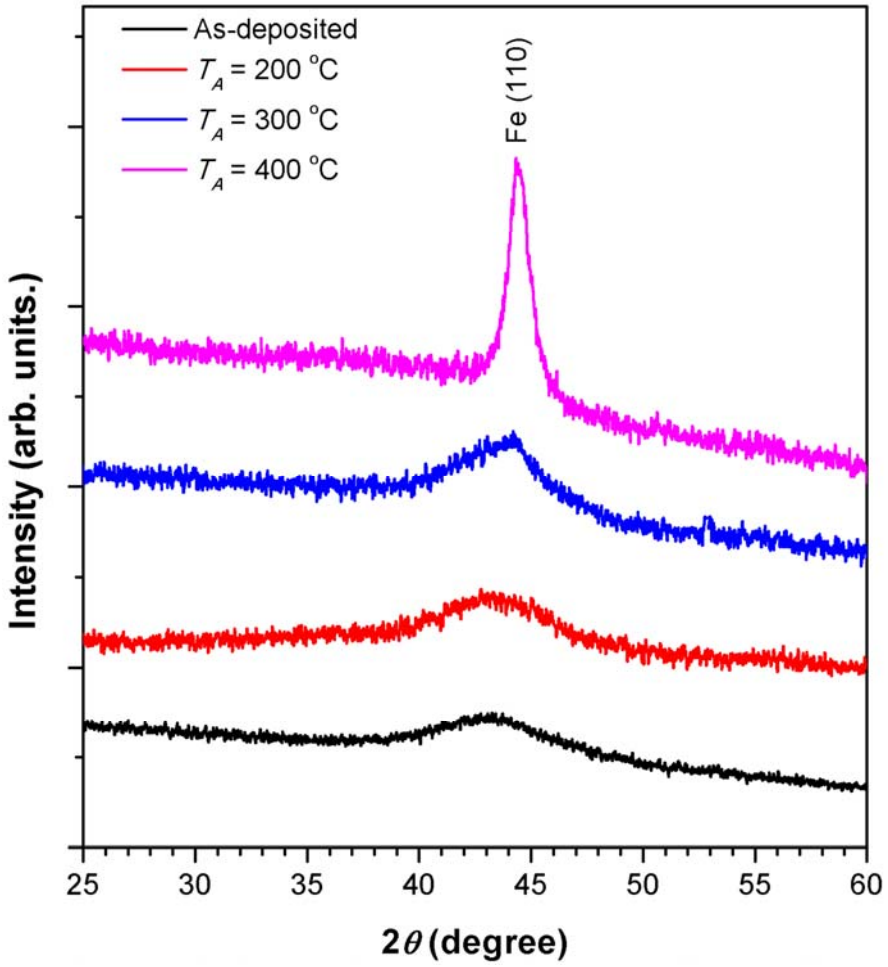

Figure 6.01: Room temperature XRD patterns of multilayer [[FeTaC (50 nm)/Ta (1 nm)]$_3$/FeTaC (50 nm)] films annealed at different temperatures.

6.2. Structural properties:

Figure 6.01 depicts the typical room temperature XRD patterns of multilayer films with x = 1 and n = 3 annealed at different T_A. It is clearly seen from the figure that the films annealed at temperatures below 200 ºC exhibit only a broad peak around 2θ = 43º indicating the

existence of amorphous structure. On the other hand, the films annealed at 300 °C reveal a decrease in the broadness of the peak along with a shift in the peak position to a higher angle. This confirms the nucleation of α-Fe nanocrystals in the residual amorphous matrix. On further increasing T_A to 400 ºC, a clear diffraction peak was observed around $2\theta = 44.44^{o}$ and its peak value approaches to α-Fe diffraction angle. This reveals the formation of well-defined α-Fe nanocrystals in the residual amorphous matrix [HASE1990, PERU2009]. The average crystallite size calculated from the XRD peak at $2\theta = 44.44^{o}$ using the Scherer's formula for the films annealed at 400 ºC is found to be around 10 nm in size. In order to further confirm the formation of α-Fe nanocrystals in the residual amorphous matrix of all the ferromagnetic layers, the cross sectional microstructural studies were carried out using TEM. Figure 6.02 displays cross-section TEM images for single layer and multilayer films

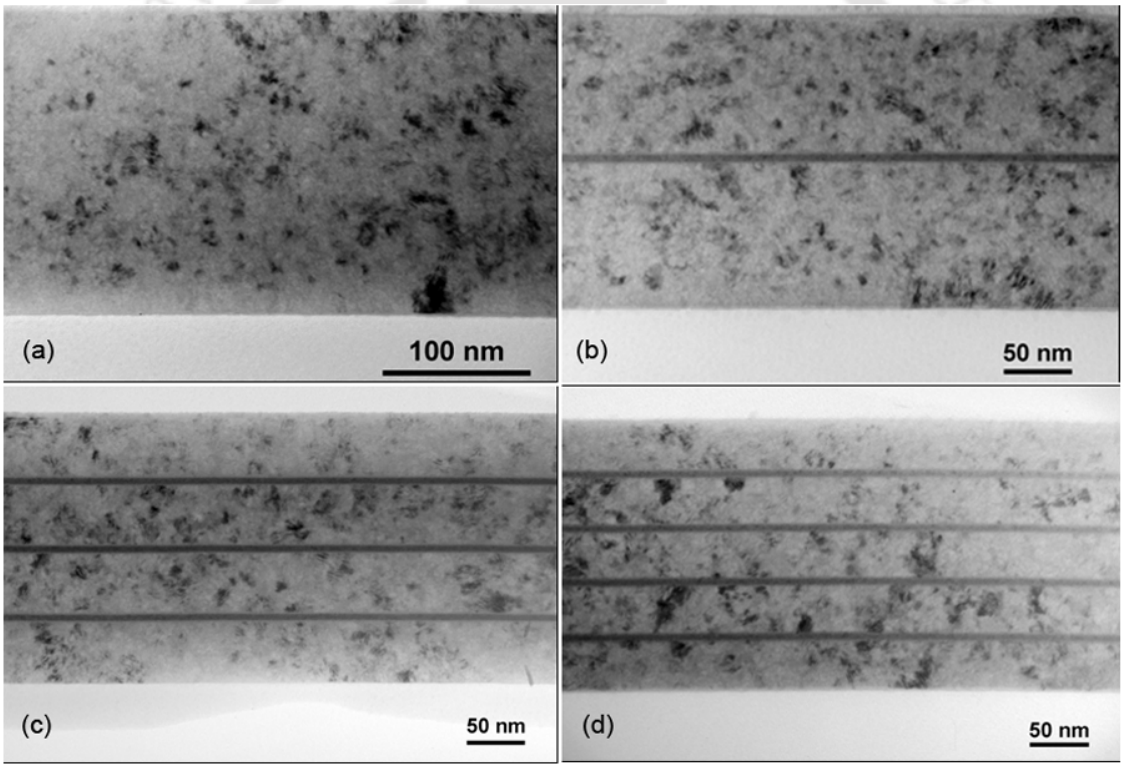

Figure 6.02: Cross sectional TEM micrographs of (a) FeTaC (200 nm) single layer film and multilayer [[FeTaC (y nm)/Ta (4 nm)]$_n$/FeTaC (y nm)] films with n = 1, 3 and 4 annealed at 400 ºC.

with x = 4 nm and for different n values. It is obvious from the figure that the formation of α-Fe nanocrystals is randomly distributed in the amorphous matrix. The average size of the crystallites calculated from the bright-field TEM image is also found to be around 10 nm in

size. These results are in good agreement with XRD results. The above results also confirm that the annealed films at T_A = 400 ºC exhibit two phase microstructure.

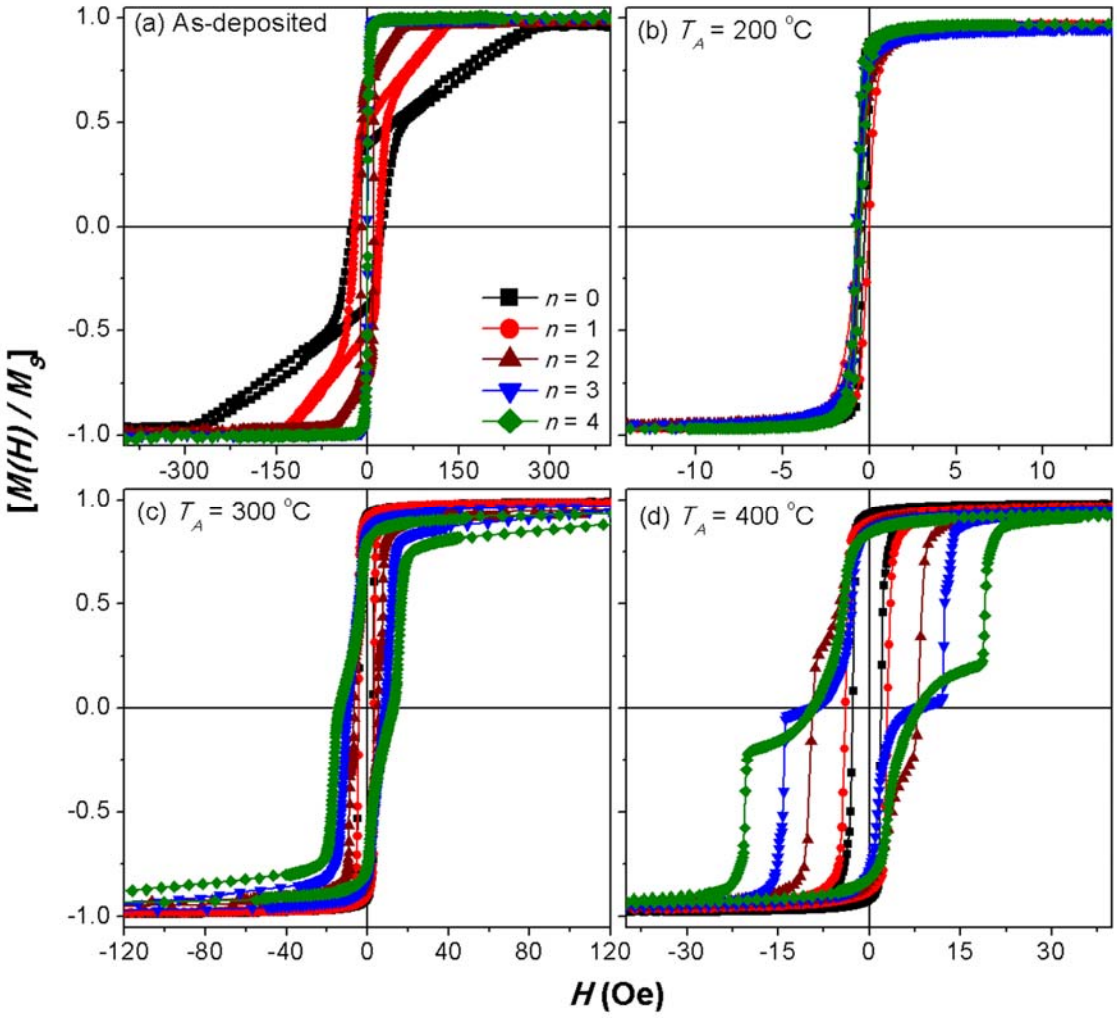

Figure 6.03: Room temperature M-H loops of (a) as-deposited and annealed single and multilayer films at (b) 200 ºC, (c) 300 ºC and (d) 400 ºC.

6.3. Magnetic properties:

As demonstrated in the chapter 5 for the as-deposited films, the magnetic properties of the annealed multilayer films were also investigated in two different aspects: (i) the effect of number of multilayers (n) and temperature on the magnetic properties by fixing the Ta spacer layer thickness (x), and (ii) the effect of thickness of the spacer layers and temperature on the magnetic properties by fixing number of Ta spacer layers (n). The value of n was varied

between 0 and 4 by keeping *x* at 1 nm in the first case, while the later part had the *n* value as 3 and varied the values of *x* between 0 and 4 nm.

6.3.1. Effect of multilayer structure on the magnetic properties:

6.3.1.1. Room temperature magnetic properties:

Figure 6.03 depicts room temperature normalized in-plane magnetic hysteresis (*M-H*) loops of as-deposited and annealed single and multilayer films with different *n* values at 200 ºC, 300 ºC and 400 ºC. As explained earlier in chapter 5, the shape of the *M-H* loops for the as-deposited films changed from transcritical to flat loop with increasing *n* values above 2 (see figure 6.03(a)). On the other hand, the single layer film and multilayer films with different *n* values annealed at 200 ºC exhibit narrow flat loops, which are considerably shifted to a negative axis for all the films as shown in figure 6.03(b). Interestingly, these loops saturate at low applied fields (< 10 Oe). This can be ascribed to the release of the stress in the as-deposited films and thereby reducing the perpendicular anisotropy. This eventually fades out the existence of strip domain structure in the annealed films [JICW2005, SHAR2006,

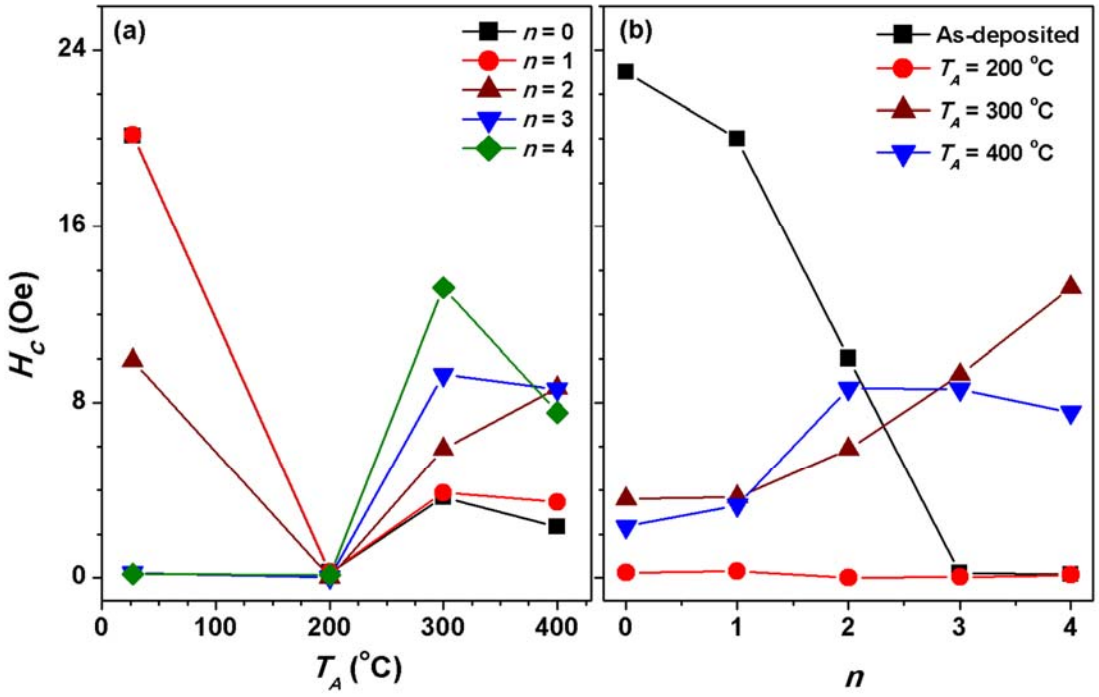

Figure 6.04: The variations of H_C with (a) T_A and (b) n in as-deposited and annealed single and multilayer films at (T_A =) 200 ºC, 300 ºC and 400 ºC.

SHAH2010] as compared to amorphous precursors and results in the in-plane orientation of the magnetization for all the single layer and multilayer films, exhibiting narrow *M-H* loops. The shift in the loop can be understood from the two-layers model as discussed in chapter 4. In the presently investigated films, the hard magnetic properties of the layers around the interface of the substrate and the rest of the upper soft magnetic layers can produce a considerable shift in the hysteresis, as observed by Lai et al in FeTaCN films with hard magnet bias [LAIC2003]. With increasing T_A above 200 ºC, the shape of the *M-H* loops changes completely as shown in the figures 6.03(c) and 6.03(d) and pronounced multistep magnetization reversal behaviour was observed even at room temperature for multilayer films with $n > 1$. In addition, number of steps in the reversal behaviour and its nature depend on the values of n and T_A. For multilayer films annealed at 400 ºC, the position of the second reversal process shifts from second quadrant to third quadrant with increasing the n values from 2 to 4. Note that such magnetization reversal behaviour was observed at temperatures only below 80 K for the as-deposited multilayer films. These results suggest that the interface roughness is enhanced with increasing T_A and hence resulting multistep magnetization reversal behaviour even at room temperature. The extracted values of H_C from the *M-H* loops are summarized as a function of T_A and n in figure 6.04. H_C not only decreases with increasing number of multilayers in as-deposited films, but also decreases largely for the films annealed at 200 ºC and approaches to a minimum of around 0.02 Oe for $n = 2$ multilayer film. While the former one could be understood based on the transition from stripe domain structure to in-plane orientation of magnetization with increasing n values [MISH2011], the latter is dominated by the reduction in the stress of the films with moderate annealing, which results the annihilation of the perpendicular anisotropy and the stripe domain structure even in FeTaC (200 nm) single layer film [NAKA1997, CHOU2003, JICW2005, SHAH2010]. On the other hand, H_C increases significantly not only with increasing T_A to 300 ºC, but also increases with increasing the n values. H_C reduces slightly for all the films annealed at 400 ºC as compared to the films annealed at 300 ºC. Similarly, the variations of H_C with n show that (i) H_C increases with increasing n for the 300 ºC annealed films and (ii) for the films annealed at 400 ºC, H_C increases initially with increasing n up to 2 and remains almost constant for $n \geq 2$. Although the development of random α-Fe nanocrystals with size less than ferromagnetic exchange correlation length in FeTaC amorphous matrix is expected to decrease H_C [HERZ1990, PERU2009] due to the presence of random anisotropy in the nanocrystalline microstructure, the interface roughness

developed at the interface between the ferromagnetic and the non-magnetic layers during the annealing process controls the magnetization reversal process. As a result, a significant increase in H_C was observed in multilayer films as compared to single layer film. Furthermore, the variations of H_C with number of multilayers are mainly dominated by the multilayer structure driven reversal process as seen from the *M-H* loops (see figure 6.03).

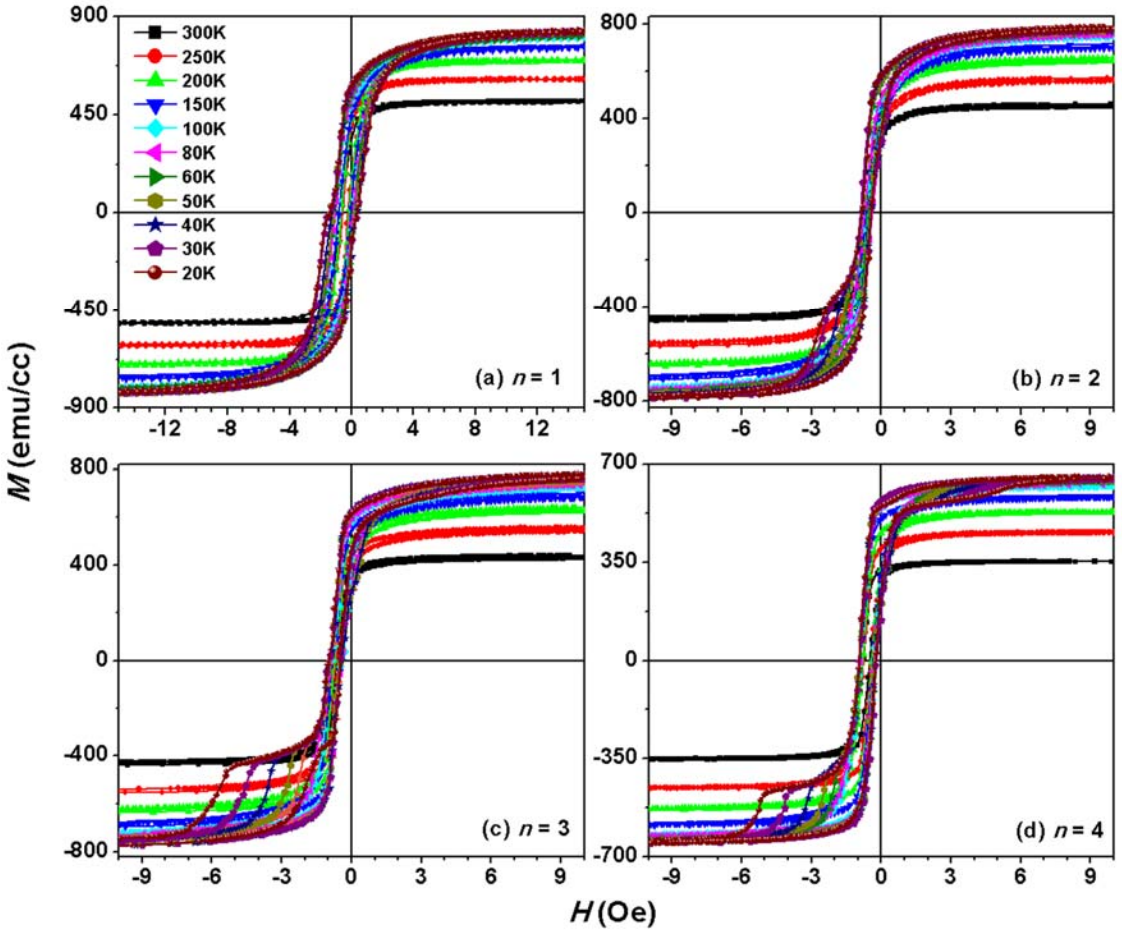

Figure 6.05: Temperature dependent M-H loops of multilayer films annealed at 200 °C with different values of n.

6.3.1.2. Low temperature magnetic properties:

To understand the magnetization reversal behaviour in details and its effect on the resulting magnetic properties, temperature dependent *M-H* loops are measured using VSM from 300 K to 20 K for all the multilayer films annealed at different T_A. The properties are explained separately for the films annealed at different T_A.

(a) Properties of the films annealed at (T_A =) 200 ℃:

Figure 6.05 displays temperature dependent *M-H* loops of multilayer films annealed at 200 ^{o}C. It is observed that the shape of the loops was not changed with temperature for the films with n = 1. However, the values of H_C and the field necessary to saturate the films' magnetization increase with decreasing temperature. This is a typical behaviour in many ferromagnetic materials. On the other hand, for the films with $n \geq 2$, the *M-H* loops display the multistep magnetization reversal behaviour at temperatures below 80 K. The magnetization switching in the individual ferromagnetic layer depends on number of multilayers. There is an additional step of magnetization reversal appearing in the third quadrant of the *M-H* loops for temperatures below 80 K for all the films with $n \geq 2$. By considering the relative variation of the magnetization of the films with respect to the saturation magnetization, it can be understood that the additional step is mainly due to the switching of the bottom most layer deposited directly on the substrate in each multilayer films. In addition, the loops are shifted significantly towards the negative field axis. The shifting of the loops increases with increasing n up to 3 and reduces slightly for n = 4 films. The extracted values of H_C for all the films are plotted in figure 6.08(a). H_C of single layer FeTaC film (n = 0) increases considerably with decreasing temperature down to 200 K and varies almost linearly in logarithmic scale with decreasing temperature from 200 K to 20 K. On the other hand, all the multilayer films show almost a linear variation of H_C with temperature in logarithmic scale and the rate of increase in H_C depends strongly on number of multilayers. The variations of M_S with temperature plotted in figure 6.09(b) reveal that the values of M_S decrease not only with increasing temperature, but also decrease significantly with increasing number of multilayers. This may be influenced by the inter-diffused layers, which increases with increasing number of multilayers. However, the values of M_S are found to be almost similar to the as-deposited films.

(b) Properties of the films annealed at (T_A =) 300 ℃:

Figure 6.06 shows temperature dependent *M-H* loops of 300 ºC annealed multilayer films. The temperature dependent *M-H* loops reveal the following features: (1) For the films with n = 1, the shape of the *M-H* loops remains the same with decreasing temperature from 300 K to 20 K. (2) With increasing $n \geq 2$, the shape of the *M-H* loops depends strongly on the temperature and exhibits multistep magnetization reversal behaviour. The number of steps, its nature and position of the steps in the loops vary with the temperature and n values. For

example, the multilayer film with n = 2 (see figure 6.06(b)) having three FeTaC (67 nm) layers displays three steps in the magnetization reversal process at 300 K. This is due to the individual switching of FeTaC layers upon the application of reverse field after its saturation in the positive direction. With decreasing temperature down to 80 K, the size of the second and third steps decreases gradually and disappears at temperatures below 80 K. This results only two steps in the magnetization reversal process, which confirms that the top layer

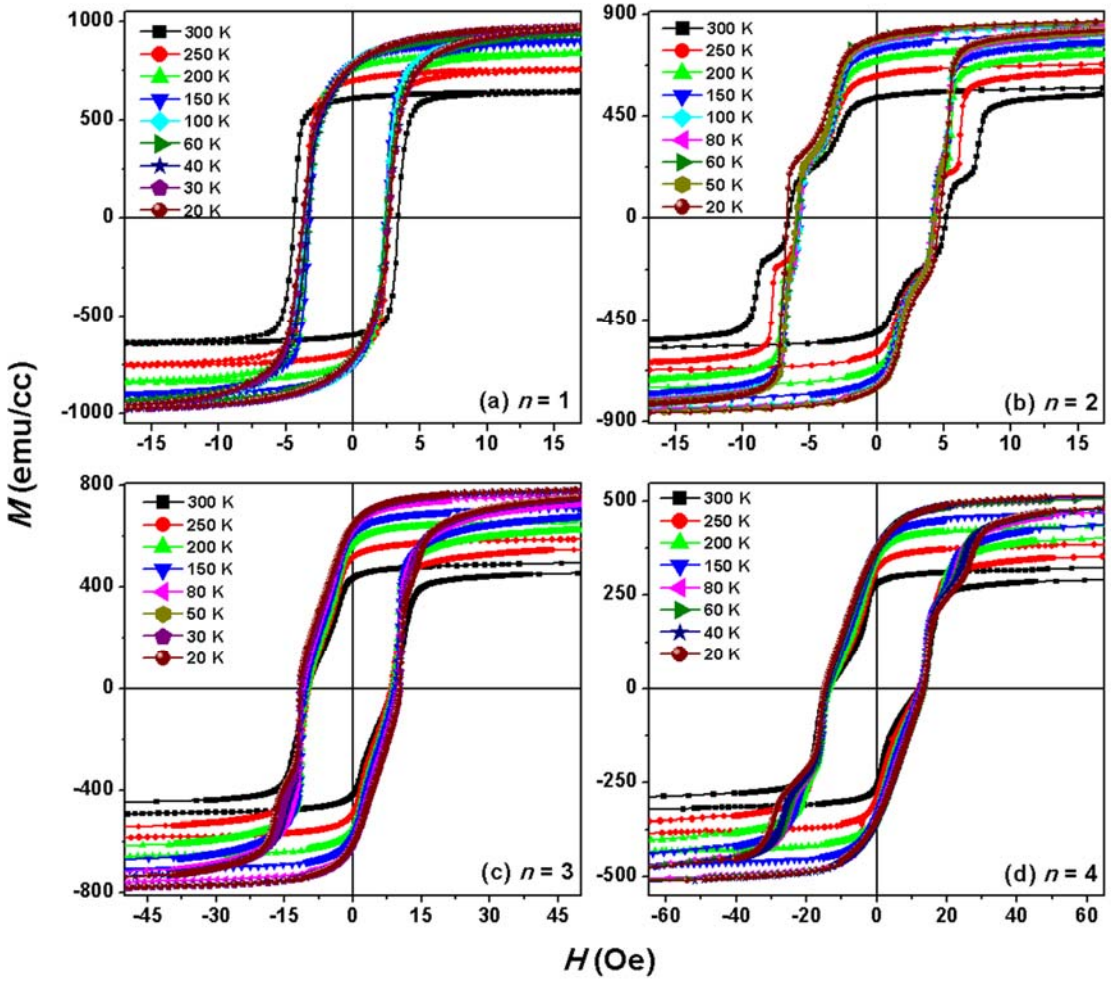

Figure 6.06: Temperature dependent M-H loops of multilayer films annealed at 300 ºC with different values of n. M-H loops at selected temperatures are shown to display the variations clearly.

switches freely followed by the collective switching of the next two layers. A detailed explanation regarding the magnetization reversal is discussed in the later part. With increasing n > 2, the magnetization reversal changes significantly as compared to n = 2 films, i.e., at 300 K, the magnetization decreases gradually with increasing the reverse field

resulting two steps in the magnetization reversal. However, the magnetization in the third quadrant changes quickly with the applied field and with decreasing temperature. On further reducing the temperature below 40 K, the third step of the reversal occurs due to the individual switching of bottom most layer on the substrate in multilayer films. The appearance of the third step is more noticeable for the films with n = 4 even at 80 K (see figure 6.06(d)). However, the third step in n = 4 films is due to the collective switching of the

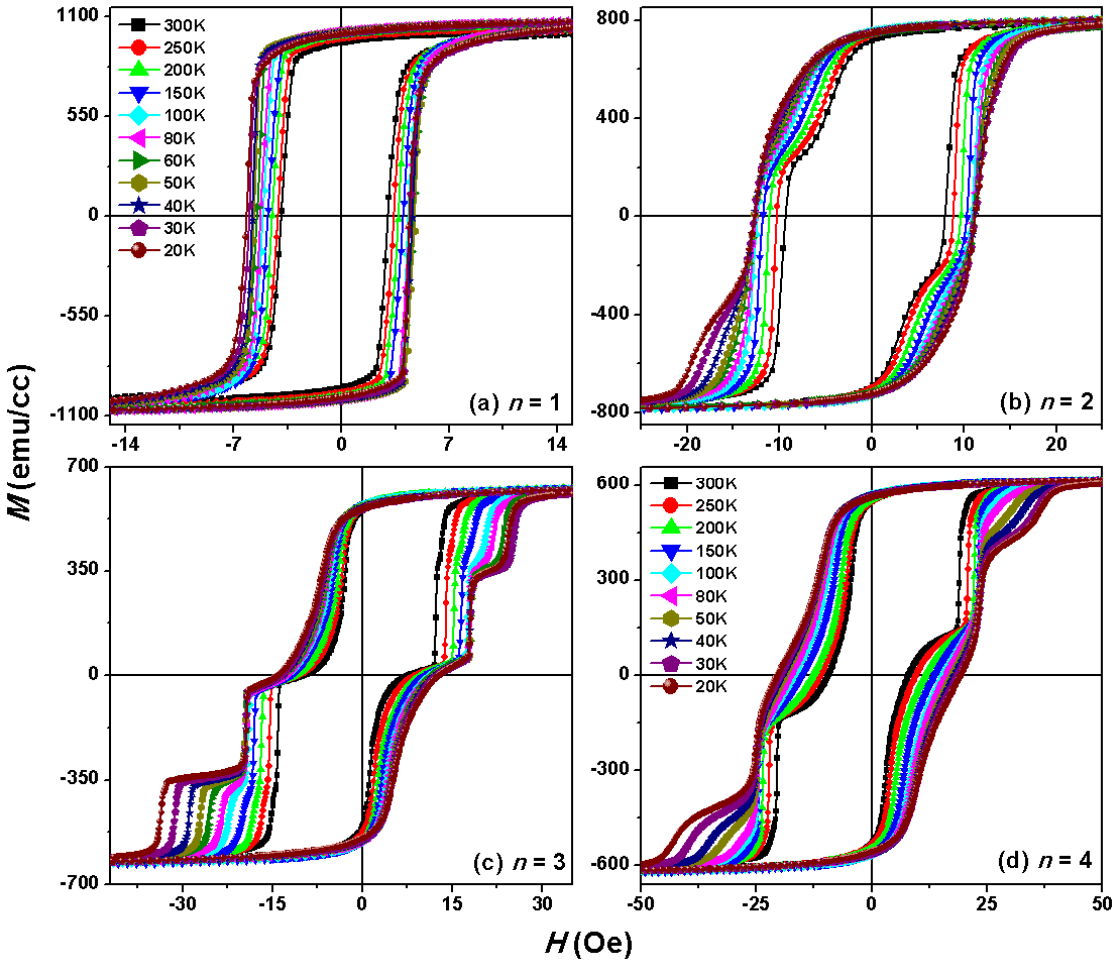

Figure 6.07: Temperature dependent M-H loops of multilayer films annealed at 400 ºC with different values of n. M-H loops at selected temperatures are displayed to show the variations clearly.

bottom two layers. The extracted values of H_C as displayed in figure 6.08(b) show unusual and interesting features: (i) H_C of the single layer film (n = 0) annealed at 300 ºC increases almost linearly in logarithmic scale with decreasing temperature which is the typical nature of a ferromagnetic material. (ii) For n = 1 multilayer film, H_C decreases up to 150 K and then

increases significantly at lower temperatures leaving a broad minimum in the temperature range between 200 K and 75 K. In addition, H_C at 21 K is lower than the H_C at 300 K. (iii) A similar behaviour of H_C with temperature is observed for n = 2 film, but the values of H_C at low temperatures increase largely as compared n = 1 film. (iv) On further increasing $n \geq 3$, H_C decreases slightly at 250 K as compared to the value at 300 K, but increases almost linearly with decreasing the temperature below 250 K. Nevertheless, the actual values of H_C in multilayer films increase with increasing number of multilayers, which can be attributed to number of interfaces hindering the collective switching of the FeTaC ferromagnetic layers. Figure 6.09(c) depicts the variations of M_S with temperature for multilayer films with different n values. M_S values increase considerably as compared to the as-deposited films and films annealed at 200 ºC. This could be correlated to the nucleation of α-Fe nanocrystals in the amorphous matrix as discussed in the structural properties, which results an increase in the magnetization. The variations of M_S with temperature reveal that the values of M_S decrease not only with increasing temperature, but also decrease significantly with increasing number of multilayers. This may be influenced by the diffusion at the interfaces, which is possibly increasing with increasing number of multilayers.

(c) Properties of the films annealed at* (T_A =) *400 ℃:

Figure 6.07 displays temperature dependent *M-H* loops of the multilayer films annealed at 400 ºC. The features obtained from the figure are: (1) For the films with n = 1, the shape of the *M-H* loops measured at different temperatures remains the same, as observed for the films annealed at 200 and 300 ºC. (2) With increasing $n > 1$, *M-H* loops exhibit strong temperature dependent magnetization reversal behaviour, i.e., the shape of the *M-H* loops is different at different temperatures for different multilayer films. (3) For the films with n = 2 (having three FeTaC layers), the *M-H* loop at 300 K exhibits two step reversal process due to the switching of top FeTaC layer followed by the collective switching of the bottom two layers. This behaviour remains unchanged with decreasing temperature down to 60 K, but the nature of the steps in the second quadrant varies gradually with decreasing temperature due to the change in the interlayer coupling. On further reducing the temperature below 60 K, the bottom most layer in the film tries to switch individually due to the temperature dependent interface roughness induced by the annealing process. As a result, the coupling between the top two layers is enhanced resulting a collective switching of top two layers followed by the individual gradual switching of the bottom most layer in the multilayer film. (4) With

increasing n to 3, the M-H loop displays two switching processes at 300 K due to the collective nature of the switching of the top two layers followed by the bottom two layers. With decreasing temperature below 150 K, one more additional switching starts appearing possibly due to the individual switching of the bottom most layer depending on the temperature dependent interface roughness as seen in the film with n = 2. The size of the step

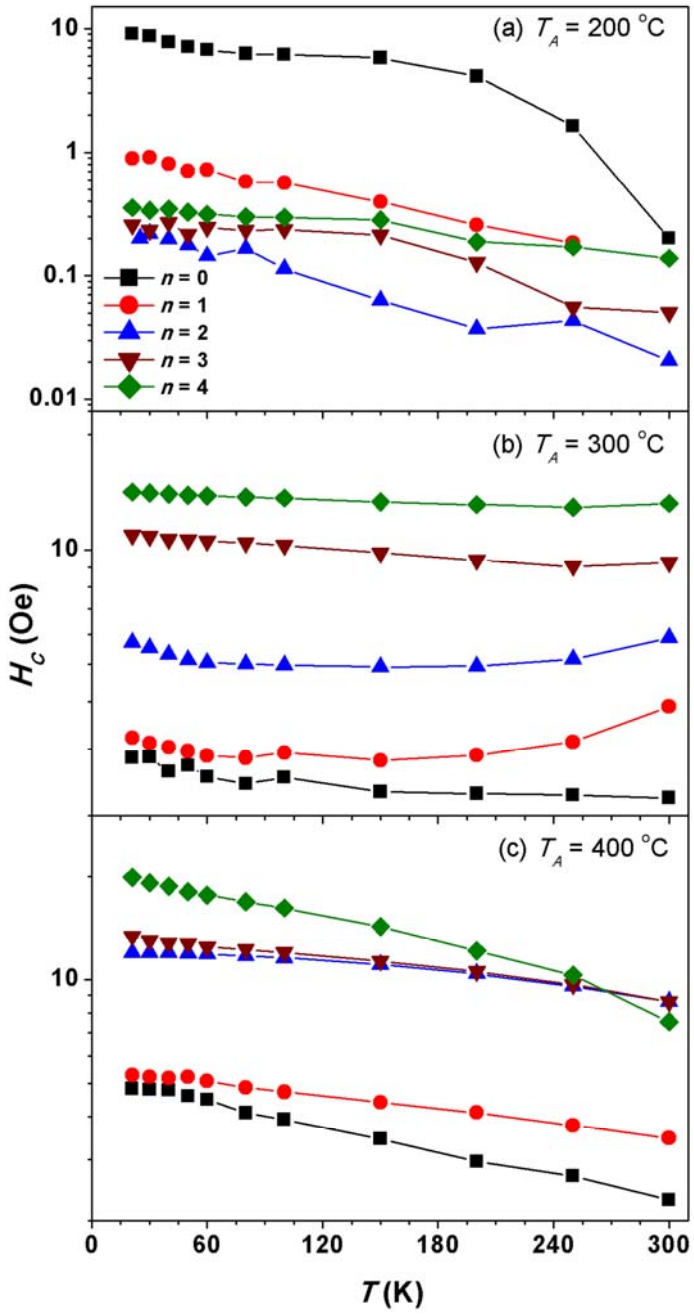

Figure 6.08: Temperature dependent H_C of multilayer films annealed at (a) 200 °C, (b) 300 °C and (c) 400 °C with different values of n.

increases significantly with decreasing temperature and therefore the field required to switch the bottom most layer also increases from 24 Oe to 33 Oe with decreasing temperature from 60 K to 20 K. (5) On further increasing *n* to 4, the *M-H* loops exhibit different nature as compared to *n* = 2 and 3 films. However, number of layers switching collectively with respect to the top layer increases to 3. In addition, there exists an additional switching at low temperature similar to the *n* = 2 and 3 films due to the individual switching of the bottom most layer in the multilayer film. It is important to note that number of FeTaC layers switches collectively with respect to the top free layer increases from 1 to 3 with increasing number of multilayers from 2 to 4, respectively. In addition, the effect of bottom most layer switching in all multilayer films is clearly pronounced with reducing the temperature. The variations of H_C with temperature for different multilayer films annealed at 400 ºC are depicted in figure

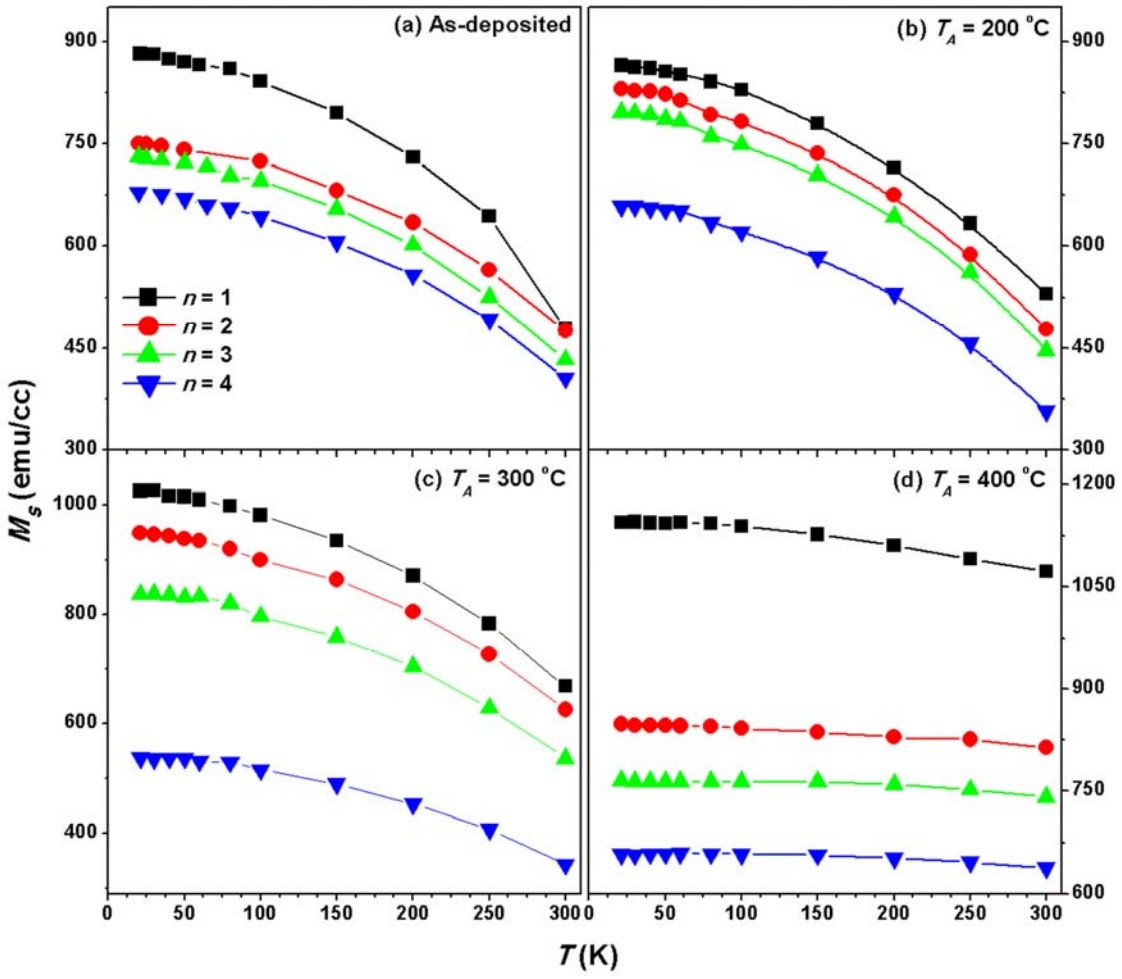

Figure 6.09: Temperature dependent M_S of (a) as-deposited and annealed multilayer films at (b) 200 ºC, (c) 300 ºC and (d) 400 ºC with different values of n.

6.08(c). H_C increases not only almost linearly with decreasing temperature down to 50 K for all the multilayer films, but also increases with increasing number of multilayers. In order to estimate the rate of increase in H_C with increasing n values, $H_C(T)$ data were fitted to a linear equation in the temperature range 250 K to 50 K. It is observed that the slope increases from 0.0065 Oe/K for n = 1 film to 0.0418 Oe/K for n = 4 film. Figure 6.09(d) depicts the temperature dependent M_S for the multilayer films with different n values. The values of M_S increase largely, as compared to the as-deposited films due to the existence of well-defined α-Fe nanocrystals in the amorphous matrix. In addition, M_S values are found to be nearly the same in the temperature range between 20 K and 300 K for each multilayer film except for n = 1 film. Nevertheless, M_S decreases significantly with increasing number of multilayers due to the interface diffusion, which increases with increasing number of multilayers.

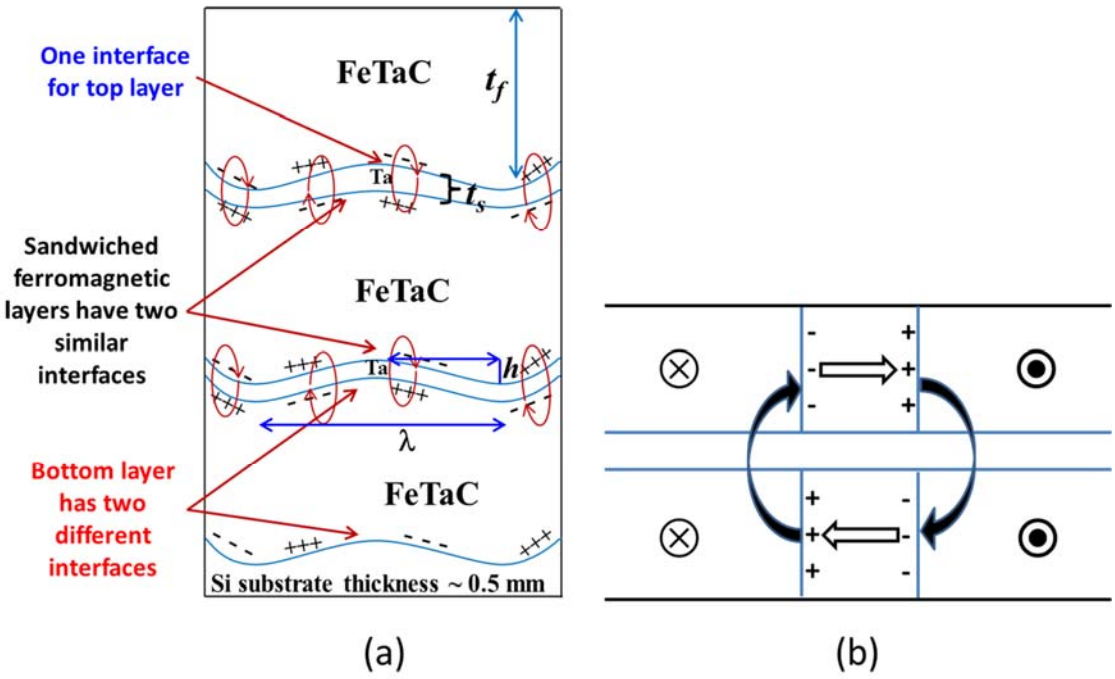

Figure 6.10: Schematic drawing of (a) Néel's orange peel coupling and (b) magnetostatic coupling between the stray fields of domain walls in multilayer thin films [CHOP2000, CHOP2005].

The above results clearly reveal that the magnetization reversal behaviour in the presently investigated multilayer thin films is strongly depending on number of multilayers, annealing temperature and the measurement temperature. This can be attributed to the change in the interlayer coupling between the ferromagnetic layers in multilayer films with

temperature and the values *x* and *n*. In general, the interlayer coupling to reverse the magnetization in the multilayer films can have four different origins [YANG2009]: (1) direct ferromagnetic coupling through pinholes in the thin spacer layer as demonstrated earlier in chapter 5 [PONG2008], (2) indirect exchange coupling through Ruderman-Kittel-Kasuya-Yosida (RKKY) interactions [NIST2010], (3) magnetostatic coupling through the stray fields at the edges of the finite sized thin films [CHOP2000, THOM2000, CHOP2005, BALT2007, STOB2009], (4) orange peel (Néel) coupling due to correlated interfacial roughness [MORI2004, NEEL1954, ZHAN19961, ZHAN19962, SCHR2000, TEGE2001] and (5) magnetostatic coupling between the stray fields of domains walls in different layers giving rise to Néel walls [CHOP2000, CHOP2005]. The observed results in figures 6.06 and 6.07 and considering the large electrical resistivity of Ta (spacer layer) as compared to Cu and Ag, the interlayer coupling due to the direct ferromagnetic coupling through pinhole and the indirect exchange coupling through RKKY interaction is nearly negligible. The stray field coupling is always present in magnetic multilayers, because each ferromagnetic layer is placed in the demagnetization field of the others, which tends to align the magnetization of adjacent layers antiparallel. However, the interlayer magnetostatic interaction through the stray fields at the edges of the continuous film of larger dimensions is weak and any contribution to the net coupling from stay fields is almost negligible [ANGU2000, LIUX2012]. The Néel coupling is magnetostatic in nature and the model by Néel considers two ferromagnetic layers with in-plane magnetization separated by a non-magnetic spacer. If the surface of ferromagnetic layers has correlated roughness, dipoles are set up at homologous protrusions and bumps at the interfaces as shown in figure 6.10(a). This tends to ferromagnetically align the magnetization in the nearest magnetic layers. Therefore, the Néel coupling caused by the correlated interface roughness as shown in figure 6.10(a) and magnetostatic coupling between the stray fields of domain walls as demonstrated in figure 6.10(b) play a key role on the magnetization reversal process of the presently investigated multilayer films. The magnitude of Néel coupling is given by [NEEL1962, SCHR2000],

$$H_N = \frac{\pi^2}{\sqrt{2}}\left(\frac{h^2}{\lambda t_f}\right) M_S exp\left(-\frac{2\pi\sqrt{2}t_s}{\lambda}\right) \qquad (6.01)$$

where, h and λ are the amplitude and wavelength of the interface roughness, M_S is saturation magnetization of the free layer, and t_f and t_s are the thicknesses of the top layer and spacer layer, respectively. As the values of M_S change with temperature and number of multilayers,

the magnitude of the Néel coupling is expected to vary accordingly [ZHAO1999, CHOU2003, MARK2010, HUYM2011]. With increasing number of multilayers, the thickness of the individual ferromagnetic layer decreases, resulting a transition from strip domain patterns to in-plane magnetization. Therefore, the magnetostatic coupling between the stray fields of the domain walls is also expected to vary with number of multilayers. Furthermore, the temperature dependent interfacial strain arising from the different thermal expansion coefficient of the materials at the interface [CHAE1999, CHEN20072, WANG2014] can contribute a significant role in the coupling process.

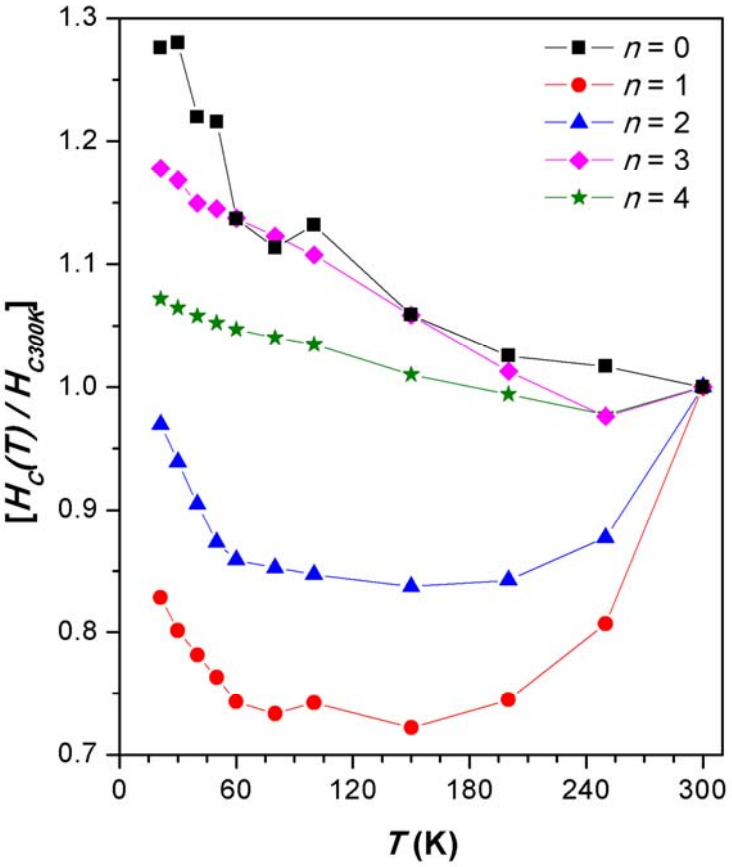

Figure 6.11: The variations of normalized coercivity with temperature for multilayer films with different n values annealed at 300 ºC.

For the multilayer films with n = 1 annealed at 300 ºC and 400 ºC, the *M-H* loops exhibit only a single loop with rectangular shape for all the measurement temperatures (see figures 6.06(a) and 6.07(a)). This suggests that FeTaC ferromagnetic layers are coupled strongly as the stray fields emanating from the domain walls are able to close its flux by magnetostatic locking-in with the stray fields from the domain walls in the adjacent layers, as

shown in figure 6.10(b). However, H_C increases linearly with decreasing temperature for 400 ºC annealed film, as expected for a typical ferromagnetic material, while the film annealed at 300 ºC exhibits a broad minimum in $H_C(T)$ versus T curve (see figure 6.11). This could be explained based on the variations of Néel coupling and the magnetostatic coupling between the stray fields of the domain walls. As discussed earlier, the multilayer film annealed at 300 ºC exhibits a large temperature dependent M_S down to 80 K and hence the Néel coupling and the magnetostatic coupling between the stray fields of domain walls increase with decreasing temperature. This enhances the interlayer coupling between the ferromagnetic layers and reduces switching field. Hence, a considerable reduction in H_C was observed. On further decreasing the temperature below 80 K, M_S almost remains constant and hence the contributions from the above two couplings do not reduce the switching field. On the other

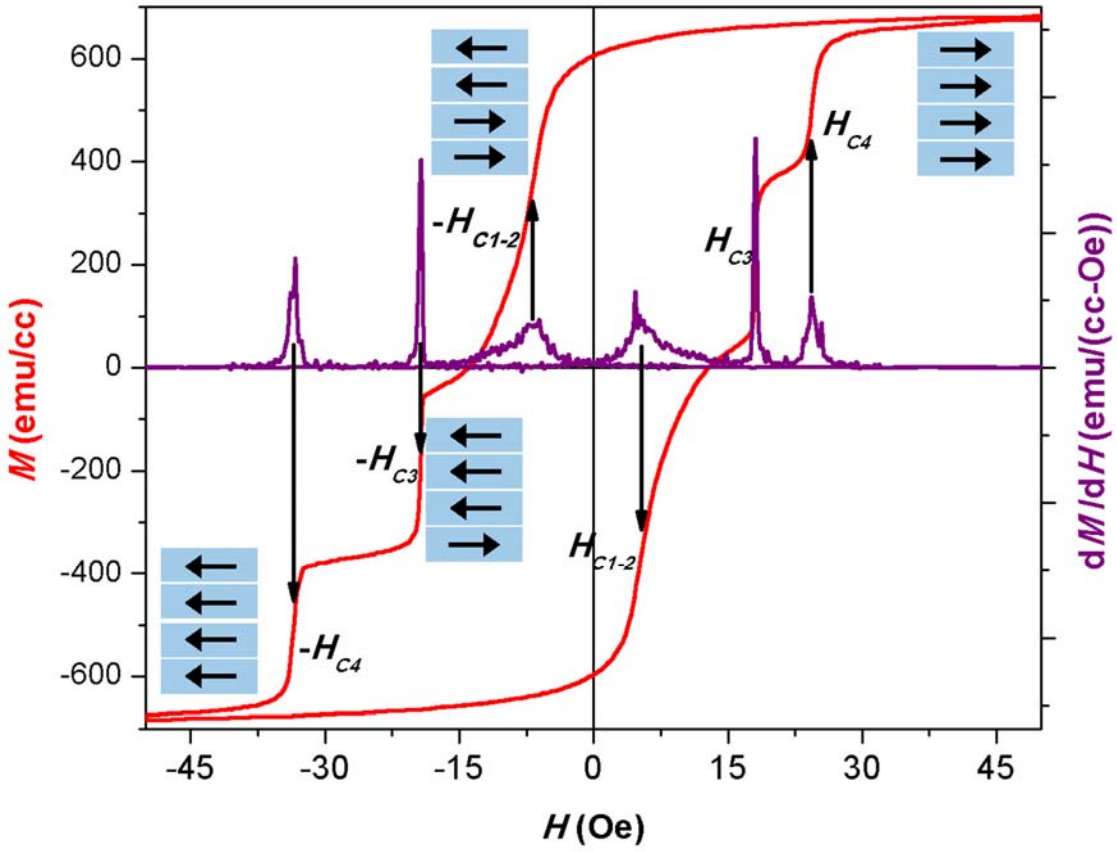

Figure 6.12: M-H loop measured at 21 K and the field derivative of magnetization for multilayer film with n = 3 and x = 1 annealed at 400 ºC.

hand, the contribution from the interface roughness increases with decreasing temperature. Therefore, H_C increases with decreasing temperature below 80 K. On the other hand, the film

with n = 1 annealed at 400 ºC shows a weak temperature dependence of M_S. This results no progressive change in the above couplings with reducing temperature. Hence, H_C vary almost linearly with decreasing temperature. With increasing $n \geq 2$, number of ferromagnetic layers and spacer layers increases resulting different interfaces as shown in figure 6.10(a), i.e., the top ferromagnetic layer has only one interface with Ta layer, which increases to two for the intermediate ferromagnetic layers and the bottom most ferromagnetic layer has two different interfacial natures: one from Ta spacer layer and other from the substrate. This provides a different magnitude of topological coupling for the top layer, intermediate layers and the bottom layer. Therefore, the top layer switches first either separately with low values of coercivity or collectively with the intermediate layers depending on the coupling between the layers followed by the intermediate layers with increased coercivity. The bottom most layer switches lastly either in coupling with the nearest intermediate layers or separately with higher coercivity. For example, the multilayer film with n = 2 annealed at 300 ºC exhibits individual ferromagnetic layer switching at 300 K (see figure 6.06(b)) due to the enhanced roughness amplitude, resulting a weak coupling between the ferromagnetic layers [GUSE2011, MAJN1976, YANB1989]. With decreasing temperature, the values of M_S show a strong dependent on temperature and following the eqn.(6.01), the Néel coupling field increases with decreasing temperature. At the same time, the magnetostatic coupling between the stray fields of domain walls also varies significantly with decreasing temperature. As a result, the individual switching changes gradually with decreasing temperature and exhibits eventually a collective switching between the intermediate and bottom layers. This would not only reduce number of switching from 3 to 2, but also reduces H_C significantly (see figure 6.11) down to 150 K as observed for n = 1 film annealed at 300 ºC. With increasing the values of $n > 2$, the thickness of individual ferromagnetic layer reduces to 50 nm or below. This exhibits a reduction in the values of M_S and an increase in the interface roughness of the films with increasing number of multilayers. Therefore, number of domains in the ferromagnetic layer is expected to decrease, resulting a reduction in the stray field coupling. In addition, the strain induced by the substrate on the bottom layer of the films is more visible with decreasing temperature. Therefore, the switching of the bottom layer is more pronounced with decreasing temperature and with increasing number of multilayers. Similarly, for the multilayer films annealed at 400 ºC, the realization of the interface effect between the substrate and the bottom layer is observed even for n = 2 films. Such effect is enhanced with increasing number of multilayers. Furthermore, the values of M_S remain

almost constant in the temperature range 20 K to 300 K for multilayer films annealed at 400 ºC and hence the Néel coupling mainly depends on the roughness parameters.

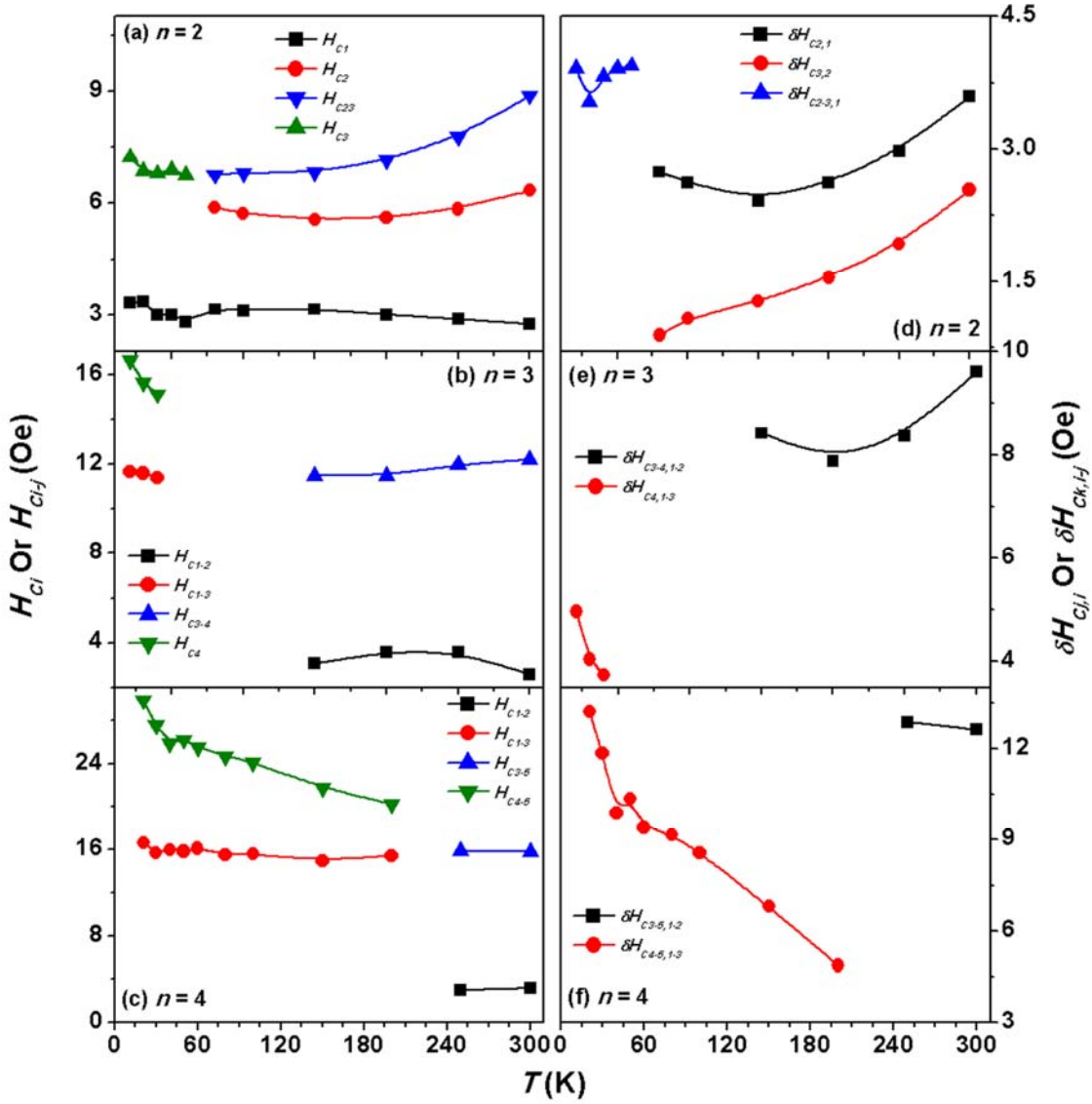

Figure 6.13: The variations of H_{Ci} or H_{Ci-j} and $\delta H_{Cj,i}$ or $\delta H_{Ck,i-j}$ for multilayer films with different n values annealed at 300 ºC.

In order to understand the individual and/or collective switching behaviours of the ferromagnetic FeTaC layers in detailed manner and to study the relative switching of the ferromagnetic layers as a function of temperature, we have carefully analysed the coercivity of the ferromagnetic layers by taking the derivative of the *M-H* loop as demonstrated in figure 6.12 [LIUX2012]. H_C of the individual steps is defined as either H_{Ci} or H_{Ci-j} depending on whether the switching occurs individually by a single layer or collectively between the

ferromagnetic layers in multilayer films. The switching behaviour was determined based on the relative variation of magnetization with respect to the saturation magnetization using the schematic drawing illustrated in figure 6.12. The fundamental concept behind such magnetization reversal is that when the interlayer coupling is strong enough as compared to

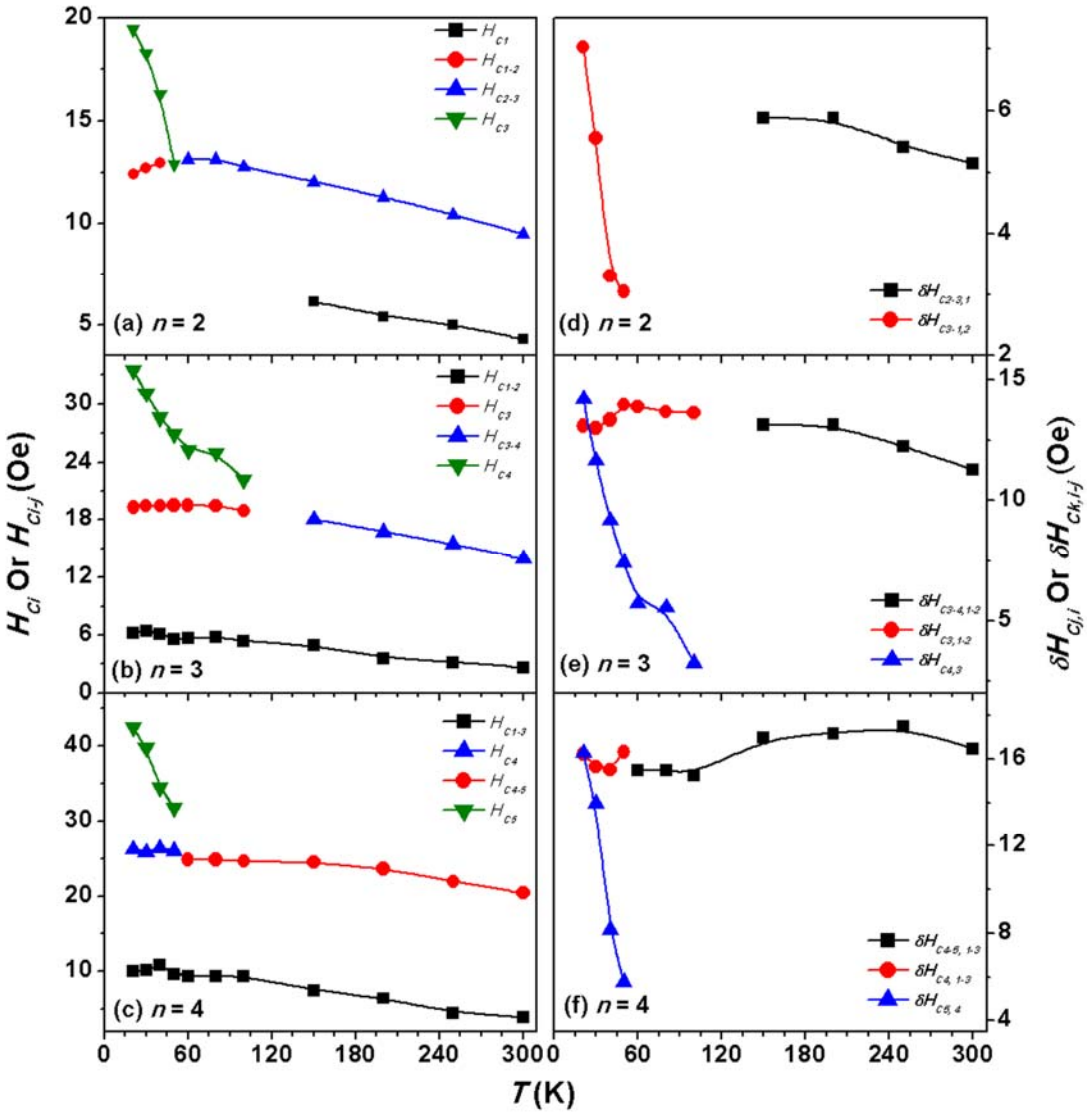

Figure 6.14: The variations of H_{Ci} or $H_{Ci\text{-}j}$ and $\delta H_{Cj,i}$ or $\delta H_{Ck,i\text{-}j}$ for multilayer films with different n values annealed at 400 ºC.

the coercivity of the individual ferromagnetic layers then they switch all together resulting a single loop in the hysteresis [LIUX2011, LIUX2012] as observed for n = 1 film. Otherwise, one would expect the individual switching of the ferromagnetic layers, which would result in a stepped hysteresis [HUAN2001]. It may be noted that the multilayer film with n = 3 has four number of FeTaC (50 nm) layers and hence it should have displayed four steps in the

reversal process provided all the layers switch individually. However, the multilayer film with $n = 3$ and $x = 1$ annealed at 400 ºC exhibits only three steps in the magnetization reversal process. Therefore, it is assumed that the top two layers switch together as shown schematically in figure 6.12 and the coercivity of such switching is defined as $H_{C1\text{-}2}$. This situation provides almost zero magnetization in film, as observed in figure 6.12. On further increasing the applied field in the reverse direction, two more steps were observed in the third quadrant and related to the switching of third (H_{C3}) and fourth (H_{C4}, bottom most) layers, respectively. Similarly, the relative switching of the ferromagnetic layers was analysed by introducing another set of parameters $\delta H_{Cj,i}$ (= H_{Cj} - H_{Ci}) and $\delta H_{Ck,i\text{-}j}$ (= H_{Ck} - $H_{Ci\text{-}j}$) representing the difference in the coercivity of the two individual switching of the nearest ferromagnetic layers and the difference in the coercivity of the one individual and collective switching of the nearest ferromagnetic layers, respectively. For example, one can determine $\delta H_{C4,3}$ (= H_{C4} - H_{C3} = 33.3 - 19.2 = 14.1 Oe) and $\delta H_{C3,1\text{-}2}$ (= H_{C3} - $H_{C1\text{-}2}$ = 19.2 - 6.9 = 12.3 Oe) from figure 6.12. Following the above procedures, the values of H_{Ci} (or $H_{Ci\text{-}j}$) and $\delta H_{Cj,i}$ (or $\delta H_{Ck,i\text{-}j}$) obtained for the multilayer films annealed at 300 ºC and 400 ºC are summarized as a function of temperature in figures 6.13 and 6.14, respectively. The variations of H_{Ci} (or $H_{Ci\text{-}j}$) and $\delta H_{Cj,i}$ (or $\delta H_{Ck,i\text{-}j}$) show a strong dependent on the temperature. A careful analysis of the bottom layer switching with respect to the above layers reveals that with increasing T_A and number of multilayers, the rate of change of $\delta H_{Cj,i}$ (or $\delta H_{Ck,i\text{-}j}$) increases largely in the low temperature region (< 100 K) due to substrate induced strain on multilayer films. With increasing temperature above 100 K, the values of $\delta H_{Cj,i}$ (or $\delta H_{Ck,i\text{-}j}$) increase for the films annealed at 300 ºC due to the reduction in the coupling field between the ferromagnetic layers. However, the films annealed at 400 ºC do not show any significant variation in $\delta H_{Cj,i}$ (or $\delta H_{Ck,i\text{-}j}$) values due to the weak temperature dependence of M_S, which further confirms a weak temperature dependent Néel coupling and magnetostatic coupling between the stray fields of the domain walls.

6.3.1.3. High temperature magnetic properties:

Figure 6.15 displays the high temperature thermo-magnetization (M-T) curves of as-deposited and annealed (T_A = 200 ºC, 300 ºC and 400 ºC) multilayer films with different n (= 2, 3 and 4) values measured along the film plane under 500 Oe applied magnetic field. In order to compare all the data of the films with a particular n value in a single graph, $M(T)$ data are normalized with respect to their room temperature magnetization. Figure 6.15 reveals the following features: (i) as-deposited multilayer films and the multilayer films annealed 200 ºC

exhibit a complete transition from ferromagnetic state to paramagnetic state in the temperature below 200 ºC. (ii) On the other hand, the multilayer films annealed at 300 ºC display a large decrease in magnetization with increasing temperature up to 160 ºC and

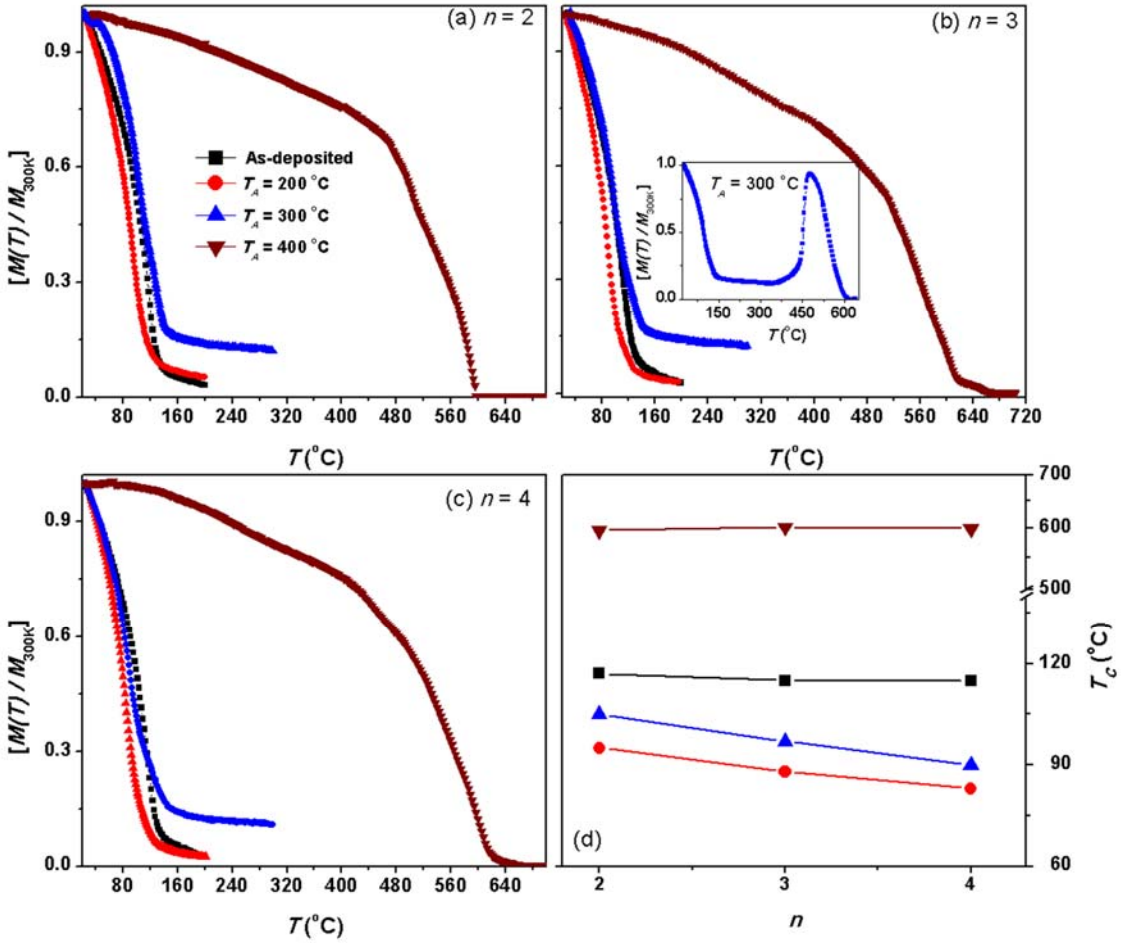

Figure 6.15: High temperature M-T curves of as-deposited and annealed (T_A = 200 ºC, 300 ºC and 400 ºC) multilayer films with different n (= 2 (a), 3 (b) and 4 (c)) values. All the curves were measured along the film plane under 500 Oe applied magnetic field and normalized with respect to their room temperature magnetization. Inset: M-T curve for the multilayer film with x = 1 and n = 3 annealed at 300 ºC. (d) The variations of T_C with n values for the multilayers films annealed at different temperatures.

remains constant with the further increase in temperature up to 300 ºC measurement temperature. This confirms the existence of around 13 % magnetization even at 300 ºC measurement temperature. In order to understand this unusual behaviour, *M-T* measurement was carried out up to 700 ºC for n = 3 film as shown in inset of figure 6.15(b). It is observed that the magnetization remains constant in the temperature range 160 ºC to 350 ºC and

increases largely up to 480 ºC. On further increasing the temperature, the magnetization decreases rapidly and approaches to nearly zero around 630 ºC. These results confirm that the large decrease in the magnetization up to 160 ºC is due to the magnetic phase transition of the amorphous phase from ferromagnetic state to paramagnetic state and the existence of considerable magnetization in the temperature range 160 ºC to 350 ºC is due to the presence of the nucleated α-Fe nanocrystals as revealed from the structural investigations (see figure 6.01). These nanocrystals further grow in size with increasing temperature resulting a clear magnetic phase transition of the α-Fe nanocrystals [HERZ1990, HERZ1995, MCHE1999]. (iii) On further increasing T_A to 400 ºC, the presence of well defined α-Fe nanocrystals in the amorphous matrix as observed from the structural studies using XRD and TEM (see figures 6.01 and 6.02) results in the magnetic phase transitions from ferromagnetic state to paramagnetic state of α-Fe around 600 ºC. In order to monitor the effect of number of multilayers on the possible variations of T_C, the values of T_C are determined from the thermal derivative of *M-T* curves and depicted in figure 6.15(d). For a given multilayer structure (fixed *n*), T_C decreases after annealing at 200 °C due to the release of quenched in stress [GORR2009]. On the other hand, films annealed at 300 °C exhibit a slightly higher T_C values due to the nucleation of nanocrystalline microstructure in the amorphous matrix. T_C values are shifted largely to around 600 ºC for the films annealed at 400 ºC due to the strong exchange interaction between the α-Fe nanocrystals in the residual amorphous matrix. A careful observation of T_C reveals that T_C depends not only on the T_A but also depends significantly on number of multilayers [PITC1993]. While as-deposited multilayer films exhibit no change in T_C with number of multilayers, T_C of the films annealed at 200 ºC and 300 ºC shows a considerable decrease with increasing number of multilayers. This could be attributed to the change in the interface nature and microstructure of FeTaC ferromagnetic layers.

6.3.2. Effect of spacer layer thickness on the magnetic properties:

The effect of annealing and number of multilayers on the temperature dependent magnetic properties of multilayer films revealed that the interlayer coupling resulting from Néel coupling and magnetostatic coupling between the stray fields of domain walls plays a major role in the magnetic properties and magnetization reversal process of the multilayer films with a fixed spacer layer thickness. Since the interlayer coupling between the ferromagnetic layers vary exponentially with the thickness of the spacer layers [ZHAN19961, LIUX2012],

the effect of spacer layer thickness on the temperature dependent magnetic properties of the multilayer films annealed at different temperatures was investigated by varying the spacer layer thickness from 1 to 4 nm in multilayer [[FeTaC (50 nm)/Ta (*x* nm)]$_3$/FeTaC (50 nm)] films and discussed in the following sections.

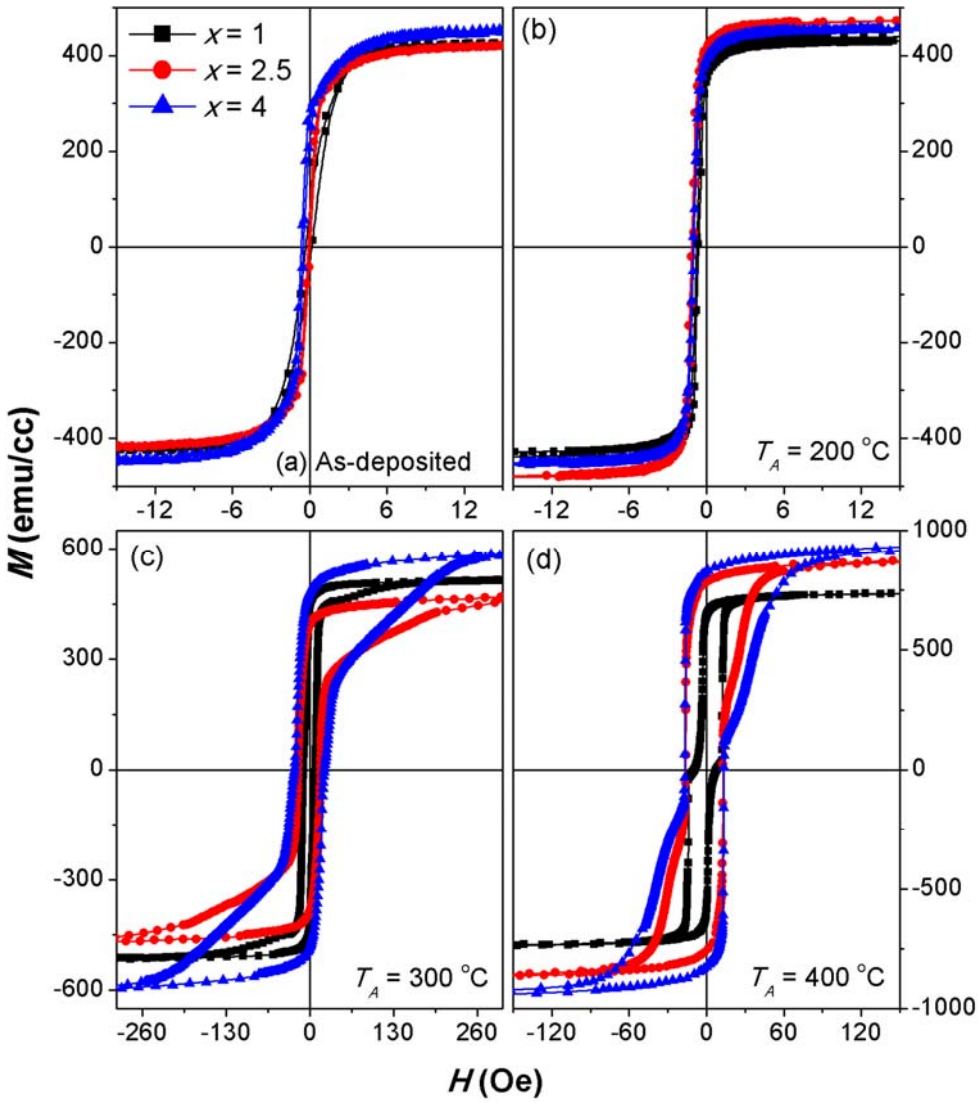

Figure 6.16: Room temperature M-H loops of as-deposited (a) and annealed (T_A = 200 ºC (b), 300 ºC (c), 400 ºC (d)) multilayer films with different spacer layer thicknesses (x = 1, 2.5 and 4 nm).

6.3.2.1. Room temperature magnetic properties:

Figure 6.16 shows room temperature *M-H* loops of as-deposited and annealed (T_A = 200 ºC, 300 ºC, 400 ºC) multilayer films with different spacer layer thicknesses (*x* = 1, 2.5 and 4 nm).

All the loops were measured along the film plane. Figure 6.16 reveals the following features: (1) as-deposited films and films annealed at 200 ºC exhibit almost similar loops, except that the loops for 200 ºC annealed films are shifted considerably to the negative *x*-axis. As discussed earlier, this is due to the control of switching of the soft ferromagnetic layers by the significant hard magnetic layer caused by the interface diffusion of the bottom most ferromagnetic layer on the substrate. Such effect is more significant only in the films annealed at 200 ºC. (2) When T_A is increased to 300 ºC, the shape of the loops change differently and the multistep magnetization reversal behaviour is observed at room temperature. With increasing *x* values from 1 to 4 nm, the switching of the bottom most layer (fourth layer from the top) is more pronounced and provides a substantial restriction on the intermediate layers to switch at a relatively slower rate. Therefore, a large applied field (> 250 Oe) is required to saturate the films with x = 4 nm. Nevertheless, the top two layers

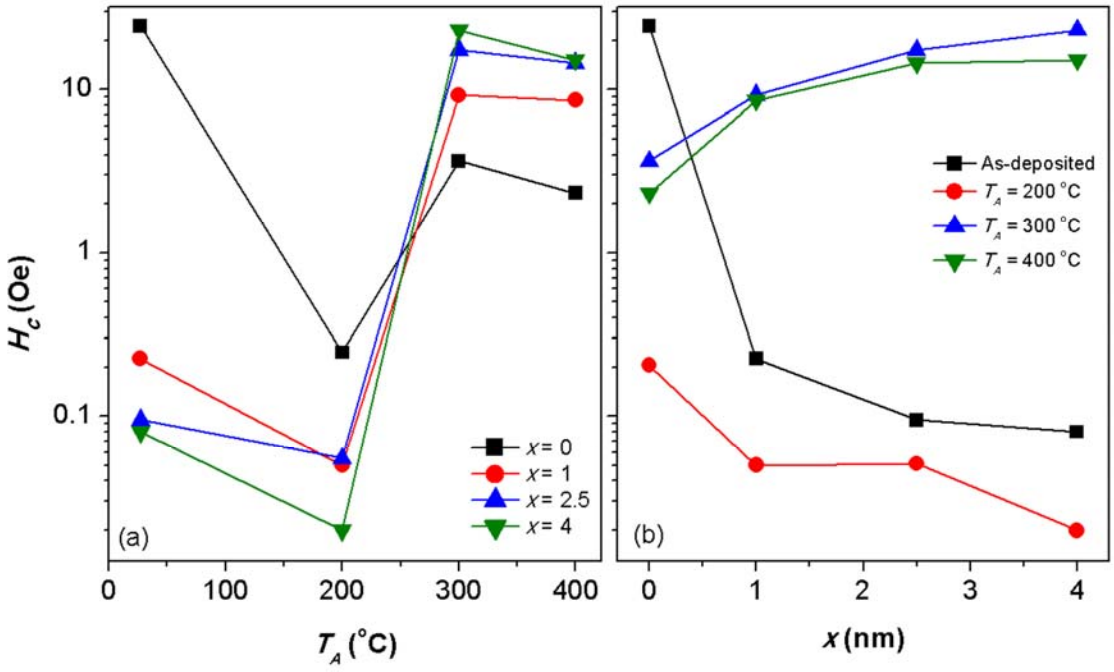

Figure 6.17: The variations of H_C with T_A (a) and x (b) in as-deposited and annealed single and multilayer films at 200 ºC, 300 ºC and 400 ºC.

switch collectively for all the films. (3) On further increasing T_A to 400 ºC, the restriction from the fourth layer on the third layer enhances further and results a collective switching between the third and fourth layers for all the films. Therefore, the switching process slows down with increasing *x*. However, the field required for saturation is reduced considerably (< 150 Oe) as compared to the films annealed at 300 ºC. This could be attributed to the

enhanced coupling between the ferromagnetic layers by the increase in the saturation magnetization due to the existence of α-Fe nanocrystals (as evidenced from figures 6.02).

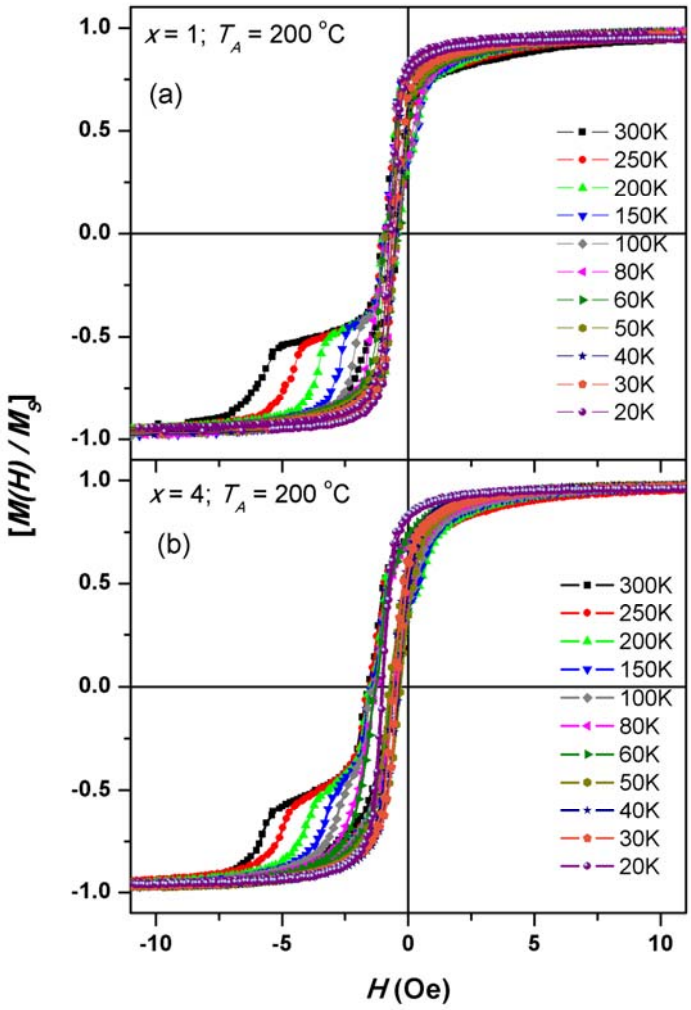

Figure 6.18: Temperature dependent M-H loops for multilayer [[FeTaC (50 nm)/Ta (x nm)]$_3$/FeTaC (50 nm)] films annealed at 200 ºC with different values of x.

The extracted values of H_C from the *M-H* loops are plotted in figure 6.17. H_C reduces to a minimum value for 200 ºC annealed films for all the x values followed by a large increase in H_C for the films annealed at 300 ºC depending on the x values. On further increasing T_A to 400 ºC, H_C decreases slightly for all the films with different x values. On the other hand, the variations of H_C with x (see figure 6.17(b)) show that H_C reduces significantly with increasing x for the as-deposited and films annealed at 200 ºC and attains a minimum value of 20 mOe. This could be attributed to the release of stress by annealing and the

dependence of interlayer coupling on x values. On the other hand, the films annealed above 200 ºC exhibit contradictory behaviour, i.e., H_C increases moderately with increasing the x values. This could be ascribed to the enhanced interface roughness with increasing T_A and the reduction in the coupling between the ferromagnetic layers with increasing x values.

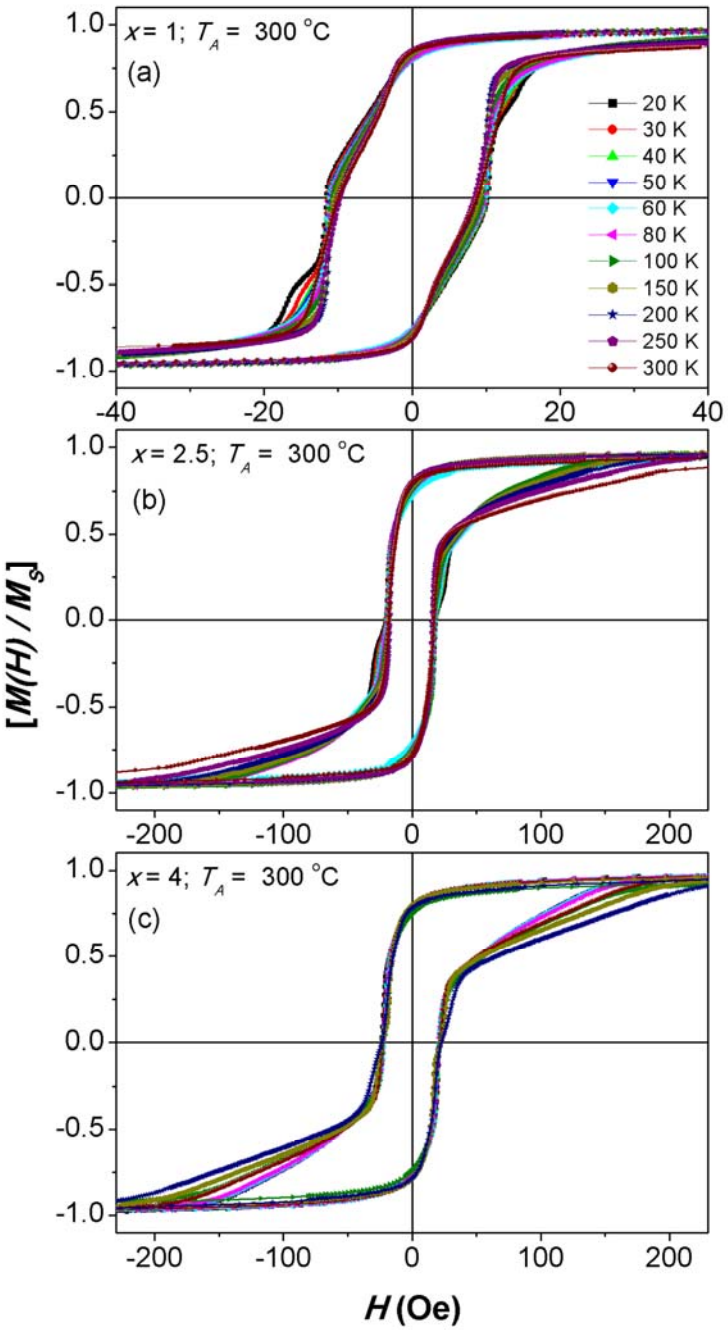

Figure 6.19: Temperature dependent M-H loops for multilayer [[FeTaC (50 nm)/Ta (x nm)]$_3$/FeTaC (50 nm)] films annealed at 300 ºC with different values of x.

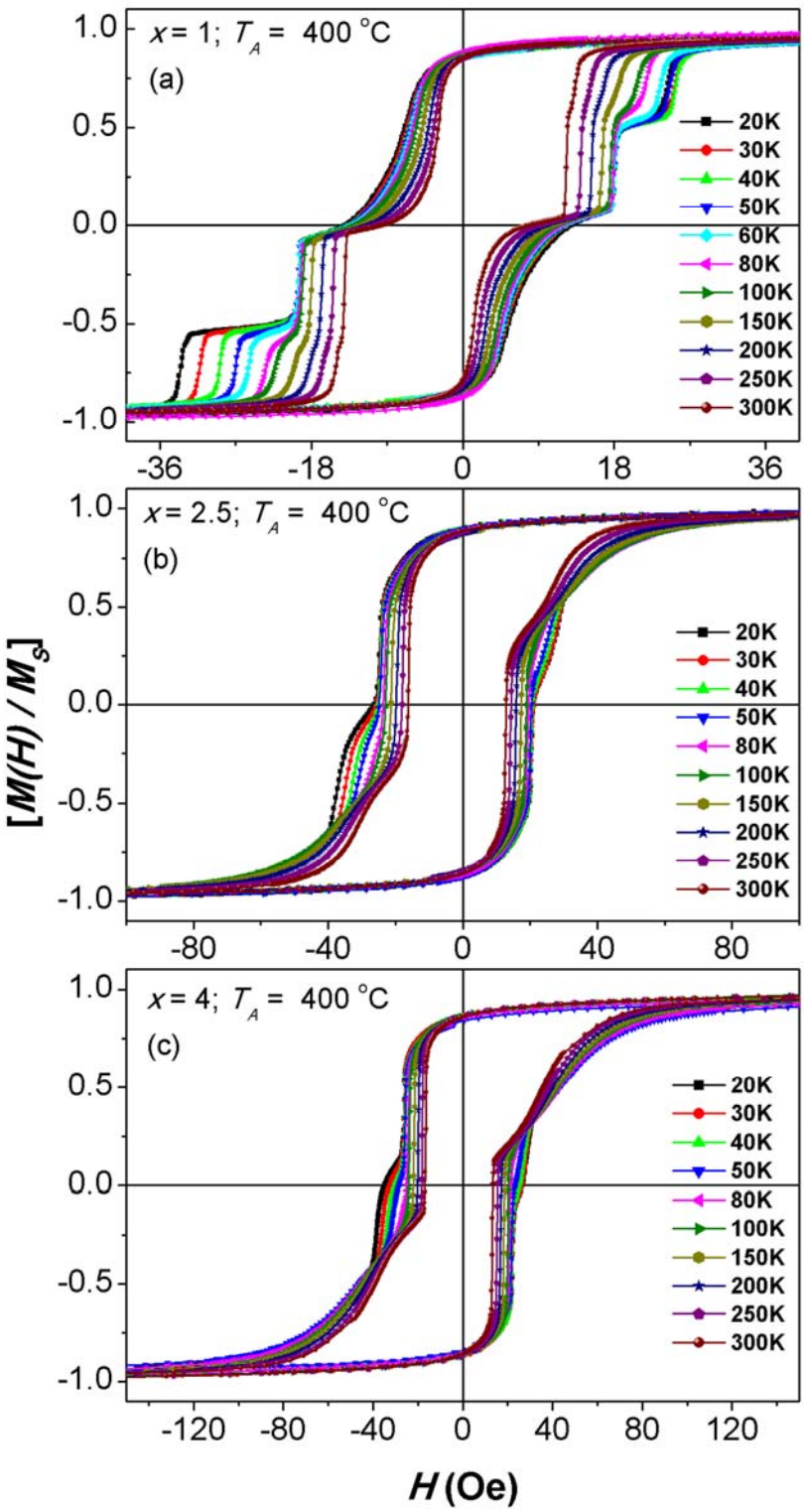

Figure 6.20: Temperature dependent M-H loops for multilayer [[FeTaC (50 nm)/Ta (x nm)]$_3$/FeTaC (50 nm)] films annealed at 400 ºC with different values of x.

6.3.2.2. Low temperature magnetic properties:

In order to understand the effect of spacer layer thickness on the magnetic properties of annealed multilayer films, temperature dependent *M-H* loops were recorded for all the films with different x and T_A from 300 K to 20 K using VSM and the observed magnetic properties are discussed in this section.

(a) Properties of the films annealed at (T_A =) 200 ℃:

Figure 6.18 displays temperature dependent normalized *M-H* loops of the multilayer films annealed at 200 ºC for different x values. It is observed that the shape of the *M-H* loops is not changed with decreasing temperature down to 80 K. With further reducing the temperature below 80 K, *M-H* loops exhibit two step magnetization reversal behaviour due to the separate switching of the bottom most layer with respect to field caused by the interface roughness at the substrate and film interface. Similar phenomena were observed for all the films with different x. Figure 6.21(b) shows the variations of H_C with temperature for multilayer films with different x values annealed at 200 ºC. H_C increases almost linearly at a rate of 7.8×10^{-4}, 1.1×10^{-3} and 1.8×10^{-3} Oe/K with decreasing temperature for multilayer films with x = 1, 2.5 and 4, respectively. The increase in the rate of H_C variation with temperature and x can be related to the relative increase in the interfacial strain with reducing temperature and with increasing x value.

(b) Properties of the films annealed at (T_A =) 300 ℃:

Figure 6.19 depicts temperature dependent normalized *M-H* loops of multilayer films with different x values annealed at 300 ºC. All the loops are normalized with respect to saturation magnetization. It is observed that (1) *M-H* loop of the multilayer film with x = 1 at 300 K shows that the magnetization decreases gradually with increasing the reverse field resulting two steps in the magnetization reversal. However, the magnetization variation in the third quadrant with the applied field changes quickly with decreasing temperature. On further reducing the temperature below 40 K, the third step of reversal occurs due to the individual switching of the bottom layer. (2) With increasing $x \geq 2.5$, the switching of the bottom most layer (fourth layer from the top) is more pronounced and provides a substantial restriction on the intermediate layers to switch at a relatively slower rate. Hence, the additional switching for the third layer occurs at temperatures below 80 K. Nevertheless, the top two layers switch collectively indicating that the interfacial roughness between the ferromagnetic and non-

magnetic layers induced by the annealing process is relatively lower than the strain realized from the substrate on the bottom layer. However, the field required to saturate the magnetization decreases with decreasing temperatures. Figure 6.21(c) displays the variations of H_C extracted from the *M-H* loops with temperature for different x values. H_C reduces initially from 300 K to 250 K for x = 1 film and then increases linearly with decreasing temperature down to 20 K. This provides a minimum in $H_C(T)$ versus T curve. The point of

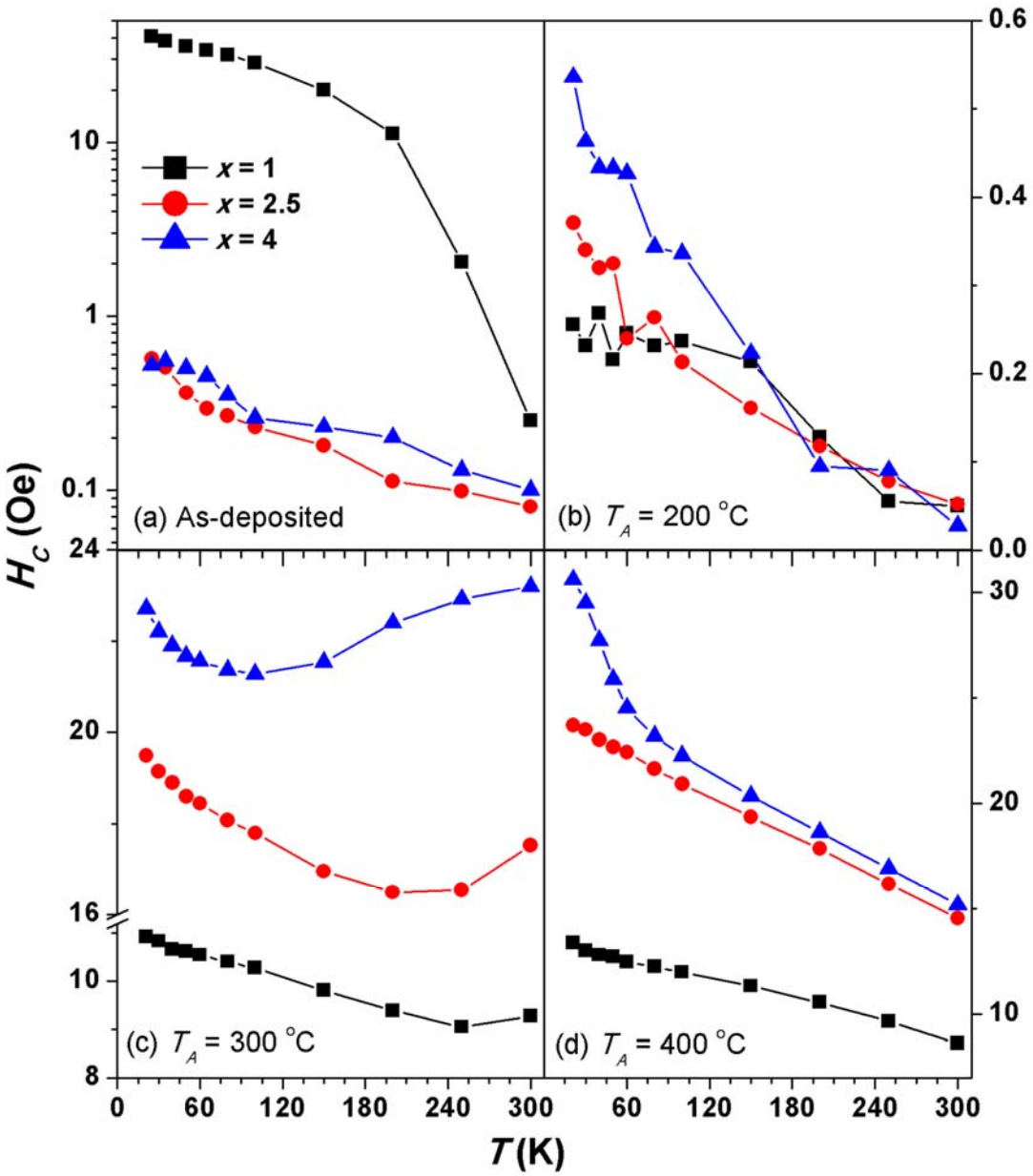

Figure 6.21: Temperature dependent H_C of (a) as-deposited and annealed (T_A = 200 ºC (b), 300 ºC (c) and 400 ºC (d)) multilayer [[FeTaC (50 nm)/Ta (x nm)]$_3$/FeTaC (50 nm)] films with different values of x.

minimum in H_C is shifted to around 200 K and 80 K when x is increased to 2.5 and 4, respectively. Furthermore, the values of H_C increase with increasing x values at a given temperature. This is an unusual behaviour for a typical ferromagnetic material. Such behaviours can be attributed to the variations in the interlayer couplings as given in eqn.(6.01) with increasing x. According to eqn.(6.01), the interlayer coupling field decreases exponentially with increasing the spacer layer thickness [ZHAN19961, SCHR2000, LIUX2012]. In addition, the multilayer film with n = 3 has four number of FeTaC (50 nm) ferromagnetic layers. Hence, they show large sized magnetic domains resulting the weak magnetostatic coupling between the stray fields of domain walls, which is further decreased with increasing x. Since the multilayer films with different x values annealed at 300 ºC show a large temperature dependent M_S, the interlayer coupling between the ferromagnetic layers is reduced at 300 K. With decreasing temperature, the interlayer coupling for a given space layer thickness increases due to the increase in M_S resulting an enhanced collective switching with decreasing temperature. Hence, H_C and the field necessary to saturate the film decrease with decreasing temperature. On further lowering the temperature below certain range, H_C increases with decreasing temperature due to the additional strain realized from the substrate on the magnetization reversal process. This provides a significant minimum in $H_C(T)$, which shifts to lower temperature with increasing x due to increasing separation between the ferromagnetic layers. Nevertheless, large interfacial strain between substrate and bottom ferromagnetic layer desists the bottom ferromagnetic layer from the interlayer coupling and makes them to switch separately.

(c) Properties of the films annealed at (T_A =) 400 ℃:

Figure 6.20 shows temperature dependent normalized *M-H* loops of multilayer films with different x values annealed at 400 ºC. It is observed that (1) *M-H* loop of the films with x = 1 displays two switching processes at 300 K due to the collective nature of the switching of the top two layers followed by the bottom two layers. With decreasing temperature below 150 K, one more additional switching starts appearing possibly due to the individual switching of the bottom most layer depending on the temperature dependent interface roughness. The size of the step increases significantly with decreasing temperature and therefore the field required to switch the bottom most layer also increases from 24 Oe to 33 Oe with decreasing temperature from 60 K to 20 K. (2) With increase x = 2.5, *M-H* loops show different behaviours with respect to temperature, i.e., the switching of the bottom most layer is more pronounced even

at room temperature and provides a substantial strain on the intermediate layers to switch at a relatively slower rate. On lowering the temperature below 300 K, the bottom two layers couple around 60 K due to the enhanced coupling between the bottom and intermediate layers. This results a collective switching of third and fourth layers for temperature below 60 K. On the other hand, the top two layers switch always together from 300 K to 20 K. (3) On further increasing the x value to 4 nm, the strain from the bottom layer is more visible at room temperature and effect of the bottom layer on the intermediate layer increases with decreasing temperature. Hence, the switching of the third layer is well separated from the top two layers with decreasing temperature and fourth layer switches progressively with increasing the field. As a result, the step appearing closed to H_C shifts to second quadrant with decreasing temperature below 150 K. In all these films, the top two layers switch collectively indicating that the interfacial roughness between the ferromagnetic and non-magnetic layers induced by the annealing process is considerably weaker than the strain realized from the substrate on the bottom layer. As discussed earlier, the values of M_S remain almost constant in the temperature range 20 K to 300 K for the multilayer films due to the existence of α-Fe nanocrystals in the amorphous matrix. To understand the effect of spacer layer thickness on the temperature dependent H_C values, the values of H_C are extracted from the M-H loops and depicted in figure 6.21(d). H_C decrease almost linearly with increasing temperature for the films with x = 1 and 2.5 at a rate of 0.0158 Oe/K and 0.0327 Oe/K, respectively. On the other hand, with increasing x to 4, there are two different variations in $H_C(T)$ versus T curve in the temperature range of 20 K to 300 K. While the linear behaviour of H_C variation between 80 K and 300 K at a rate of 0.0351 Oe/K is similar to those observed for the films with x = 1 and 2.5, the large increase in H_C (0.1613 Oe/K) at temperatures below 80 K is mainly due to the individual switching of the third ferromagnetic layer (see figure 6.20(c)) influenced by the bottom most layer with decreasing temperature below 80 K. The actual values of H_C increases with increasing spacer layer thickness and the rate of decrease in H_C with increasing temperature increases with increasing the values of x. This confirms the enhancement in the interlayer roughness by the annealing process with decreasing temperature and causes a large H_C change with increasing x values.

6.3.2.3. High temperature magnetic properties:

Figure 6.22 depicts high temperature M-T curves of as-deposited and annealed (T_A = 200 ºC, 300 ºC and 400 ºC) multilayer films with different x (= 1, 2.5 and 4) values measured along

the film plane under 500 Oe applied magnetic field. In order to compare all the data of the films with a particular x value in a single graph, $M(T)$ data are normalized with respect to

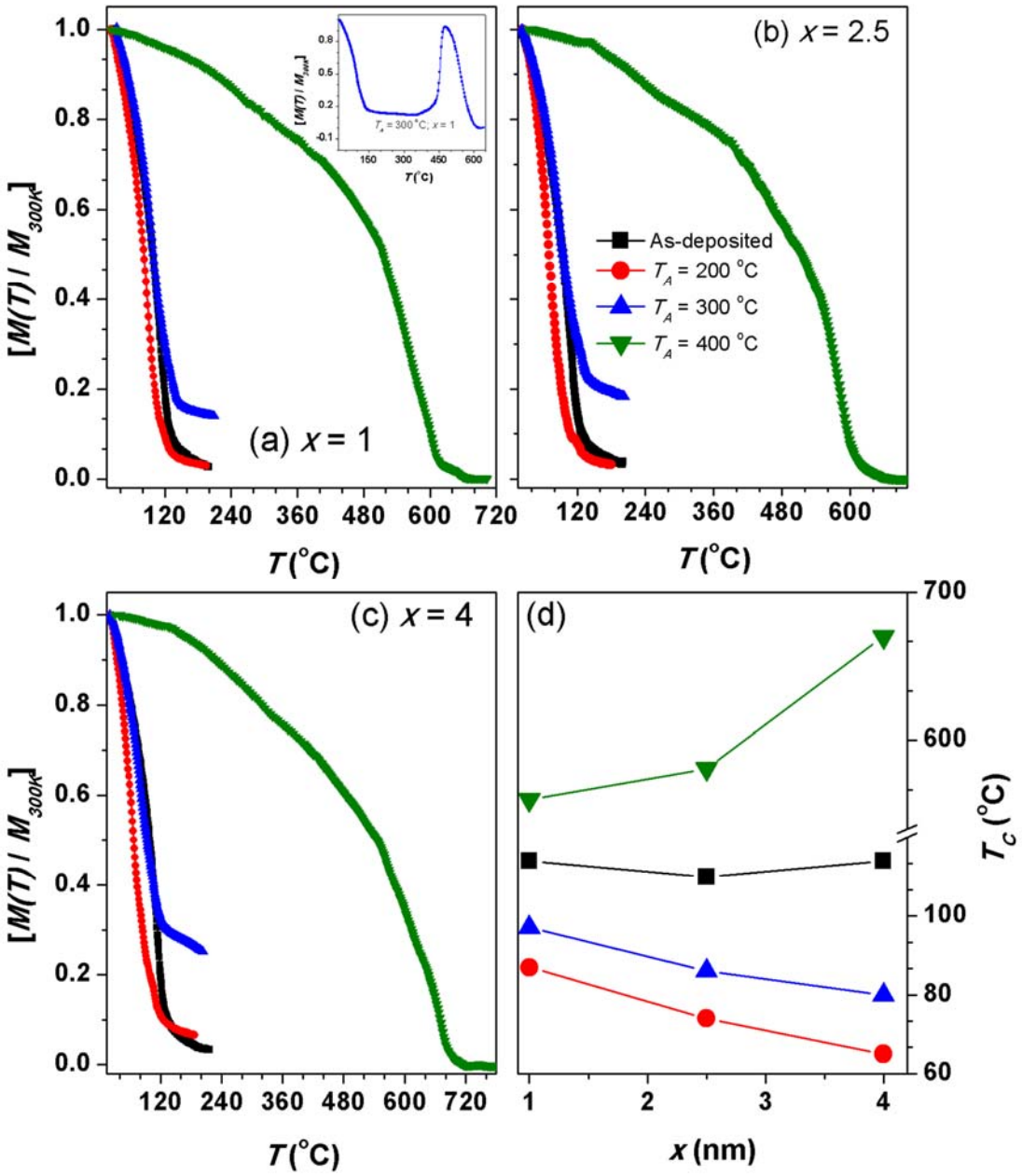

Figure 6.22: High temperature M-T curves of as-deposited and annealed (T_A = 200 ºC, 300 ºC and 400 ºC) multilayer films with different x (= 1 (a), 2.5 (b) and 4 (c)) values. All the curves were measured along the film plane under 500 Oe applied magnetic field and normalized with respect to their room temperature magnetization. Inset: M-T curve for the multilayer film with x = 1 and n = 3 annealed at 300 ºC. (d) The variations of T_C with x values for the multilayers films annealed at different temperatures.

their room temperature magnetization. The following features are observed from figure 6.22: (i) as-deposited multilayer films and the multilayer films annealed 200 ºC exhibit a complete transition from ferromagnetic state to paramagnetic state in the temperature below 200 ºC. (ii) On the other hand, the films with different x values annealed at 300 ºC display a large decrease in magnetization with increasing temperature up to 160 ºC and remains constant with the further increase in temperature up to 300 ºC measurement temperature. This confirms the existence of constant magnetization even at 300 ºC measurement temperature. A careful observation of residual magnetization around 200 ºC reveals that the amount of magnetization increases from 13 % for x = 1 to 19 % and 25 % with increasing x values of 2.5 and 4, respectively. The spacer layer dependence of magnetization at 200 ºC could be correlated to the enhanced diffusion across the interface causing a non-reversal of magnetization. This is further supported by the observation of almost linear variation of magnetization switching in the *M-H* loops for the films with x = 2.5 and 4 (see figure 6.19). These results confirm that the large decrease in the magnetization up to 160 ºC is due to the magnetic phase transition of the amorphous phase from ferromagnetic state to paramagnetic state and the existence of considerable magnetization in the temperature range 160 ºC to 350 ºC is due to the presence of the nucleated α-Fe nanocrystals as revealed from the structural investigations. In order to understand this unusual behaviour, *M-T* measurement was carried out up to 700 ºC for n = 3 film as shown in inset of figure 6.22(a). It is observed that the magnetization remains constant in the temperature range 160 ºC to 350 ºC and increases largely up to 480 ºC. On further increasing the temperature, the magnetization decreases largely and approaches to nearly zero around 630 ºC. This confirms that the nanocrystals are further grown in size with increasing the temperature resulting a clear magnetic phase transition of the α-Fe nanocrystals [HERZ1990, HERZ1995, MCHE1999]. (iii) On further increasing the T_A to 400 ºC, the presence of well defined α-Fe nanocrystals in the amorphous matrix as observed from the structural studies using XRD and TEM (see figures 6.01 and 6.02) results a magnetic phase transition of α-Fe nanocrystals from ferromagnetic state to paramagnetic state around 600 ºC. Interestingly, the transition temperature shifts to higher values with increasing x. In addition, the manner in which *M-T* curves of 400 ºC annealed films decreases is not smooth. This might be due to the release of stress induced by the interface diffusion with increasing temperature [GORR2009]. In order to monitor the effect of spacer layer thickness on the possible variations of T_C, the values of T_C are determined from the thermal derivative of *M-T* curves and depicted in figure 6.22(d). For a given spacer

layer thickness (fixed x), T_C decreases after annealing at 200 °C due to the release of quenched in stress [GORR2009]. On the other hand, the films annealed at 300 °C exhibit a slightly higher T_C values due to the nucleation of nanocrystalline microstructure in the amorphous matrix. On further increasing the T_A to 400 ºC, T_C values are shifted more than 550 ºC due to the strong exchange interaction between α-Fe nanocrystals in the residual amorphous matrix. A careful observation of T_C reveals that T_C depends not only on the T_A but also depends significantly on the spacer layer thickness [PITC1993]. While the as-deposited multilayer films exhibit no considerable change in T_C with the spacer layer thickness, T_C of the films annealed at 200 ºC and 300 ºC show a significant decrease with increasing the spacer layer thickness. This could be attributed to the change in the interface nature, which modifies the interlayer coupling depending on the spacer layer thickness. As the interlayer diffusion in the films annealed at 400 ºC increases significantly, the thickness of the stressed layer at the interface increases with increasing x values. Therefore, the magnetic phase transition temperature is expected to increase significantly with an increase in the stress induced in the ferromagnetic layers [GORR2009].

6.4. Summary:

A systematic study on the effect of post deposition annealing on the structural and magnetic properties of multilayer [[FeTaC (y nm)/Ta (x nm)]$_n$/FeTaC (y nm)] films with different multilayers and the spacer layer thicknesses was carried out in this chapter. The salient features of annealed multilayer films from the current investigations are as follows:

- The annealing process of the amorphous multilayer [[FeTaC (y nm)/Ta (x nm)]$_n$/FeTaC (y nm)] films under controlled heating conditions up to 400 ºC shows the following crystallization sequence of the amorphous films → amorphous (stress released) (at 200 ºC) → α-Fe (nucleated) + amorphous residue (at 300 ºC) → α-Fe (rich) + amorphous residue (at 400 ºC).
- All the multilayer films annealed at 200 ºC exhibit narrow and shifted hysteresis loops with a large reduction in coercivity. These are due to the release of stress accumulated during the film deposition, which annihilates the existence of strip domain patterns in higher thickness films.
- Temperature dependent M-H loops of multilayer films annealed at 200 ºC exhibit multistep magnetization reversal behaviour only at temperatures below 80 K. The multistep reversal behaviour was, on the other hand, observed even at room

temperature for multilayer films annealed at $T_A \geq 300$ ºC due the enhanced interface roughness and change in the microstructure of the films.

- The nature of coupling between the ferromagnetic layers in the multilayer films strongly depends on the annealing temperature, number of multilayers, spacer layer thicknesses and measurement temperatures.
- Temperature dependent coercivity of multilayer films annealed at 200 ºC and 400 ºC decrease with increasing temperature as observed for typical ferromagnetic materials. However, multilayer films annealed at 300 ºC show a broad minimum in $H_C(T)$ curves. Moreover, the temperature at which the minimum in H_C occurs strongly depends on number of multilayers and the spacer layer thickness. This was explained on the basis of change in the interlayer coupling caused by the Néel coupling and magnetostatic coupling between the stray fields of domain walls with temperature, number of multilayers and spacer layer thickness.
- The switching behaviour of the bottom most layer and its effect on the subsequent layers are strongly depending on the annealing temperature, number of multilayers, spacer layer thickness and the measurement temperature.
- High temperature thermo-magnetization data reveal that Curie temperature depends on annealing temperature, number of multilayers and spacer layer thickness, as the magnitude of interlayer diffusion changes considerably with annealing temperature, number of multilayers and spacer layer thickness. All the multilayer films annealed at 200 ºC exhibit low Curie temperature in the range of 65 ºC to 95 ºC due to the release of accumulated stress in the amorphous films, while the multilayer films annealed at 400 ºC exhibit high Curie temperature in the temperature range of 560 ºC to 670 ºC due to the formation of well-defined α-Fe nanocrystals.

Chapter 7

Summary and scope for future work

The overall summary of the salient results obtained on the structural and magnetic properties of FeTaC (t) single layer films of different thicknesses and multilayer [[FeTaC (y nm)/Ta (x nm)]$_n$/FeTaC (y nm)] films is listed in this chapter. Highlights of the current investigations and the possibilities for future work are also summarized below:

7.1. Summary of the results:

Amorphous FeTaC (t) films with different thicknesses (t = 20, 50, 100 and 200 nm) and the multilayer [[FeTaC (y nm)/Ta (x nm)]$_n$/FeTaC (y nm)] films with n = 0 – 4 and x = 0 – 6 nm were prepared using DC magnetron sputtering technique at ambient temperature directly on the thermally oxidized Si substrates. The thickness of the individual FeTaC layers in the multilayer films was controlled using the relation $y = 200/(n+1)$, where n is number of multilayers and the total thickness of FeTaC films was maintained at 200 nm for all the multilayer films. In order to form the nanocrystalline microstructure, all the as-deposited amorphous FeTaC (200) film and multilayer [[FeTaC (y nm)/Ta (x nm)]$_n$/FeTaC (y nm)] films with n = 1 - 4 and x = 1 - 4 nm were annealed ex-situ in a home-made high vacuum (< 10^{-6} Torr) annealing set-up at different temperatures (T_A) of 200 ºC, 300 ºC and 400 ºC for 30 minutes duration.

Structural investigations of all the as-deposited single layer and multilayer films using X-ray diffraction and transmission electron microscopy techniques confirm their amorphous nature. Similarly, the films annealed at 200 ºC also exhibit the amorphous structure. With increasing annealing temperature above 200 ºC, the nucleation (at 300 ºC) and subsequent growth (at 400 ºC) of α-Fe nanocrystals in the residual amorphous matrix were observed.

The magnetic properties of FeTaC (t) single layer films reveal strong thickness dependent magnetic properties in the thickness range between 20 nm and 200 nm. FeTaC ($t \leq$ 50 nm) films exhibit soft magnetic nature due to the in plane orientation of the magnetization. Interestingly, FeTaC (50 nm) film exhibits in-plane uniaxial anisotropy with large sized magnetic domains. However, soft magnetic properties of FeTaC ($t \geq$ 100 nm) films are degraded due to the transition from the in-plane magnetization to the dense stipe domain magnetic structure caused by the growth of the perpendicular anisotropy. The development of perpendicular anisotropy occurs due to the stress induced during the deposition of the amorphous films. This results in a transcritical hysteresis loop. Therefore, the room temperature coercivity (H_C) increases by an order of magnitude as the film thickness is increased from 50 nm to 100 nm. The temperature dependent magnetic properties at low

temperature region exhibit a considerable shift in the magnetic hysteresis (*M-H*) loops for low thickness films, which is analyzed using the two-layers model. Although the room temperature perpendicular anisotropy constant is almost constant for 100 and 200 nm thick films, their temperature variation strongly depends on the thickness of the films. Low temperature thermo-magnetization (*M-T*) data reveal that the magnetic disorder observed at low temperature increases with increasing film thickness above 50 nm. The observed results therefore suggest that the soft magnetic properties degrade in FeTaC ($t \geq 100$ nm) films. Curie temperature (T_C) of the films obtained from the thermal derivative of *M-T* data increases marginally with decreasing the films thickness. In addition, the magnetic susceptibility critical exponent displays a cross over from 3D Ising model to 3D Heisenberg values with decreasing FeTaC film thickness.

In order to control the development of perpendicular anisotropy and the soft magnetic properties of FeTaC films at higher thicknesses, the multilayer structured [[FeTaC (y nm)/Ta (x nm)]$_n$/FeTaC (y nm)] films were fabricated with different n (= 0 - 4) and x (= 0 – 6 nm) and then characterized. Room temperature H_C and the field necessary to saturate the magnetization (H_{Sat}) decreased drastically with increasing number of multilayers, while they show weak dependence on the spacer layer thickness for a given multilayer structure. The improvement in the magnetic properties of multilayer films is due to the suppression of perpendicular anisotropy in FeTaC ferromagnetic layers by the insertion of the Ta spacer layers causing a transition from the magnetic stripe domain structure to the in-plane orientation of the magnetization. Furthermore, temperature dependent magnetic study reveals that the shape of the *M-H* loops depend strongly on number of multilayers and thickness of the spacer layers. The multilayer film with x = 1 showed a strong temperature dependent magnetic nature induced by the direct exchange coupling through the pinholes. In addition, multilayer films exhibit pronounced multistep magnetization reversal process for the temperature below 70 K and thermal activation results in smooth and narrow hysteresis loops for temperatures above 70 K. The number of steps in the reversal behavior depends on number of multilayers and thickness of the spacer layers. The magnetic disorder observed at low temperature in a single layer film decreases and the bifurcation observed between ZFC and FC data shifts to lower temperature and disappears eventually for the multilayer films with increasing number of multilayers and thickness of the spacer layers. The magnetic parameters (H_C, H_{Sat} and perpendicular anisotropy constant) of the multilayer films depend strongly on temperature and vary at different rates for different multilayers and spacer layer

thicknesses. With increasing number of multilayers, the saturation magnetization of the multilayer films decreases significantly due to an increase in the magnetic dead layers with increasing number of interfaces.

In order to enhance the soft magnetic properties of FeTaC films further and to study the interface effects in more details, all the multilayer films were annealed ex-situ at different T_A of 200 ºC, 300 ºC and 400 ºC in home-made high vacuum (< 10^{-6} Torr) chamber. All the multilayer films annealed at 200 ºC exhibit narrow but shifted hysteresis loops with a large reduction in the values of H_C. This is due to the release of stresses accumulated during the deposition of the films, which annihilates the existence of strip domain patterns in higher thickness films. Temperature dependent *M-H* loops of multilayer films annealed at 200 ºC exhibit multistep magnetization reversal behavior only at temperatures below 80 K. However, such magnetization reversal behavior was observed even at room temperature for the multilayer films annealed at $T_A \geq 300$ ºC due the enhanced interface roughness and change in the microstructure of the films. The nature of coupling between the ferromagnetic layers in multilayer films strongly depends on the annealing temperature, number of multilayers, spacer layer thickness and measurement temperature. While the temperature dependent coercivity of multilayer films annealed at 200 ºC and 400 ºC decrease with increasing temperature as like typical ferromagnetic materials, multilayer films annealed at 300 ºC show a broad minimum in $H_C(T)$ curves and the temperature at which the minimum in H_C occurs strongly depends on number of multilayers and the spacer layer thickness. This is correlated to the change in the interlayer coupling caused by the Néel coupling and magnetostatic coupling between the stray fields of domain walls with temperature, number of multilayers and spacer layer thickness. The switching behavior of the bottom most layer and its effect on the subsequent layers are strongly depending on the annealing temperature, number of multilayers, thickness of the spacer layers and the measurement temperature.

High temperature *M-T* data reveal that while T_C of all the as-deposited multilayer films is not influenced significantly by the multilayer structures and the spacer layer thickness, the annealed multilayer films exhibit a strong dependence of T_C on annealing temperature, number of multilayers, and spacer layer thickness. This is mainly due to the change in the microstructure of FeTaC films and the interlayer diffusion with T_A, n and x. All the multilayer films annealed at 200 ºC exhibit low T_C in the range of 65 ºC to 95 ºC due to the release of stress in the amorphous films, while the multilayer films annealed at 400 ºC

exhibit high T_C in the temperature range of 560 ºC to 670 ºC due to the formation of α-Fe nanocrystals.

7.2. Scope for future work:

The current investigations have brought out some new and interesting aspects and characteristics of FeTaC single layer and multilayer structured films. These observations have not only exposed the potential of this material and multilayer structure for specific applications in modern magnetoelectronic devices but have also shown paths for future scope of work in FeTaC single and multilayer structured films. Some of the possibilities are briefly discussed below to serve as appropriate conclusion to the current thesis work.

Since the multilayer structured films exhibit the multistep magnetization reversal behavior and the changeover in the magnetic domains from stripe domain patterns to in-plane magnetization with increasing number of multilayers, it would be interesting to measure the electrical transport properties in these multilayer films as a function of applied magnetic field (magnetoresistance) and temperature. This would reveal a correlation between the magnetic and transport properties, provided the transport properties are affected by the change in the domain structure and number of multilayers. The nature of the interlayer coupling between the ferromagnetic layers in the multilayer films depends strongly on the annealing temperature, number of multilayers and the spacer layer thicknesses. In the current investigation, we have kept the total thickness of FeTaC ferromagnetic films as 200 nm and the individual thickness of FeTaC layer in the multilayer films was controlled using the relation $y = 200/(n+1)$. Such multilayer structure provides a different magnetostatic coupling between the stay fields of the domain walls with increasing number of multilayers and their dependence on the temperature. This is mainly due to the reduction in the thickness of the ferromagnetic layers with increasing number of multilayers. On the other hand, Huang et al [HUAN2001] reported H_C variation in FeCoZrBCu/SiO_2 multilayer films, i.e., H_C decreases largely from 25 Oe for a single layer FeCoZrBCu (150 nm) film to 0.25 Oe for the multilayer film of [FeCoZrBCu(150 nm)/ SiO_2(2 nm)]$_2$/ FeCoZrBCu (150 nm)/glass substrate. In this case, the thickness of the individual FeCoZrBCu layer is kept same as the single layer films. Therefore, the interlayer coupling between the ferromagnetic layers plays a major role on deciding the resulting magnetic properties. Hence, a study on variation of interlayer coupling at different temperatures in these types of multilayer structures would provide a new direction for evaluating the magnetic properties of multilayer thin films. Similarly, if the individual

thickness of the ferromagnetic layers in multilayer films is varied randomly, then the magnetization reversal behavior is expected to be strongly dependent on the thickness of the individual ferromagnetic layers. As a result, the variation of temperature dependent coercivity could be mainly determined by the interlayer coupling between the ferromagnetic layers in multilayer films. This would be completely different from the typical variation of coercivity of a simple ferromagnetic material. Furthermore, as the room temperature saturation magnetization of the amorphous films is considerably low and decreases further with increasing number of multilayers, addition of Co in FeTaC amorphous and nanocrystalline films is expected to not only enhance the saturation magnetization, but also enhances the T_C, which would be useful for high temperature applications [DEBA2010].

References

[ABID1999] Abid M, Ouahmane H, Lassri H, Khmou A, Krishnan R, J. Magn. Magn. Mater. 202 (1999) 335.

[ACHA2004] Acharya B.R, Zhou J.N, Zheng M, Choe G, Abarra E.N, Johnson K.E, IEEE Trans. Magn. 40 (2004) 2383.

[ALBE1978] Alben R, Becker J.J, Chi M.C, J. Appl. Phys. 49 (1978) 1653.

[ALLE1990] Allenspach R, Stampanoni M, Bischof A, Phys. Rev. Lett. 65 (1990) 3344.

[ALLE1994] Allenspach R, J. Magn. Magn. Mater. 129 (1994) 160.

[AMOS2008] Amos N, Fernandez R, Ikkawi R, Lee B, Lavrenov A, Krichevsky A, Litvinov D, Khizroev S, J. Appl. Phys. 103 (2008) 07E732.

[ANGU2000] Anguelouch A, Schrag B.D, Xiao G, Trouilloud Y.L.P.L, Wanner R.A, Gallagher W.J, Parkin S.S.P, Appl. Phys. Lett. 76 (2000) 622.

[ANTO1992] Antonion B, Principles and Applications of Superconducting Quantum Interference Device, World Scientific, U.K (1992).

[BACK1995] Back C.H, Wursch Ch, Vaterlaus A, Ramsperger U, Maier U, Pescia D, Nature (London) 378 (1995) 597.

[BAIB1988] Baibich M.N, Broto J.M, Fert A, Dau F.N.V, Petroff F, Eitenne P, Creuzet G, Friederich A, Chazelas J, Phys. Rev. Lett. 61 (1988) 2472.

[BALT2007] Baltz V, Marty A, Rodmacq B, Dieny B, Phys. Rev. B 75 (2007) 014406.

[BERG2011] Bergman A, Skubic B, Hellsvik J, Nordstrom L, Delin A, Eriksson O, Phys. Rev. B 83 (2011) 224429.

[BITO1997] Bitoh T, Makino A, Hatanai T, Inoue A, J. Appl. Phys. 81 (1997) 4634.

[BLUN2001] Blundell S, Magnetism in Condensed Matter, Oxford University Press Inc., New York (2001).

[BRAJ2010] Brajpuriya R, J. Appl. Phys. 107 (2010) 083914.

[BRAN1992] Brandes E.A, Brook G.B, Smithells Metals Reference Book 7th edn, Butterworth-Heinemann, UK (1992).

[BRAN2008] Brandon D, Kaplan W.D, Microstructural Characterization of Materials, Wiley, UK (2008).

[BRUN1989] Bruno P, Renard J.P, Appl. Phys. A 49 (1989) 499.

[BRUN1991] Bruno P, Chappert C, Phys. Rev. Lett. 67 (1991) 1602.

[BRUN1992] Bruno P, Chappert C, Phys. Rev. B 46 (1992) 261.

[CAIN1996] Cain W, Payne A, Baldwinson M, Hempstead R, IEEE Trans. Magn. 32

(1996) 97.

[CAST19971] Castano F.J, Stobiecki T, Gibbs M.R.J, Czapkiewicz M, Kopcewicz M, Gacem V, Speakman J, Cowlam N, Blythe H.J, J. Phys.: Condens. Matter 9 (1997) 10603.

[CAST19972] Castano F.J, Stobiecki T, Gibbs M.R.J, Blythe H.J, J. Phys.: Condens. Matter 9 (1997) 1609.

[CHAE1999] Chae J.-H, Lee J.-Y, Kang S.-W, Sensors and Actuators A 75 (1999) 222.

[CHAN2002] Chang J.Yu C, Karns D, Ju G, Kubota Y, Eppler W, Bruker C, Weller D, J. Appl. Phys. 91 (2002) 8357.

[CHAP1988] Chappert C, Bruno P, J. Appl. Phys. 64 (1988) 5736.

[CHEN20071] Chen J.S, Lim B.C, Hu J.F, Liu B, Chow G.M, Ju G, Appl. Phys. Lett. 91 (2007) 132506.

[CHEN20072] Chen Y.B, Sun H.P, Katz M.B, Pan X.Q, Choi K.J, Jang H.W, Eom C.B, Appl. Phys. Lett. 91 (2007) 252906.

[CHOM2001] Cho M.-H, Ko D.-H, Choi Y.G, Jeong K, Lyo I.W, Noh D.Y, Kim H.J, Whang C.N, J. Vac. Sci. Technol. A 19 (2001) 192.

[CHOP2000] Chopra H.D, Yang D.X, Chen P.J, Parks D.C, Egelhoff W.F, Phys. Rev. B 61 (2000) 9642.

[CHOP2005] Chopra H.D, Sullivan M.R, Ludwig A, Quandt E, Phys. Rev. B 72 (2005) 054415.

[CHOU2003] Chou C.Y, Kuo P.C, Yao Y.D, Chen S.C, Sun A.C, Lie C.T, J. Appl. Phys. 93 (2003) 7205.

[CLAR1994] Clarke R, Barlett D, Tsui F, Chen B, Uher C, J. Appl. Phys. 75 (1994) 6174.

[COEY2010] Coey J.M.D, Magnetism and Magnetic Materials, Cambridge university press, Cambridge (2010).

[COIS2008] Coisson M, Celegato F, Olivetti E, Tiberto P, Vinai F, Baricoo M, J. Appl. Phys. 104 (2008) 033902.

[COIS2009] Coisson M, Vinai F, Tiberto P, Celegato F, J. Magn. Magn. Mater. 321 (2009) 806.

[CRAI1965] Craik D.J, Tebble R.S, Ferromagnetism and Ferromagnetic Domains, North-Holland Publishing Company, New York (1965).

[CRAU2002] Craus C.B, Chezan A.R, Siekman M.H, Lodder J.C, Boerma D.O, Niesen L, J. Magn. Magn. Mater. 240 (2002) 423.

[CRAU2003] Craus C.B, Magnetic Properties of Nanocrystalline Materials for High Frequency Applications, Thesis (PhD), University of Groningen (2003).

[CULL2001] Cullity B.D, Stock S.R, Elements of X-ray diffraction, 3rd edn, Pearson Eduaction, Boston (2001).

[DAHL1988] Dahlberg E.D, Riggs K, Prinz G.A, J. Appl. Phys. 63 (1988) 4270.

[DEBA2010] Mishra D, Magnetic Properties of Co and Mn Substituted Fe-Zr-B Alloy Prepared by Melt Spinning and Mechanical Alloying Processes, Thesis (PhD) Indian Institute of Technology Guwahati, India (2010)

[DIAZ2002] Díaz J, Hamdan N, Jalil P, Hussain Z, Valvidares S.M, Alameda J.M, IEEE Trans. Magn. 38 (2002) 2811.

[DUNL2004] Dunlavy I.M.J, Venus D, Phys. Rev. B 69 (2004) 094411.

[FENG1994] Feng Y.C, Laughlin D.E, Lambeth D.N, IEEE. Trans. Magn. 30 (1994) 3960.

[FENG1995] Feng Y.C, Laughlin D.E, Lambeth D.N, IEEE. Trans. Magn. 31(1995) 2845.

[FELD1971] Feldtkeller E, J. De Physique 32 (1971) 452.

[FUJI2006] Fujii I, Shima T, Takanashi K, Mater. Trans. 47 (2006) 47.

[GARR2005] Garreau G, Hajjar S, Bubendorff J.L, Pirri C, Berling D, Mehdaoui A, Stephan R, Wetzel P, Zabrocki S, Gewinner G, Boukari S, Beaurepaire E, Phys. Rev. B 71 (2005) 094430.

[GORR1996] Gorria P, Orue I, Gubieda M.L.F, Plazaola F, Zabala N, Barandiaran J.M, J. Magn. Magn. Mater. 157-158 (1996) 203.

[GORR2009] Gorria P, Blanco D.M, Perez M.J, Blanco J.A, Hernando A, Marco M.A.L, Haskel D, Neto N.S, Smith R.I, Marshall W.G, Garbarino G, Mezouar M, Martinez A.F, Chaboy, J, Barquin L.F, Castrillon J.A.R, Moldovan M, Alonso J.I.G, Zhang J, Liobet A, Jiang J.S, Phys. Rev. B 80 (2009) 064421.

[GUER2007] Guerrero M.G, Prieto J.L, Ciudad D, Sanchez P, Aroca C, Appl. Phys. Lett. 90 (2007) 162501.

[GUSE2011] Gusenbauer C, Ashraf T, Stangl J, Hesser G, Plach T, Meingast A, Kothleitner G, Koch R, Phys. Rev. B 83 (2011) 035319.

[HAND2005] Ha N.D, Yoon T.S, Gan'shina E, Phan M.H, Kim C.G, Kim C.O, J. Magn. Magn. Mater. 295 (2005) 126.

[HANS1991] Hansen P, Magnetic Amorphous Alloys, Handbook of Magnetic Materials, vol. 6, ed. Buschow K. H. J, Elsevier, Amsterdam, (1991).

[HART1999] Hartmann U, Magnetic Multilayers and Giant Magnetoresistance: Fundamentals and Industrial Applications, Springer, New York (1999).

[HASE1990] Hasegawa N, Saito M, Kojima A, Makino A, Misaki Y, Watanabe T, J. Magn. Soc. Jpn. 14 (1990) 319.

[HASE1995] Hasegawa N, Makino A, Kataoka N, Fujimori H, Tsai A.P, Inoue A, Masumoto T, Mater. Tran. JIM 6 (1995) 952.

[HEIN1987] Heinrich B, Urquhart K.B, Arott A.S, Cochran J.F, Myrtle K, Purcell S.T, Phys. Rev. Lett. 59 (1987) 1756.

[HEIS1928] Heisenberg V.W, für. Z, Phys. 49 (1928) 619.

[HERN1995] Hernando A, Navarro I, Gorria P, Phys. Rev. B 51 (1995) 3281.

[HERN2002] Hernando A, Crespo P, Flores M.S, Bianco L.D, Briones F, Mater. Sci. Forum 386–388 (2002) 447.

[HERN2008] Herndon N.B, Oh S.H, Abiade J.T, Pai D, Sankar J, Pennycook S.J, Kumar D, J. Appl. Phys. 103 (2008) 07D515.

[HERZ1989] Herzer G, IEEE Trans. Magn. 25 (1989) 3327.

[HERZ1990] Herzer G, IEEE Tran. Magn. 26 (1990) 1397.

[HERZ1992] Herzer G, J. Magn. Magn. Mater. 112 (1992) 258.

[HERZ1995] Herzer G, Scr. Metall. Mater. 33 (1995) 1741.

[HERZ2005] Herzer G, Properties and Applications of Nanocrystalline Alloys from Amorphous Precursors, NATO Science Series II: Mathematics, Physics and Chemistry, vol. 184, ed. Idzikowski B, Svec P, Miglierini M, Kluwer Academic Publishers, Dordrecht (2005).

[HILL1993] Hill E.W, Tomlinson S.L, Li J.P, J. Appl. Phys.73 (1993) 5978.

[HIND2011] Hindmarch A.T, Rushforth A.W, Campion R.P, Marrows C.H, Gallagher B.L, Phys. Rev. B 83 (2011) 212404.

[HIRA2000] Hirayama Y, Kikukawa A, Honda Y, Shimizu N, Futamoto M, IEEE

Trans. Magn. 36 (2000) 2396.

[HORS2006] Czichos H, Saito T, Smith L, Handbook of Materials Measurements methods, Springer, Berlin (2006).

[HUAN2001] Huang M-Q, Hsu Y.N, McHenry E, Laughlin D.E, IEEE Trans. Magn. 37 (2001) 2239.

[HUBE2009] Hubert A, Schäfer R, Magnetic Domains: the Analysis of Magnetic Microstructures, Springer, New York (2009).

[HUYM2011] Hu Y.M, Li S.S, Chia C.H, Appl. Phys. Lett. 98 (2011) 052503.

[IKED2008] Ikeda S, Hayakawa J, Ashizawa Y, Lee Y.M, Miura K, Hasegawa H, Tsunoda M, Matsukura F, Ohno H, Appl. Phys. Lett. 93 (2008) 082508.

[INOU1997] Inoue A, Zhang T, Takeuchi A, Appl. Phys. Lett. 71 (1997) 464.

[ITOS1980] Ito S, Aso K, Makino Y, Uedaira S, Appl. Phys. Lett. 37 (1980) 665.

[JANS2004] Svoboda J, Magnetic Technique for the Treatment of Materials, Kluwer Academic Publishers, Dordrecht (2004).

[JIAN2005] Jiang R.F, Lai C.H, J. Appl. Phys. 97 (2005) 10N302.

[JICW2005] Ji C.W, Kim S.H, Kim I, Kim K.H, Yamaguchi M, IEEE Trans. Magn. 41 (2005) 3277.

[JILE1997] Jiles. D, Introduction to Magnetism and Magnetic Materials, Chapman and Hall, Boca Raton (1997).

[JUNG2006] Jung H.S, Velu E.M.T, Malhotra S.S, Jiang W, Bertero G, J. Appl. Phys. 99 (2006) 08E702.

[KARM2006] Kar M, Perumal A, Ravi S, Phys. Status Solidi 243 (2006) 1908.

[KASU1956] Kasuya T, Progress of Theoretical Physics 16 (1956) 45.

[KAZI2013] Kazimierczuk M.K, High-Frequency Magnetic Components 2nd edn, Wiley, Chichester (2013).

[KHIZ20041] Khizroev S, Litvinov D, J. Appl. Phys. 95 (2004) 4521.

[KHIZ20042] Khizroev S, Litvinov D, Perpendicular Magnetic Recording, Kluwer Academic Publishers, New York (2004).

[KIKU2000] Kikukawa A, Honda Y, Hirayama Y, Futamoto M, IEEE Trans. Magn. 36 (2000) 2402.

[KIKU2001] Kikukawa A, Tanahashi K, Honda Y, Hirayama Y, Futamoto M, J. Magn. Magn. Mater. 235 (2001) 68.

[KIMD2002] Kim D, Zink B.L, Helmann F, Coey J.M.D, Phys. Rev. B 65 (2002) 214424.

[KIMJ2003] Kim J.G, Han K.H, Song S.H, Reilly A, Thin Solid Films 440 (2003) 54.

[KIMY2000] Kim Y.M, Choi D, Kim K.H, Kim J, Han S.H, Kim H.J, J. Magn. 5 (2000) 120.

[KITT2004] Kittel C, Introduction to Solid state Physics, 7th edn Wiley, Singapore (2004).

[KOBL1978] Kobliska R.J, Aboaf J.A, Gangulee A, Cuomo J.J, Klokholm E Appl. Phys. Lett. 33 (1978) 473.

[KOOL1999] Kools J.C.S, Kula W, Mauri D, Lin T, J. Appl. Phys. 85 (1999) 4466.

[KOON1987] Koon N.C, Jonker B.T, Volkening F.A, Krebs J.J, Prinz G.A, Phys. Rev. Lett. 59 (1987) 2463.

[KORE2012] Korelis P.T, Jonsson P.E, Liebig A, Wannberg H.E, Nordblad P, Hjorvarsson B, Phys. Rev. B 85 (2012) 214430.

[KRAV2012] Kravets A.F, Timoshevskii A.N, Yanchitsky B.D, Bergmann M.A, Buhler J, Andersson S, Korenivski V, Phys. Rev. B 86 (2012) 214413.

[KRON2003] Kronmuller H, Fahnle M, Micromagnetism and the Microstructure of Ferromagnetic Solids, Cambridge University Press, New York (2003).

[KYPR1996] Kyprianidis I.M, Achilleos C.A, Tsoukalas I.A, Bremers H, J. Hesse, J. Magn. Magn. Mater. 161 (1996) 203.

[LAIC2003] Lai C.H, Jiang R.F, J. Appl. Phys. 93 (2003) 8155.

[LEED2006] Lee D.W, Wang S.X, J. Appl. Phys. 99 (2006) 08F109.

[LIUX2011] Liu X.H, Liu W, Guo S, Lv X.K, Gong W.J, Zhang Z.D, J. Alloys Compds. 509 (2011) 1448.

[LIUX2012] Liu X.M, Ho P, Chen J.S, Adeyeye A.O, J. Appl. Phys. 112 (2012) 073902.

[LIUZ2006] Liu Z.W, Liu Y, Yan L, Tan C.Y, Ong C.K, J. Appl. Phys. 99 (2006) 043903.

[LIW2005] Li W, Sun Y, Sullivan C.R, IEEE Trans. Magn. 41 (2005) 3283.

[LIXW2007] Li X.W, Song C, Yang J, Zeng F, Geng K.W, Pan F, J. Magn. Magn. Mater. 315 (2007) 120.

[MAJC2007] Majchrak P, Derer J, Lobotka P, Vavra I, Frait Z, Horvath D, J. Appl.

Phys. 101 (2007) 113911.

[MAJN1976] Majni G, Ottavniani G, Prudenziati M, Thin Solid Films 38 (1976) 15.

[MAKI1995] Makino A, Inoue A, Masumoto T, Mat. Trans. JIM 36 (1995) 924.

[MARK2010] Marko D, Strache T, Lenz K, Fassbender J, Kaltofen R, Appl. Phys. Lett. 96 (2010) 022503.

[MCHE1999] McHenry M.E, Willard M.A, Laughlin D.E, Prog. Mater. Sci. 44 (1999) 291.

[MAPP1991] Mapps D.J, Akhter M.A, Pan G, J. Appl. Phys. 69 (1991) 5178.

[MIDD1963] Middelhoek S, J. Appl. Phys. 34 (1963) 1054.

[MISH2011] Mishra D, Singh A.K, Shyni P.C, Sharma D, Perumal A, J. Appl. Phys. 109 (2011) 07A304.

[MORI2004] Moritz J, Garcia F, Toussaint J.C, Dieny B, Nozieres J.P, Europhys. Lett. 65 (2004) 123.

[MURA1966] Murayama Y, J. Phys. Soc. Jpn. 21 (1966) 2253.

[NAKA1997] Nakagawa S, Suemitsu K, Naoe M, J. Appl. Phys. 81 (1997) 3782.

[NAKA2001] Nakamura F, Hikosaka T, Tanaka Y, J. Magn. Magn. Mater. 235 (2001) 64.

[NAOE1996] Naoe M, Nakagawa S, J. Appl. Phys. 79 (1996) 5015.

[NAOE1998] Naoe M, Matsumiya H, Ichihara T, Nakagawa S, J. Appl. Phys. 83 (1998) 6673.

[NEAL1994] Neal H.B, Theory of Magnetic Recording, Cambridge University Press, New York (1994).

[NEEL1954] Neel L, J. Phys. Rad. 15 (1954) 376.

[NEEL1962] Néel L, Comptes. Rendus Acad. Sci. 255 (1962) 1676.

[NIST2010] Nistor L.E, Rodmacq B, Auffret S, Schuhl A, Chshiev M, Dieny B, Phys.Rev. B 81 (2010) 220407.

[OEPE1990] Oepen H.P, Benning M, Ibach H, Schneider C.M, Kirschner J, J. Magn. Magn. Matt. 86 (1990) L137.

[OHAN1987] O'Handley R.C, J. Appl. Phys. 62 (1987) R15.

[OHAN2000] O'Handley R.C, Modern Magnetic Materials Principles and Applications, Wiley, New York (2000).

[OHNU2003] Ohnuma S, Fujimori H, Masumoto T, Xiong X.Y, Ping D.H, Hono K,

Appl. Phys. Lett. 82 (2003) 946.

[OHRI1992] Ohring M, Materials Science of Thin Films, Academic Press, London (1992).

[OLIV1999] Oliveira A.J.A.de, Ortiz W.A, Mosca D.H, Mattoso N, Mazzaro I, Schreiner W.H, J. Phys.: Condens. Matter. 11 (1999) 47.

[OSHI2002] Oshima H, Nagasaka K, Seyama Y, Shimizu Y, Tanaka A, Phys. Rev. B 66 (2002) 140404.

[PAPO2006] Papon P, Leblond J, Meijer P.H.E, The Physics of Phase Transitions: Concepts and Applications, Springer, Berlin (2006).

[PARK1990] Parkin S.S.P, More N, Roche K.P, Phys. Rev. Lett. 64 (1990) 2305.

[PERU2008] Perumal A, Takahashi Y.K, Hono K, Appl. Phys. Exp. 1 (2008) 101301.

[PERU2009] Perumal A, Takahashi Y.K, Hono K, J. Appl. Phys. 105 (2009) 07A304.

[PERU2010] Perumal A, Zhang L, Takahashi Y.K, Hono K, J. Appl. Phys. 108 (2010) 083907.

[PESC1987] Pescia D, Stampanoni M, Bona G.L, Vaterlaus A, Willis R.F, Meier F, Phys. Rev. Lett. 58 (1987) 2126.

[PETZ2002] Petzold J, J. Magn. Magn. Mater. 242-245 (2002) 84.

[PIRA2007] Piramanayagam S.N, J. Appl. Phys. 102 (2007) 011301.

[PITC1993] Pitcher P.G, Miller J, Pearson D.P.A, Gurney P.D, J. Magn. Soc. Jpn. 17 (1993) 95.

[PONG2008] Pong P.W.T, Dennis C.L, Castillo A, J. Appl. Phys. 103 (2008) 07A902.

[PORR2002] Porrati F, Spatially Varying Magnetic Anisotropies in Ultrathin Films, Thesis (PhD) Martin-Luther-University (2002).

[PRAD1997] Prado L.M.A, Pérez G.T, Morales R, Salas F.H, Alameda J.M, Phys. Rev. B 56 (1997) 3306.

[PRAD2004] Prado L.M.A, Alamedo J.M, Physica B 343 (2004) 241.

[PRUT1964] Prutton M, Thin Ferromagnetic Films, Butterworth Inc, University of California (1964).

[REIM1993] Reimer L, Transmission Electron Microscopy, Springer-verlag, Germany (1993).

[RIET1997] Riet V.D.E, Klaassens W, Roozeboom F, J. Appl. Phys. 81 (1997) 806.

[RUDE1954] Ruderman M.A, Kittel C, Phys. Rev. 96 (1954) 99.

[SAIP2012] Saipriya S, Kurian J, Singh R, J. Appl. Phys. 111 (2012) 07C110.

[SAIT1964] Saito N, Fujiwara H, Sugita Y, J. Phys. Soc. Jpn. 19 (1964) 1116.

[SAIT2002] Saitoh E, Matumoto H, Nakamura T, Miyajima H, J. Appl. Phys. 91 (2002) 7215.

[SAKI2008] Saki T.O, Takahashi Y.K, Hono K, J. Appl. Phys. 103 (2008) 023910.

[SCHA2007] Schäfer R, Novel Techniques for Characterizing and Preparing Samples in Handbook of Magnetism and Advanced Magnetic Materials, ed. H. Kronmüller, Parkin S, Vol. 3, Wiley, Chichester (2007).

[SCHR2000] Schrag B.D, Anguelouch A, Ingvarsson S, Xiao G, Trouilloud Y.L.P.L, Gupta A, Wanner R.A, Gallagher W.J, Rice P.M, Parkin S.S.P, Appl. Phys. Lett. 77 (2000) 2373.

[SELL2006] Sellmyer D, Skomski R, Advanced Magnetic Nanostructures, Springer, New York (2006).

[SESH2002] Seshan K, Handbook of Thin-film Deposition Processes and Techniques: Principles, Methods, Equipment, and Applications, Noyes publication, New York (2002).

[SHAH2010] Shah L.R, Fan X, Kou X, Wang W.G, Zhang Y.P, Lou J, Sun N.X, Xiao J.Q, J. Appl. Phys. 107 (2010) 09D909.

[SHAR2006] Sharma P, Kimura H, Inoue A, Arenholz E, Guo J.H, Phys. Rev. B 73 (2006) 052401.

[SHIR1990] Shirakawa K, Yamaguchi K, Hirata M, Yamaoka T, Takeda F, Murakami K, Matsumi H, IEEE Trans. Magn. 26 (1990) 2262.

[SHIZ1994] Shi Z-P, Levy P.M, Fry J.L, Phys. Rev. B 49 (1994) 15159.

[SING2012] Singh A.K, Kisan B, Mishra D, Perumal A, J. Appl. Phys. 111 (2012) 093915.

[SPAL2011] Spaldin N.A, Magnetic Materials: Fundamental and Applications, Cambridge University Press, New York (2011).

[STIL2005] Stiles M.D, Interlayer Exchange Coupling in Ultrathin Magnetic Structures III: Fundamentals of Nanomagnetism ed. Bland J.A.C, Heinrich B, Springer, New York (2005).

[STOB2009] Stobiecki F, Urbaniak M, Szymański B, Kuświk P, Schmidt M, Aleksiejew J, Weis T, Engel D, Lengemann D, Ehresmann A, Kopcewicz

M, Acta Phys. Polo. A 115 (2009) 345.

[SUZU1993] Suzuki K, Makino A, Inoue A, Masumoto T, J. Appl. Phys. 74 (1993) 3316.

[SUZU1994] Suzuki K, Makino A, Inoue A, Masumoto T, J. Magn. Soc. Jpn. 18 (1994) 800.

[SUZU19981] Suzuki K, Herzer G, Cadogan J.M, J. Magn. Magn. Mater. 177 (1998) 949.

[SUZU19982] Suzuki K, Cadogan J.M, Phys. Rev. B 58 (1998) 2730.

[TAKA2000] Takano H, Nishida Y, Futamoto M, Aoi H, Nakamura Y, presented at Intermag 2000, AD-06, Toronto, 9–13 April 2000.

[TANA2002] Tanahashi K, Kikukawa A, Takahashi Y, Hosoe Y, Futamoto M, J. Magn. Magn. Mater. 242-245 (2002) 325.

[TANA20031] Tanahashi K, Kikukawa A, Hosoe Y, J. Appl. Phys. 93 (2003) 8161.

[TANA20032] Tanahashi K, Kikukawa A, Takahashi Y, Hosoe Y, J. Appl. Phys. 93 (2003) 6766.

[TATE1998] Tate B.J, Parmer B.S, Todd I, Davies H.A, Gibbs M.R.J, Major R.V, J. Appl. Phys. 83 (1998) 6335.

[TEGE2001] Tegen S, Monch I, Schumann J, Vinzelberg H, Schneider C.M, J. Appl. Phys. 89 (2001) 8169.

[THOM2000] Thomas L, Samant M.G, Stuart S.P.P, Phys. Rev. Lett. 84 (2000) 1816.

[TSAN1994] Tsang C, Fontana R.E, Lin T, Heim D.E, Sperious V.S, Gurney B.A, Williams M.L, IEEE Trans. Magn. 30 (1994) 3801.

[VELU1988] Velu E, Dupas C, Renard D, Renard J.P, Seiden J, Phys. Rev. B 37 (1988) 668.

[VOLK2011] Volkerts J.P, Magnetic Thin Films: Properties, Performance, and Applications, Nova Science Pub. Incorporated, New York (2011).

[WAGE1994] Wagendristel A, Wang Y, An Introduction to Physics and Technology of Thin Films, World Scientific, Singapore, 1994.

[WANG2014] Wang X, Shen S, Comput. Mater. Sci. 84 (2014) 13.

[WEIV2000] Wei V.F, Wu D, Zheng D, Ma B, Yang Z, Mater. Sci. Engg. B 68 (2000) 156.

[WUAY2002] Wua Y, Li K, Qiu J, Guo Z, Han G, Appl. Phys. Lett. 80 (2002) 4413.

[WUYM1998] Wu Y.M, Lo J.-T, Jpn. J. Appl. Phys. 37 (1998) 4943.

[YAMA1975] Yamada K, Ishikawa Y, Endoh Y, Masumoto T, Solid State Commun. 16 (1975) 1335.

[YANB1989] Yan B, Lin T, Yang D.C, Thin Solid Films 173 (1989) 51.

[YANG2009] Yang P.Y, Zhu X.Y, Zeng F, Pan F, Appl. Phys. Lett. 95 (2009) 172512.

[YANG2011] Yang W, Liu H, Dun C, Zhao Y, Dou L, J. Low Temp. Phys. 164 (2011) 272.

[YILD20091] Yildiz F, Przybylski M, Kirschner J, J. Appl. Phys. 105 (2009) 07E129.

[YILD20092] Yildiz F, Przybylski M, Ma X.D, Kirschner J, Phys. Rev. B 80 (2009) 064415.

[YOSH19881] Yoshizawa Y, Yamauchi K, J. Appl. Phys. 64 (1988) 6047.

[YOSH19882] Yoshizawa Y, Oguma S, Yamauchi K, J. Appl. Phys. 64 (1988) 6044.

[YOSH19891] Yoshizawa Y, Yamauchi K, J. Magn. Soc. Jpn. 13 (1989) 231.

[YOSH19892] Yoshizawa Y, Oguma S, Hiraki A, Yamuchi K, Hitachi Metals Tech. Rev. 5 (1989) 13.

[YOSH2001] Yoshizawa Y, Scripta Mater. 44 (2001) 1321.

[YOSI1957] Yosida K, Phys. Rev. 106 (1957) 893.

[YOUS2004] Youssef J.B, Vukadinovic N, Billet D, Labrune M, Phys. Rev. B 69 (2004) 174402.

[ZENG2005] Zeng F, Gen Q.W, Gao Y, Pan F, Appl. Surf. Sci. 245 (2005) 39.

[ZHAN19961] Zhang J, White R.M, J. Appl. Phys. 79 (1996) 5113.

[ZHAN19962] Zhang J, White R.M, IEEE Trans. Magn. 32 (1996) 4630.

[ZHAN2003] Zhang Z.G, Kang K, Suzuki T, Appl. Phys. Lett. 83 (2003) 1785.

[ZHAO1999] Zhao Y.P, Palasantzas G, Wang G.C, Hosson J.T.M.D, Phys. Rev. B 60 (1999) 1216.

Publications

LIST OF PUBLICATIONS:

IN JOURNALS:

Published

[1]. Spacer layer and temperature driven magnetic properties in multilayer structured FeTaC thin films
Akhilesh Kr. Singh, Srijani Mallik, Subhankar Bedanta, and A. Perumal
Journal of Physics D: Applied Physics 46 (2013) 445005.

[2]. Effect of post annealing and multilayer structure on soft magnetic properties of FeTaC thin film
Akhilesh Kr. Singh, Srijani Mallik, Subhankar Bedanta, and A. Perumal
IEEE Transactions on Magnetics 50 (2013) 2000804.

[3]. Enhanced soft magnetic properties in stress free amorphous FeTaC/Ta multilayer thin films
Akhilesh Kr. Singh and A. Perumal
AIP Conference Proceedings 1512 (2013) 630.

[4]. Thickness dependent magnetic properties of amorphous FeTaC films
Akhilesh K. Singh, Bhagaban Kisan, Debabrata Mishra, and A. Perumal
Journal of Applied Physics 111 (2012) 093915.

[5]. Enhanced soft magnetic properties in multilayer structured amorphous Fe-Ta-C films
D. Mishra, **Akhilesh Kr. Singh**, P. C. Shyni, D. Sharma, and A. Perumal
Journal of Applied Physics 109 (2011) 07A304.

Under Submission

[6]. Microstructure and multilayer structure driven magnetic properties of FeTaC/Ta thin films
Akhilesh Kr. Singh and A. Perumal.

[7]. Effect of heat treatment on spacer layer thickness dependent magnetic properties of FeTaC/Ta multilayer structure films
Akhilesh Kr. Singh and A. Perumal.

[8]. Temperature dependent magnetic properties of post annealed multilayer structured FeTaC thin films.
Akhilesh Kr. Singh and A. Perumal.

In Conferences

[1]. Effects of magnetostatic interaction and topological coupling on magnetic properties of multilayer structured FeTaC thin films
Akhilesh Kr. Singh and A. Perumal
Presented in International Conference on Magnetic Materials and Applications 2013 (MagMA-2013), December 5-7, 2013, IIT Guwahati, Guwahati.

[2]. Effect of post annealing and multilayer structure on soft magnetic properties of FeTaC thin film
Akhilesh Kr. Singh, Srijani Mallik, Subhankar Bedanta, and A. Perumal
Presented in the 3rd International Symposium on Advanced Magnetic Materials and Applications (ISAMMA 2013), July 21-25, 2013, Taichung, Taiwan.

[3]. Enhanced soft magnetic properties in stress free amorphous FeTaC/Ta multilayer thin films
Akhilesh Kr. Singh and A. Perumal
Presented in 57th DAE Solid State Physics Symposium, December 3-7, 2012, IIT Bombay, India.

[4]. Role of nanostructure on the magnetic properties
A. Perumal, **Akhilesh Kr. Singh**, P. C. Shyni, K. Bhagaban, Anabil Gayen,
Presented in National Seminar on Nanoscience and Nanotechnology, MC College, Barpeta, August 31- September 01, 2012, India.

[5]. Soft magnetic properties of multilayer structured amorphous FeTaC films
Akhilesh Kr. Singh and A. Perumal,
Presented in National Conference on Magnetism and Magnetic Materials (MagMa-2012), March 12-13, 2012, IIT Madras, India.

[6]. Role of soft magnetic films in magnetic recording media for futuristic hard disk drive applications
Akhilesh Kr. Singh, Bhagaban Kisan, and A. Perumal,
Presented in International Conference on Nanomaterials and Applications, February 28-29, 2012, Mother Therasa University, Kodaikanal, India.

[7]. Thickness dependent magnetic properties of amorphous FeTaC thin films
Akhilesh Kr. Singh, P. Gogoi, and A. Perumal,
Presented in International Conference on Advanced Nanoscience and Nanotechnology (ICANN-2011), December 8-10, 2011, IIT Guwahati.

[8]. Enhanced soft magnetic properties in multilayer structured amorphous Fe-Ta-C films

D. Mishra, **Akhilesh Kr. Singh**, P. C. Shyni, D. Sharma, and A. Perumal,
Presented in International Conference on Magnetism and Magnetic Materials (55 MMM Conference), November 14-18, 2010, Atlanta, USA.

PUBLICATIONS OUTSIDE THESIS WORK:

[1]. Effect of post annealing and multilayer structure on soft magnetic properties of FeTaC thin film
P Saravanan, Jen-Hwa Hsu, Anabil Gayen, **Akhilesh Kr. Singh**, A Perumal, G L N Reddy, Sanjiv Kumar and S V Kamat
Journal of Physics D: Applied Physics 46 (2013) 155002.

[2]. High temperature magnetic properties of indirect exchange spring FePt/M(Cu,C)/Fe trilayer thin films
A. Gayen, B. Biswas, **Akhilesh Kr. Singh**, P. Saravanan, and A. Perumal
J. Nanomaterials 2013 (2013) 718365.